The University Of Sheffield.

The role of versican in the development of the inner ear and in cancer progression

By Elvira Diamantopoulou

A thesis submitted in partial fulfilment of the requirements for the degree of Doctor of Philosophy

The University of Sheffield Department of Biomedical Science

August 2018

Με πολλή αγάπη, στη γιαγιά και τον παππού μου

To my beloved grandparents

ACKNOWLEDGMENTS

First of all, I would like to thank my first supervisor Professor Tanya Whitfield, for trusting me with the opportunity of this PhD and guiding me through its rambling path. I am only grateful to her for all the advice, the support, the encouragement and the time she generously devoted to me. Special thanks to my second supervisor, Dr Daniel W. Lambert, for his valuable input to this work.

Also, I would like to thank the University of Sheffield for funding my PhD and the travel opportunities it offered me.

Thank you to all my friends and colleagues in Firth Court and the School of Clinical Dentistry, who made my days fun and lunch breaks amusing. Special thanks to Dr Sarah Baxendale and Dr Sarah Burbridge for their friendship and guidance in the lab. Thanks to Dr Hellen Colley, Prof Keith Hunter, Brenka McCabe and Kirsty Franklin, for providing cells and technical support.

A huge thank you to my family, without the support of whom, I would have never imagined I would be able to complete this PhD. Thanks to my Mum, for all the uplifting words and the care packages coming all the way from Greece, and to my Dad for believing in me like no one else. To my αγάπη, George Sutherland, thank you for the constant support; academic, emotional, tangible and for all the cooking while I was writing up!

ABSTRACT

Cancer is the second leading cause of death and its high mortality rate is due to metastasis; a complex process that involves cross talk between cancer cells, and their cellular and acellular microenvironment. However, metastasis treatment is a highly challenging task, due to its resistance to existing therapeutic strategies. The extracellular matrix gene versican *(VCAN)* is overexpressed by fibroblasts of the stroma in many human cancer types, and its increased expression is linked to enhanced metastasis and poor patient outcome. While anticancer therapies typically target cancer cells directly, in the project herein, the zebrafish model organism is used as a novel approach to identify chemical compounds that can manipulate the gene expression of the chondroitin sulphate proteoglycan VCAN in the tumour microenvironment.

Versican core protein genes are also expressed in the zebrafish inner ear, where morphogenesis of semicircular canals requires a fusion event between epithelial projections. *Versican* transcripts are strongly expressed in the projections before this fusion event and sharply down-regulated as soon as it is complete, suggesting a potential role for Versican in the fusion process. In the zebrafish *adgrg6* (*gpr126*) mutant ear, *versican* genes remain expressed at high levels, fusion fails and the ear shows concomitant morphological defects.

In this study, I showed that zebrafish *versican* mutants do not exhibit a clear abnormal ear phenotype, suggesting that other extracellular matrix components may compensate for *versican* loss. I demonstrated that heparan sulphate proteoglycans are essential for epithelial projection outgrowth, as in the homozygous *ext2* mutant ear the projections fail to elongate and fuse. Using the zebrafish *adgrg6* mutant embryo as an *in vivo* drug screening tool, I built upon previous work of the Whitfield lab and identified 74 compounds that can strongly down-regulate otic *versican* mRNA expression. To investigate whether these compounds are likely to down-regulate *versican* through modulation of Adgrg6 signalling, I performed a secondary assay using *mbp* (*myelin basic protein*), a gene whose expression is down-regulated in *adgrg6* mutants. Many of the compounds that were able to both suppress *versican* and rescue *mbp* expression in *adgrg6* mutants are calcium-channel blockers or adrenoceptor antagonists. One compound was also able to suppress *VCAN* mRNA levels in experimentally-derived cancer-associated

fibroblasts, the major cellular component of the tumour microenvironment, as shown by qPCR. The present study highlights the importance of the extracellular matrix on cellular behaviour. A greater understanding of the regulation of *versican* expression will shed light on the biological processes underlying development and may also contribute to the development of new antineoplastic therapies.

CONTENTS

CHAPTER 1. Introduction 13

1.1 Background 17

1.1.1 Zebrafish as a model for development and disease 18

1.2 The extracellular matrix (ECM) 20

1.2.1 Function and components of the ECM 20

1.2.2 Chondroitin & Heparan Sulphate Proteoglycans 22

1.2.3 The versican molecule 26

1.2.4 Regulation of versican expression 29

1.2.5 The roles of versican 30

1.3 Auditory and vestibular system 33

1. .3.1 Overview of the vertebrate inner ear 33

1.3.2 The zebrafish inner ear and lateral line function 34

1.3.3 Semicircular canal development in zebrafish 35

1.3.4 Involvement of the ECM in the formation of the inner ear 37

1.3.5 Adgrg6 (Gpr126) 38

1.4 Cancer 42

1.4.1 The tumour microenvironment 42

1.4.2 The ECM of the tumour microenvironment 45

1.4.3 The role of versican isoforms in cancer 47

1.5 Main hypothesis and aims 51

CHAPTER 2. Materials and Methods 52

2.1 Zebrafish work 52

2.1.1 Zebrafish lines 52

2.1.2 Zebrafish care and mating 53

2.1.3 Microscopy and photography 53

2.1.4 *In vivo* drug screening 54

2.1.5 Whole-mount *in situ* hybridisation (ISH) 55

2.1.6 Molecular analysis 57

2.2 Human cell culture 60

2.2.1 Cell lines 60

2.2.2 Cell culture 60

2.2.3 TGF-β and drug treatments 61

2.2.4 Western Blot 61

2.2.5 Molecular Analysis 63

2.2.6 Statistical Analysis 64

CHAPTER 3. The role of versican in the zebrafish inner ear development 65

3.1 Introduction 65

3.2 Results 67

3.2.1 *Versican a* wild-type expression pattern 67

3.2.2 *Versican b* wild-type expression pattern 70

3.2.3 *Versican a* mutant phenotype 73

3.2.4 *Versican b* mutant phenotype 76

3.2.5 *Versican a* and *b* double mutant phenotype 79

3.3 Discussion 82

3.4 Conclusions 84

CHAPTER 4. The role of heparan sulphate proteoglycans in the zebrafish inner ear development 86

4.1 Introduction 86

4.2 Results 87

4.2.1 Epithelial projections in the *dak*$^{to273b-/-}$ mutant ear stay small and do not fuse 87

4.2.2 Saccular otoliths are not properly tethered on the posterior macula of the *dak*$^{to273b-/-}$ mutant ear 89

4.2.3 Improper otolith tethering in *dak*^{to273b} mutants is due to the otolithic membrane lacking *otogelin* ... 91

4.2.4 *Versican* mRNA expression abnormally persists in the unfused projections in the *dak*^{to273b} mutant ear, while *adgrg6* shows ectopic expression ... 93

4.3 Discussion ... 96

4.4 Conclusions ... 98

CHAPTER 5. *In vivo* drug screening using the *adgrg6* zebrafish mutant ... 99

5.1 Introduction ... 99

5.2 Results ... 102

5.2.1 Small molecules that rescue *versican* mRNA expression in *adgrg6* mutants ... 102

5.2.3 Secondary assay based on *myelin basic protein* (*mbp*) expression ... 111

5.2.4 Tracazolate hydrochloride, FPL 64176, nifedipine and cilnidipine down-regulate *versican* mRNA expression in a dose-dependent manner. ... 124

5.2.5 Tracazolate hydrochloride, FPL 64176, nifedipine and cilnidipine restore pillar formation in the *adgrg6* mutant ear in a dose-dependent manner. ... 129

5.3 Discussion ... 131

5.3.1 Primary *versican* screens ... 131

5.3.2 Secondary *myelin basic protein* screens ... 132

5.3.3 Putative downstream effectors of the Adgrg6 pathway ... 132

5.3.4 Putative Adgrg6 receptor modulators ... 135

5.4 Conclusions ... 136

CHAPTER 6. Regulation of Versican in Human Fibroblasts ... 137

6.1 Introduction ... 137

6.2 Results ... 138

6.2.1 TGF-β1 upregulates *VCAN* mRNA expression in oral fibroblasts to an extent that is dependent on the cell type. ... 138

6.2.2 The effect of nifedipine on *VCAN* expression in TGF-β-induced oral fibroblasts ... 140

6.2.3 The effect of cilnidipine on *VCAN* expression in TGF-β-induced oral fibroblasts ... 146

6.2.4 *ADGRG6* is expressed in oral fibroblasts ... 149

6.3 Discussion **151**

6.3.1 The effect of TGF-β1 on *VCAN* expression in oral fibroblasts 151

6.3.2 The use of DMSO as a solvent for drug treatments on oral fibroblasts 151

6.3.3 CCBs as a tool to down-regulate *VCAN* in fibroblasts 152

CHAPTER 7. Synopsis **154**

7.1 Overview of the results **154**

7.2 The role of chondroitin and heparan sulphates in the development of the inner ear **156**

7.3 Drug screening approach: the translation from *in vivo* to *in vitro* systems **158**

7.4 Relevance of my study to other fields of research and therapeutics **159**

7.5 Concluding remarks **161**

BIBLIOGRAPHY **162**

APPENDIX **189**

LIST OF ABBREVIATIONS

ADAMTS – a disintegrin and metalloprotease with thrombospondin motifs

ALL – anterior lateral line

AP-1 – activator protein 1

AVC – atrioventricular canal

B2M – β2 microglobulin

BCA – bicinchoninic acid

BMP – bone morphogenetic protein

BSA – bovine serum albumin

CAF – cancer-associated fibroblast

cAMP – cyclic adenosine monophosphate

CCB – calcium-channel blocker

chsy1 – chondroitin synthase 1

CNS – central nervous system

CREB – cAMP-responsive-element-binding protein

CRI – cancer-related inflammation

CRP – complement regulatory protein

CS – chondroitin sulphates

CSPG – chondroitin sulphate proteoglycan

CTF – C-terminal fragment

DC – dendritic cell

DIC – differential interference contrast

DLS – dorsolateral septum

DMEM – Dulbecco's modified eagle medium

DMSO – dimethyl-sulfoxide

ECM – extracellular matrix

EDTA – ethylenediaminetetraacetic acid

EGF – epidermal growth factor

EMT – epithelial-to-mesenchymal transition

ENU – *N*-ethyl-*N*-nitrosourea

ER – endoplasmic reticulum

ERK – extracellular-signal-regulated kinase

ext – exostosin

FBS – foetal bovine serum

FGF – fibroblast growth factor

GAG – glycosaminoglycan

GAIN – G-autoproteolysis-inducing domain

GalNAc – *N*-acetylgalactosamine

GAPDH – glyceraldehyde 3-phosphate dehydrogenase

GlcA – glucuronic acid

GlcNAc – *N*-acetylglucosamine

GPCR – G-protein-coupled receptor

GPS – GPCR proteolytic site

HA – hyaluronan

HABR – hyaluronan-binding repeats

HM – hybridisation mix

hpf – hours post fertilisation

HRP – horseradish peroxidase

HS – heparan sulphates

HSPG – heparan sulphate proteoglycans

IBMX – 3-isobutyl-1-methylxanthine

Ig – immunoglobulin

IL – interleukin

ISH – *in situ* hybridisation

JNK – c-Jun N-terminal kinase

LC – C-type-lectin domain

LD_{50} – median lethal dose

LDL – low-density lipoproteins

LOX – lysyl oxidase

LWT – London wild type

MAPK – mitogen-activated protein kinase

MBP – myelin basic protein

MET – mesenchymal to epithelial transition

miRNA – microRNA

MMPs – matrix metalloproteinases

NFκB – nuclear factor kappa B

NK – natural killer cells

NMDA – *N*-methyl-D-aspartate receptor

NOF – normal oral fibroblast

NTF – N-terminal fragment

OSCC – oral squamous cell carcinoma

PBS – phosphate buffered saline

PDGF – platelet-derived growth factor

PG – proteoglycan

PKA – protein kinase A

PLLg – posterior lateral line ganglion

PNS – peripheral nervous system

PSGL-1 – P-selectin glycoprotein ligand-1

qRT-PCR – quantitative real-time polymerase chain reaction

RIPA – radio-immunoprecipitation assay

RNA – ribonucleic acid

SAP – shrimp-alkaline phosphatase

SC – schwann cell

SCC – semicircular canal

Shh – sonic hedgehog

SMC – smooth muscle cell

TAM – tumour-associated macrophages

TANs – tumour-associated neutrophils

TBS – tris-buffered saline

TBS-T – tris-buffered saline- tween

TGF-β – transforming growth factor beta

TLR – toll-like receptor

ugdh – UDP-glucose dehydrogenase

UTR – untranslated region

uxs1 – UDP-glucuronate decarboxylase 1

VCAN – versican

VEGF – vascular endothelial growth factor

α-SMA – alpha smooth muscle actin

7TM – seven-transmembrane helix domain

LIST OF FIGURES

Figure 1.1 Biosynthesis of Chondroitin and Heparan Sulphate Proteoglycans in vertebrates..... 24

Figure 1.2 Schematic representation of the structure of versican and its isoforms in mammals and zebrafish..... 27

Figure 1.3 The vertebrate inner ear evolution..... 34

Figure 1.4 Schematic comparison of semicircular canal formation in the zebrafish ear and the amniote ear..... 35

Figure 1.5 Development of the semicircular canal system in the zebrafish embryo. 36

Figure 1.6 Schematic representation of Adgrg6 protein structure..... 39

Figure 1.7 Adgrg6 signalling in a myelinating Schwann Cell..... 41

Figure 1.8 The tumour microenvironment..... 43

Figure 1.9 The binding partners of versican and the main functions of its domains.....50

Figure 2.1 Normalisation of ear width..... 54

Figure 3.1 Schematic diagram of the predicted Vcana and Vcanb proteins, showing the C-type-lectin-like motif..... 66

Figure 3.2 *vcana* mRNA expression pattern in wild-type 14 hpf- 22 hpf zebrafish embryos 67

Figure 3.3 *vcana* mRNA expression pattern in wild-type 50 hpf- 5 dpf zebrafish embryos 69

Figure 3.4 *vcanb* mRNA expression pattern in wild-type 19 hpf- 26 hpf zebrafish embryos 70

Figure 3.5 *vcanb* mRNA expression pattern in wild-type 48 hpf- 5 dpf zebrafish embryos 72

Figure 3.6 The *vcana*^{sa1460} mutant phenotype is variable 75

Figure 3.7 The *vcanb*^{sa923} mutant phenotype is incompletely penetrant 78

Figure 3.8 *sa1460;sa923* double homozygous mutant phenotype is variable 81

Figure 4.1 The *dak*^{to273b} mutant phenotype is characterised by inner ear defects... 88

Figure 4.2 Saccular otoliths are not properly tethered in the homozygous *dak*^{to273b} mutant ear at 5 dpf. 90

Figure 4.3 Expression of *otomp*, *otog* and *stm* is reduced from the saccular macula in the *dak*^{to273b} mutant ear 92

Figure 4.4 Expression of *versican* abnormally persists on the unfused projections of *dak*^{to273b} mutants 94

Figure 4.5 *adgrg6* shows ectopic expression in *dak*^{to273b} mutants 95

Figure 5.1 Schematic showing the positions of the most studied *adgrg6* mutant alleles ..101

Figure 5.2 A Primary drug screen identified 92 (Tocris) and 205 (Spectrum) putative hit compounds able to down-regulate *versican* mRNA expression in *adgrg6*^{tb233c} mutants... 105

Figure 5.3 Combined data from the Tocris and Spectrum libraries revealed widespread chemical clustering 106

Figure 5.4 85% of the hit compounds that passed the first retest scored A-C in the second retest 108

Figure 5.5 *mbp* scoring system and classification of the compounds 112

Figure 5.6 Classification of putative Adgrg6 modulators 116

Figure 5.7 Visualisation of the compounds presumed to interact with the Adgrg6 receptor directly 119

Figure 5.8 Classification of the *versican* hit compounds that did not affect *mbp* expression (group I) 121

Figure 5.9 Classification of the *versican* hit compounds that also down-regulated *mbp* expression, which may represent general transcription inhibitors (group J) 123

Figure 5.10 Tracazolate hydrochloride, FPL 64176, nifedipine and cilnidipine down-regulate *versican* mRNA expression in the *adgrg6*^{tb233c} mutant ear in a dose-dependent manner 125

Figure 5.11 Tracazolate hydrochloride, FPL 64176, nifedipine and cilnidipine down-regulate *versican* levels of expression and reduce the number of projections that express *versican* in the *adgrg6*^{tb233c} mutant ear, in a dose-dependent manner 127

Figure 5.12 LD_{50} curves from the treatment of wild-type embryos for the adjusted exposure time (60-110 hpf) 128

Figure 5.13 Tracazolate hydrochloride, FPL 64176, nifedipine and cilnidipine restore pillar formation and ameliorate the swelling in the *adgrg6*^{tb233c} mutant ear in a dose-dependent manner 130

Figure 5.14 Dihydrofissinolide, carapin-8(9)-ene, deoxygedunin, alpha-dihydrogedunol and danazol share structural similarities that may be important for interaction with the binding pocket of Adgrg6 receptor 135

Figure 6.1 The effect of TGF-β1 on *VCAN* mRNA expression in normal and cancer-associated oral fibroblasts.. 139

Figure 6.2 Nifedipine induced a variable decrease in VCAN expression in TGF-β1-induced NOF804 oral fibroblasts, which was not dose-dependent..... 143

Figure 6.3 Treatment of TGF-β1 induced NOF316 fibroblasts with nifedipine did not affect V0 or V1 expression levels..... 144

Figure 6.4 Treatment of cancer-associated fibroblasts with nifedipine induced a dose-dependent down-regulation of V0, but not V1 expression 145

Figure 6.5 Treatment of TGF-β1-induced normal fibroblasts with cilnidipine induced a down-regulation of V0, but not V1 expression 148

Figure 6.6 *ADGRG6* is expressed in low levels in NOF316 and CAF003 cells, but is found expressed at high levels in NOF804 cells 150

LIST OF TABLES

Table 1.1 Summary of the main effects of mammalian versican isoforms…….. ……..32

Table 2.1. List of zebrafish lines used in the study..... 52

Table 2.2. List of ISH reagents..... 57

Table 2.3. List of previously synthesised ISH template constructs used for ISH 59

Table 2.4. List of primers used for DNA sequencing 60

Table 2.5. List of antibodies used for western blotting..... 63

Table 2.6. Reverse Transcription reaction..... 64

Table 5.1 Brief description of the two compound libraries used for the *versican* screening assay……..103

Table 5.2 Overview of the hit compounds identified in versican screens. ……..109

Table 5.3 Hit compounds best able to down-regulate *versican* mRNA expression in the ear of *adgrg6*^{tb233c} mutants. The compounds listed were classed as A-C in both rounds of retesting……..110

Table 5.4 List of the 42 hit compounds that were able to rescue the expression of *vcanb* and *mbp* in *adgrg6*^{tb233c} mutants, thus representing putative Adgrg6 pathway modulators……116

Table 5.5 List of the hit compounds that were unable to rescue the expression of *vcanb* in *adgrg6*^{fr24} mutants, thus representing putative Adgrg6 receptor modulators…….. 119

Table 5.6 List of the 26 versican hit compounds that did not affect *mbp* expression in *adgrg6*^{tb233c} mutants……121

Table 5.7 List of the 21 versican hit compounds that also down-regulated *mbp* expression in *adgrg6*^{tb233c} mutants, which may represent general transcription inhibitors……..123

CHAPTER 1.

Introduction

1.1 BACKGROUND

In developed countries, cancer is the second leading cause of death and it has been shown that its high mortality rate is due to metastasis (Kung et al., 2008). Cancer is a group of diseases that involve abnormally increased cell growth in the body. Cancer cells have the ability to invade normal tissue by reactivating gene expression programs, normally employed during embryonic development, that control functions, such as cell proliferation, migration and invasion.

It is generally accepted that the biochemical composition of a cell's surroundings is one of the most important factors that may prompt it to undergo such functions. The group of extracellular molecules, secreted by cells, that provides structural support and biochemical information to the surrounding cells is referred to as the extracellular matrix (ECM).

This work focuses on the ECM component versican, a chondroitin sulphate proteoglycan (CSPG), known to influence many key cellular processes involved in development and disease. Versican has been reported to be associated with cancer progression in a large number of malignancies in the past few years and its main source is believed to be the tumour stromal microenvironment (reviewed in Ricciardelli et al., 2009).

From a developmental point of view, *versican* genes are strongly expressed during the formation of several tissues in the body, including the semicircular canals in the inner ear of zebrafish embryos, which are responsible for detecting angular acceleration in three-dimensional space (Geng et al., 2013). The Whitfield lab identified a signalling pathway in the zebrafish inner ear required for the generation of an epithelial pillar, essential for the formation of the semicircular canals. The essential mediator of this pathway is the G-protein coupled receptor (GPCR) Adgrg6 (Gpr126). Homozygous *adgrg6* mutants fail to down-regulate *versican* expression, fusion to form pillars is impeded (Geng et al., 2013) and adult canal ducts are defective (Whitfield lab, unpublished data).

This finding suggests that Versican might have a role in the changes cells undergo in order to adhere, recognise each other and fuse, allowing for successful semicircular canal development, and its expression may be regulated by Adgrg6.

The main aim of this work is to improve understanding of versican biology, elucidate its role during semicircular canal development, as well as investigate the regulatory mechanisms that drive *versican* expression in the zebrafish inner ear *in vivo* and *in vitro* in human stromal models.

1.1.1 Zebrafish as a model for development and drug screening

Zebrafish (*Danio rerio*) is a tropical freshwater fish of the minnow family, native to Asia, comprising a very well-established model for the study of development, pathology, and regeneration of numerous vertebrate organs (Detrich et al., 2010). The popularity of zebrafish as an animal model can be attributed to the numerous practical advantages it offers, including its small size, the transparency of its embryo, its rapid development, the relative simplicity of its handling and the availability of tools for genetic manipulation (Whitfield et al., 2002).

Large-scale genetic studies revealed that genetic similarity between zebrafish and human is astonishingly high, as 70 per cent of protein-coding human genes have a zebrafish orthologue and 84 per cent of genes linked with human diseases have a zebrafish counterpart (Howe et al., 2013). Thus, numerous zebrafish models for various human genetic diseases, including cancer, have been developed over the years (reviewed in Kaslin and Gibert, 2017).

The availability of zebrafish disease models, in combination with the fact that the embryos are permeable to small chemical compounds, makes them uniquely suited for *in vivo* high-throughput drug screens. Unlike *in vitro* screens, zebrafish drug screening offers early insight into toxicity, absorption and metabolism of the tested compounds, due to the existence of functioning organ systems in the larvae (e.g. kidney, liver). At the same time, it provides the opportunity for counter screens, which can exclude compounds with undesirable effects.

As the zebrafish embryo offers all the advantages of whole-organism, phenotypic drug screening, numerous phenotype-based small molecule zebrafish screens have been conducted over the years (Owens et al., 2008; Baxendale et al., 2012; Macrae and Peterson,

2015; Bruni et al., 2016; Bremer et al., 2017; Bossé and Peterson, 2017). Successful examples include large-scale drug screens using zebrafish models of leukemia or melanoma identifying efficacious antineoplastic compounds, such as lenaldekar and leflunomide (White et al., 2011; Cusick et al., 2012). Lenaldekar was initially identified as a T-cell expansion inhibitor in zebrafish larvae and was soon afterwards shown to selectively kill primary human leukemia cells (Cusick et al., 2012; Ridges et al., 2018). Leflunomide was shown to decrease melanoma growth in zebrafish embryos, mouse xenograft models and in human melanoma cell lines (White et al., 2011). A thriving case was the identification of clemizole by a small molecule screen using *scn1a* zebrafish embryos, a mutation that recapitulates Dravet syndrome patient symptoms (Baraban et al. 2013). A few years later, clemizole was proved to clinically reduce the frequency and severity of seizures in Dravet syndrome patients (Griffin et al., 2017). Such cases of rapid translation of zebrafish screening-derived data to murine models or even human patients exemplifies the potency of zebrafish as a reliable model for *in vivo* drug screening.

1.2 THE EXTRACELLULAR MATRIX (ECM)

1.2.1 Function and components of the ECM

The extracellular matrix (ECM) is a sophisticated, dynamic and highly organised network that surrounds and supports cells within tissues, having various physiological functions (Zhang et al., 2012). Before the 1980s, the ECM's sole function was considered to be structural, providing a scaffold which cells can adhere to and form tissues. This opinion completely changed after the discovery of integrins (Tamkun et al., 1986), as it became clear that these physical linkages could bind to receptors and transport bidirectional intracellular and extracellular messages that affect cell behaviour.

The ECM is composed of water, ions and a wide spectrum of molecules, which can be classified in collagenous and non-collagenous glycoproteins, glycosaminoglycans (GAGs) and proteoglycans (PGs) (reviewed in Rozario and Desimone, 2010).

Collagenous glycoproteins make up one of the most abundant protein classes found in the animal kingdom. A typical collagen molecule is comprised of a triple helix made up of coiled α-chains (Shoulders and Raines, 2009). The majority of collagen molecules in the ECM are produced by cells called fibroblasts, and they can be organised in fibrils, sheets or networks, that vary among different tissues (reviewed in Theocharis et al., 2016). Non-collagenous glycoproteins of the ECM form a much more diverse group, which includes laminins, fibronectins, fibrillins and tenascins (reviewed in Theocharis et al., 2016).

GAGs are repeats of a disaccharide pair consisting of an amino sugar and a uronic acid (glucuronic acid or iduronic acid) or galactose (Lindahl et al., 2017; Chapter 17). Based on the composition of these residues, GAGs can be clustered in chondroitin, dermatan, keratan, heparan sulphates and the non-sulphated hyaluronic acid (HA) (reviewed in Hascall and Esko, 2017; Chapter 16).

Due to their negative charge, GAGs possess very strong osmotic properties, which cause the 'swelling' of GAG-rich matrices (reviewed in Rozario and Desimone, 2010). Apart from HA, all GAGs are covalently attached to a core protein, creating a proteoglycan (PG) (reviewed in Lindahl et al., 2017; Chapter 17). Differential splicing of genes encoding core proteins generates a plethora of proteoglycans, which are correspondingly named after the type of GAG chains they incorporate.

ECM composition is not static, but rather dynamic and can change to serve the needs of a

cell at different stages. A change in the ECM composition can block or transmit signals regulating cell adhesion, apoptosis, proliferation, migration, invasion or form concentration gradients of morphogens. For example, the vertebrate embryonic ECM constitution is distinct from the ECM surrounding adult tissues. Due to the extensive cell migration, folding and branching of tissues that take place during embryogenesis, a highly specialised and compact adult ECM, characterised by a well-established collagenous structure, would obstruct successful development. Instead, the provisional matrix is high in hyaluronan, fibronectin and proteoglycans, such as versican (VCAN), which keep it hydrated and flexible (reviewed in Nandadasa et al., 2014). On the other hand, the ECM surrounding a tumour is often stiffer, due to alterations in ECM deposition by cancer-associated fibroblasts (CAFs, discussed in section 1.4.1) and builds a track whereby cancer cells can migrate. At the same time, ECM deposition could also operate as a barrier, impeding immune cells, apoptotic signals, or drugs from reaching the tumour site (reviewed in Venning et al., 2015). Although anticancer therapies have traditionally targeted tumour cells directly, ECM molecules have recently started to draw increasing attention as key therapeutic targets (reviewed in Venning et al., 2015 and Theocharis et al., 2016).

1.2.2 Chondroitin & Heparan Sulphate Proteoglycans

Proteoglycans are expressed at the cell surface of the majority of eukaryotic cell types. As described above, proteoglycans of the ECM incorporate core proteins coupled with GAG chains. The two main proteoglycan groups of the ECM are chondroitin sulphate proteoglycans (CSPGs) and heparan sulphate proteoglycans (HSPGs), which carry GAGs of chondroitin sulphate (CS) and heparan sulphate (HS) type, respectively. Although CSs and HSs incorporate polysaccharide backbones of different constitution, they both contain numerous *O*-sulphate groups, the location of which affects their ability to bind various growth factors (Ashikari-Hada et al., 2004). CSPGs and HSPGs have also been shown to bind a variety of other ligands, including morphogens, chemokines, cell adhesion molecules, and other extracellular matrix proteins, through interaction with GAGs or specific core protein motifs (Kreuger et al., 2006).

The CSPG family consists of nine submembers: CSPG1 (aggrecan), CSPG2 (versican), CSPG3 (neurocan), CSPG4 (melanoma-associated chondroitin sulphate proteoglycan or neuron-glial antigen 2), CSPG5, CSPG6 (structural maintenance of chromosomes protein 3, SMC-3), CSPG7 (brevican), CSPG8 (cluster of differentiation 44, CD44) and phosphacan. Versican, brevican, aggrecan and neurocan belong to the large aggregating CSPG family, also called the hyalectan or lectican family (Du et al., 2012). All members of this family are characterised by an amino-terminal hyaluronan-binding domain and a C-type-lectin domain (LC) at the carboxy-terminal end (reviewed in Wu et al., 2005 and Lindahl et al., 2017). The LC domain is highly conserved among lectican members in vertebrates and is known to bind carbohydrates in a calcium-dependent manner (Aspberg et al., 1995; Cummings and McEver, 2017; Chapter 34).

Whilst most CSPGs are extracellular molecules, HSPGs are found either on the cell surface or the basement membrane (reviewed in Theocharis et al., 2016). Cell surface representatives of this family include glypicans, syndecans and betaglycan, but the main HSPGs of the ECM are the pericellular members perlecan, agrin and collagen XVIII.

Biosynthesis of both CS and HS chains starts in the endoplasmic reticulum (ER) and is completed in Golgi apparatus (Silbert and Sugumaran, 2002). It initiates with the formation of a tetrasaccharide linker, mediated by xylosyltransferase, which transfers xylose from UDP-xylose to specific serine residues of the core protein (Baker et al., 1972; Figure 1.1). The next transferase to act, N-acetylglucosaminyl-transferase I (GlcNAcT-I) or N-acetylgalactosaminyl-tranferase I (GalNAcT-I), drives synthesis to HS or CS, respectively

(Esko and Zhang, 1996). Studies on the synthesis of syndecan, which incorporates both types of glycosaminoglycans, revealed that specific amino acid sequences within the core protein were the key determinants for HS or CS attachment (Kokenyesi and Bernfield, 1994). These sequences create a hydrophobic or hydrophilic environment, in which the activity of one of the two acetyltransferases is favoured (Kokenyesi and Bernfield, 1994).

If CS synthesis is promoted, the polymerisation of the chondroitin chain continues with the alternating addition of glucuronic acid (GlcA) and N-acetylgalactosamine (GalNAc) residues by an enzyme with GlcA- and GalNAc- transferase activities, called chondroitin synthase (Silbert and DeLuca, 1969; Silbert and Sugumaran, 2002). If HS synthesis is favoured, elongation is continued with the alternating addition of GlcA and N-acetylglucosamine (GlcNAc) residues by GlcA- and GlcNAc- transferases, whose genes belong to the exostosin (EXT) gene family of tumour suppressors. Once the CS or HS chain is assembled, it is modified by a number of enzymes, which are summarised below in Figure 1.1. Although HA also consists of repeating GlcNAc and GlcA residues, these are not modified and its synthesis normally occurs at the inner surface of the plasma membrane and not in the Golgi apparatus (Hascall and Esko, 2017; Chapter 16).

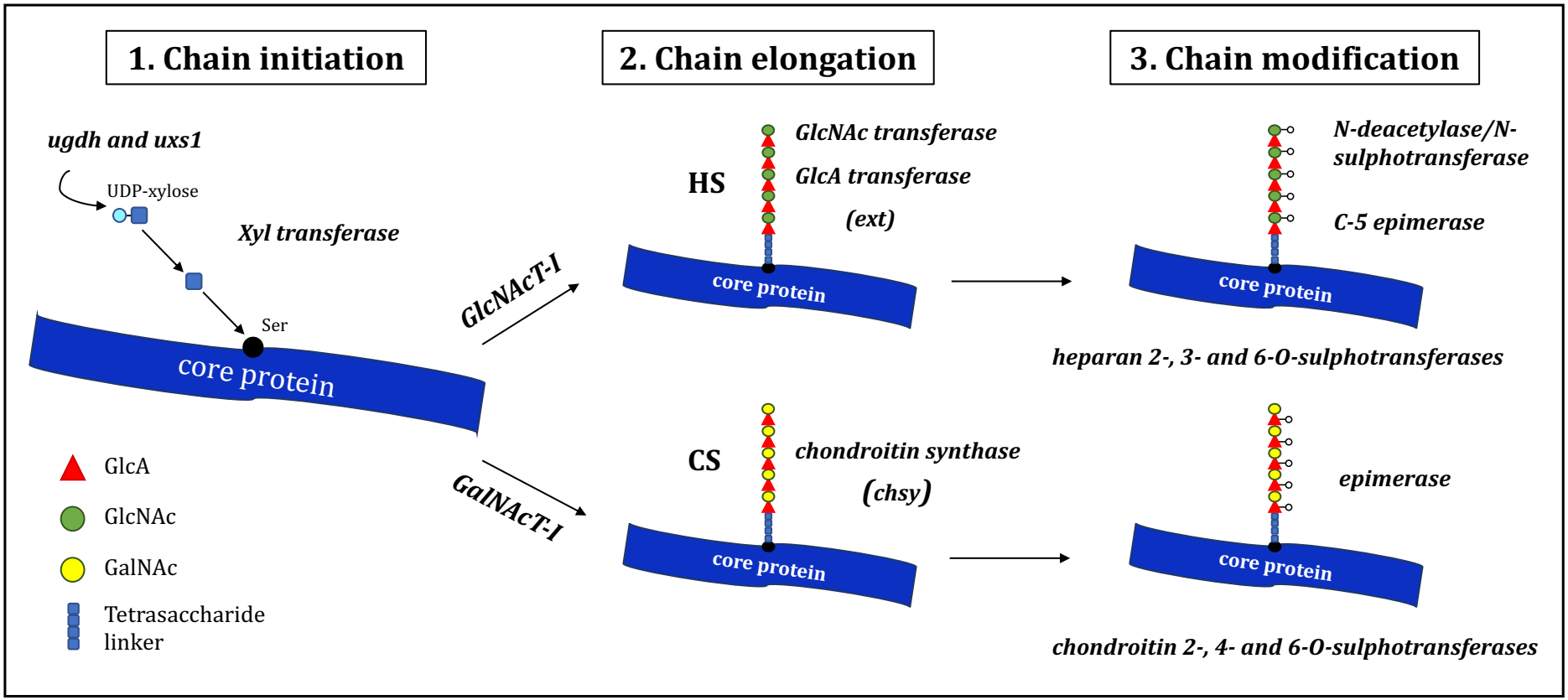

Figure 1.1 Biosynthesis of Chondroitin and Heparan Sulphate Proteoglycans in vertebrates. The first step for the synthesis of both CS and HS is the production of UDP-xylose from UDP-glucose by two enzymes, UDP-glucose dehydrogenase (ugdh) and UDP-glucuronate decarboxylase 1 (uxs1). Xyl transferase transfers xylose from UDP-xylose to serine residues on the core protein. Subsequently, Gal and GlcA transferases add three residues to the xylose, thus forming the tetrasaccharide linker: GlcA-Gal-Gal-Xyl. The next enzyme to act, GlcNAc transferase-I or GalNAc transferase-I, directs the synthesis towards HS or CS. Note that chondroitin synthase possesses both GlcA and GalNAc transferase features. Modification of the chain includes phosphorylation, epimerisation and *O*-sulphation (indicated by –o) in places that vary for each proteoglycan member.

In zebrafish, numerous genes that encode enzymes involved in CS and HS biosynthesis have been reported to be important for skeletal and craniofacial development, as well as the development of the fin, the heart and the retina. These include *udp-glucuronic acid decarboxylase 1* (*uxs1*), *udp-glucose dehydrogenase (ugdh/jekyll), exostosin 2* (*ext2/dackel*), *exostoses-like 3* (*extl3/boxer*), *chondroitin synthase 1* (*chsy1), and chondroitin sulphate N-Acetylgalactosaminyltransferases (csgalnact1 and 2)* (Neuhauss et al., 1996; van Eeden et al., 1996; Becker et al., 2002; Eames et al., 2010; Holmborn et al., 2012). In *ext2* zebrafish mutants in particular, high-performance liquid chromatography (HPLC) and immunostaining data have shown that HS chain levels are drastically reduced (89% reduction compared to wild-type siblings at 5 dpf) (Lee et al., 2004). As HS are essential for chondrocyte differentiation, homozygous mutant larvae have a defective pharyngeal cartilage and do not form functional pectoral fin buds (van Eeden et al., 1996; Clement et al., 2008).

Similarly, mutations in the same genes cause impaired skeletal or limb development in humans. For example, *CHSY1* mutations result in Syndromic Brachydactyly through increased NOTCH signalling (Tian et al., 2010). Inactivating mutations in the *EXT1* or/and *EXT2* genes (chromosome 8 and 11, respectively) lead to Human Hereditary Multiple Osteochondromas (MO/Multiple Hereditary Exostosis syndrome, MHE), an autosomal dominant inherited skeletal disorder, characterised by the formation of multiple benign cartilage-capped tumours within the context of the same bone (Jochmann et al., 2014). Depending on the dimensions and the location of the tumours, they may limit motion, cause extensive pain (Jochmann et al., 2014) and may even transform into malignant osteosarcomas (Schmale et al., 1994).

1.2.3 The versican molecule

Versican (also called dermacan, PG-M, br146 or CSPG2) was first isolated from the culture medium of fibroblasts in 1979 (Coster et al., 1979) and, unlike other hyalectans, which are specifically expressed in the cartilage (aggrecan) or the central nervous system (neurocan, brevican), it is a major ECM component of various soft tissues in all vertebrates with significant and diverse biological roles (reviewed in Nandadasa et al., 2014).

In general, versican expression is high in developing tissues and decreased in most mature tissues, with the exception of the brain (Du et al., 2013; Schmalfeldt et al., 1998). Versican is found in low amounts in healthy adult tissues, but sees increased expression during wound repair, inflammation and as a consequence of some diseases, including cancer (Keire et al., 2014).

The versican core protein consists of three distinct subdomains: an N-terminal G1 domain, a central chondroitin-sulphate (CS)-binding domain and a C-terminal G3 domain. The G1 domain includes the hyaluronan-binding repeats (HABR) and an immunoglobulin (Ig)-like site. The CS-binding domain harbours attachment sites for the GAG chains. The G3 domain consists of two epidermal growth factor (EGF)-like repeats, a complement regulatory protein (CRP)-like motif, also called complement control protein (CCP) or Sushi domain and a C-type-lectin-like (LC) motif, also known as carbohydrate-recognition domain (CRD) (Andersson-Sjoland et al., 2015; Figure 1.2A).

The G1 and G3 domains are highly conserved in vertebrates and play a vital role in proteoglycan function (Kang et al., 2004). There are two large exons encoding the core CS-binding domain, each of which gives rise to an αGAG or a βGAG region. Alternative splicing of these exons gives rise to four different versican isoforms: V0, V1, V2 and V3 (reviewed in Andersson-Sjoland et al., 2015; Figure 1.2A).

In the early 1990's, Iozzo and co-workers (1992) mapped the versican core protein gene (*VCAN*) to the long arm of human chromosome 5 (5q13-q14), and a few years later, Naso et al., (1995) were able to map the homologous murine *Vcan* gene to chromosome 13. The nucleotide sequence of the mouse *Vcan* gene was also shown to share 86% identity with the human *VCAN* gene (Naso et al., 1995). The mammalian *VCAN* gene includes 15 exons, spanning over 90 kbp of DNA (Wu et al., 2005). The middle region of the versican core protein is encoded by exons 7 and 8 that specify the GAG attachment regions (Wight, 2002).

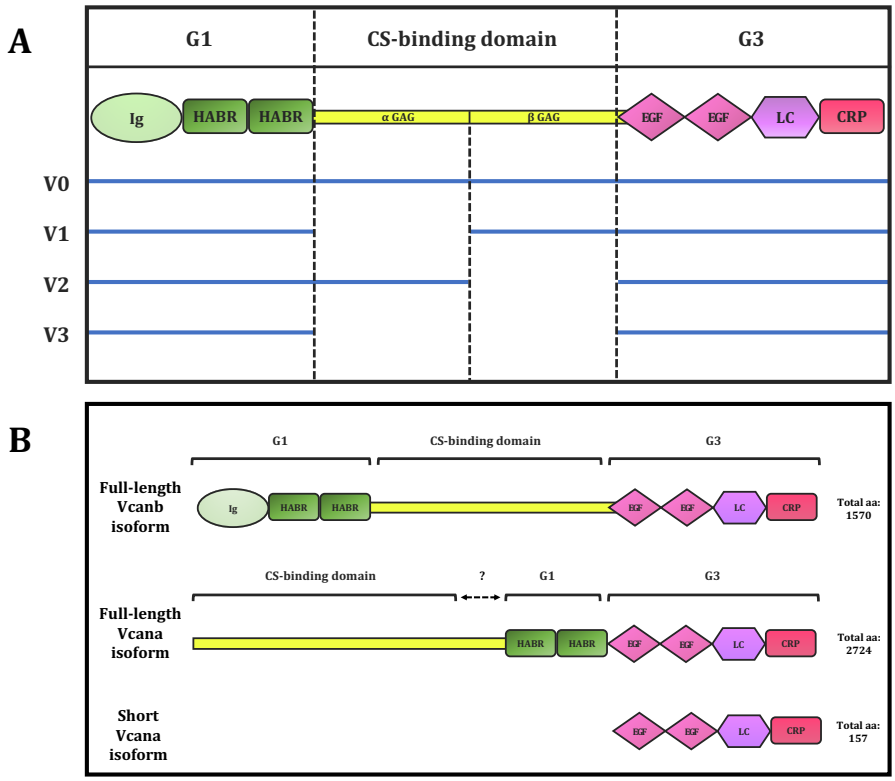

Figure 1.2 Schematic representation of the structure of versican and its isoforms in mammals and zebrafish. (A) Mammalian versican protein structure. G1 domain is the N-terminal domain and contains an immunoglobulin-like site (Ig) and hyaluronan-binding repeats (HABR). G2 is at the C-terminal end of the protein and contains two EGF repeats (EGF), a lectin-like motif (LC) and a CRP-like motif. The core protein consists of CS–binding sites, which attach GAG chains to a various extent depending on the splice variant (V0, V1, V2, V3). V0 is the largest versican isoform (370 kDa) and encompasses one αGAG and one βGAG region. V1 (263 kDa) contains only one βGAG region, V2 (180 kDa) contains one αGAG region, whereas V3 (74 kDa) contains no GAG regions at all. **(B)** Predicted zebrafish Vcanb and Vcana protein structures. Note that Vcana CS-binding domain is located at the N-terminal end, with the HABD immediately after it, before the G3 domain at the C-terminal end.

In the zebrafish genome, there are two *versican* core protein genes, *vcana* and *vcanb*, which are located on chromosome 5 and 10, respectively. The dominant theory is that the two genes in the zebrafish genome arose after duplication of a common ancestor *versican* gene (Kang et al., 2004). The *vcana* gene is 91 kbp long and consists of 49 exons (ZFIN). Alternative splicing leads to two known transcript variants, a full-length variant consisting of 49 exons and a short 3-exon fragment. Both transcripts are protein-coding; full-length Vcana protein is 290 KDa, consisting of 2724 amino acids, whereas the short isoform is just 157 aa long and it only consists of a G3 domain (Figure 1.2B). *Vcanb* gene was first identified by Kang et al., (2004) as a distinct gene from *versican*, and it was named *dermacan,* due to its participation in dermal bone formation. It is about 74 kbp in length, consisting of 15 exons. There are two predicted *vcanb* splice variants, both encoding the same 170 kDa-protein sequence, consisting of 1570 aa (http://www.uniprot.org; Figure

1.2B).

The amino-acid sequence of the G3 domain is highly conserved (70% identity) among human VCAN and zebrafish Vcana and b proteins. While the human G1 domain presents very high similarity to the Vcanb G1 (55% identity, both Ig-like and HABR domains are conserved), it shows significantly lower similarity to the Vcana G1, where only a part of HABD is conserved. Interestingly, Vcana protein structure shows a significant difference to both Vcanb and human isoforms; the CS-binding domain is located at the N-terminal end, with the HABD immediately after it before the G3 domain at the C-terminal end. The CS-binding domains are generally not conserved between the two species, apart from a small fraction of βGAG, which is conserved between the human VCAN and zebrafish Vcanb proteins. Consequently, zebrafish Vcanb protein is very similar to the human V0 and V1 isoforms (65% similarity), while Vcana is generally less similar to human isoforms (highest similarity is 17% with V2) (NCBI BLASTProtein, Henikoff and Henikoff, 1992).

1.2.4 Regulation of versican expression

VCAN expression is regulated by several levels of control in different tissues. At the transcription level, *VCAN* expression can be regulated either positively or negatively by three main regulatory elements located upstream of the *VCAN* gene: a promoter, an enhancer and a negative element. The human *VCAN* promoter harbours a typical TATA box, attachment sites for many transcription factors and a cAMP-responsive element (CRE) (Naso et al., 1994; reviewed in Wu et al., 2005). The vast majority of studies delineating the proteins that can interact with *VCAN* promoter come from human cell culture models. Transforming growth factor (TGF)-β1 can up-regulate *VCAN* gene through Smad phosphorylation in many cell types, such as lung fibroblasts and prostate cancer cells (Wight, 2002; reviewed in Andersson-Sjoland et al., 2015). Interestingly, TGF-β2 and TGF-β3 preferentially increase the expression of the V0 and V1 isoforms (Berdiaki et al., 2008). Another pathway that activates *VCAN* transcription in humans is the Wnt pathway, where the β-catenin-TCF/LEF (Transcription/Lymphoid enhancer-binding factors) complex interacts directly with the *VCAN* promoter (Rahmani et al., 2005). In some cancer cell lines, *VCAN* mRNA expression has been shown to be increased by p53, steroid hormones and gonadotrophins (Yoon et al., 2002; Ricciardelli et al., 2009). In melanoma cell lines in particular, *VCAN* transcription has been shown to be activated through ERK/MAPK and JNK signalling pathways acting on the AP-1 site of the promoter (Domenzain-Reyna et al., 2009). In addition, altered methylation of the *VCAN* gene in either neoplastic or stromal cells has been reported to affect transcription levels and may also be related to predisposition to tumourigenesis in cases such as colon cancer (Adany et al., 1990).

At the post-transcriptional level, *VCAN* expression can also be regulated by microRNAs (miRNAs); small, single-stranded RNA molecules, which bind sequence-specifically to complementary mRNA, thereby repressing gene expression (Yang and Yee, 2014). In addition, tyrosine kinase activity stimulated by mitogens, such as the platelet-derived growth factor (PDGF), upregulates versican core protein and CS synthesis (Syrokou et al., 1999).

At the protein level, matrix metalloproteinases (MMPs) and a disintegrin and metalloproteinase with thrombospondin motifs (ADAMTS) can cleave versican to bioactive forms that contain different fragments of G1 and/or G3 domains, thus temporally and spatially restricting versican function (reviewed in Andersson-Sjoland et al., 2015 and Nandadasa et al., 2014). Moreover, the versican GAG chains can undergo

several modifications that affect cell behaviour, the most common being the sulphation of the GAGs, which is essential for chemokine and selectin binding to versican (Hitchcock et al., 2006).

It is clear that the complexity of the versican regulatory system is crucial for sustaining normal functioning in various tissues, as failure in the regulation of either expression levels or the isoform balance can lead to developmental abnormalities or specific diseases.

1.2.5 The roles of versican

Deriving its name from the versatility of its activity, the complex protein structure of versican is responsible for the multiple biological roles it carries out. Due to the strong negative charge of GAG chains, as well as the variety of binding sites versican incorporates, it can bind many other matrix molecules (hyaluronan, tenascins, fibulin, fibrillin and fibronectin), cell surface proteins (selectins, chemokines, CD44, integrin, EGFR, and P-selectin glycoprotein ligand-1 (PSGL-1)) and low-density lipoproteins (LDL) (reviewed in Wu et al., 2005). These interactions allow versican to be involved in diverse cellular processes, such as cell proliferation, adhesion, migration and apoptosis. In most cases, versican expression is reduced soon after the development of a tissue. Overexpression of versican in mature tissues has been associated with a number of diseases, such as cancer and lung disorders (Chronic obstructive pulmonary disorder-COPD, asthma) (Hallgren et al., 2010; reviewed in Andersson-Sjoland et al., 2015). Similarly, failure in the regulation of the isoform balance ratio (V0+V1):(V2+V3) results in vitreo-retinopathies, such as Wagner Syndrome (Ronan et al., 2009).

Interestingly, different isoforms are expressed in different tissues and may have dissimilar, possibly contradictory, effects. Mammalian versican isoforms V1 and V0 are mainly expressed during embryonic development and are the predominant isoforms found in cancer tissues, contributing to cell proliferation and migration. In contrast, V2 and V3 are expressed in mature tissues and inhibit tumour growth (reviewed in Nandadasa et al., 2014). V2 is the predominant isoform of the adult brain and V3 is variably expressed in adult tissues of endothelial origin (Table 1.1).

The role of versican in cancer progression and cancer-related inflammation (CRI) is discussed in more detail in section 1.4.3. In the section that follows, the role of versican during embryonic development is reviewed.

1.2.5.i Versican in Development

Versican is expressed from many cell types in a large number of vertebrate developing tissues, having a central role in the development of the craniofacial dermal bones, the lungs and limbs, while it is also involved in neural crest cell migration (Kang et al., 2004; Kim et al., 2014).

In 1993, cDNA analysis of a chick gene known to be expressed in the limbs and to encode the core protein of the CSPG PG-M, revealed that it is the chick homologue of the human *VCAN* gene. The same team reported that versican in limbs is implicated in tissue differentiation and chondrogenesis, by regulating cell adhesion both positively, through the C-terminus of the core protein, and negatively, through its GAG chains (Shinomura et al., 1993). Later, versican V0 and V1 isoforms were reported to also have a guidance role during neural crest migration in chick and mouse embryos (Dutt et al., 2006). In murine models, *Vcan* is also highly expressed in the developing lungs around day E13.5 and then it substantially declines through to adulthood (Snyder et al., 2015). As high levels of expression are found mainly in the pulmonary interstitium, versican is believed to play a role on scaffolding for tissue development and migration (Snyder et al., 2015).

Versican plays a central role in the vertebrate heart valve development (Schroeder et al., 2003; Kim el al., 2014), as it is a major component of the cardiac jelly, which is the ECM that separates myocardium from endocardium. During valve formation, a group of endocardial cells from the atrioventricular (AVC) region differentiates and migrates into the cardiac jelly, where it forms the endocardial cushions, the precursors of the heart valve leaflets (Henderson and Copp, 1998). Kim et al. (2014) recently reported that suppression of *versican a* in the AVC region of 48 hpf zebrafish embryos by another gene, *crip2*, is essential for normal heart valve formation. In another zebrafish study, morpholinos targeting *versican b* mRNA caused high levels of lethality (about 80 %) in the first 7 days post fertilisation. The surviving larvae exhibited serious craniofacial malformations, including a smaller head, malformed jaws, and absent dermal bones, suggesting that Versican is important in the morphogenesis of these facial structures (Kang et al., 2004). *Versican* genes are also highly expressed in the developing zebrafish inner ear, but their role in this context is yet to be elucidated (Geng et al., 2013).

Table 1.1 Summary of the main effects of mammalian versican isoforms. V0 is synthesised by prechondrogenic mesenchymal cells, smooth muscle cells, fibroblasts and other non-neural cell lines. V1 is produced by endothelial and various fetal cells, and both isoforms contribute to cancer cell proliferation, migration and metastasis. Versican V2 is almost exclusively expressed in the mature central nervous system (CNS), where it induces cell apoptosis and angiogenesis, while it inhibits tumour growth. V3 is expressed in various adult tissues of endothelial origin activated by cytokines/growth factors and inhibits tumour growth as well. There is controversy about its effect on cell migration (see chapter 1.4.2). Question marks are used to show that there is no bibliography to date to support any specific effect, or that the results have been inconclusive.

Versican isoform	Cell type	Inflammation	Tumour growth	Invasion and metastasis	Apoptosis	References
V0	prechondrogenic mesenchymal, smooth muscle cells, fibroblasts, cancer tissues	↑	↑	↑	**?**	Arslan et al., 2007; Wight et al., 2014 ; Potter-Perigo et al., 2010
V1	embryonic, endothelial, smooth muscle cells, fibroblasts, cancer tissues	↑	↑	↑	↓	Onken et al., 2014; Sheng et al., 2006; Li et al., 2013 ; Potter-Perigo et al., 2010
V2	mature CNS	**?**	↓	**?**	↑ in CNS ↓ in glioblastoma	Schmalfeldt et al., 1998; Yang and Yee, 2013
V3	mature primary endothelial cells	↓	↓	↑	**?**	Serra et al., 2005; Miquel-Serra et al., 2006; Kang et al., 2014; Fanhchaksai et al., 2016

1.3 AUDITORY AND VESTIBULAR SYSTEM

Auditory and vestibular systems have co-evolved in close proximity and they cooperate to provide important mechanosensory input from the environment, which is advantageous not only towards predation for many species, but also towards the development of cognition and language in humans. Although the vestibular system is conserved among vertebrates, the auditory system has evolved to serve the different needs of aquatic or terrestrial lifestyles and shows variability across phyla (Fritzsch et al., 1998; Chapter 3; Riley, 2000).

The sensory receptors for both auditory and vestibular systems are hair cells (Schwander et al. 2010). Although hair-cell-like cells have been traced back to lower chordata, the first organised assembly of hair cells forming a primitive inner ear and lateral line evolved in aquatic craniates, around 540 million years ago (Burighel et al., 2011; Fritzsch et al., 2007). The timing of the evolution of hearing is controversial, but it is generally accepted that audition helped aquatic tetrapods to adapt more efficiently to the new challenges of the terrestrial environment (Popper and Fay, 1973; Hester, 2005). Recent studies in salamander show that even if these early tetrapods only possessed an inner ear compartment, without outer or middle ears, they were capable of detecting airborne sound to some extent (Christensen et al., 2015). The middle ear was evolved later in amphibians and facilitated the conversion of aerial sound pressure to particle motion in the inner ear (Hetherington, 1987).

1. .3.1 Overview of the vertebrate inner ear

The vertebrate inner ear comprises two to three fluid-filled semicircular canals (SCCs) and one or more sensory patches, the maculae (Fritzsch et al., 2007). In the fish inner ear, mineralised deposits named otoliths are tethered, one to each macula, whereas in mammals, otoliths are replaced by collections of smaller crystals (otoconia). Inertial relative movement between otoconia/otoliths and the hair cells of the macula in response to gravity, sound or linear acceleration, activates the hair cells, which transmit the signal to the brain. Similarly, the SCCs detect angular acceleration through a swelling at the end of each canal, which contains a sensory epithelium, the crista.

In the inner ear of some agnatha (hagfish), there is only one common macula and a single canal with two cristae. In jawed fish, a third horizontal (lateral) canal is added and there are three maculae; the utricle, the saccule and the lagena (Fritzsch et al., 2007). The

mammalian inner ear has also got three SSCs, but differs from the one found in fish in that it only has two maculae and a cochlea (Figure 1.3).

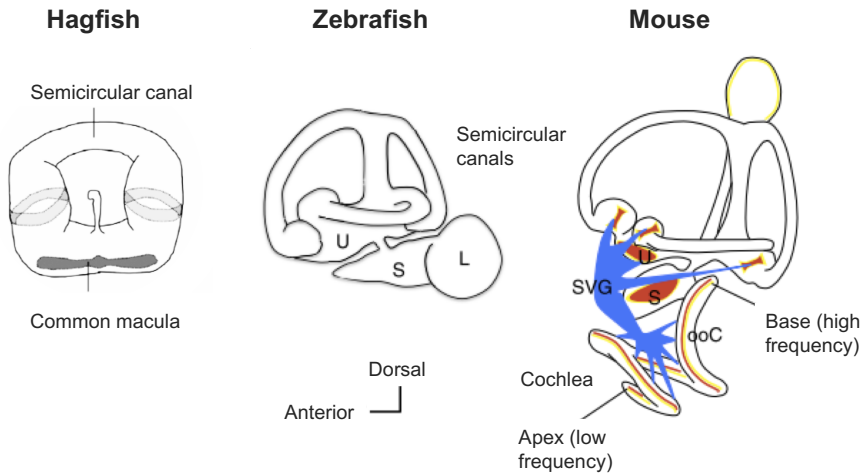

Figure 1.3 The vertebrate inner ear evolution. The inner ear of the three depicted vertebrate species differ in the number of semicircular canals (hagfish has one, zebrafish and mouse have three), number of vestibular organs (hagfish has one [common macula], zebrafish has three [utricle, U; saccule, S; lagena, L] and mouse has two [utricle, U; saccule, S]). Major morphological evolutionary changes are the addition of a horizontal canal in gnathostomata and the transformation of the utricle into several recesses containing the saccule, lagena and cochlea. Sensory (red), neuronal (blue) and endolymph-regulating (yellow) cells are shown for the mouse ear. Abbreviations: L, lagena; ooC, organ of Corti; S, saccule; SVG, spiral and vestibular ganglion; U, utricle. Modified after Whitfield (2005).

1.3.2 The zebrafish inner ear and lateral line function

The vestibular organs in zebrafish are the inner ear and the lateral line (reviewed in Ghysen and Dambly-Chaudiere, 2004). The lateral line is a sensory system on the surface of the head and body, made up of hair cell clusters, called neuromasts, which can detect movement and pressure gradients in the water and pass the information to the spinal cord through afferent nerve fibres. Neuromasts on the head are part of the Anterior Lateral Line (ALL), the nerves of which cluster in a ganglion (ALLg) located between the eye and the ear. Neuromasts on the trunk and tail are part of the Posterior Lateral Line (PLL), the ganglion of which is posterior to the ear (PLLg). Neurons of the lateral line are supported and ensheathed by Schwann cells, glial cells that are in intimate contact with axons and generate the insulating myelin sheath (Monk et al., 2015).

The zebrafish inner ear has been shown to have both vestibular and auditory roles. Like other jawed fish, it contains three orthogonally placed, fluid-filled SCCs and one otolith resting on each of the three maculae (utricle, saccule and lagena). Among these, the utricle and the SCCs have been shown to have important vestibular functions; the saccule is

presumed to exert primarily auditory roles, while the lagena has been attributed with both vestibular and auditory functions (Riley and Moorman, 2000; Lu and DeSmidt, 2013; reviewed in Abbas and Whitfield, 2010). Although the function and morphology of SCCs is conserved between zebrafish and mammals, the developmental process that leads to their formation is different (Figure 1.4) (Bok et al., 2007; Baxendale and Whitfield, 2014).

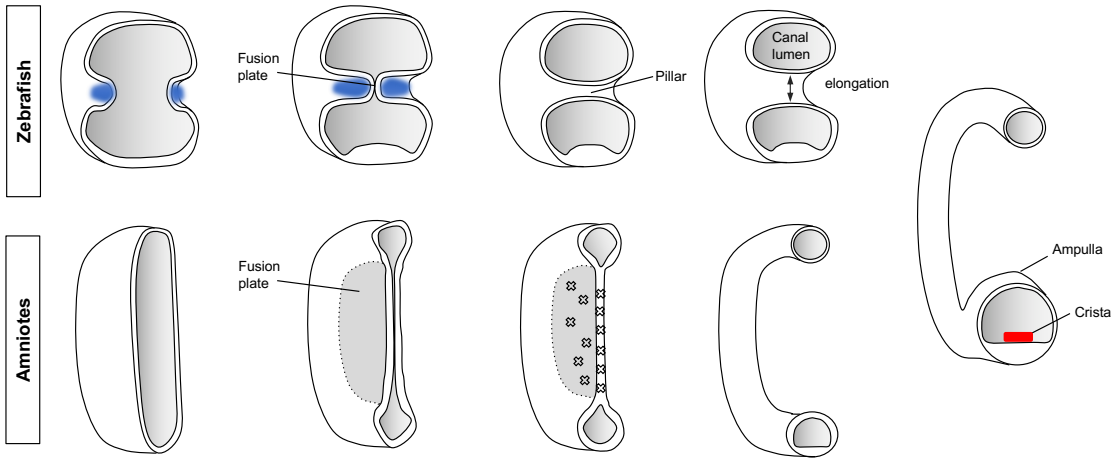

Figure 1. 4 Schematic comparison of semicircular canal formation in the zebrafish ear and the amniote ear. In zebrafish (top row), the otic vesicle forms finger-like epithelial projections, which adhere and fuse with each other to create a fusion plate, which resolves into a pillar of epithelium. In amniotes (bottom row), flattened canal pouches are generated as outpocketings from the otic vesicle, and their apical sides touch and fuse to generate a much bigger fusion plate, which also resolves into a pillar (reviewed by Bok et al., 2007). Both processes lead to the same result; the epithelial pillar enlarges, giving rise to a semicircular canal duct (right hand side picture). Note that the development of only one semicircular canal is shown. Modified after Whitfield (2015).

1.3.3 Semicircular canal development in zebrafish

In the zebrafish embryo, each ear develops rapidly from an ectodermal thickening, the otic placode, which appears 16 hours post fertilisation (hpf). During the first day of zebrafish development (24 hpf), the otic placode forms a ball of epithelium, the otic vesicle (Figure 1.5A), which contains the developing saccular and utricular otoliths. At around 42 hpf, finger-like epithelial projections begin to protrude into the otic vesicle (Figure 1.5B), and gradually elongate until they fuse at their tips to create three pillars of epithelial tissue, each making up the hub of a SCC duct (Figure 1.5C-D).

The first comprehensive study describing the morphogenetic process by which epithelial projections fuse and perforate to give rise to semicircular canals in the zebrafish embryo was made by Waterman and Bell (1984). Electron and light micrographs showed that the cells of the projections first reorganise in a way that allows contact, before they start

fusing around 55 hpf (Waterman and Bell, 1984). The site where the epithelial projections meet and adhere with each other is called the fusion plate, the perforation of which gives rise to a pillar of epithelium that spans the ear lumen (Figure 1.4; Waterman and Bell, 1984; Baxendale and Whitfield, 2014). This pillar gradually elongates and gives rise to the adult SCC ducts. Each SCC duct ends in a chamber called the ampulla, which contains the associated sensory crista (Figure 1.4).

The underlying mechanism by which the cells of the epithelial projections recognise each other, adhere and fuse is not yet fully elucidated. It has been shown that various ECM components are highly up-regulated during projection growth and repressed immediately after fusion (Geng et al., 2013), but their role is not completely understood. Chapters 3 and 4 aim to elucidate the involvement of the ECM in this morphogenetic process.

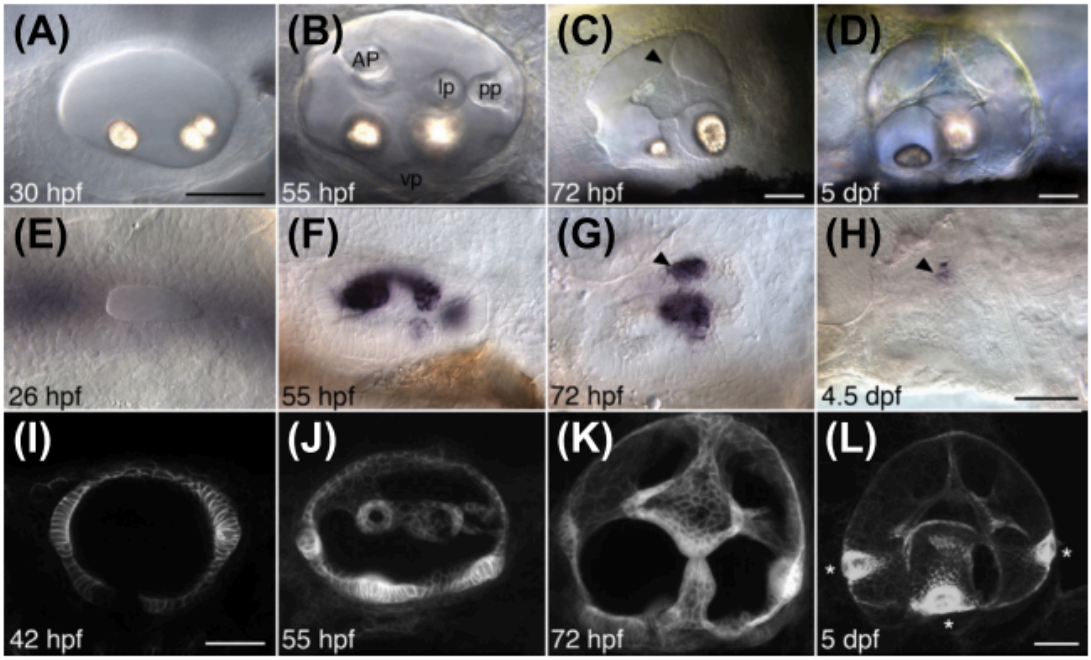

Figure 1.5 Development of the semicircular canal system in the zebrafish embryo. Development of the semicircular canal ducts between 1 dpf and 5 dpf shown with a live view **(A–D)**, *versican* expression by *in situ* hybridisation **(E–H)**, and a transgenic line expressing GFP in the cell membranes of the otic vesicle **(I–L).** Epithelial projections that extend and fuse to form the three pillars, around which the semicircular canals form, are not present before 42 hpf **(I)**, and *versican* expression in the otic vesicle is not seen at this early stage **(E)**. At 55 hpf, the anterior pillar (AP) is formed and the posterior (pp) and ventral (vp) projections are growing to meet the central lateral projection (lp). By 3 dpf all three pillars have fused **(C, K)**. *Versican* expression is still present at the fusion plate of the ventral pillar and also in the dorsolateral septum (DLS, arrowhead) but is down-regulated in the anterior and posterior pillars. At 5 dpf fusion is complete **(D, L)** and *versican* expression is down-regulated, remaining only in the DLS (**H**, arrowhead). Cristae (asterisks) are shown in L. All images are lateral views, with anterior to the left. Scale bars, 50μm: B, E,F, G as in A; J, K as in I. Reproduced with permission from Baxendale and Whitfield (2014).

1.3.4 Involvement of the ECM in the formation of the inner ear

The ECM plays an important role in the cell migration and adhesion changes that take place during the morphogenesis of the inner ear from a very early stage. Enzymatic degradation of hyaluronan, chondroitin sulphates, or heparan sulphates of the otic region inhibited folding of the otic placode in the chick embryo, suggesting a role for these ECM components in otic vesicle formation (Gerchman et al., 1995; Moro-Balbás et al., 2000).

Waterman and Bell (1984) were the first to observe the ECM accumulation in the core of the epithelial projections in the developing zebrafish inner ear using electron microscopy. Haddon and Lewis (1991) showed that the main constituent of the epithelial projection core is HA. Hyaluronidase injections into the developing epithelial projections in the zebrafish and *Xenopus* inner ear resulted in the collapse of these projections, showing that HA is essential for the propulsion of the projections into the otic lumen before they fuse to form the SCC hubs (Haddon and Lewis, 1991; Geng et al., 2013). Alternative approaches that block HA production using zebrafish *jekyll* (*ugdh*) mutants and *dfna5* (deafness-associated tumour suppressor 5) morphants, lead to a similar ear phenotype, confirming that HA (and possibly CS and/or HS) is important for the outgrowth of the epithelial projections (Neuhauss et al., 1996; Busch-Nentwich et al., 2004). Contrary to HA, CS have been reported to localise primarily at the periphery of the elongating epithelial projections in *Xenopus,* creating a sheath (Haddon and Lewis, 1991), but the role of this CS covering is not yet elucidated. A more recent zebrafish study revealed that the core protein genes of the CSPG Versican (*vcana* and *vcanb*) are strikingly overexpressed in the outgrowing epithelial projections before fusion and get down-regulated immediately after the fusion of the projections is complete (Geng et al., 2013; Baxendale and Whitfield, 2014). The role of Versican in the zebrafish inner ear has not yet been reported and it is the subject of Chapter 3.

A similar expression pattern with *versican* is followed by other ECM molecules or ECM producing enzymes, including hapln1 (Hyaluronan and Proteoglycan link Protein 1), collagen II, chondroitin synthase 1 (chsy1) and has3 (Hyaluronic Acid Synthase 3) (Geng et al., 2013). Contrary to the wild-type developing ear, *adgrg6* (formerly *gpr126*) mutants fail to down-regulate the expression of the ECM genes mentioned above; the projections overgrow and do not fuse, resulting in no pillar formation (Geng et al., 2013). This finding suggests that Adgrg6 is essential for the recognition, adhesion and fusion of canal projections, through regulation of the ECM gene expression program.

1.3.5 Adgrg6 (Gpr126)

G-protein-coupled receptors (GPCRs) constitute one of the biggest receptor families in the human genome (reviewed in Bjarnadóttir et al., 2006). GPCRs are transmembrane receptors that function by binding various extracellular ligands to convey their signal into the cell through G-protein activation (Bockaert et al., 1999). GPCRs exert numerous important roles in the progression of development and disease and they are one of the most popular drug targets worldwide (Drews, 2000; Bjarnadóttir et al., 2006).

Adgrg6 (formerly Gpr126) is one of the 33 members of the adhesion G-protein coupled receptor family (aGPCR), with essential roles in neural, cardiac and ear development (reviewed in Patra et al., 2014). Like all aGPCR members, Adgrg6 consists of a long extracellular (ECD) domain and a seven-transmembrane helix (7TM) domain, separated by an autoproteolysis-inducing domain (GAIN), which incorporates a highly-conserved GPCR proteolytic site (GPS) (Fredriksson et al., 2003; Stehlik et al., 2004; Langenhan et al., 2013; Figure 1.6). The GAIN domain is linked to the 7TM motif via a 20-amino-acid sequence hidden between β-sheets, the *Stachel* sequence (Liebscher et al., 2014). Autoproteolysis at the GPS results in two fragments, the NTF (N-terminal fragment) and CTF (C-terminal fragment), which then remain together on the cell surface, noncovalently bound (Patra et al., 2014; Figure 1.6). Upon ligand binding, the NTF dissociates from the CTF, thus exposing the *Stachel* peptide （Liebscher et al., 2014; Mehta et al., 2017). Unmasking of the *Stachel* sequence enables it to act as a tethered agonist, thereby stimulating CTF activity (Liebscher et al., 2014). Cleaved NTF can interact with ECM components, such as Collagen and Laminin or with surface receptors of neighbouring cells, while the activated CTF transduces the signal in the cell via G-protein activation (Mogha et al., 2013). G-proteins then recruit second messengers such as small GTPases and kinases, that ultimately lead to changes in gene expression (Langenhan et al., 2013). These features provide Adgrg6 with a variety of CTF-dependent or independent signalling capabilities, that orchestrate cell adhesion and cell-cell or cell-matrix interactions.

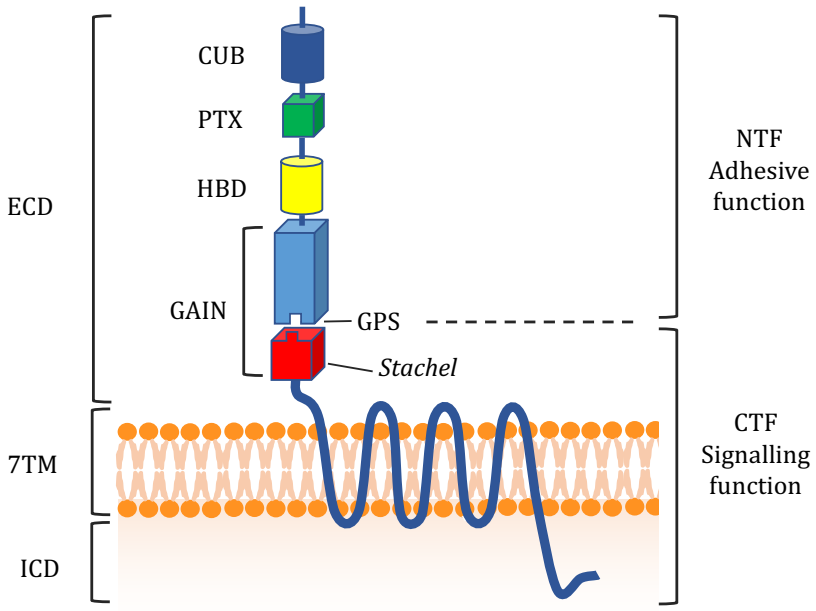

Figure 1. 6 Schematic representation of Adgrg6 protein structure. The extracellular domain (ECD) of Adgrg6 incorporates a Complement C1r/C1s, Uegf, BMP1 domain (CUB, dark blue cylinder), a Pentraxin domain (PTX, green cube), a hormone binding domain (HBD, yellow cylinder) and a GPCR auto-proteolysis domain (GAIN, light blue/red cube), which includes the GPCR proteolytic site (GPS) and the *Stachel* sequence (red part of the GAIN domain). The carboxy-terminal fragment (CTF) includes the 7-transmembrane domain (7TM) and the intracellular domain (ICD). Proteolysis at the GPS domain triggers the binding of the *Stachel* sequence to the 7TM domain, thereby activating the CTF.

Zebrafish *adgrg6* (*lauscher*) mutants, exhibit a severe ear phenotype, where the epithelial projections that form the semicircular canal ducts fail to fuse as per normal, overgrow and the ear shows concomitant morphological defects (Geng et al., 2013). Gene expression analysis of the *adgrg6* mutant ear showed a constant and uncontrolled *versican* overexpression, which abnormally persists at late larval stages, thus suggesting a role for Adgrg6 in *versican* regulation. This finding in combination with the fact that Versican possesses known binding sites for other ECM components also found abnormally up-regulated (HA, hapln), suggests that Versican may be one of the main mediators that orchestrates the cellular changes underlying fusion and pillar formation. Although the *adgrg6* mutant ear phenotype was ameliorated by treatment with cyclic AMP (cAMP) agonists (Geng et al., 2013), the mechanism of Adgrg6 signalling in the inner ear is largely uncharacterised (discussed in Chapter 5).

In contrast, the role of Adgrg6 in peripheral nerve development and myelination has been extensively studied in the last decade (Monk et al., 2009; Monk et al., 2011; Glenn and Talbot, 2013; Mogha et al., 2013; Petersen et al., 2015; Monk et al., 2015; Mogha et al.,

2016). In humans, mutations in *ADGRG6* cause congenital contracture syndrome 9, which is a severe type of arthrogryposis multiplex congenita, and peripheral nerves from affected individuals show significantly reduced expression of Myelin Basic Protein (MBP) (Ravenscroft et al., 2015). In *adgrg6* zebrafish and mouse mutants, peripheral myelination is also severely impaired, suggesting that the function of Adgrg6 in myelination is evolutionarily conserved in vertebrates (Waller-Evans et al., 2010; Monk et al., 2011). In zebrafish *adgrg6* mutants, Schwann cells (SCs) associate with axons, but never spiral their membrane to generate a myelin sheath and show down-regulation or loss of the *mbp* gene (Monk et al., 2009; Geng et al., 2013; Glenn et al., 2013).

The myelination defects present in *adgrg6* zebrafish and mouse mutants have been shown to be ameliorated after chemically induced cAMP elevation, suggesting Adgrg6 signals through Gs-proteins (Monk et al., 2009; Mogha et al., 2013). Additional zebrafish data show that *Stachel* unmasking is essential for Schwann cell myelination, as it causes the 7TM domain to undergo important conformational changes which activate $G\alpha_s$-protein signalling (Liebscher et al., 2014). $G\alpha_s$-protein activation triggers a signalling cascade which involves activation of the cAMP-response element binding protein (CREB) pathway and ultimately of transcription factors that induce the expression of myelination genes, including *mbp* (reviewed in Monk et al., 2015; Figure 1.7). *Stachel* availability has been shown to be further modulated in Schwann cells by the interaction of NTF with laminin-211 (Petersen et al., 2015). Nevertheless, the *in vivo* mechanism whereby a ligand contributes to the exposure of *Stachel* is not clear; it is presumed this is either due to the physical removal of the NTF or due to conformational changes in the NTF caused by the ligand (Liebscher et al., 2014). The chemical nature of these agonistic ligands is also not elucidated.

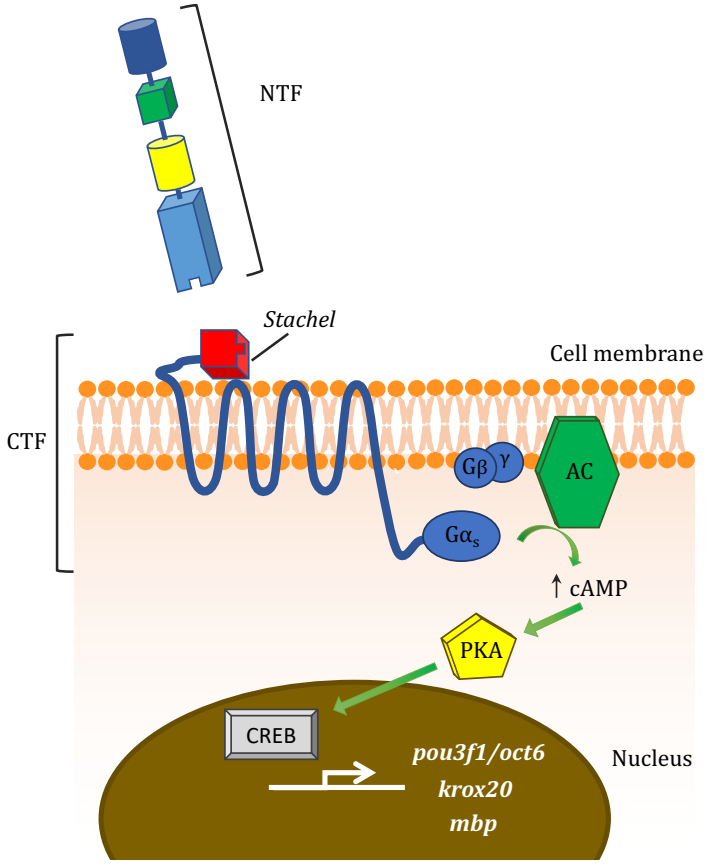

Figure 1.7 Adgrg6 signalling in a myelinating Schwann Cell. Unmasking of the *Stachel* sequence triggers conformational changes to the CTF, which activate $G\alpha_s$-protein signalling. $G\alpha_s$-protein activation triggers adenylate cyclase (AC) to generate cAMP, which in turn phospholylates Protein Kinase A (PKA) and activates the cAMP-response element binding protein (CREB) pathway. Ultimately, major transcription factors Oct-6 (Pou3f1) and Krox-20 (Egr2) are activated to induce the expression of genes involved in myelination, including *mbp*.

Other members of the adhesion aGPCR receptor family include GPR98 (also known as VLGR1), GPR112, and members of the brain-specific angiogenesis inhibitor (BAI), cadherin EGF LAG seven-pass G-type receptors (CELSR1–3) and latrophilin (LPHN1–3) subfamilies, all of which are often mutated in multiple human cancers (reviewed in O'Hayre et al., 2013). As the ligands for most aGPCRs are still not known, it is evident that the importance of identifying ligands for these receptors is substantial (Mehta et al., 2017).

1.4 CANCER

Cancer derives from the sequential acquisition of mutations, resulting in the conversion of proto-oncogenes to oncogenes, the malfunction of tumour-suppressor genes and may also involve epigenetic changes, as well as changes in the extracellular matrix (Jones and Baylin, 2002; Nelson and Bissel, 2006). Cancer is a group of more than a hundred diseases, characterised by uncontrolled growth of abnormal cells in the body, which have the ability to invade and metastasise to other body parts.

Hanahan and Weinberg (2000, 2011) delineated eight acquired capabilities of cancer cells: insensitivity to anti-growth signals, self-sufficiency in growth signals, evasion of apoptosis, limitless replicative potential, sustained angiogenesis, tissue invasion and metastasis, reprogramming of energy metabolism and evading immune destruction. Due to the critical role of infiltrating immune cells in cancer progression, cancer-related inflammation (CRI) has been established as a hallmark of cancer, which not only affects proliferation, survival and migration of malignant cells, but also induces genetic instability (Colotta et al., 2009; Hanahan and Weinberg, 2011; Diakos et al., 2014).

Tissue invasion and metastasis is a highly sophisticated, multi-step process, responsible for approximately ninety per cent of cancer mortality. It initiates with cell detachment from the ECM, partial degradation of the basement membrane, migration through the stroma and intravasation into the circulatory system, which transports the cells to other body regions (reviewed in Ricciardelli et al., 2009; Lambert et al., 2016). These phenotypic changes are induced by many alterations in gene expression and functions, the most outstanding of which is the switch from an epithelial to a mesenchymal gene expression program, a process termed epithelial–mesenchymal transition (EMT) (Yeung and Yang, 2017; Singh et al., 2018). After dissemination of cancer cells via blood or lymphatic circulation, they may extravasate, proliferate and give rise to a secondary tumour. Depending on the cancer type, tumour cells may follow different patterns of invasion; during single cell invasion, individual cancer cells disperse in a neighbouring tissue in a disorganised manner, while when collective cell migration occurs, the tumour mass invades as a whole, maintaining cell-cell adhesions and displacing the healthy adjacent tissue (Yilmaz et al., 2007; Clark and Vignjevic, 2015).

Although cancer cell properties have been studied extensively during the past four decades, the role of the microenvironment in which tumour cells subsist has only started being examined during the last decade. As existing therapies that directly target neoplastic

cells have not been greatly successful in withholding metastasis and improving survival rates, the tumour cell-centric view of cancer is starting to change and the tumour microenvironment is gaining increasing attention as a potential therapeutic target to modify cancer cell behaviour (reviewed in Pietras and Östman, 2010; Smyth et al., 2016; Ding et al., 2018).

1.4.1 The tumour microenvironment

The tumour microenvironment is composed of numerous non-cancerous cells, including fibroblasts, endothelial cells and cells of the immune system, together with the acellular ECM (reviewed in Balkwill and Hagemann, 2012; summarised in Figure 1.8).

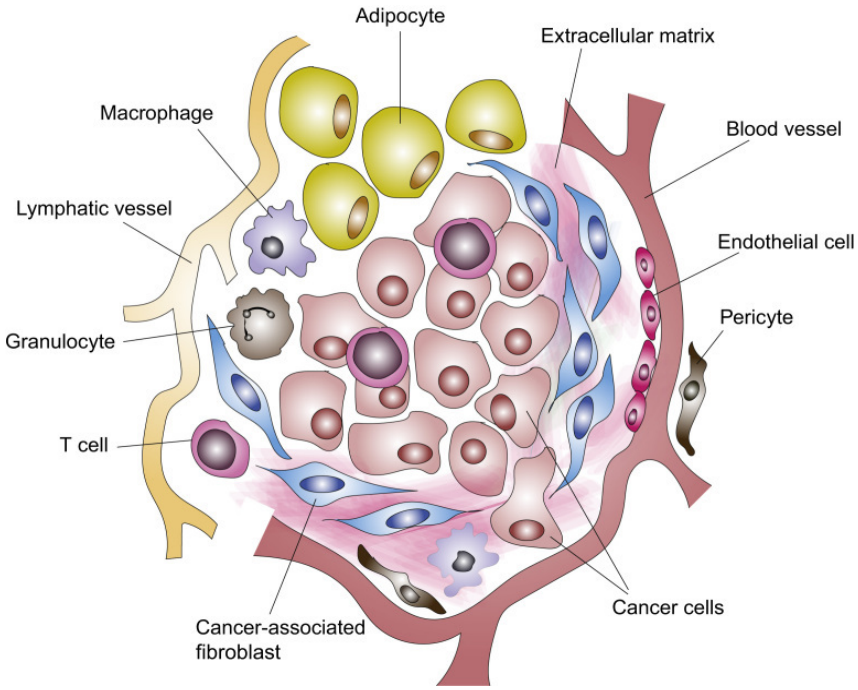

Figure 1.8 The tumour microenvironment. Schematic presenting the major components of the tumour microenvironment, including cancer cells (pink), cancer associated fibroblasts (blue), adipocytes (yellow), granulocytes (grey), pericytes (brown), macrophages (purple) and T-cells (dark pink). Reproduced with permission from Prajapati and Lambert (2016).

The immune cells of the tumour microenvironment include T and B lymphocytes, natural killer (NK) cells, and myeloid cells, such as tumour-associated macrophages (TAMs), neutrophils (TANs) and dendritic cells (DCs). The effect of these specialised cells can be either pro- or anti-tumourigenic and is attributable to the existence of different subpopulations with distinct localisation within the tumour site (reviewed in Joyce and Pollard, 2009).

The lymphatic and vascular endothelial cells of the tumour microenvironment can be stimulated by angiogenic factors, such as vascular endothelial growth factor (VEGF) and fibroblast growth factor (FGF), triggering new vessels to sprout from the existing vasculature. The newly formed microvessels, which are supported by specialised perivascular cells, called pericytes, supply cancer cells with oxygen and nutrients (reviewed in Armulik et al., 2011). In some cancer types, adipocytes present in the tumour microenvironment favour cancer cell migration through secretion of adipokines, and contribute to rapid malignant progression by nourishing tumour cells with fatty acids (Nieman et al., 2011).

The most abundant cellular constituents of the tumour microenvironment are commonly cancer-associated fibroblasts (CAFs). CAFs are differentiated, contractile fibroblasts of the tumour microenvironment, which are activated upon tissue injury and promote wound healing (Li and Wang, 2011). Upon differentiation, CAFs start expressing α-smooth muscle actin (α-SMA), a differentiation marker of smooth muscle cells (SMCs), which enhances cell contractility (Hinz et al., 2001). CAFs also produce various growth factors that aid proliferation, and TGF-β, which stimulates adjacent epithelial cells to acquire mesenchymal characteristics (EMT) and become migratory (Mamuya et al., 2012). In addition, CAFs are the major source of ECM components and ECM remodeling enzymes in the tumour microenvironment (reviewed in Attieh and Vignjevic, 2016). Due to the impact of CAFs on cancer cell invasion through their secretome and their effect on matrix modification, CAFs are becoming attractive therapeutic targets in various clinical and preclinical studies (reviewed in Chen and Song, 2018).

.

1.4.2 The ECM of the tumour microenvironment

The ECM of the tumour microenvironment plays a pivotal role in cancer progression, as it affects every stage of the metastatic cascade (reviewed in Walker et al., 2018). Not only does it aid migration, attachment, survival or proliferation of cancer cells, but may also act as a shield, protecting them from immune cells or drugs (reviewed in Venning et al., 2015).

During the early onset of metastasis, the primary tumour microenvironment is characterised by increased deposition of ECM molecules, such as HA and collagen, coupled with elastin. Changes in collagen deposition, degradation, crosslinking, as well as altered collagen fibre orientation around a primary tumour are important factors for migration initiation and intravasation into the blood stream (reviewed in Walker et al., 2018). *In vitro* and *in vivo* studies have shown that increased collagen I deposition along with enhanced collagen crosslinking catalysed by lysyl oxidases (LOX) increases ECM stiffness and prompts adjacent epithelia to acquire an invasive mesenchymal phenotype (Shintani et al., 2006; Xiao and Ge, 2012; Gilkes et al., 2013). As described, LOX-mediated collagen crosslinking activates integrin and Rho signalling pathways, which result in focal adhesion formation and induction of EMT (Levental et al., 2009). In addition, localised alignment of linear collagen fibres along the leading edge of a tumour has been associated with enhanced invasiveness, as it is thought to create a migrating path for cancer cells out of the tumour (Han et al., 2016; Walker et al., 2018). Similar to collagen, increased pericellular HA deposition and processing can also promote EMT, mainly through interaction with CD44. As shown previously, HA-mediated translocation of CD44 to the nucleus leads to the upregulation of LOX enzymes, which activate EMT transcription factors, such as TWIST-1 (El-haibi et al., 2012). In cases such as ovarian cancer and leiomyosarcoma, versican has been suggested to be essential for the aggregation of this pericellular HA sheath, not only because it stimulates HA synthesis, but also because it prevents it from degradation (Ween et al., 2011; Keire et al. 2014). Additional ECM remodelling by MMPs can also facilitate the onset of cancer cell invasion by degrading ECM physical barriers and by activating growth factors, such as TGF-β (reviewed in Kessenbrock et al., 2010).

Once the cancer cells enter the blood or lymphatic circulation, they are protected from immune surveillance by two mechanisms; the first is the recruitment and activation of platelets by the ECM proteins fibrinogen and tenascin-C. As shown previously, fibrinogen and its active form fibrin, can form complexes with activated platelets through integrin αIIbβ3 (Gay and Felding-Habermann, 2011). This physical linkage promotes the accumulation of platelets, which functions as a shield that protects cancer cells from

immune-cell attack (reviewed in Sharma et al., 2014). As tenascin-C has also been shown to efficiently bind and activate platelets *in vitro*, it could also contribute to the protection of cancer cells from immune cells (Schaff et al., 2011). Another mechanism described is HA aggregation acting as a physical barrier for lymphocytes, thereby increasing the chances of cancer cell survival in the circulation (McBride and Bard, 1979; Singha et al., 2015).

In order to extravasate from the circulatory system, cancer cells first need to attach and then break through the endothelial barrier. HA is one of the most important regulators of vascular integrity and endothelial cell-cell contact maintenance, coating the endothelial cells with a thick glycocalyx. Cancer cells have the ability to attach to the HA-rich glycocalyx through cell surface CD44, while the disintegration of the glycocalyx is catalysed by tumour-cell secreted hyaluronidases (reviewed in Singleton, 2014). Enzymatic degradation of HA to low molecular weight HA fragments (LMW-HA) triggers a cascade of events, which activates Rho-associated protein kinases, thus promoting actin fibre formation and the disruption of the endothelial barrier (Singleton, 2014).

After breaking free from the endothelial barrier, cancer cells are exposed to an inhospitable microenvironment. In order to transform it to a favourable niche that allows for tumour proliferation and engraftment, cancer cells dictate the production of ECM components, such as collagen, hyaluronan, periostin, tenascin-C and versican from the surrounding stromal cells. *In vitro* and *in vivo* studies confirm that versican, through suppression of SNAIL, promotes mesenchymal to epithelial transition (MET) in the early metastatic niche (Sheng et al., 2006; Gao et al., 2012); a process that is the reverse of EMT, which prompts migratory cancer cells to acquire a non-invasive phenotype that favours cell adhesion and quick proliferation. The interaction of versican with hyaluronan, as well as MMP-related ECM remodelling have been shown to promote angiogenesis in the secondary tumour microenvironment (Koyama et al., 2007; Kessenbrock et al., 2010). Interestingly, cancer cells can also dictate ECM remodelling in distant premetastatic sites indirectly, before they actually arrive at those. This is achieved by tumour-derived extracellular vesicles (EVs), which can transfer matrix-remodelling enzymes such as MMPs, heparanases and hyaluronidases to recipient cells of the premetastatic niche (reviewed in Nawaz et al., 2018).

1.4.3 The role of versican isoforms in cancer

In the past decade, an increasing body of evidence has associated elevated levels of versican expression in tumour samples with poor patient outcome. This finding has been observed in numerous cancer types, including hepatocellular carcinoma (Fang et al., 2013), osteosarcomas, leiomyosarcomas (Keire et al., 2014), melanomas (Domenzain-Reyna et al., 2009), gliomas (Onken et al., 2014), lymphomas, brain, breast (Du et al., 2013), prostate, colon (Wit et al., 2013), lung (Said et al., 2012), pancreatic (Barry et al., 2013), gastric (Zhang et al., 2012), oral (Pukkila et al., 2007) and ovarian (Li et al., 2013) cancer. Although Mauri et al. (2005) reported that endothelial pancreatic cancer cells can produce versican, whether and to what extent cancer cells can actually secrete versican by themselves is still a matter of controversy. However, it is generally accepted that cancer cells can dictate versican expression by the surrounding stromal cells. CAFs are the predominant source of versican in the peritumoural microenvironment, but it can also be expressed by myeloid cells (Ricciardelli et al., 2009; Gao et al., 2012).

The versican domains that are important for tumour cell growth, invasion and migration are thought to be the G1 and G3 domains. The G1 domain has been shown to enhance the ability of cancer cells to invade, migrate and resist apoptosis by destabilising cell adhesion (Ricciardelli et al, 2009). ADAMTS proteases can cleave versican isoforms to produce a bioactive protein fragment named versikine, which only contains the G1 domain and has important developmental roles in interdigital web regression (McCulloch et al., 2009). On the other hand, G3 is the most commonly found versican fragment in brain tumours and it has been shown to enhance tumour cell proliferation and blood vessel formation, most likely through interaction with fibronectin and VEGF (Zheng et al., 2004).

The predominant versican isoforms found in tumour tissues are V0 and V1. These two isoforms inhibit cancer cell adhesion to the ECM, thereby contributing to enhanced cell motility and the initiation of micrometastasis in prostate, melanoma and glioma cell lines (Ricciardelli et al., 2009; Onken et al., 2014). The most popular mechanism proposed for V1/V0 function is the one that supports the formation of a polarised ‘pericellular sheath’, consisting of CD44 and HA/versican complexes (Onken et al., 2014). This triple interaction activates various pathway mediators, including LOX, Rho and Rac1 GTPases, erbB2 tyrosine kinase, Src-related tyrosine kinases and nuclear factor-κB (NF-κB), thereby affecting the cytoskeletal organisation, cell adhesion and migration (Wu et al., 2005). As described, this pericellular sheath is formed at the trailing edge of a migratory cell, inhibiting cellular adhesion to ECM, but absent in the leading edge, allowing attraction and

binding to ECM, thus enhancing the forward motion of the cells (Ricciardelli et al., 2009). In addition, V1 has been shown to aid apoptotic resistance and enhance cancer cell proliferation, as well as facilitate cancer cell engraftment in the secondary tumour site, through the induction of MET in both fibroblasts and metastatic tumour cells (Sheng et al., 2006; Gao et al., 2012).

In contrast, overexpression of the V2 and V3 isoforms inhibit cancer cell growth, as shown by multiple *in vitro* and *in vivo* studies on fibroblasts, melanoma, sarcoma and glioma models (Sheng et al., 2005; Miquel-Serra et al., 2006; Yang and Yee, 2013; Fanhchaksai et al., 2016). This discrepancy between the effects of V0/V1 and V2/V3 isoforms on proliferation implies an important proliferative role for the βGAG domain, which is absent in V2 and V3 (Figure 1.2A). Yang and Yee (2012) showed that, although V2-transfected glioma cells proliferate at a slower rate, their ability to escape cell death is enhanced. In the same study, V2 was also shown to enhance angiogenesis, through interaction with fibronectin. In a melanoma study, although V3 was found to inhibit cell growth *in vivo*, it appeared to stimulate metastasis to the lung (Miquel-Serra et al., 2006). The role of V3 in apoptosis is contentious; V3-overexpressing melanoma cells did not show a different apoptotic rate compared to controls *in vitro* (Serra et al., 2005), but when the same cell line was injected in mice, it stimulated higher levels of apoptosis (Miquel-Serra et al., 2006).

Versican isoforms also play a central role in the control of inflammation, which is inextricably associated with cancer (CRI) (reviewed in Colotta et al., 2009; Zhang et al., 2012; Andersson-Sjöland et al., 2014). Versican, which is abundantly expressed during inflammation, can interact with cell receptors of myeloid and lymphoid cells to influence their adhesion properties and production of inflammatory cytokines (Wight et al., 2014). Apart from stromal and tumour cells, VCAN can be expressed by monocytes and TAMs, suggesting that myeloid cells can transform the surrounding ECM to amplify the inflammatory response (Li et al., 2013; Masuda et al., 2013; Sotoodehnejadnematalahi et al., 2015). The role of versican during inflammation has been extensively studied, with an emphasis on the elucidation of the contribution of each structural domain on the inflammatory cascade (reviewed in Wight et al., 2014). The results implicate many versican binding partners, including TLR2, PSGL-1, CD44, selectins, HA and fibronectin, in the regulation of the inflammatory response. For example, matrices rich in versican/HA complexes have been shown to promote monocyte adhesion, but at the same time, due to versican acting as an antagonist that prevents CD44 from binding to HA, they can also

dampen the immune response (Evanko et al., 2012). Interaction of V1 GAG chains with TLR2 has been shown to stimulate macrophages to produce pro-inflammatory cytokines (mainly TNF-α), which contribute to tumour growth in a number of malignancies, including lung and ovarian cancer (Li et al., 2013; Xu et al., 2016).

The CS-containing versican isoforms have been shown to have pro-inflammatory properties, as they contribute to the formation of an elastin-depleted ECM that attracts monocytes (Hinek et al., 1991; Potter-Perigo et al., 2010; Wight et al., 2014). V3 has been shown to have the opposite effect in arterial smooth muscle cells, as it creates an ECM rich in elastic fibers, thereby preventing monocyte adhesion (Kang et al., 2014; Kang et al., 2015). The underlying reason seems to be the absence of CS chains from the V3 isoform, suggesting a critical pro-inflammatory role for this region.

It is evident from the above, that versican exerts distinct, often opposing roles in each step of the metastatic cascade, due to its ability to interact, directly or indirectly, with a wide repertoire of ECM mediators and cell surface receptors (summarised in Figure 1.9). Apart from its contribution to the metastatic cascade, versican can affect cancer progression through regulation of the CRI. The different modes of action versican possesses can be attributed not only to the numerous protein motifs and the GAGs it incorporates, but also to the existence of different isoforms, which can be further cleaved into bioactive fragments, adding another level of complexity to versican functions. The final outcome of versican activity is dependent on the spatiotemporal availability of versican fragments and is the product of antagonism between the different domains and isoforms.

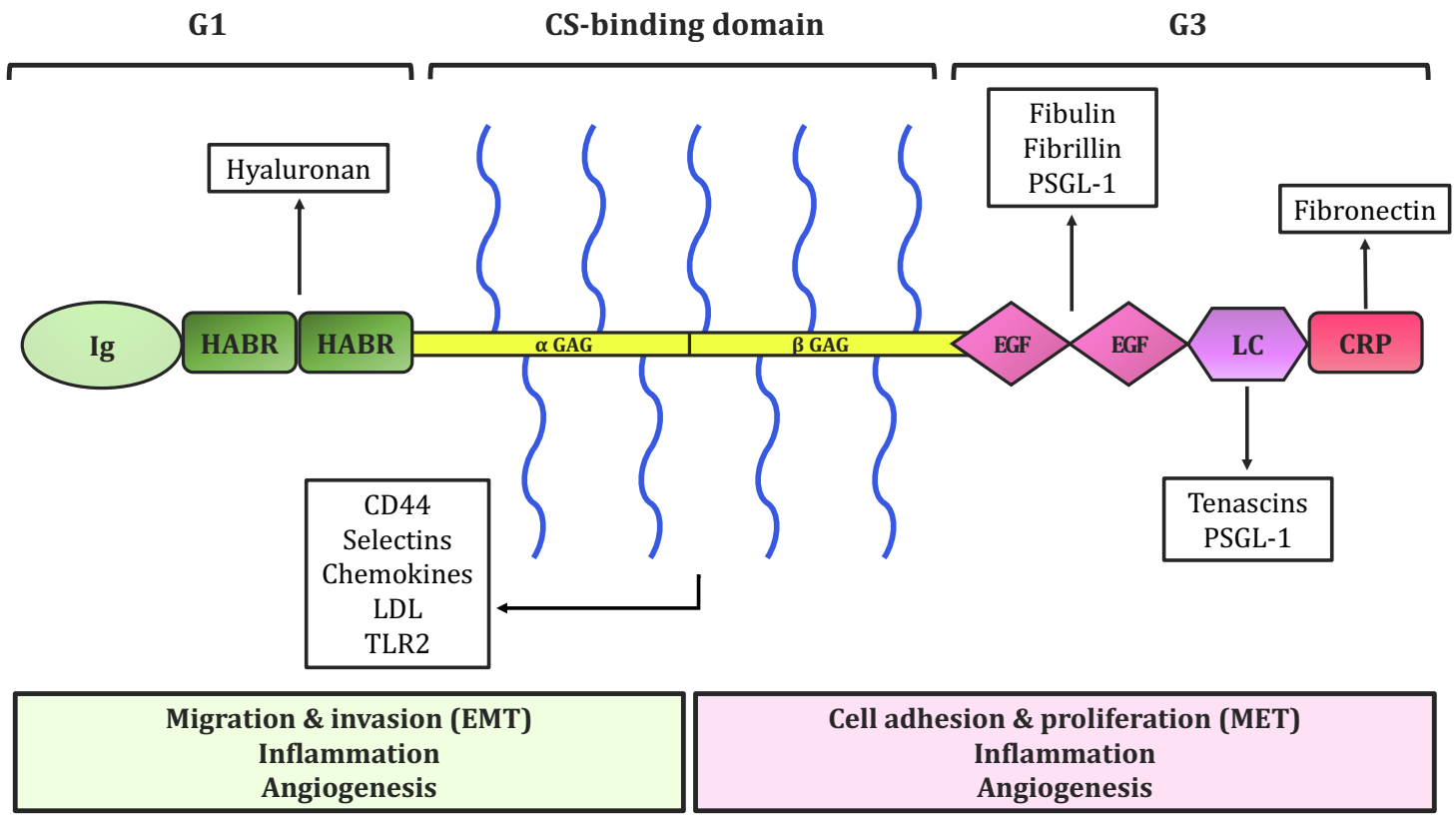

Figure 1.9 The binding partners of versican and the main functions of its domains. Black arrows indicate sites of interaction. The HABR domain of versican (dark green) can bind hyaluronan, while GAG chains (blue) provide docking sites for CD44, selectins, chemokines, LDL and TLR2. Fibullin, fibrillin and PSGL-1 can bind to the EGF repeats (pink), fibronectin can bind to the CRP domain (red) and tenascins and PSGL-1 interact with the LC domain (purple). The interaction of versican with selectins, chemokines, PSGL-1, TLR2, HA, tenascin-C, fibrillin and fibulin is associated with inflammation. Versican interaction with fibronectin and hyaluronan can stimulate angiogenesis. Although the G1 domain stimulates EMT through interaction with HA and CD44, the βGAG and G3 domains are important for the induction of MET. Versican G3 domain can also bind to integrin β1, but the exact site of this interaction is not known (Wu et al., 2005; Wight et al., 2014).

1.5 MAIN HYPOTHESIS AND AIMS

This project aims to combine multiple approaches for the study of versican, both in the whole animal model (zebrafish embryo) and in human stromal cells. More specifically, I aimed to exploit the developing zebrafish inner ear as a convenient *in vivo* model, in which to manipulate *versican* mRNA expression and monitor effects on cell behaviour. I have used *adgrg6* homozygous zebrafish mutants as an *in vivo* drug screening system to identify compounds able to down-regulate *versican* expression*. mbp* expression was used as a secondary screening assay to investigate which of the hit compounds are likely to act through modulation of Adgrg6 signalling. A subset of the positive hit compounds were tested on human stromal cell models *in vitro* to investigate whether versican regulatory pathways are conserved between zebrafish and human.

I hypothesise that:

1. *versican* expression is essential for epithelial fusion and pillar formation that leads to semicircular canals, and thus zebrafish *versican a* and/or *b* mutants will show defects on the above process.
2. Zebrafish *ext2* mutant embryos (low heparan sulphate biosynthesis) will exhibit a defective inner ear phenotype and
3. as CS have been previously suggested to be up-regulated under circumstances where HS is low (Holmborn et al., 2012), we hypothesise that *versican* mRNA levels would be higher in these mutants.
4. Some of the compounds identified in a zebrafish *adgrg6* screening system on the basis of their ability to down-regulate *versican* expression in the inner ear will restore the canal defects displayed by these mutants.
5. A subset of the hit compounds will also rescue *myelin basic protein (mbp)* expression in *adgrg6* zebrafish mutants, possibly through interaction with Adgrg6 pathway.
6. A subset of the hit compounds will down-regulate *VCAN* expression in human fibroblasts.

CHAPTER 2.

Materials and methods

2.1 ZEBRAFISH WORK

2.1.1 Zebrafish lines

The wild-type strains used were AB (ZDB-GENO-960809-7) and London wild type (LWT). Embryos of the *nac* (*mitfa*$^{w2/w2}$) strain (ZDB-GENO-990423-18), which lack melanophores (Lister et al., 1999), were used as wild types for the drug screening experiments. The mutant alleles used in this study are listed in Table 2.1.

Table 2.1. List of zebrafish lines used in the study

Mutant allele	Gene mutated	Source
lau^{tb233c} *(bge*^{tb233c}*)*	*adgrg6*	Whitfield et al., 1996, Geng et al., 2013
lau ^{tk256a}	*adgrg6*	Whitfield et al., 1996
dak^{to273b}	*ext2*	van Eeden et al., 1996
sa1460	*vcana*	Sanger Institute
sa923	*vcanb*	Sanger Institute

2.1.2 Zebrafish care and mating

Adult fish were kept in circulating water, maintained at 28.5 °C with a 14-hour light/10-hour dark cycle. Fish were mated either as pairs in containers with a removable partition to allow for timed mating, or marbled, by placing a mesh-bottom container with marbles over a collection tank in the main fish tank. Embryos were collected, sorted into pre-warmed E3 medium (5 mM NaCl, 0.17 mM KCl, 0.33 mM $CaCl_2$, 0.33 mM $MgSO_4$) containing methylene blue and placed in a 28.5 °C incubator. Embryos were staged according to Kimmel et al., (1995). All experimental work conformed to UK Home Office regulations on the use of animals in research (Animals Scientific Procedures Act 1986) and was undertaken under the animal license 40/3655 (01/10/2014-24/07/2017) and P66302E4E (25/07/2017-01/07/2018).

2.1.3 Microscopy and photography

For live imaging, zebrafish embryos were anaesthetised in 4% (w/v) tricaine (MS222) in E3 medium and mounted in 3% (w/v) methyl-cellulose in a cavity created by cutting a small "window" in three layers of electrical insulation tape stuck on an imaging slide. A coverslip was added at the top and images were taken using an Olympus BX-51 microscope, C3030ZOOM camera and CELL B software, and assembled with Adobe Photoshop CC. In all images, anterior is towards the left and dorsal towards the top.

Drug-treated embryos were imaged in Multiscreen plates (Millipore) containing 50% (v/v) glycerol using a Nikon AZ100 microscope fitted with an automated stage (Prior). Extended depth of focus images from *z*-sections through the embryos were compressed using the NIS-Elements software (Nikon).

In order to assess the ear swelling in drug-treated *adgrg6*^{tb233c} mutant embryos, the ear-to-ear-width was calculated taking into account three variables (A, B and C) that were measured from photographs of live embryos mounted dorsally using CELLB software (Figure 2.1). Value A was the distance between the two horizontal lines designating the two widest points of the ears of the embryo. As I was comparing *adgrg6* mutant embryos to LWT wild-types, I wanted to eliminate any strain differences concerning the size of the head. Therefore, I introduced values B and C; value B was the distance between the two horizontal lines that cross the most medial point of the ear (i.e. the medial edge of the saccular otolith). Value C was the distance between the two points where the edge of the ear joins the rest of the body and it was used as an indicator of the overall size of the

embryo. In order to give a normalised quantification of the ear width in the assay, I subtracted B from A and divided this number by the value of C.

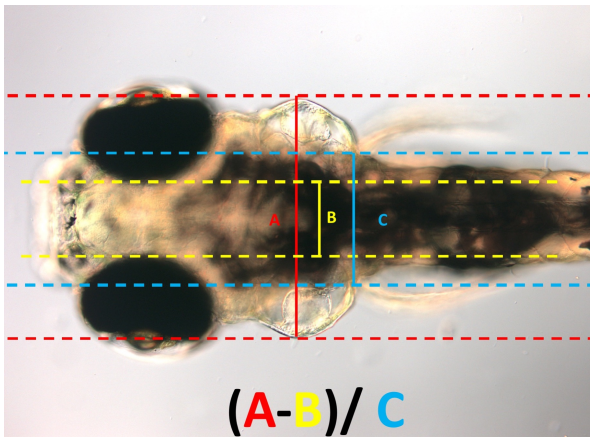

Figure 2.1 Normalisation of ear width. Live DIC image of an *adgrg6* ^{tb233c} mutant embryo at 110 hpf, mounted dorsally, showing the parameters used to calculate the normalised ear width. This value was used in section 5.2.5 to assess how the ear swelling is affected after treatment with different compounds.

2.1.4 *In vivo* drug screening

All *in vivo* drug screening assays were performed at the Sheffield Zebrafish Screening Unit. Chemical compounds from Tocris Total (Tocriscreen collections, 1120 compounds) and The Spectrum Collection (Microsource Discovery Systems, 2000 compounds) were stored at a concentration of 5 mM in DMSO in v-bottomed 96-well microtitre plates (Matrix) at -80 °C. Assay plates contained compounds diluted to 25 µM in E3 medium for drug screening. Wild-type (*nac*) and homozygous *adgrg6*^{tb233c} mutant embryos were raised to 50 hours post fertilisation (hpf), dechorionated manually with forceps and then moved to 20 °C overnight to slow down development and facilitate experiment times. Embryos at the equivalent of the 60 hpf stage (as estimated according to Kimmel et al.,1995) were aliquoted at three embryos per well into Multiscreen mesh-bottomed plates (100 mm; Millipore) and transferred to Multiscreen 96-well culture receiver trays (Millipore) containing the compounds at 25 µM in columns 2-11, with control wells containing either IBMX (3-isobutyl-1-methylxanthine, Sigma, 50 µM in E3), DMSO (Sigma, 1% (v/v) in E3) or E3, in columns 1 and 12. Assay plates were incubated at 28.5 °C for 30 hours and the embryos were then transferred to 4% (v/v) paraformaldehyde (PFA) and stored at 4 °C overnight. Fixed embryos were bleached with a 3% (v/v) H_2O_2/0.5% (w/v) KOH solution until pigmentation completely disappeared, according to the standard protocol in Thisse and Thisse (2008) and stored at -20 °C in methanol, until required for *in situ* hybridisation. In order to facilitate screening, samples were kept in the same 96-well mesh-bottomed

Multiscreen plate during drug treatment, *in situ* hybridisation and hit detection. Hits identified in the primary screen were selected and retested using the same protocol. Selected compounds were then purchased separately from Sigma and tested in dose-response assays.

2.1.5 Whole-mount *in situ* hybridisation (ISH)

Whole-mount *in situ* hybridisation was performed based on the standard procedure described in Thisse and Thisse (2008) with small modifications. The reagents used are described in Table 2.2 and were purchased from Sigma, unless otherwise stated. Normally, a batch of 40-50 embryos was analysed per condition.

Preparation: 4% PFA fixed embryos were bleached with a 3% H2O2/0.5% KOH solution until pigmentation completely disappeared (~20 minutes). The reaction was stopped with 25% (v/v) methanol in PBS, and then embryos were dehydrated by gradually increasing methanol concentration to 100%, with 5-minute washes in 50% and 75% (v/v) methanol in PBS. Embryos were then stored at -20 °C until needed.

Day 1: Embryos were rehydrated by gradually decreasing methanol and increasing Phosphate-Buffered Saline (PBS) concentration to 100%. Four 5-minute washes with 100% PBT were carried out before digestion with proteinase K solution (10 µg/mL), the duration of which was critical and dependent on the stage of the embryo (9-18 somites for 3 minutes, 18 somites-24 hpf for 10 minutes, 36 hpf-5 dpf for 30 minutes). Digestion was stopped with a 20-minute wash in 4% PFA/PBS solution followed by four PBT washes before prehybridising for 3 hours at 70 °C in hybridisation mix (HM). 30-50 ng of appropriate antisense RNA probe (diluted in HM at 1: 450) were incubated for 16 hours at 70 °C.

Day 2: The probe was washed with HM (without tRNA and heparin) pre-warmed at 70 °C and then HM was gradually replaced by 2xSSC, through serial 70 °C washes in 25%, 50%, 75% and 100% (v/v) 2xSSC. Two 30-minute washes in 0.2xSSC at 70 °C were performed before 0.2xSSC was progressively changed to PBT by successive washes in 0.2xSSC/PBT solutions of the same dilutions used previously (25%, 50%, 75% and 100% (v/v) PBT). The embryos were then blocked for 3 hours at 20 °C, using the blocking buffer described below, and an anti-DIG antibody (diluted at 1/2000 in blocking buffer) was added for an overnight incubation at 4 °C with gentle agitation.

Day 3: The antibody was washed with six 15-minute washes in PBT before embryos were incubated in alkaline Tris buffer and eventually staining solution. Embryos were checked regularly under the microscope until desired intensity was achieved (normally 1-4 hours). The reaction was stopped with stop solution and the embryos were equilibrated in 50% and 100% (v/v) glycerol in distilled H2O were carried out to improve the optical transparency of the samples, which were then ready for mounting and imaging.

When performing *in situ* hybridisation on drug-treated embryos, all steps were carried out in multiscreen mesh-bottomed plates using the Biolane HTI 16V *in situ* robot (*Intavis*) to increase throughput.

Table 2.2. List of ISH reagents

Reagent	**Consistency**
PBT	0.1% Tween-20 in PBS
Hybridization mix (HM)	50% formamide, 5xSSC, 0.1% Tween-20, 50 µg/mL heparin, 500 µg/mL tRNA, pH 6.0
20xSSC	175 g NaCl, 88 g Sodium citrate, 800 mL H_2O, pH 7.0
Blocking buffer	2% Fetal Bovine Serum, 2 mg/mL BSA, 1xPBT
Alkaline Tris buffer	100 mM Tris HCl, pH 9.5, 50 mM $MgCl_2$, 100 mM NaCl, 0.1% Tween-20
Staining solution	225 µL of 50 mg/mL NBT, 175 µL of 50 mg/mL BCIP in 50 mL Alkaline Tris buffer.
Stop solution	1xPBS, 1 mM EDTA, 0.1% Tween-20

2.1.6 Molecular analysis

2.1.6.i Polymerase-Chain-Reaction (PCR)

All primers for PCR amplification were purchased from IDT. Primers were re-suspended in milliQ H2O to give a 100 µM stock concentration and diluted to a working concentration of 10 µM. Both were stored at -20 °C. PCR reactions were assembled in PCR tubes or 96-well plates on ice. The polymerase used was 2x Taq Reddymix polymerase (Thermo-Fisher Scientific). The reactions were set up as recommended by the manufacturer. The annealing temperatures used for 2x Taq Reddymix reactions were approximately 5 °C below the melting temperature (Tm) of the primers.

2.1.6.ii Synthesis of DIG-labelled RNA probes

The DNA templates used for synthesising RNA ISH probes were produced by linearising previously published modified plasmids containing the cloned DNA sequence of interest (Table 2.3). The plasmid was linearised using a restriction enzyme which has a unique cleavage site located 5' to the insert (for anti-sense probes). To do this, 1 µg plasmid DNA was incubated with the appropriate restriction enzyme and buffer in a 20 µL reaction containing 10 µg/µl acetylated BSA. Linearised DNA was then purified with GenElute PCR kit (Sigma). DNA was then transcribed to RNA *in vitro* by incubating 1 µg of DNA template, 2 µL 10x transcription buffer, 1µL RNase inhibitor, 2 µL RNA polymerase (T7 or SP6), 1 µL DIG-labelled RNA mix and milliQ water to 20 µL at 37 °C for 2 hours. Subsequent incubation with DNase I for 20 minutes at 37 °C was carried out to digest the DNA and the synthesized RNA was purified by precipitation in ammonium acetate (NH4Ac). The RNA was added to 10 µL of 7.5 M NH4Ac and 75 µL of cold ethanol before being centrifuged at 1000 xg, 4 °C for 20 minutes. The pellet was then washed with 100 µL of 70% ethanol and centrifuged at 1000 xg, 4 °C for 5 minutes. The ethanol wash was then discarded and the pellet resuspended in 20 µL of RNase-free water. Purified RNA was checked by gel electrophoresis and an equal volume of formamide was added to it before being stored at -80 °C.

Table 2.3. List of previously synthesised ISH template constructs used for ISH

Gene	ZFIN ID	Reference
*vcana**	ZDB-GENE-011023-1	Kang et al., 2004
*vcanb**	ZDB-GENE-030131-2185	Kang et al., 2004
gpr126	ZDB-GENE-041014-357	Geng et al., 2013
chsy1	ZDB-GENE-030131-3127	Thisse and Thisse, 2004
mbpa	ZDB-GENE-030128-2	Brösamle and Halpern, 2002
tecta	ZDB-GENE-110411-120	Stooke-Vaughan et al., 2015
myo7aa	ZDB-GENE-020709-1	Ernest et al., 2000
otog	ZDB-GENE-120228-1	Stooke-Vaughan et al., 2015
otomp	ZDB-GENE-040709-1	Murayama et al., 2005
stm	ZDB-GENE-031112-4	Söllner et al., 2003

* For the exact nucleotide sequence of the RNA probe refer to the Appendix.

2.1.6.iii Genotyping by sequencing

For genotyping, genomic DNA (gDNA) was extracted from live adult fin clips or live/fixed embryonic tissue using the HotSHOT method described by Meeker et al. (2007). Primers were designed on primer3 software around the mutation site using the Sanger Institute webpage for information (http://www.sanger.ac.uk/sanger/Zebrafish_Zmpgene/ENSDARG00000078680#sa1460, http://www.sanger.ac.uk/sanger/Zebrafish_Zmpgene/ENSDARG00000009401#sa923).

The tissue was heated in 50 mM sodium hydroxide at 95 °C to lyse cells and denature the DNA. The solution was then cooled at 4 °C, neutralised by adding 1/10th volume of Tris pH 8 and centrifuged to pellet cell debris. The supernatant, which contains the gDNA, was used in PCR to amplify the gDNA fragment of interest. Primers and NTPs were removed from the PCR products by ExoSAP, where 2 µL of SAP (Shrimp-Alkaline Phosphatase) and 0.25 µL of Exonuclease I (NEB) was added to 8 µL of the PCR product and incubated at 37

°C for 45 minutes. After this incubation, the reaction was heated to 80 °C for 15 minutes to deactivate the enzymes. Samples were sequenced with the relevant sequencing primer (Table 2.4).

Table 2.4. List of primers used for DNA sequencing

Primer (Gene/allele)	Genotyping direction	Sequence
vcana sa1460	Forward (5'-3')	AGCAGTCTCATTCATAAATTCAACA
vcana sa1460	Reverse (3'-5')	CCGCAGTTTGAAACCACATTAAA
vcanb sa923	Forward (5'-3')	GCTTATGCCGTTTGAATAGGAGT
vcanb sa923	Reverse (3'-5')	CATACGGAGAGGAGAATTTGTCG

2.2 HUMAN CELL CULTURE

2.2.1 Cell lines

Primary human normal oral fibroblasts were isolated from human gingival tissue and were kindly supplied by Dr Helen Colley, as previously described (Hearnden et al., 2009) with South Yorkshire ethical committee approval at the Charles Clifford Dental hospital (National Ethical Approval number 09/H1308/66). NOF804 and 316 from two different donors were used at passage 5-11. Primary human cancer-associated fibroblasts (CAF003) were isolated from OSCC resection specimens (Hearnden et al., 2009) within the university hospital by Prof Keith Hunter (Sheffield Research Ethics Committee reference number 13/NS/0120) and used between passages 5-9.

2.2.2 Cell culture

All reagents used in tissue culture were purchased from Sigma Aldrich (UK): Dulbecco's modified Eagle medium (DMEM), foetal bovine serum (FBS), L-glutamine, phosphate buffered saline (PBS), trypsin /EDTA (ethylenediaminetetraacetic acid), penicillin and streptomycin. All culture plates were purchased from Griener Bio one (UK). Glass coverslips with a diameter of 13mm were purchased from VWR International (UK).

Primary normal oral fibroblasts were maintained in 99% humidity, 5% (v/v) CO2 at 37 °C, in antibiotic-free DMEM containing 10% (v/v) FBS and 2 mM L-glutamine. All cell lines were routinely cultured in T75 flasks (Greiner bio-one), passaged once a week and the culture medium was changed twice a week. Every 3 months, cells were checked by Kirsty Franklin for the presence of mycoplasma using the EZ-PCR mycoplasma kit (GeneFlow) on conditioned media from the cells.

When confluent, cells were passaged using trypsin/EDTA. The cells were washed twice with phosphate buffered saline (PBS), and an appropriate amount of trypsin/EDTA was added according to the culture size (1.5 mL for T75 and 300 µL for 6 well plate), and the flask was placed in the incubator for 2-5 minutes. After detachment of cells from the culture flask or plate, serum containing media was used to neutralise the enzymatic action of the trypsin/EDTA. The cell suspension was then centrifuged at 1000 xg for 5 minutes, resuspended in fresh culture media and the appropriate amount was placed in a new flask.

2.2.3 TGF-β and drug treatments

Oral fibroblasts were seeded at 250000 cells/well in a 6-well plate. When confluent (normally 72 hours after seeding), the cells were serum-starved for 24 hours by replacing the medium with serum-free DMEM (plus L-glutamine), before being treated with 5 ng/mL recombinant human TGF-β1 (RD systems, reconstituted in 4 mM HCl plus 1 mg/mL BSA). 24 hours later, cells were treated with freshly diluted nifedipine (Sigma) or cilnidipine (Sigma) in DMSO (final concentrations ranged from 0.05 to 100 ng/mL), which also contained 5 ng/mL TGF-β1. For every experiment, DMSO (0.1 %) was used as a negative control, while the drug treatment lasted for 24 hours. At the end of the treatment, cells were harvested by scraping, using either a RIPA (Radio-Immunoprecipitation Assay) buffer/protease inhibitor mixture (for protein analysis, 30 µL/well) or an RLT buffer/β-mercaptoethanol mixture (for RNA analysis, 350 µL/well). Cell lysates were then stored at -80 °C until needed.

2.2.4 Western Blot

Cell lysates were prepared by scraping cells from each well of a 6-well plate into 30 µL RIPA buffer supplemented with Complete Mini Protease Inhibitor Cocktail (Roche). The protein concentration was calculated using a bicinchoninic acid (BCA) assay kit (Thermo-Fisher Scientific), whereby standards of various BSA concentrations were prepared and used to generate a standard curve. Absorbance of standards and protein samples was measured at 595 nm using an Infinite M200 TECAN spectrophotometer and the sample concentration was interpolated from the standard curve.

15-20 µg of total protein sample was resolved by 8-10% (w/v) SDS-polyacrylamide gel (Life-Technologies) electrophoresis (SDS-PAGE) in Tris-acetate buffer (Life-Technologies). The protein was transferred onto a nitrocellulose membrane (Millipore) by semi-dry transfer system Trans-Blot Turbo (Bio-rad), and protein presence was checked using Ponceau Red (1:10 diluted in dH2O). Ponceau dye was washed off with Tris buffered saline with 0.05% (v/v) Tween 20 (TBS-T), before blocking the membrane in 5% (w/v) milk powder in TBS-T. The primary antibody was diluted in the same blocking solution and incubated at 4 °C overnight (see Table 2.5 for information on the antibodies used). The membrane was washed 3 times, 5 minutes per wash, with TBS-T, before being incubated with the appropriate horseradish peroxidase-conjugated (HRP) secondary antibody diluted 1 in 3000 in the above blocking solution, for 1 hour at room temperature. The membrane was washed 3 times in TBS-T, before being exposed to Clarity Western

enhanced chemoluminescent (ECL) Substrate mixture (Biorad) for 5 minutes, after which, HRP activity was detected using a C-Digit Blot Scanner (Li-Cor).

Table 2.5. List of antibodies used for western blotting

Antibody target	Description	Dilution	Supplier
alpha smooth muscle actin (α-SMA)	mouse anti-human monoclonal IgG2a, clone 1A4	1:500	Sigma Aldrich (A5228)
glyceraldehyde 3-phosphate dehydrogenase	rabbit anti-human monoclonal IgG, HRP-conjugated, clone EPR6256	1:7500	Abcam
Versican (full length)	Goat anti-human polyclonal IgG	1:1000	R & D systems
mouse IgG	horse anti-mouse IgG, HRP-conjugated	1:3000	Cell Signalling Technologies
goat IgG	Rabbit anti-goat IgG, HRP-conjugated	1:3000	Promocell

2.2.5 Molecular Analysis

RNA extraction

Frozen samples in RLT buffer/β-mercaptoethanol mixture were thawed on ice and an equal volume of 70% ethanol was added. RNA was purified using RNeasy Mini Kit (Qiagen) according to the manufacturer's instructions. After purification, RNA was retrieved in 35 µL RNase-free water and its concentration was measured using Nanodrop 1000 spectrophotomer (Thermo-Fisher), before being stored at -80 °C.

cDNA synthesis

cDNA was synthesised by setting up the 20 µL reaction described in Table 2.6 and incubating at 25 °C for 10 minutes, at 37 °C for 120 minutes and at 85 °C for 5 minutes. cDNA was stored at -80 °C.

Table 2.6. Reverse Transcription reaction

Reagent	Volume
10x Reverse Transcriptase Buffer (Applied Biosystems)	2 µL
dNTP mix (Applied Biosystems)	0.8 µL
10x RT random primers (Applied Biosystems)	2 µL
Multiscribe Reverse Transcriptase (Thermo-Fisher)	1 µL
350 ng RNA	Variable (<14.2 µL)
Nuclease-free H_2O	to 20 µL

Quantitative Polymerase-Chain Reaction (qRT-PCR)

cDNA was subjected to Taqman real time quantitative PCR reactions using a Rotor-Gene Q (Qiagen). Taqman primers used for versican isoforms V0, V1 and V3 were HS01007944, HS01007937 and HS01007941 respectively, purchased from Thermo-Fisher Scientific. For each reaction, 5 μL Taqman Master Mix (AB), 0.5 μL β2macroglobin (B2M) (HS00187842), 3 μL RNase-free H2O, 0.5 μL primer and 1 μL cDNA were added into qPCR tubes and inserted into the machine.

The mRNA expression was quantified via the delta delta C_T method (2ΔΔCT) (Livak and Schmittgen, 2001), where the C_T value is the number of thermal cycles at which the amount of fluorescence reaches a detectable threshold and it corresponds to the amount of template at the beginning of the reaction. C_T values of the gene of interest were normalised to B2M expression levels, as a reference control.

2.2.6 Statistical Analysis

Graphpad Prism 7 (Graphpad Prism Software, Inc.) was used to perform all statistical analyses and to plot graphs. Data were initially checked for normal distribution. When comparing two different groups of normally distributed data (e.g. TGF-β1 treatments; section 6.2.1), two-tailed, unpaired Student's t-tests were used. To assess the statistical difference between more than one groups (e.g. nifedipine-treated fibroblasts; section 6.2.2) one-way ANOVA tests were performed, with appropriate post-test corrections for multiple samples. Error bars correspond to the standard deviation (SD), unless otherwise stated.

CHAPTER 3.

The role of versican in the zebrafish inner ear development

3.1 INTRODUCTION

Versican is an ECM gene with a dramatically dynamic expression pattern during the first days of zebrafish development (see sections 1.2.5i and 1.3.4 for more details). Although previous studies have described *versican* expression in specific regions of the zebrafish embryo (Thisse et al., 2001 (ZFIN, direct data submission); Kang et al., 2004; Baxendale and Whitfield, 2014), this work aims to take a more holistic approach and present a comparative study of the *vcana* and *vcanb* expression pattern in the whole embryo. The finding that *versican* fails to be down-regulated in the abnormal *adgrg6* mutant ear (Geng et al., 2013), raised a number of questions regarding the role of *versican* in the inner ear development and motivated the work presented in this chapter.

The vast majority of studies regarding the function of versican in zebrafish and mice have focused on its role in the differentiation of the atrioventricular (AV) boundary in the heart (Mjaatvedt et al., 1998; Walsh and Stainier, 2001). In zebrafish, *versican* genes (mainly *vcana*) have been extensively used as an AV canal differentiation marker by many groups studying mutations that affect heart development; among these, *id4*, *tbx5*, *tbx1* and nephronectin (*npnt*) mutants exhibited altered *versican* expression in the heart (Garrity et al., 2002; Patra et al., 2011; Choudhry and Trede, 2013; Ahuja et al., 2016;). In *tbx5* mutants and morphants, *versican* expression was also missing from the malformed pectoral fins (Parrie et al., 2013).

Knockdown of *vcanb* with antisense morpholinos led to malformation of cover craniofacial structures in the injected zebrafish embryos, such as the jaw and gill (Kang et al., 2004). In a different study, *vcana* morpholino injections at the same concentration led to pericardial edemas of variable severity, ranging from mild to very severe, but the experiments were limited by high lethality of injected embryos (Müller-Deilea et al., 2016). A similar heart phenotype was observed in *ugdh* (*jekyll)* mutants (which lack HS, CS and HA), where

pericardial edema and blood accumulation in the two heart chambers was attributed to failure of valve formation, but no embryonic lethality was recorded (Walsh and Stainier, 2001). As morpholino-mediated knockdown has been reported to have off-target effects in many cases, the high lethality of *vcana* morphants could be a toxic artefact of this approach (Rossi et al., 2015). In addition, none of the above studies described the ear morphology and apart from these morpholino approaches, there is no record of studies on *vcana* or *vcanb* zebrafish mutants. In this chapter, I present the findings from the study of *sa1460* (*vcana*) and *sa923* (*vcanb*) single and double mutants with a focus on inner ear development.

The *vcana sa1460* allele is a nonsense point mutation that introduces a premature stop codon. The predicted truncated protein would consist of 230 aa (as opposed to the normal full-length isoform that is 2724 aa long), lacking all the structural motifs of the G1 and G3 domains (Figure 3. 1; https://www.sanger.ac.uk/sanger/Zebrafish_Zmpgene/ENSDARG00000078680#sa1460) . However, the predicted short Vcana isoform should not be affected by the mutation (Figure 3.1). The *vcanb sa923* allele is also a nonsense point mutation presumed to affect both predicted *vcanb* transcript variants, as it lands at amino acid 96 (part of the G1 domain, which is present in both predicted *vcanb* transcript variants) (https://www.sanger.ac.uk/sanger/Zebrafish_Zmpgene/ENSDARG00000009401#sa923).

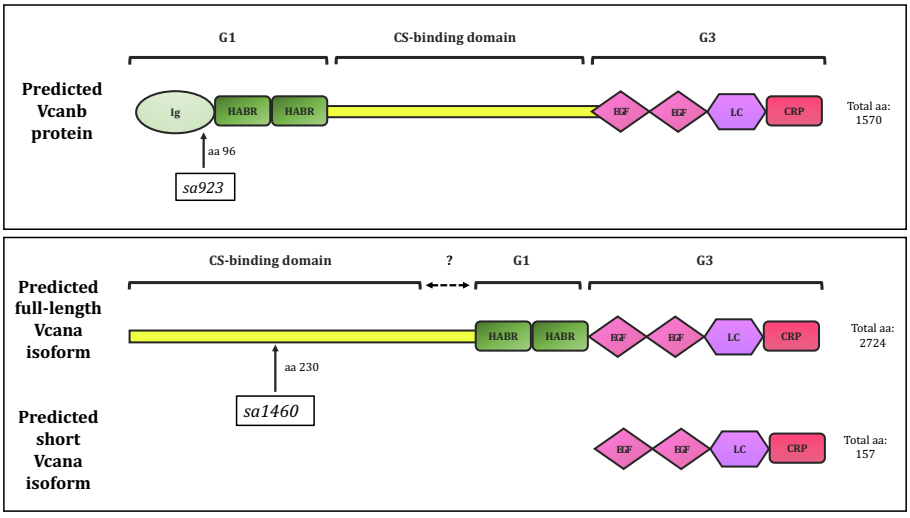

Figure 3.1 Schematic diagram of the predicted Vcana and Vcanb proteins, showing the position of *sa1460* and *sa923* mutations. Abbreviations: CRP, complement regulatory protein-like motif; HABR, hyaluronan-binding repeats; Ig, immunoglobulin-like site; LC, C-type-lectin-like motif.

3.2 RESULTS

3.2.1 *Versican a* wild-type expression pattern

In order to study *vcana* expression pattern, wild-type (LWT) zebrafish larvae were fixed at developmental timepoints ranging from 12-120 hpf and whole-mount *in situ* hybridisation was carried out. In Figure 3.2, *vcana* mRNA expression pattern in an early zebrafish larva is shown. In correlation with directly submitted data on ZFIN, *vcana* expression could be detected for the first time at around 14 hpf in the eye field and the adaxial cells (Thisse et al., 2001; Figure 3.2A,A'). At 16 hpf, the expression was stronger in the lateral plate mesoderm (Figure 3.2B'), while the expression in the adaxial cells was progressively weaker. From 19 hpf until 24 hpf, *vcana* was strongly expressed in the lens primordium, the developing heart tube and the fin fold (Figure 3.2C,C',D,D'). At these stages, there was no detectable expression in the otic placode and vesicle.

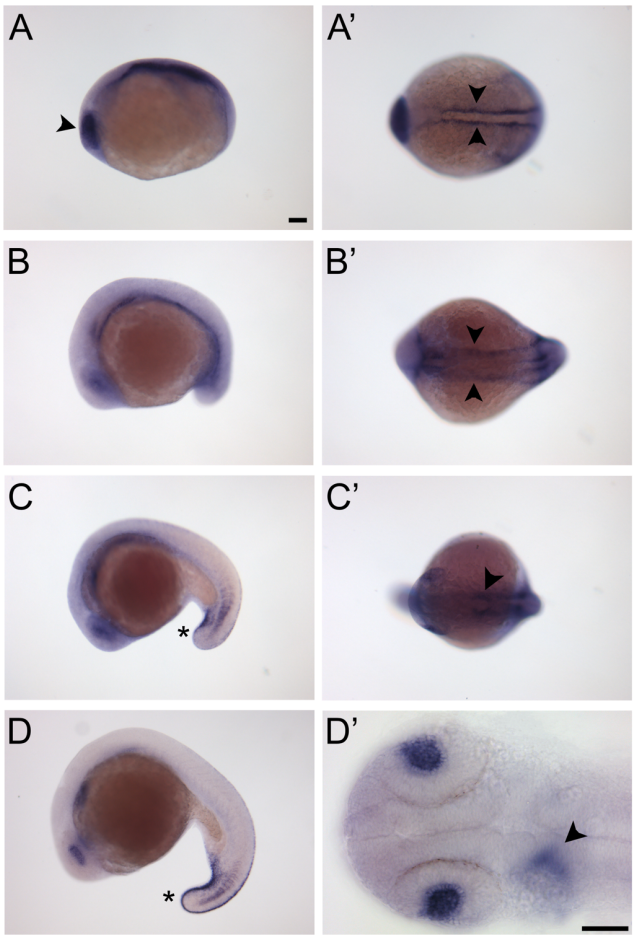

Figure 3.2 *vcana* mRNA expression pattern in wild-type 14 hpf- 22 hpf zebrafish embryos. (A,A') At 14 hpf, *vcana* mRNA is expressed in the forebrain, the eye field (arrowhead in A) and in the adaxial cells (arrowheads in A'); *n*=60. **(B,B')** At 16 hpf, *vcana* expression is present in the lens primordium and the lateral mesoderm (arrowheads in B'); *n*=60. **(C,C')** At 19 hpf, *vcana* expression appears in the ventral epidermis and paraxial mesoderm of the forming fin bud (asterisk), and in the developing heart tube (arrowheads in C' and D'); *n*=60. **(D,D')** This expression persists until 23 hpf, when *vcana* is strongly expressed in both the ventral and dorsal epidermis of the fin fold (asterisk); *n*=60. Left panels are lateral views, with anterior to the left. Right panels are dorsal views, with anterior to the left. A-D and A'-C' were taken using brightfield optics; D' was taken using differential interference contrast (DIC) optics. Scale bars: in A, 100 µm for A–D and A'-C'; in D', 100 µm. Data representative of two individual experiments, each analysing 30 embryos per embryonic stage.

At 48 hpf, *vcana* expression was very high in the developing epithelial projections of the otic vesicle, as previously reported (Thisse et al., 2001; Geng et al., 2013; Figure 3.3A'). Apart from the known expression on the epithelial projections, *vcana* expression was detected for the first time at the tip of the hair cells that comprise the anterior macula (Figure 3.3A'). At the same time, the expression in the heart was restricted to a very narrow zone which comprises the AV boundary, as shown previously (Garrity et al., 2002), while a weak expression was apparent in the opercle (gill cover) (Figure 3.3Ai). At 72 hpf, when the epithelial projections have fused to create three pillars that span the otic lumen, *vcana* expression in the pillars was gradually weakened until it disappeared, and only a trace of expression remained at the dorsolateral septum (DLS) between 4 and 5 dpf (Figure 3.3B',C').

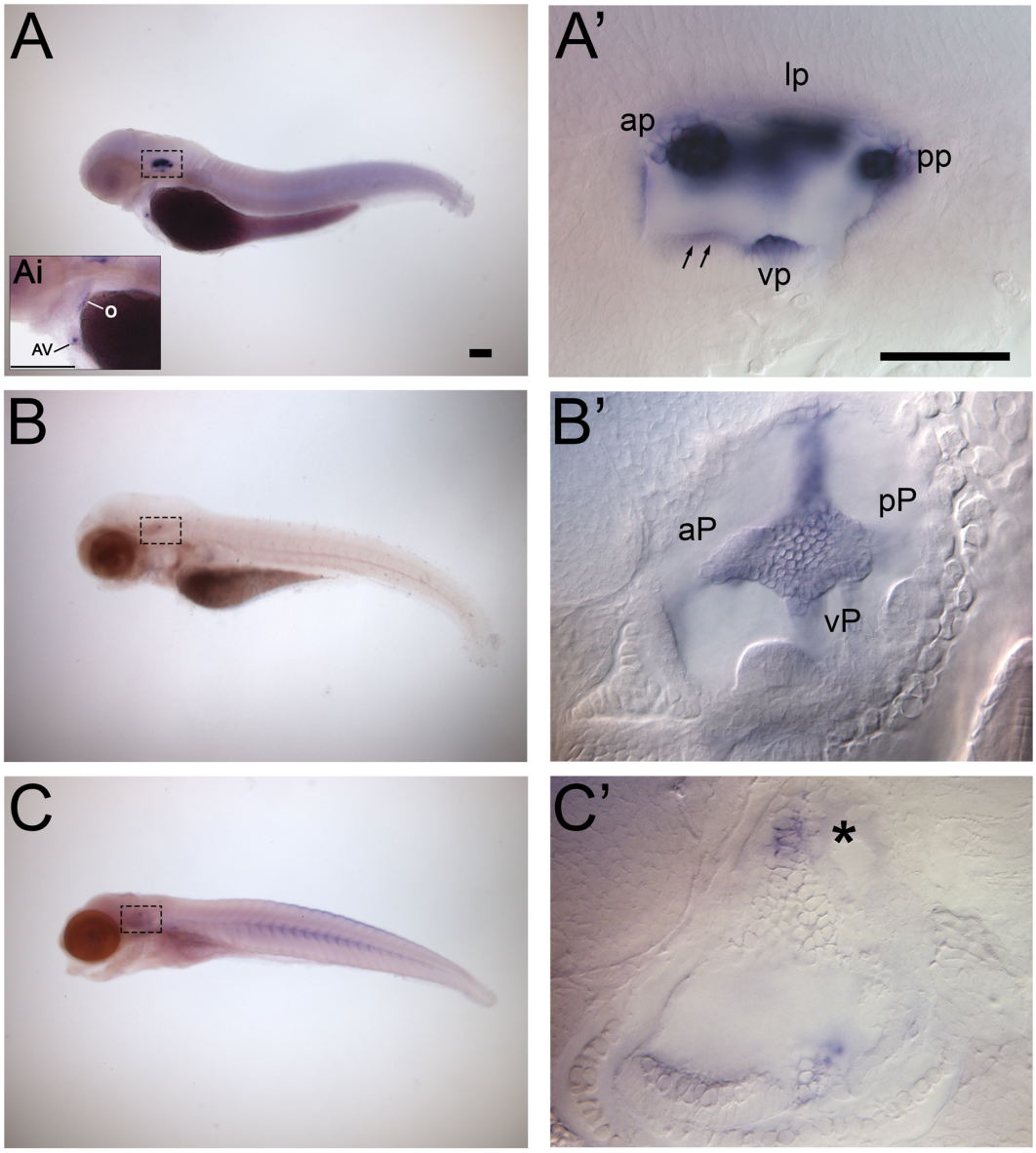

Figure 3.3 *vcana* mRNA expression pattern in wild-type 50 hpf- 5 dpf zebrafish embryos. Right panels are magnified pictures of the otic vesicle of the fish depicted in the left panels. **(A,A')** At 50 hpf, *vcana* mRNA is highly expressed in the otic vesicle, specifically in the developing anterior (ap), posterior (pp), lateral (lp), ventral projections (vp) and the anterior macula (arrows). (Ai) Magnified view of A. Expression in the heart is restricted in the AV boundary (AV), while there is a weak expression in the opercle (o); *n*=100. **(B,B')** At 72 hpf, the expression in the otic vesicle decreases significantly as the fusion gets towards completion; *n*=100. **(C,C')** At 5dpf, only a trace of *vcana* is detected in the dorsolateral septum (asterisk); *n*=100. All panels are lateral views, with anterior to the left and were taken using DIC optics. Scale bars: in A, 100 μm for B, C; in Ai, 100 μm; in A', 50 μm for B', C'. Abbreviations: ap, anterior projection; aP, anterior pillar; AV, atrioventricular boundary; lp, lateral projection; lP, lateral pillar; o, opercle; pp, posterior projection; pP, posterior pillar. Data representative of two individual experiments, each analysing 50 embryos per embryonic stage.

3.2.2 *Versican b* wild-type expression pattern

In order to study the *vcanb* expression pattern, wild-type (LWT) zebrafish larvae were fixed at developmental timepoints ranging from 12-120 hpf and whole-mount *in situ* hybridisation was carried out. *Vcanb* expression could not be detected earlier than 18 hpf, when expression started to appear in the cephalic paraxial mesoderm (Figure 3.4A'). Expression in the developing heart tube started four hours later (Figure 3.4B') and peaked at 26 hpf (Figure 3.4D'). Although expression in the heart at 24 hpf has been previously observed by Kang et al. (2004), this is the first time strong expression of *vcanb* in the heart at 26 hpf is shown, in a zone presumed to be the second heart field. Consistent with previous observations (Lee et al., 2015), *vcanb* was no longer expressed in the heart at 48 hpf. *Vcanb* could be seen in the sclerotome from 22 hpf and the expression got stronger as the embryos developed (Figure 3.4C), until it was no longer detectable at 48 hpf (Figure 3.5A).

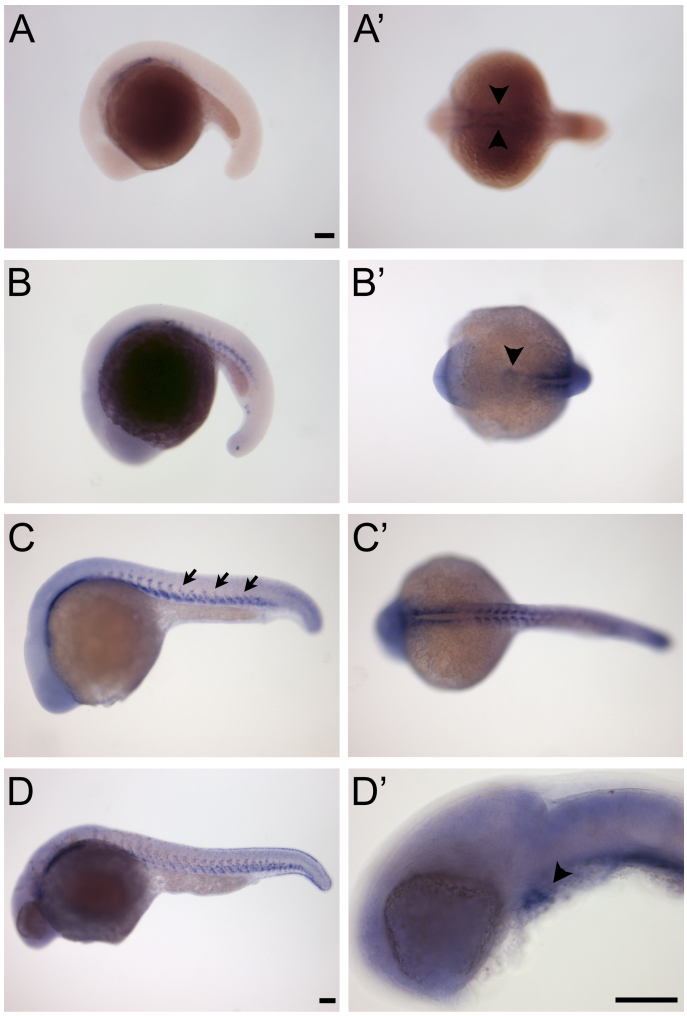

Figure 3.4 *vcanb* mRNA expression pattern in wild-type 19 hpf- 26 hpf zebrafish embryos. (A,A') At 18 hpf, *vcanb* mRNA was expressed in the cephalic paraxial mesoderm (arrowheads in A'); *n*=60. **(B,B')** At 22 hpf, *vcanb* expression was present in the developing heart tube (arrowhead in B'); *n*=60. **(C,C')** Expression in the sclerotome could be observed from 22 hpf, but it was more obvious at 24 hpf (arrows in C); *n*=60. **(D,D')** At 26 hpf, *vcanb* expression was detected in the second heart field (arrow in D'); *n*=60. Left panels and D' are lateral views, with anterior to the left. A'-C' are dorsal views, with anterior to the left. A-D and A'-C' were taken using brightfield optics; D' was taken using DIC optics. Scale bars: 100 μm (scale bar in A applies to A–C and A'-C'). Data representative of two individual experiments, each analysing 30 embryos per embryonic stage.

As shown previously, at 48 hpf, *vcanb* expression was observed in the developing pectoral fin buds, the opercle (Figure 3.5Ai) and in the epithelial projections of the otic vesicle (Kang et al., 2004; Geng et al., 2013; Figure 3.5A'). Like *vcana*, *vcanb* was also expressed at the tip of the anterior macula (Figure 3.5A') Although strong *vcanb* expression at 72 hpf in the opercle has been shown before, I show for the first time that *vcanb* at this stage is also present in the anterior end of the basihyal cartilage (Figure 3.5B,Bi). The otic *vcanb* expression decreased as soon as the fusion of the projections was complete, at approximately 72 hpf; at that stage, the expression in the anterior macula was no longer detectable (Figure 3.5B'). From 4 until 5 dpf, *vcanb* expression was restricted to the DLS (Figure 3.5C').

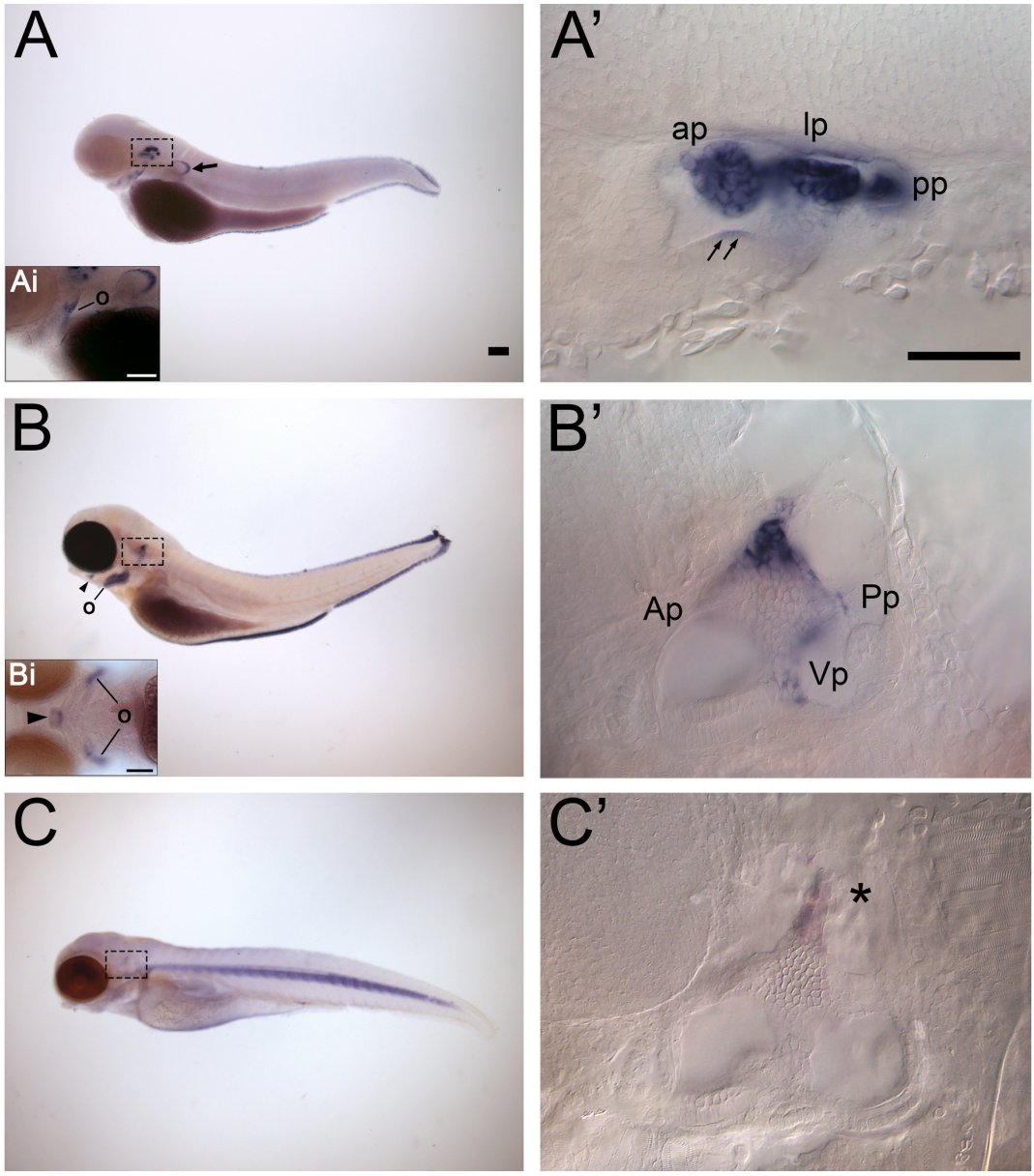

Figure 3.5 *vcanb* mRNA expression pattern in wild-type 48 hpf- 5 dpf zebrafish embryos. Right panels are magnified pictures of the otic vesicle of the fish depicted in the left panels. **(A,A')** At 48 hpf, *vcanb* mRNA is expressed in the pectoral fin bud (arrow in A), the opercle (o) and the otic vesicle, specifically in the developing anterior (ap), posterior (pp), lateral (lp) and ventral projections; It is also weakly expressed in the anterior macula (arrows in A'); *n*=100. (Ai) Magnified view of A. **(B,B')** At 72 hpf, the expression in the otic vesicle decreases significantly as the fusion gets towards completion and the opercle expression is stronger (arrowhead); *n*=100. (Bi) Magnified view of B. **(C,C')** At 5 dpf, only a trace of *vcanb* is detected in the dorsolateral septum (asterisk); *n*=100. All panels are lateral views, with anterior to the left and were taken using DIC optics. Scale bars: in A, 100 µm for B, C; in Ai, 100 µm; in A', 50 µm for B', C'; in Bi, 100 µm. Abbreviations: ap, anterior projection; aP, anterior pillar; lp, lateral projection; lP, lateral pillar; o, opercle; pp, posterior projection; pP, posterior pillar. Data representative of two individual experiments, each analysing 50 embryos per embryonic stage.

3.2.3 *Versican a* mutant phenotype

Adult *vcana*^{sa1460} heterozygous mutants generated by ENU mutagenesis were obtained from the Sanger Institute. A new generation was raised to eliminate the possibility of background mutations in the obtained generation and genotyped by fin clip to identify *vcana*^{sa1460} heterozygous fish.

Heterozygous *vcana*^{sa1460} fish were marbled and the offspring phenotype (n=224) was recorded for the first 5 days of development. Until 72 hpf, no developmental defects or abnormalities were observed and the embryos looked healthy. A delay in projection elongation and consequently the pillar formation was recorded between 72 hpf and 96 hpf. However, due to the fact that this mating technique generates offspring that can differ in age for a few hours and the semicircular canals form rapidly, the experiment was repeated with heterozygous *vcana*^{sa1460} fish pair-mates, which allow for controlled fertilisation time. At the same time, wild-type (LWT) fish pair-mates were performed and the wild-type offspring were used as a stage control. The phenotypes of the offspring from four independent heterozygous *vcana*^{sa1460} incrosses (n=106) are summarised in Figure 3.6. For a mutation with Mendelian inheritance, 25% of the offspring should be homozygous for the mutant allele. Until 72 hpf, no developmental defects or abnormalities were observed and the embryos looked healthy. A delay in projection elongation and consequently the pillar formation was recorded in 21 out of 106 (19.8%) embryos observed at 72 hpf (Figure 3.6B). This percentage was not as high as expected (25%), implying that some of the homozygous mutants may not exhibit any abnormal ear phenotypes. Out of these 21 embryos, 10 had a normal heart phenotype, while 11 also displayed a heart edema. Based on the ear phenotype, the embryos were categorised in two groups: (1) those that formed the anterior and posterior pillars, but the ventral projection remained unfused (17.9% at 72 hpf) and (2) those that formed an anterior pillar, but the ventral and posterior projections remained unfused (1.88% at 72 hpf) (Figure 3.6Aii,iii). At 72 hpf, only 1 (0.94%) of the LWT wild-type embryos was found to have an unfused ventral projection and none fell under the second category. At 4 dpf, all the LWT embryos had formed all three pillars. At the same stage, 2 (1.88%) of the embryos from the *vcana*^{sa1460} cross had the ventral projection unfused and another 2 (1.88%) had both the posterior and the ventral projections unfused (Figure 3.6B). However, 100% of the embryos from the *vcana*^{sa1460} cross formed all three pillars by day 5. The findings were similar among the offspring of different pairs.

The same heterozygous cross was repeated and embryos were fixed at different stages, while embryos with ear defects at 72 and 96 hpf were kept separately. Whole-mount *in situ* hybridisation showed that *vcanb* expression was normal in all embryos at 48 hpf and 5 dpf, but always persisted at the tips of unfused projections between 72 and 96 hpf (Figure 3.6Avi-x). *vcana* mRNA staining appeared either weak or absent in the genotyped *vcana*^{sa1460} homozygous mutants (n=3) and was normal in the genotyped *vcana*^{sa1460} heterozygous or wild-type siblings (n=4) (Figure 3.6E). In 74-hpf fixed embryos, the staining was either lost or weak in all 9 fish (n=45) which had unfused projections between 70-74 hpf, but was also reduced in 3 embryos which had a fully wild-type ear between these stages (Figure 3.6ii,iv,vi). This finding further supports the idea that a small proportion of homozygous mutants (5-6%) does not exhibit an ear phenotype at any of the stages studied, and thus the mutation is incompletely penetrant.

As mentioned above, *vcana*^{sa1460} mutants were also characterised by pericardial edema of variable severity, ranging from mild to severe, which only became apparent after 72 hpf. At 72 hpf, 21 (6.4%) out of the 330 embryos from a heterozygous incross were recorded to have a mild pericardial edema and 34 (10.3%) had a severe edema (total 16.7%; Figure 3.6D). At 4 dpf the percentage of embryos with an apparent mild/moderated edema increased to 12.4%. However, not all the embryos with a heart edema had an ear phenotype and vice versa. Out of the 106 embryos for which both ear and heart characteristics were recorded, 18 embryos displayed a heart edema at 72 hpf (16.9%); out of these, 7 had a normal ear phenotype, while 11 also displayed a delay in the fusion of the projections at 72 hpf.

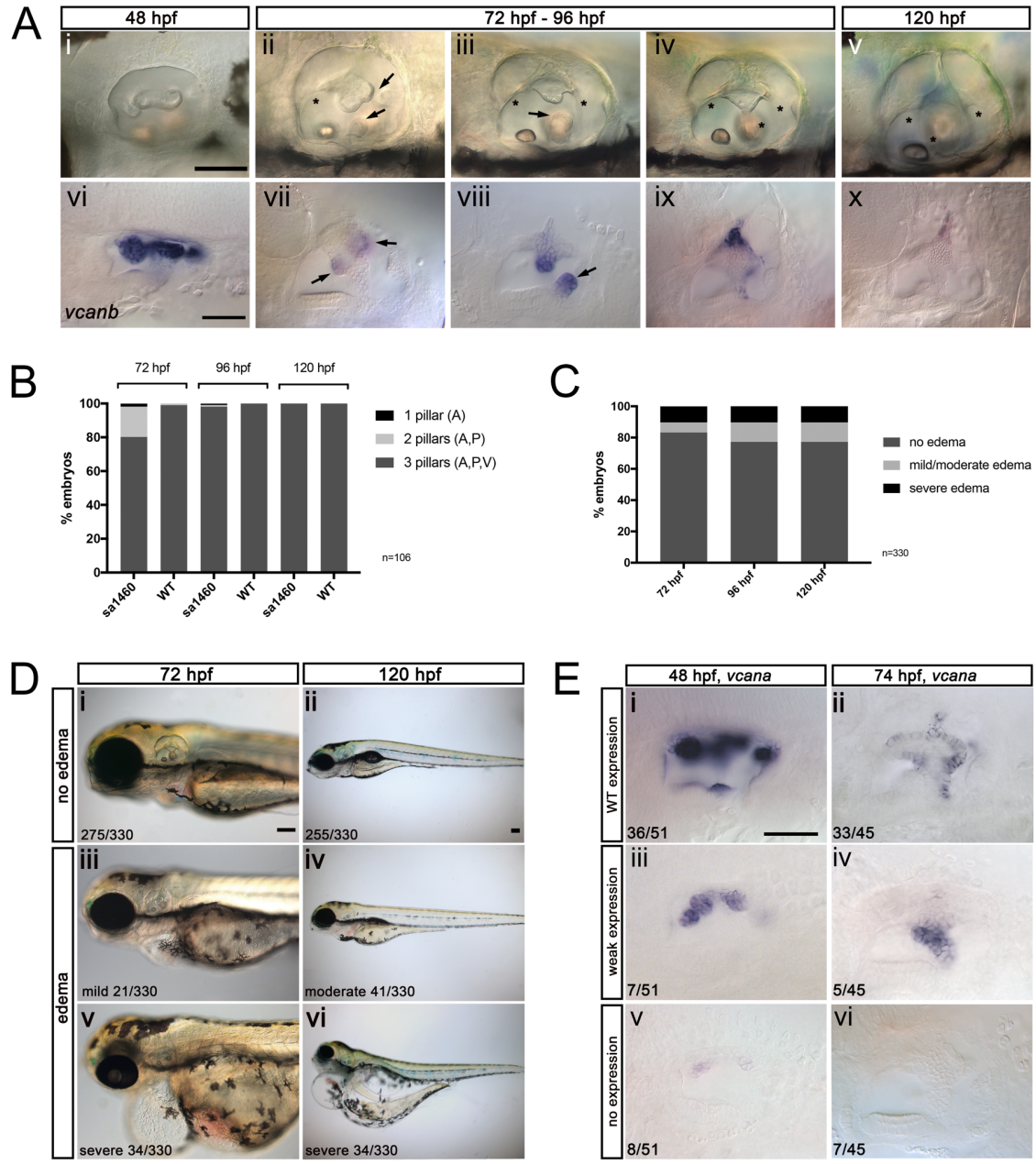

Figure 3.6 The *vcana*^{sa1460} mutant phenotype is variable. (A,B) Images and graphical representation of the inner ear phenotype of embryos from *vcana*^{sa1460} heterozygous crosses from 48 hpf to120 hpf. **(Ai-v)** Live images showing fused (asterisk) and unfused (arrows) epithelial projections of the inner ear. **(Avi-x)** Corresponding *vcanb* mRNA expression showing persisting staining in the unfused projections (arrows). **(C,D)** Live images and graphical representation of the heart phenotype of the same embryos from 72 hpf to 120 hpf. The pericardial edema varied from mild to severe. **(E)** *vcana* mRNA staining at 48 hpf (i,iii,v) and 74 hpf (ii,iv,vi) was either weak or absent in *vcana*^{sa146} homozygous mutants. Note the localisation of the stain in the unfused ventral projection in iv. Scale bars: in Ai, 50 µm for Aii-v; in Avi, 50 µm for Avii-x; in Di, 100 µm for Diii,v; in Dii, 100 µm for Div,vi; in Ei, 50 µm for Eii-vi.

3.2.4 *Versican b* mutant phenotype

Adult *vcanb*^{sa923} heterozygous mutants generated by ENU mutagenesis were obtained from the Sanger Institute. The generation obtained was characterised by low fertility yield. The offspring from a heterozygous cross had severe developmental delays and abnormalities during the first hours after fertilisation, presumably due to background mutations. To test this hypothesis and circumvent the infertility problems, healthy offspring were raised to adulthood and genotyped by fin clip to identify heterozygous fish.

Heterozygous *vcanb*^{sa923} fish were pair-mated and the offspring phenotype was recorded for the first 5 days of development, using LWT wild-type offspring as a stage control. Offspring yield dramatically improved and the early developmental abnormalities were not present in this generation. The phenotypes of 135 embryos from three independent heterozygous incrosses are summarised in Figure 3.7. For a mutation with Mendelian inheritance, 25% of the offspring should be homozygous for the mutant allele. Until 72 hpf, no developmental defects or abnormalities were observed and all the embryos looked healthy. At 72 hpf, a delay in projection outgrowth and consequently the pillar formation was recorded in 9/135 (6.7%) embryos from the *vcanb*^{sa923} cross (Figure 3.7B). This ratio was much lower than the expected, suggesting that the mutation is characterised by low penetrance. At 72 hpf, the embryos could be categorised in two groups: those that formed an anterior pillar, but the ventral and posterior projections remained unfused (5/135, 3.7%) and those that formed the anterior and posterior pillars, but the ventral projection remained unfused (4/135, 3%) (Figure panels 3.7Aii and iii, respectively). At 4 dpf, all LWT embryos had formed all three pillars (135/135). At the same stage, all the embryos from the *vcanb*^{sa923} cross had fused the posterior pillar, but 3 (2.2%) had an unfused ventral projection (Figure 3.7B). However, 100% of the *vcanb*^{sa923} embryos formed all three pillars by day 5. The findings were similar among the offspring of different pairs.

The same heterozygous cross was repeated and embryos were fixed at different stages, while embryos with ear defects at 72 and 96 hpf were kept separately. Whole-mount *in situ* hybridisation showed that *vcana* expression was normal in all embryos at 48 hpf and 5 dpf, but it always persisted at the tips of unfused projections between 72 and 96 hpf (Figure 3.7Avi-x). *vcanb* mRNA expression was absent from both the ear and the opercle in one quarter of the embryos at all stages, possibly due to nonsense-mediated decay of the mutant RNA transcript (Figure 3.7E). Specifically, *vcanb* expression was missing from

11/41 (23%) embryos at 48 hpf, from 12/52 (24.3%) embryos at 72 hpf and from 11/40 (27.5%) embryos at 120 hpf. 3 out of the 11 (2.7%) fixed samples missing *vcanb* expression had unfused projections between 72-96 hpf, while the 8 remaining samples (72.7%) with no *vcanb* expression had fully wild-type ears. Genotyping of 5 of the embryos with no staining confirmed that these were homozygous for *vcanb*^{sa923}, as opposed to the 3 genotyped embryos with staining that were either *vcanb*^{sa923} heterozygous or wild-type. These findings combined support the previously stated argument that the mutation is incompletely penetrant and show that only 2.7% of the homozygous mutants exhibit an ear phenotype.

In addition to the ear defects, 5 (3.7%) of the *vcanb*^{sa923} embryos had a mild pericardial edema at 72 hpf, which developed to moderate in later stages (Figure 3.7D). However, not all the embryos with a heart edema had an ear phenotype and vice versa. Out of the 5 embryos with a heart edema, 2 also displayed an ear phenotype at 72 hpf, while 3 had a wild-type ear from 72 hpf. The morphology of the cartilage of the jaw and the gill cover seemed slightly altered in the embryos with heart or ear defects (Figure 3.7Ciii,iv).

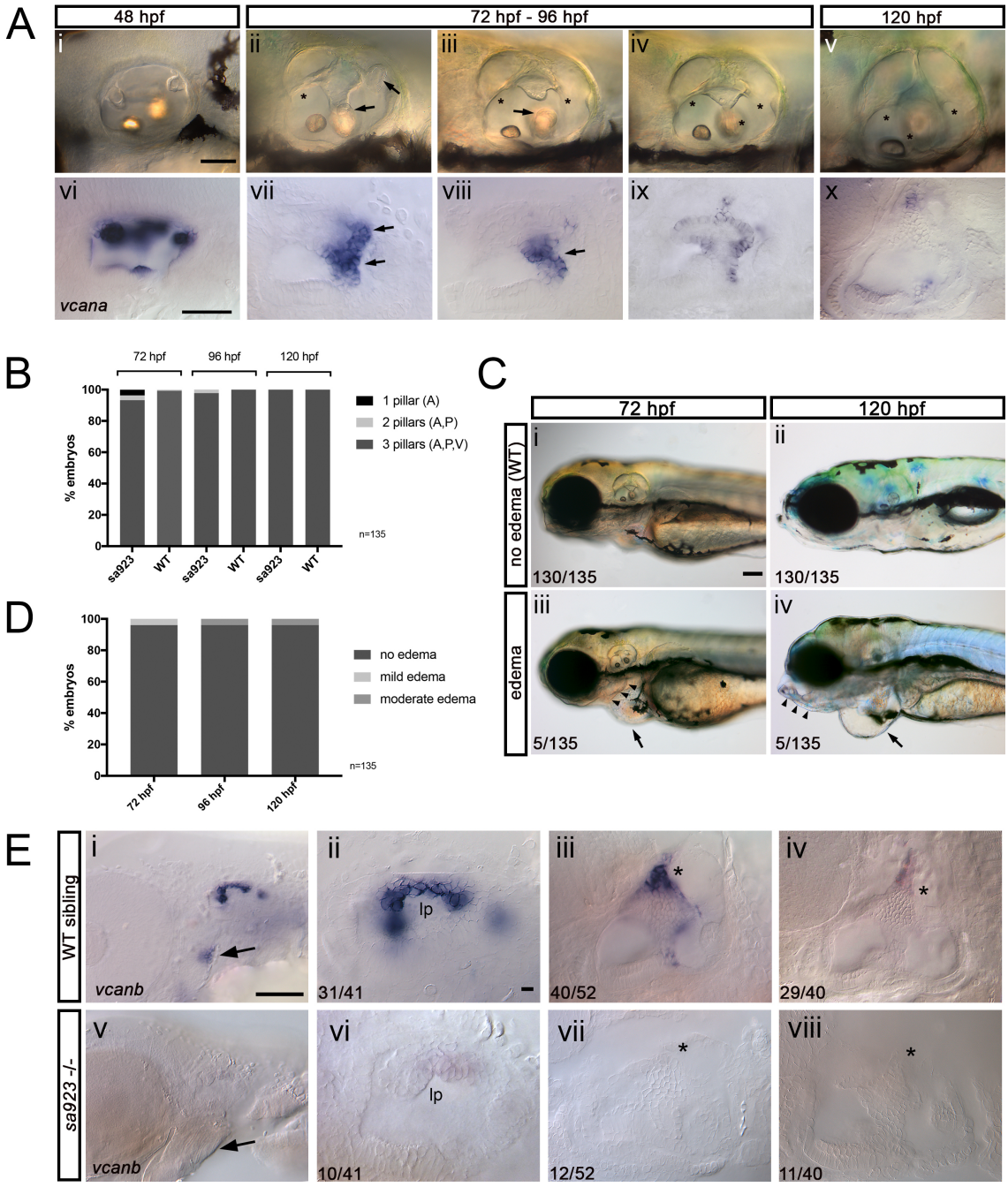

Figure 3.7 The *vcanb*^{sa923} mutant phenotype is incompletely penetrant. (A,B) Images and graphical representation of the inner ear phenotype of embryos from *vcanb*^{sa923} heterozygous crosses from 48 hpf to120 hpf. **(Ai-v)** Live images showing fused (asterisk) and unfused (arrows) epithelial projections of the inner ear. **(Avi-x)** Corresponding *vcana* mRNA expression showing persisting staining in the unfused projections (arrows). **(C,D)** Live images and graphical representation of the heart phenotype of the same embryos from 72 hpf to 120 hpf. Note the pericardial edema (arrows in Ciii,iv) and the altered morphology of the facial skeleton (arrowheads in Ciii,iv). **(E)** *vcanb* mRNA expression at 48 hpf (i,ii,v,vi), 72 hpf (iii,vii) and 120 hpf (iv,viii) was missing from the epithelial projections, the DLS (asterisks) and the opercle (arrows) of *vcanb*^{sa923} homozygous mutants. Abbreviations: lp, lateral projection. Scale bars: in Ai, 50 µm for Aii-v; in Avi, 50 µm for Avii-x; in Ci, 100 µm for Cii-iv; in Ei, 100 µm for Ev; in Eii, 10 µm for Eiii,iv, vi,vii,viii.

3.2.5 *Versican a* and *b* double mutant phenotype

As the mutant ear phenotype of *vcana*^{sa1460} and *vcanb*^{sa923} single mutants was incompletely penetrant and rescued by day 5, I wanted to investigate whether *vcana*^{sa1460}*;vcanb*^{sa923} double mutants (from now on *sa1460;sa923*) would show a more severe ear phenotype. *Sa1460*+/-;*sa923*+/- mutants were generated by outcrossing *vcana*^{sa1460} with *vcanb*^{sa923} heterozygous mutants. The offspring were raised and adults were genotyped by fin clip to identify *sa1460;sa923* double heterozygous fish.

Sa1460;sa923 double heterozygous fish were pair-mated and the offspring phenotype was recorded for the first 5 days of development. The phenotype of the offspring coming from five independent heterozygous crosses are summarised in Figure 3.8. According to the Mendelian law of independent assortment, the predicted ratio for a double homozygous genotype is 1 in 16 (6.25%), while the predicted ratios for single *vcana* or *vcanb* homozygotes are both 3 in 16 (18.75%) (Figure 3.8B). Until 72 hpf, no developmental defects or abnormalities were observed and the embryos looked healthy. At 72 hpf, a delay in the formation of the pillars was recorded in 37 (20.4%) out of the 181 embryos from the *sa1460;sa923* cross (Figure 3.8B). This number included 19 embryos (10.5%) that had not fused the ventral projection and 18 embryos (9.9%) that had not fused neither the ventral nor the posterior projection (Figure 3.8Aii,iii). At the same timepoint, all LWT wild-type embryos had a fused posterior pillar and only 2/181 (1.1%) had not fused the ventral projection. At 4 dpf, all LWT embryos had formed all three pillars, 14 (7.7%) of the embryos from the *sa1460;sa923* cross were found to have both the ventral and the posterior projections unfused and 12 (6.6%) had not completed the fusion of the ventral projection (Figure 3.8B). At 5 dpf, the pillar defects persisted in 8 (4.4%) of the *sa1460;sa923* embryos. Genotyping 4 of the embryos with persistent ear defects showed that 2 were double homozygous (aabb) and 2 were homozygous for *vcana* and heterozygous for *vcanb* (aaBb), suggesting that loss of *vcana* function can cause fusion delays that persist until day 5, when *vcanb* is completely missing (bb) or exists in a lower gene dose (Bb) (Figure 3.8F). On the other hand, none of the 4 *vcanb* single homozygous mutants (Aabb or AAbb) genotyped displayed any ear defects at 5 dpf.

Some of the embryos from the same *sa1460;sa923* double heterozygous cross were also characterised by pericardial edema of variable severity, ranging from mild to severe (Figure 3.8C). Around 23-30% of the embryos developed a heart edema from 72-120 hpf. More specifically, 44 (19.7%) out of the 223 embryos observed were recorded to have a mild pericardial edema and 25 (11.2%) had a severe edema at 72 hpf (Figure 3.8D). The

number of embryos with a severe edema increased to 37 (16.6%) at 5 dpf. However, not all the embryos with a pericardial edema had an ear phenotype and vice versa (Figure 3.8E).

3 out of the 4 genotyped *vcanb* single homozygous mutants (Aabb or AAbb) had a wild-type phenotype and only 1 (Aabb) showed an altered morphology of the facial skeleton (Figure 3.8Ciii,iv and F). The phenotype of the 2 genotyped double heterozygous mutants was normal (Figure 3.8Ci,ii and F).

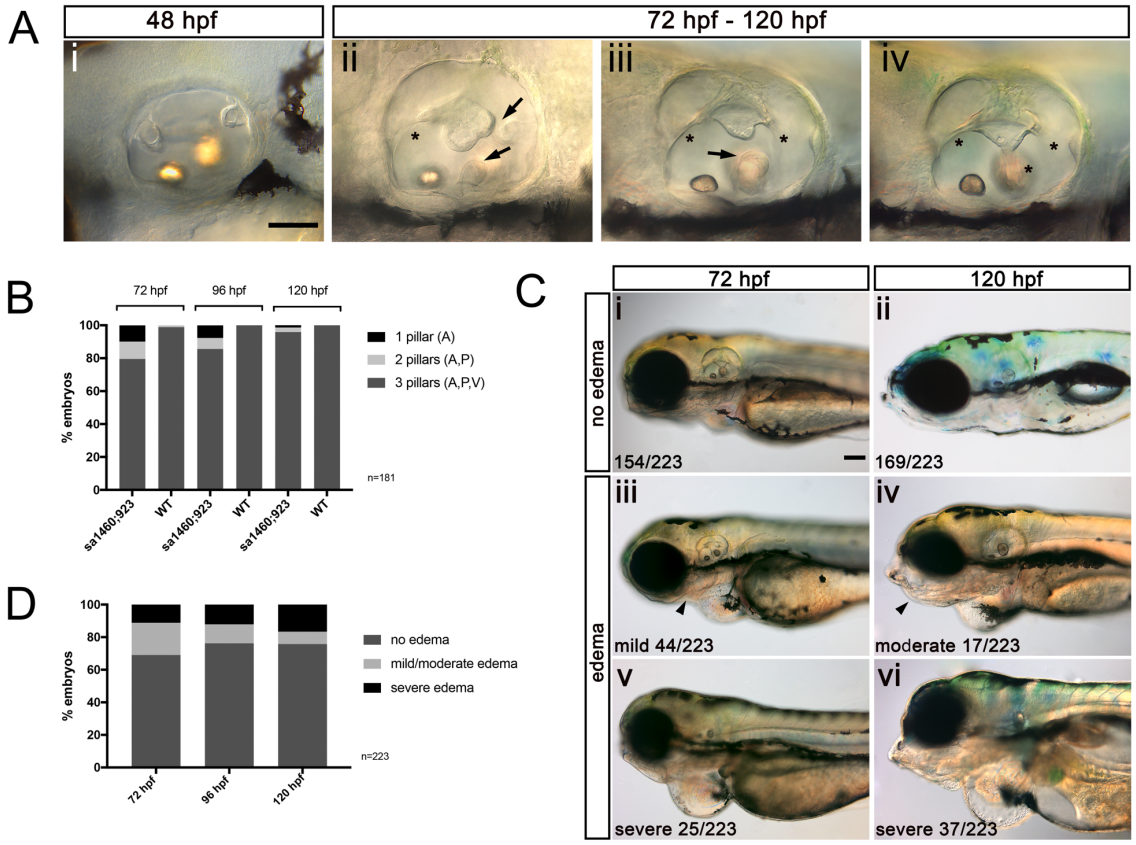

F

Genotype	Expected ratio	Number of genotyped embryos	Phenotype at 5 dpf
double homs (aabb)	6.25%	4	1 WT, 1 edema only, 1 ear defects only, 1 ear defects and edema
single a homs (aaB_)	18.75%	2 (aaBb)	ear defects only
single b homs (A_bb)	18.75%	3 (Aabb) 1 (AAbb)	2 WT, 1 jaw defects WT
double hets (AaBb)	25%	2	WT
single a hets (AaBB)	12.25%	1	WT
single b hets (AABb)	12.25%	0	-
WT (AABB)	6.25%	0	-

Figure 3.8 *Sa1460;sa923* double homozygous mutant phenotype is variable. (A,B) Images and graphical representation of the inner ear phenotype of embryos coming from *sa1460;sa923* double heterozygous crosses from 48 hpf to120 hpf. **(Ai-iv)** Live images showing fused (asterisk) and unfused (arrows) epithelial projections of the inner ear. **(C,D)** Live images and graphical representation of the heart phenotype of the same embryos from 72 hpf to 120 hpf. The pericardial edema (arrows) varied from mild to severe. **(E)** Pie chart and table showing the coincidence of the ear and heart phenotype. **(F)** Table showing the predicted genotype ratios from a double heterozygous incross, as well as the corresponding phenotypes of the genotyped embryos. Abbreviations: a and A, *vcana;* b and B, *vcanb;* WT, wild type. Scale bars: in Ai, 50 µm for Aii-iv; in Ci, 100 µm for Ciii,vi.

3.3 DISCUSSION

In this chapter, I presented the wild-type expression of *vcana* and *vcanb* genes during the first five days of zebrafish development and annotated the regions of expression. Consistent with previous data, the *versican* expression pattern during the early stages of development was highly dynamic and changed rapidly (Thisse et al., 2001, ZFIN, direct data submission). Both genes were expressed in the developing heart tube from 20 hpf. *Vcana* expression was present in the atrium (26 hpf) and the AV boundary (48 hpf), as shown previously (Garrity et al., 2002), whereas *vcanb* was shown to be expressed in the migrating cells of the second heart field (26 hpf) and was no longer detectable in this tissue at 48 hpf. Both genes were expressed in the opercle, but *vcana* expression was considerably weaker in this tissue and only present at 48 hpf, whereas the *vcanb* zone of expression in the opercle was wider, stronger and lasted for longer (Kang et al., 2004). In addition, I have shown for the first time that *vcanb* is also expressed in the anterior end of the basihyal cartilage. The expression pattern in the inner ear is the same for both genes. Consistent with previous data, expression of both genes begins in the epithelial projections of the otic vesicle from 45 hpf, reaching maximum levels of expression at 50 hpf, and decreasing after 72 hpf, until only a trace of expression is present in the DLS after 4 dpf (Geng et al., 2013). In addition to this, I have shown that both genes are also expressed at the apical surface of the anterior macula of the inner ear.

In this chapter, I have also shown that *vcana* (*sa1460*) and *vcanb* (*sa923*) single and double mutant phenotypes did not follow the classic Mendelian ratios, but were characterised by some variable, incompletely penetrant defects in the heart and the inner ear. The ear phenotype exhibited by some of the *vcana*^{sa1460} and *vcanb*^{sa923} homozygous mutants was the same; epithelial projections delayed to elongate sufficiently to permit fusion and pillar formation in the otic lumen at 72 hpf. However, the percentage of *vcana*^{sa1460} embryos with fusion delays at 72 hpf was three-fold higher compared to the one observed in *vcanb*^{sa923} mutants at the same stage. Time-lapse light-sheet microscopy over the critical window between 57-72 hpf could provide valuable information regarding the time point at which the delay in the projection elongation starts being apparent in the mutant ear. In addition, it could be used to investigate whether homozygous mutant embryos with a wild-type ear morphology at 72 hpf exhibited a short-frame delay in projection elongation at an earlier timepoint between 57-72 hpf.

Both *vcana*^{sa1460} and *vcanb*^{sa923} single mutants managed to restore the fusion delays before 5 dpf. The fact that *vcana* expression persisted in the unfused projections of *vcanb*^{sa923}

mutants and *vcanb* expression persisted in the unfused projections of *vcana*^{sa1460} mutants suggests that *vcana* possibly compensates for the loss of *vcanb* and vice versa. The fact that fusion delays persisted until day 5 in double homozygotes and in *vcana*^{sa1460} homozygotes which were heterozygous for *vcanb*^{sa923}, but not in *vcana*^{sa1460} homozygotes with two wild-type *vcanb*^{sa923} copies, suggests that the ear phenotype can be affected by the gene dosage of *versican* genes.

Similarly to zebrafish *vcana* morphants (Janina Müller-Deilea et al., 2016), *ugdh* (*jekyll*) mutants (Walsh and Stainier, 2001), and *cspg2* (*hdf)* mouse mutants (Mjaatvedt et al., 1998), a pericardial edema of varying severity was also observed in *vcanb*^{sa923} and *vcana*^{sa1460} mutants. Evidently, the *vcana*^{sa1460} mutant phenotype had a much higher penetration in the heart than *vcanb*^{sa923}, as the proportion of *vcana*^{sa1460} embryos with a pericardial edema was five-fold higher compared to *vcanb*^{sa923} and the severity of these edemas was greater as well. In the previously published cases above, the heart edema in *vcana* morphants had been attributed to proteinuria (Janina Müller-Deilea et al., 2016), whereas the edema in *ugdh* and *hdf* mutants to the failure of endothelial cells to cluster and form the AV boundary (Mjaatvedt et al., 1998; Walsh and Stainier, 2001). Further investigation is required to unravel the aetiology of the heart edema observed in *vcana*^{sa1460} mutants (eg. by studying the gene expression of other AV canal markers).

Apart from the ear and heart defects, *vcanb*^{sa923} homozygous mutants, but not *vcana*^{sa1460} mutants, exhibited an altered morphology of the facial skeleton, including the opercle. This craniofacial phenotype is similar to one observed in *vcanb* morphants (Kang et al., 2004), where the jaw, dentary, opercle, and branchiostegal ray were either malformed or absent and showed decreased ossification at later stages. Although further investigation (eg. alcian blue staining) is needed to annotate the specific regions affected by the mutation, these preliminary data further support the previously reported theory that *vcanb* plays a role in the formation of some of the facial skeleton elements (Kang et al., 2004).

The fact that the phenotype of genotyped *sa1460;sa923* double homozygous mutants included embryos with fusion problems at 5 dpf (with or without a heart edema), as well as two embryos with a fully wild-type ear, could mean that other extracellular matrix components in the inner ear can compensate for the loss of *vcana* and *vcanb.* One such candidate could be a newly identified and poorly characterised gene, *similar to versican b* (*s-vcanb)*, which follows the same expression pattern as *vcan* genes. *s-vcanb* is expressed in the AV canal of the heart, the epithelial projections of the inner ear, the opercle and the lens (Lee et al., 2015). Alternatively, other CS- or HS- containing ECM molecules might

constitute a compensatory network when *versican* expression is lost. In the next chapter, the role of the HSPGs in the formation of the epithelial pillars is discussed. Another reason why *versican* single and double mutants did not show a fully penetrant phenotype might be the numerous differential splicing sites of the *versican* genes, which might lead to 'skipping' of the mutated exon, particularly in the case of *vcana,* whose expression was not completely absent from every *vcana*^{sa1460} homozygous mutant. To circumvent this possibility, a mutation affecting the 3'-UTR region of the *vcana* mRNA transcript or a deletion mutation (eg. by using CRISPR/Cas9 CHOPCHOP technology) could be used (Montague et al., 2014).

Although there is no reference to any ear phenotypes in *ugdh* mutants, live images of 72 hpf *ugdh* homozygous mutant embryos display a very similar ear phenotype with the one observed in *versican* mutants, where projections fail to reach one another and fuse to form pillars (Walsh and Stainier, 2001). On the other hand, in *adgrg6* zebrafish mutants, where epithelial projections grow past one another without fusing, *versican* expression abnormally persists until day 5 (Geng et al., 2013). In order to investigate whether *versican* overexpression is causative for the *adgrg6* ear phenotype, triple *vcana*;*vcanb*;*adgrg6* mutants could be generated or *vcana;vcanb* double mutants could be injected with *adgrg6* morpholinos. These previous data in conjunction with my findings, suggest that *versican* genes facilitate the outgrowth and elongation of the epithelial projections, which is a prerequisite for the fusion event that takes place between 66 hpf and 70 hpf and leads to semicircular canal formation.

3.4 CONCLUSIONS

- *Vcana* and *b* are both expressed in the inner ear, the heart and the gill cover.
- The otic expression pattern of both genes is the same; they are strongly expressed in the developing epithelial projections from 48 hpf and get down-regulated at 72 hpf, when the projections have fused to form pillars of epithelium that form the semicircular canal hubs.
- *vcana*^{sa1460} and *vcanb*^{sa923} single mutant phenotypes did not follow the classic Mendelian ratios, but were characterised by some incompletely penetrant defects in the heart and the inner ear.
- In some single homozygous mutant ears, a delay in projection elongation and fusion was observed between 72 and 96 hpf. This phenotype was always rescued before 5 dpf in single mutants, but persisted in some double homozygous mutants.

- *vcana*^{sa1460} mutant phenotype exhibited higher penetration compared to *vcanb*^{sa923}.
- *versican* genes facilitate the outgrowth and elongation of the epithelial projections, which is a prerequisite for the fusion event that leads to semicircular canal formation.
- The incomplete penetrance of the *versican* mutant phenotype might be due to a compensatory network of other ECM molecules that is activated when *versican* genes are mutated.

CHAPTER 4.

The role of heparan sulphate proteoglycans in the zebrafish inner ear development

4.1 INTRODUCTION

HSPGs are cell surface mediators of receptor-ligand interactions required for the signal transduction of major pathways, like FGF, Wnt, Shh, Notch and BMP, controlling the development of sensory and non-sensory epithelial structures of the inner ear in vertebrates (Freeman et al., 2015). HS sulphation levels have been reported to be important in avian and murine inner ear development, while the HSPGs *syndecan2 (sdc2)* , *glypican1a and glypican4* (*gpc1a, gpc4)* are known to be expressed in the developing zebrafish inner ear (Thisse et al., 2001 [ZFIN directy submitted data]; Freeman et al., 2015; Sisson et al., 2015). However, their exact role in the formation of this tissue is not understood. The *ext2* gene encodes a glycosyltransferase essential for HS biosynthesis and is abundantly expressed during the first three days of zebrafish development, in regions including the retina, the brain, the branchial arches and the pectoral fins (Lee et al., 2004). *ext2 to273b* is a nonsense mutant allele and in zebrafish *ext2*^{to273b} *(dackel/dak*^{to273b}*)* homozygous mutants, heparan sulphate proteoglycan (HSPG) levels are known to be lower than half of the normal, leading to numerous developmental defects (Lee et al., 2004). As HS are essential for cartilage morphogenesis, zebrafish *dak*^{to273b} homozygous mutant larvae have been reported to show cartilage defects that resemble those seen in Hereditary Multiple Exostoses (HME) patients (Van Eeden et al., 1996; Clément et al., 2008). In both cases, chondrocytes differentiate normally, but fail to flatten and stack into columns, resulting in cartilage elements that are shorter and thicker compared to the wild-types (Clément et al., 2008). In addition, the ossification is reduced in both dermal and cartilage bones of *dak*$^{to273b-/-}$ mutants (Clément et al., 2008). Apart from the above malformations, it has been reported that the retinal ganglion cell axons fail to sort properly in the optic tract (Lee et al., 2004), while a mild lateral line phenotype has also been recorded. The collective migration speed of the primordium that deposits the neuromasts of the lateral line is reduced after 40 hpf, resulting in neuromasts placed

closely together (Venero Galanternik et al., 2015). This phenotype was attributed to reduced FGF signalling, which caused an ectopic expansion of the Wnt/β-catenin pathway activation zone in the lateral line (Venero Galanternik et al., 2015).

In addition, *dak*^{to273b} homozygous mutants do not form functional pectoral fin buds and the ear has been characterised as retarded, with no clear internal structures (Van Eeden et al., 1996; Whitfield et al., 1996). Apart from these statements, there has not been a comprehensive study of the *dak*^{to273b} ear phenotype. In this chapter, I aim to describe the *dak*^{to273b} mutant ear phenotype and study how the expression of important otic markers is affected in these mutants.

4.2 RESULTS

4.2.1 Epithelial projections in the *dak*$^{to273b-/-}$ mutant ear stay small and do not fuse

Phenotypic analysis of live *dak*^{to273b} zebrafish mutants, confirmed that the homozygous mutants do not form pectoral fin buds (Figure 4.1A, B; Van Eeden et al., 1996) and that the morphology of the cartilage of the jaw is malformed (Figure 4.1C,D,G,H; Clément et al., 2008). I show for the first time, that all homozygous *dak*^{to273b} mutants also exhibited a mild heart edema, which started to appear from 48 hpf (Figure 4.1B,D,H).

In addition, it is demonstrated for the first time that *dak*^{to273b} -/- mutants do not form pillars, as the epithelial projections do not sufficiently elongate to meet and fuse (Figure 4.1D',F',H'). It was typically observed that the projections grow at a slower rate compared to the wild-types until 72 hpf, after which they do not appear to grow any further. The lateral projection did form an anterior bulge, but did not appear to form distinguishable posterior or ventral bulges (Figure 4.1F'). The otic vesicle was slightly smaller and had a rounded, swollen morphology compared to the wild-type (Figure 4.1G',H'). The otolith size, particularly the size of the saccular otoliths, appeared smaller compared to the controls at 72 hpf, with the size difference enhanced between 4 and 5 dpf (Figure 4.1E',F' and G,H). In addition, the saccular otolith appeared misplaced in *dak*^{to273b} -/- mutants of age between 72 hpf and 5 dpf (Figure 4.1G,H), indicative of defective tethering on the corresponding hair-cell patch (posterior sensory macula).

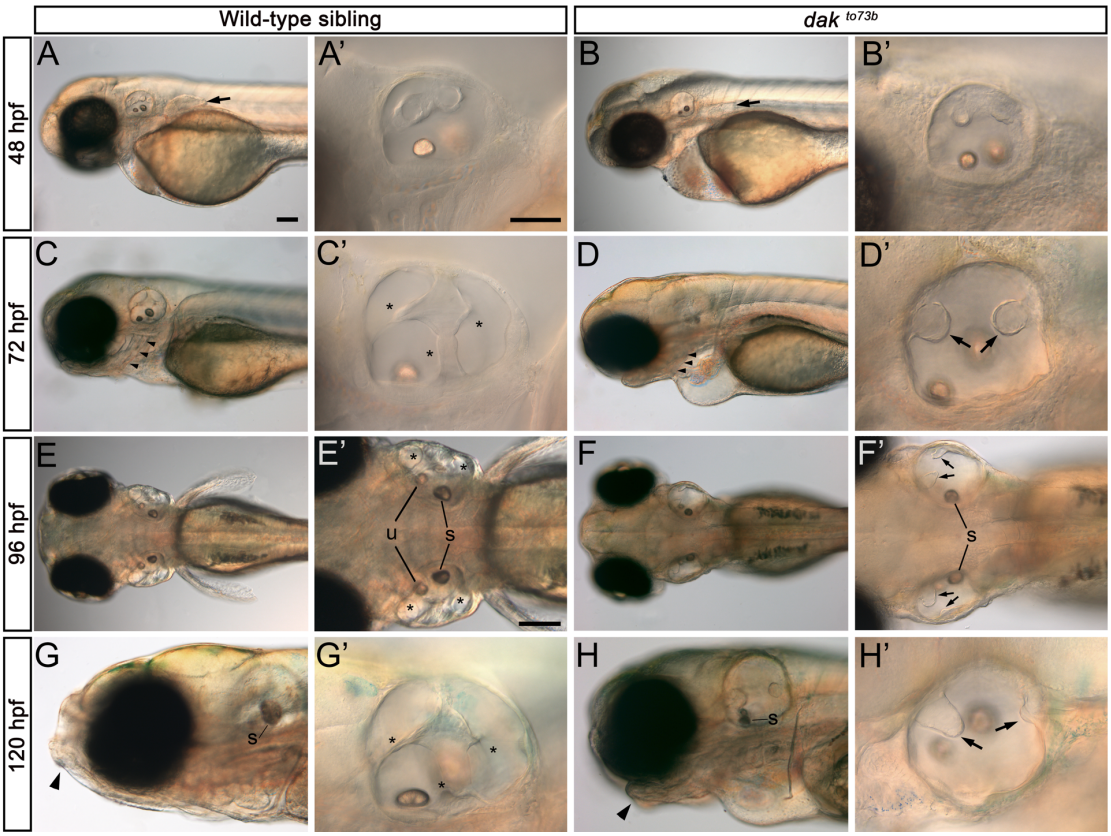

Figure 4.1 The *dak*^{to273b} mutant phenotype is characterised by inner ear defects. (A,B) Live DIC images of a wild-type (A) and *dak*^{to273b} homozygous sibling (B) at 48 hpf. Note the absence of the pectoral fin bud (arrows in A and B). **(A',B')** Magnified images of the otic vesicle of the fish depicted in A and B, respectively. **(C,D)** Live DIC images of a wild-type (C) and *dak*^{to273b} homozygous sibling (D) at 72 hpf. Note the altered morphology of the facial skeleton (arrowheads in C,D,G and H). **(C',D')** Magnified images of the otic vesicle of the fish depicted in C and D, respectively. At 72 hpf, the epithelial projections have fused and formed pillars in the WT (asterisks in C' and G'), whereas in the *dak*^{to273b} mutant ear, the projections stayed small and did not fuse (arrows in D',F' and H'). **(E,F)** Dorsal DIC images of a wild-type (E) and *dak*^{to273b} homozygous sibling (F) at 96 hpf. **(E',F')** Magnified images of the fish depicted in C and D, respectively, showing the utricular (u) and saccular otoliths (s). **(G,H)** Lateral DIC images of a wild-type (G) and *dak*^{to273b} homozygous sibling (H) at 120 hpf. Note the difference in size and position of the saccular otolith (s). **(G',H')** Magnified images of the otic vesicle at 120 hpf. Asterisks mark fused pillars; arrows mark unfused projections. In all panels, anterior is to the left. Abbreviations: u, utricular otolith; s, saccular otolith. Scale bars: in A, 100 μm for B,C,D,E,F,G,H; in A', 50 μm for B',C',D',G',H'; in E', 100 μm for F'.

4.2.2 Saccular otoliths are not properly tethered on the posterior macula of the *dak*$^{to273b-/-}$ mutant ear

In order to test whether otoliths are properly tethered on the macula in the *dak*$^{to273b-/-}$ mutant ear, I performed a simple tapping experiment (Stooke-Vaughan et al., 2015); anaesthetised 5 dpf *dak*$^{to273b-/-}$ mutants (n=8) and wild-type siblings (n=8) were individually mounted in 4% methylcellulose on a slide covered with a coverslip and the slide was gently tapped on the benchtop for 10 seconds. Pictures of the ear were taken before and after tapping. In the wild-type ear, none of the otoliths were displaced after tapping (8/8), while in 7 out of *dak*$^{to273b-/-}$ mutants, one or both saccular otoliths were displaced after tapping (Figure 4.2). Contrary to the saccular otolith, the utricular one did not appear misplaced in any of the mutants that were tapped. Interestingly, when the same experiment was repeated at 28 hpf and 50 hpf, using 5 *dak*$^{to273b-/-}$ mutants and 5 wild-type siblings per stage, none of the samples appeared to have any displaced otoliths after tapping (data not shown). These data strongly suggest that the saccular otoliths, although initially tethered on the macula, lose complete adherence between 72 hpf and 5 dpf in the *dak*^{to273b} mutant ear. This could be attributed to either the hair cells of the macula being absent/defective or to defective otolith features.

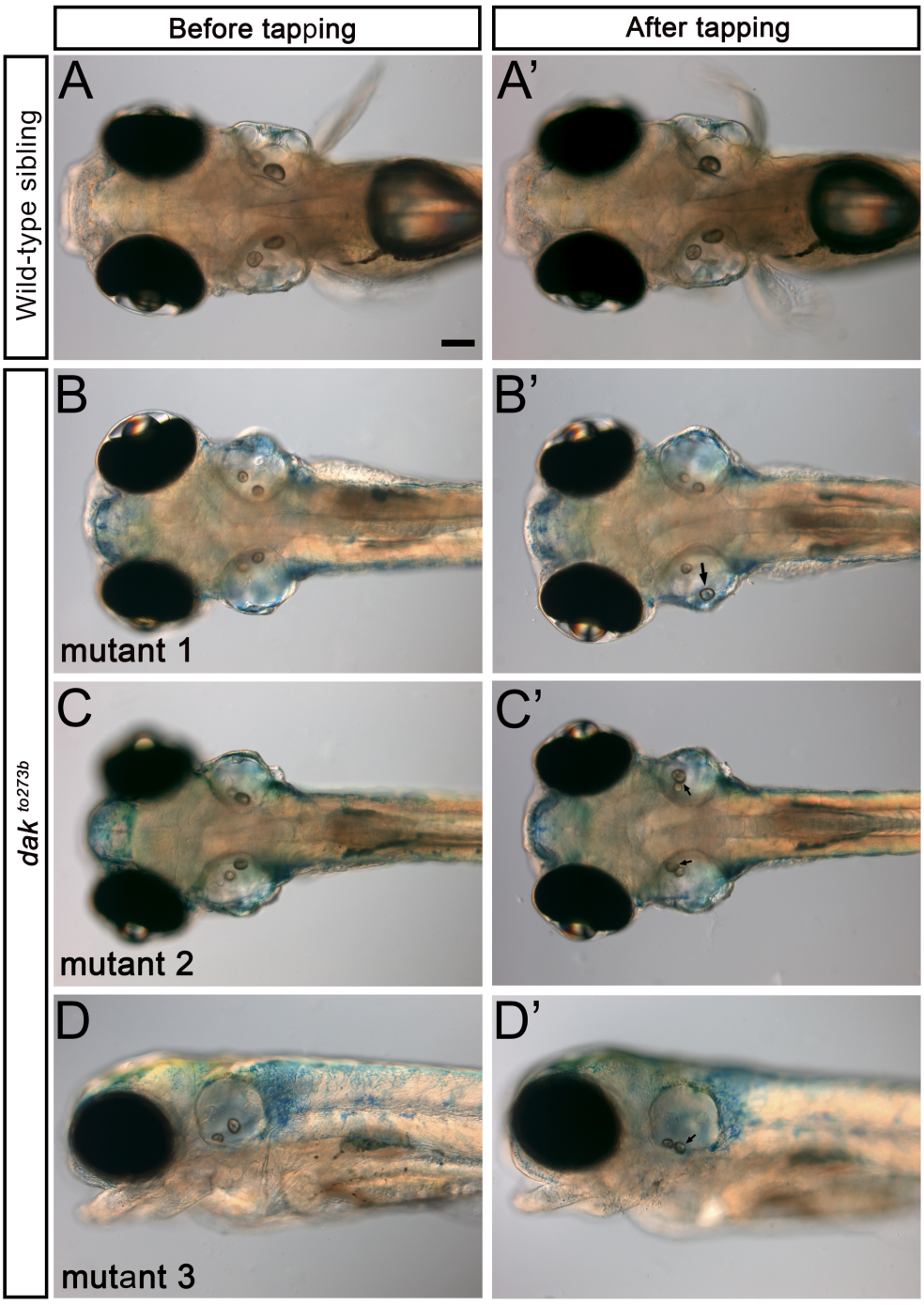

Figure 4.2 Saccular otoliths are not properly tethered in the homozygous *dak*^{to273b} mutant ear at 5 dpf. Live DIC images of a wild-type **(A,A')** and three homozygous *dak*^{to273b} siblings **(B-D')** at 5 dpf, before (left panels) and after (right panels) tapping. Arrows indicate displaced otoliths after tapping. A-C' are dorsal views; D,D' are lateral views. In all panels, anterior is to the left. Scale bars: in A, 100 μm for all panels.

4.2.3 Improper otolith tethering in *dak*^{to273b} mutants is due to the otolithic membrane lacking *otogelin*

According to the two-stage model for otolith seeding proposed by Stooke-Vaughan et al. (2015), the initial seeding step takes place around 18-22 hpf, during which otolith precursors tether to the hair cell kinocilia (Riley et al., 1997). In order to check whether the tethering defects in *dak*^{to273b} mutants were due to lack of the first sensory hair cells (tether cells), I used the expression of *myosin VIIa* (*myo7aa*), which marks differentiated tether cells. No difference was found between 23 hpf *dak*^{to273b} and sibling embryos, suggesting that the failure in otolith seeding cannot be attributed to hair cell loss (Figure 4.3G,G').

The first tethering step is followed by a second step that occurs in later developmental stages, which maintains the adhesion of the otolith to the macula during otolith growth and biomineralisation. This second step is achieved by the formation of the otolithic membrane, an ECM bed that couples the otolith to the sensory macula (Dunkelberger et al., 1980). In order to investigate whether the improper otolith tethering in *dak*^{to273b} mutants is due to otolithic membrane defects, I used the otolithic membrane markers *α-tectorin* (*tecta*) and *otogelin* (*otog*) (Stooke-Vaughan et al., 2015). Although *tecta* mRNA expression appeared normal in the *dak*^{to273b} mutant ear (Figure 4.3I-J'), *otog* expression was found significantly reduced on the anterior (utricular) macula at 24 hpf and was completely missing from the posterior (saccular) macula from 72-120 hpf (Figure 4.3C-F'). The *otog* expression in the three cristae was also reduced (Figure 4.3E,E').

As the otoliths in the *dak*^{to273b} mutant ear appeared smaller, I wanted to investigate the expression of *otolith matrix protein* (*otomp*), the loss of which has been linked with slowed otolith growth (Murayama et al., 2005). Evidently, *otomp* expression was found significantly reduced from both the anterior and the posterior maculae (Figure 4.3A-B'). In addition, the expression levels of *starmaker* (*stm*), which are known to control the shape and morphology of the otoliths (Söllner, 2003), were also reduced, particularly from the posterior macula.

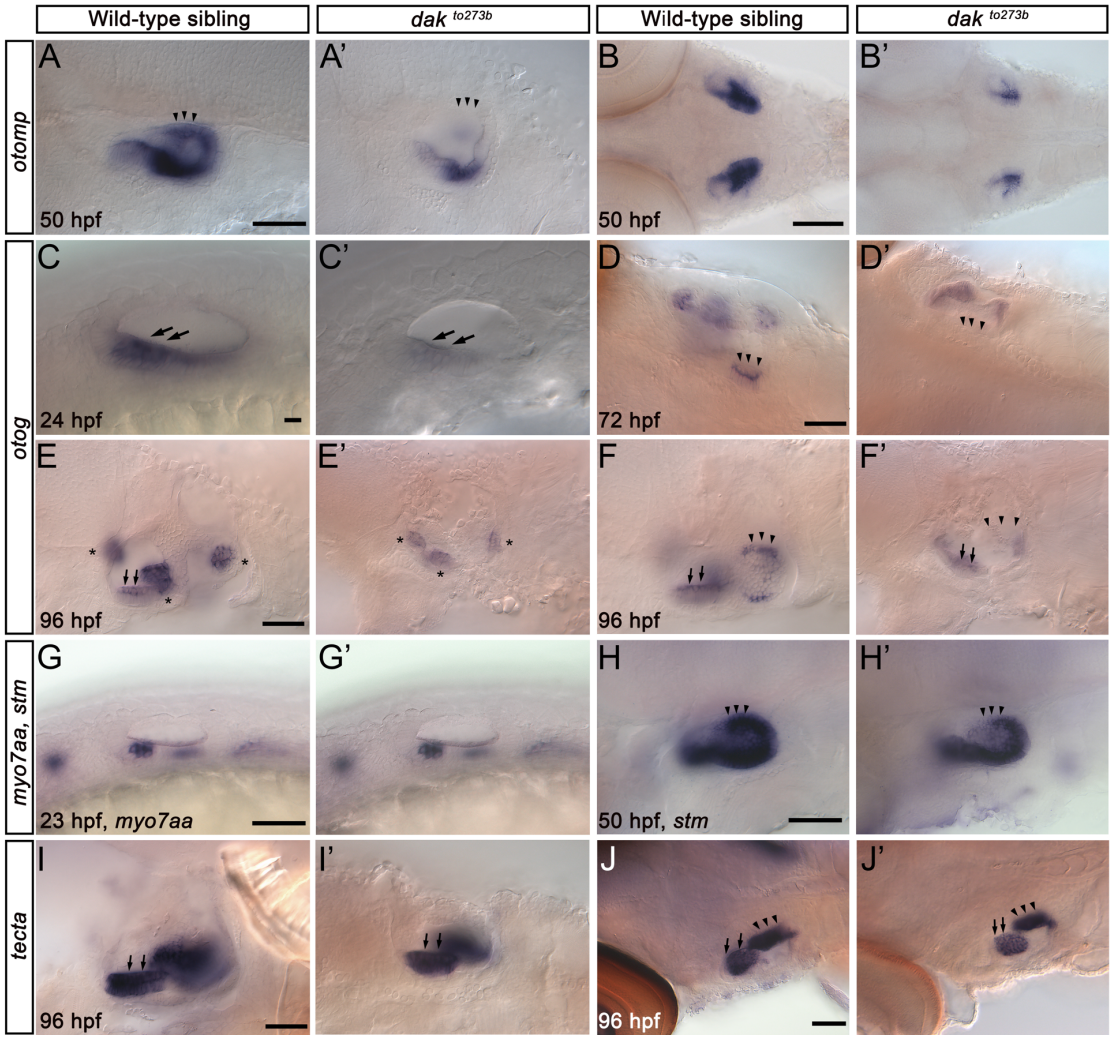

Figure 4.3 Expression of *otomp*, *otog* and *stm* is reduced from the saccular macula in the *dak*^{to273b} mutant ear. (A-B') *otomp* expression in the *dak*^{to273b} mutant ear (A',B') at 50 hpf was lower compared to the wild-type (A,B). **(C-F')** *otog* expression at 24 hpf (C,C'), 72 hpf (D,D') and 96 hpf (E-F') was significantly reduced in the *dak*^{to273b} mutant ear. F and F' are different focal planes of the same ear depicted in E and E', respectively. **(G,G')** *myo7aa* expression at 23 hpf was not altered in *dak*^{to273b} mutants. **(H,H')** *stm* expression at 50 hpf was reduced in the posterior macula (arrowheads) of the *dak*^{to273b} mutant ear. **(I-J')** *tecta* expression was unaltered at 96 hpf. Arrowheads mark the posterior (saccular) macula; arrows mark the anterior (utricular) macula; asterisks mark the cristae. B,B',D,D',J and J' are dorsal views. In all panels, anterior is to the left. Scale bars: in A, 50 µm for A'; in B, 100 µm for B'; in C, 10 µm for C'; in D, 50 µm for D'; in E, 50 µm for E'-F'; in G, 50 µm for G'; in H, 50 µm for H'; in I, 50 µm for I'; in J, 50 µm for J'. Data representative of two individual experiments; in each experiment 50 embryos for each of the embryonic stages shown were analysed per gene.

4.2.4 *Versican* mRNA expression abnormally persists in the unfused projections in the *dak*^{to273b} mutant ear, while *adgrg6* shows ectopic expression

As CS have been previously suggested to be up-regulated under circumstances where HS is low (Holmborn et al., 2012), I wanted to investigate whether *versican* levels would be higher in *dak*^{to273b} mutants. *In situ* hybridisation results showed that in *dak*$^{to273b-/-}$ mutants, *versican* genes follow a normal expression pattern until 50 hpf (data not shown). At 50 hpf, the *vcanb* fin expression was absent due to the tissue missing (Figure4.4A,A'). At the same stage, otic *vcanb* and *vcana* mRNA expression levels were both lower in all *dak*^{to273b} mutants tested (26/26), possibly due to the slower rate of projection outgrowth compared to the wild-types (Figure 4.4A,A'). However, abnormally high *vcana* and *vcanb* expression persisted on the unfused epithelial projections from 72 until 120 hpf (Figure 4.4D,D',E,E'). In addition, *vcana* and *vcanb* expression abnormally persisted on the anterior macula until 72 hpf, when the hair cells appeared disorganised compared to the wild-type (Figure 4.4D,D'). *vcana* and *vcanb* expression also marked the dorsolateral septum, which seemed to develop relatively normally (Figure 4.4C',E'). Expression of *vcanb* in the opercle was considerably reduced in *dak*$^{to273b-/-}$ mutants, possibly because part of the structure was missing or malformed (Figure 4.4B,B').

adgrg6 is another semicircular canal marker that also persisted on the unfused projections of all *dak*^{to273b} mutants tested between 72 and 120 hpf (79/79; Figure 4.5B',E'). Interestingly, *adgrg6* consistently showed a very strong ectopic expression in a zone presumed to be the cerebral vein from 96 to 120 hpf (53/53; Figure 4.5A',B',D'). *adgrg6* expression in the central zone of the olfactory epithelium was narrower in *dak*^{to273b} mutants and the morphology of the epithelium appeared subtly altered (Figure 4.5B,B'). In addition, *adgrg6* expression in the Schwann cells of the lateral line appeared stronger in 96 hpf *dak*^{to273b} mutants (26/26; Figure 4.5C,C').

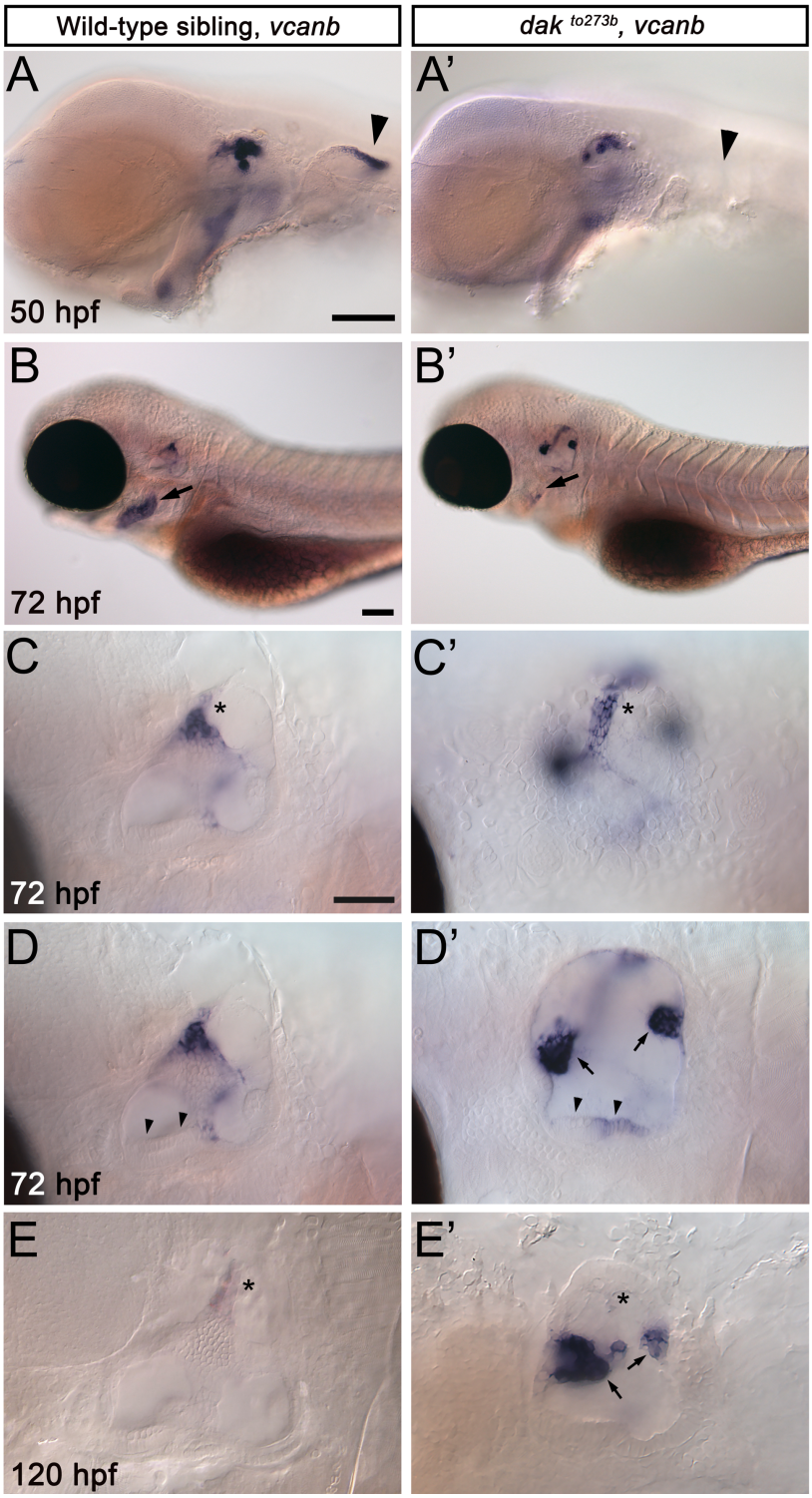

Figure 4.4 Expression of *versican* abnormally persists on the unfused projections of *dak*^{to273b} mutants. (A,A') Expression of *vcanb* in wild-type and *dak*^{to273b} mutant siblings at 50 hpf. As the pectoral fins are absent from *dak*^{to273b} mutants, *vcanb* expression is missing (arrowheads in A,A'). **(B,B')** At 72 hpf, *vcanb* expression is strongly reduced from the opercle (arrows in B,B'), **(C,C')** *Vcanb* is expressed normally on the dorsolateral septum (asterisk), but stays up-regulated on the unfused projections (arrows in D',E') and the anterior macula (arrowheads in D') of the *dak*^{to273b} mutant ear. **(D,D')** Different focal planes of the otic vesicle shown in C and C', respectively. **(E,E')** *vcanb* expression abnormally persists on the unfused projections until 120 hpf. Asterisks mark the dorsolateral septum. Scale bars: in A, 100 µm for A'; in B, 100 µm for B'; in C, 50 µm for C'-E'. Data representative of two individual experiments, each analysing 50 embryos per embryonic stage.

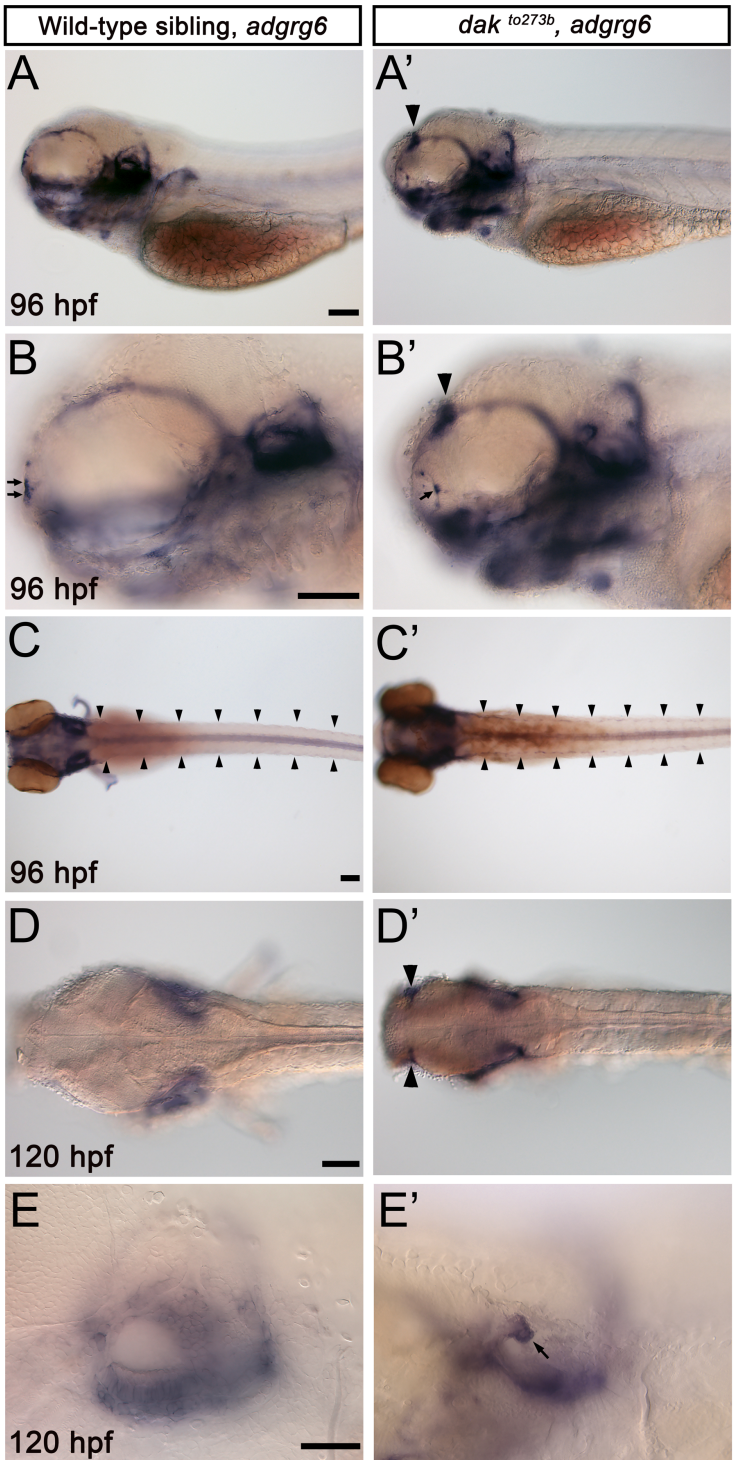

Figure 4.5 *adgrg6* shows ectopic expression in *dak*^{to273b} mutants (A,A') From 96 hpf, *adgrg6* shows ectopic expression at the cerebral vein (arrowheads in A' and B'). **(B,B')** Magnified images of the fish depicted in A and A', respectively, showing that the zone of *adgrg6* expression in the olfactory epithelium of *dak*^{to273b} mutants (arrow in B') is narrower compared to the wild type (arrows in B). **(C,C')** Dorsal images showing *adgrg6* expression in the lateral line of wild-type and *dak*^{to273b} mutants at 96 hpf. **(D,D')**Dorsal and **(E,E')** lateral images of wild-type and *dak*^{to273b} mutants at 120 hpf, showing that the *adgrg6* ectopic expression and the expression on the unfused projections persists until 120 hpf. Scale bars: in A, 100 µm for A'; in B, 100 µm for B'; in C, 100 µm for C'; in D, 100 µm for D'; in E, 50 µm for E'. Data representative of two individual experiments, each analysing 50 embryos per embryonic stage.

4.3 DISCUSSION

The observations I have made in this chapter confirm previously reported data on the defects of the *dak*^{to273b} mutant phenotype in relation to the development of the fins and the facial skeleton (Van Eeden et al., 1996; Clément et al., 2008). I have shown for the first time that in the *dak*^{to273b} mutant ear, although epithelial projections did begin to form during the second day of development, they failed to elongate further so as to meet and fuse, resulting in no semicircular canal formation. The elongation failure is unlikely to be due to low levels of epithelial growth, as HSPGs have been shown not to interfere with the epithelial cell proliferation rate in the chick otic placode (Moro-Balbás et al., 2000). Instead, the inhibition of epithelial invagination of the otic placode after heparinase injection was attributed to the destabilisation of HS complexes with the ECM (Moro-Balbás et al., 2000). The *dak*^{to273b} ear phenotype is very similar to those observed after hyaluronidase injections in the epithelial projections of wild-type zebrafish embryos, where the injected projections collapsed and were not able to elongate (Geng et al., 2013). These data combined suggest that HA and HS act in a similar, most likely cooperative way, to aid the elongation of the epithelial projections into the otic vesicle from 48 hpf, possibly by propulsing the epithelial tissue towards the inside of the lumen. In order to validate this hypothesis and confirm that the canal defects in the *dak*^{to273b} ear are not secondary abnormalities stemming from a general developmental arrest of the embryo, enzymatic degradation of HS using heparinase microinjections into the epithelial projections of wild-type embryos could be employed.

Similarly to the *adgrg6* mutant phenotype, *versican* genes remained strongly expressed on the small, unfused projections of the *dak*^{to273b} ear (Geng et al., 2013). The high *versican* gene expression in the projections of the mutant ear could be a compensatory mechanism that is activated when HS biosynthesis is low, according to the previously proposed theory that CS levels tend to increase when HS levels are depleted (Holmborn et al., 2012). Alternatively, the persistence of *versican* expression on the unfused projections might be due to the existence of a feedback loop, where the fusion event is required to trigger an *adgrg6*-mediated signal for the down-regulation of *versican*.

In addition to semicircular canal defects, the *dak*^{to273b} mutant ear phenotype was accompanied by some otolith morphogenesis and tethering defects. Phenotypic observation and tapping experiments revealed that saccular otoliths were tethered to the macula during the first two days of development, but failed to maintain a strong adhesion during otolithic growth and biomineralisation between 3 and 5 dpf. This phenotype could

be due to the absence of *otogelin* expression from the saccular macula, as this gene has been previously shown to be required for otolithic tethering (Stooke-Vaughan et al., 2015). Nevertheless, the otolith phenotype observed in *dak*^{to273b} mutants does not share many similarities with the *otogelin* (*einstein*) mutant phenotype, where only one otolith forms in each mutant ear.

The otolithic *dak*^{to273b} mutant phenotype is very similar to the *α-tectorin* (*rolling stones*) mutant phenotype, where the otolithic development was normal during the first two days of development, but between 3 and 5 dpf, misplaced saccular otoliths were detected in some of the mutants, which were sometimes moderately misshapen (Stooke-Vaughan et al., 2015). Similar to my observations on *dak*^{to273b} mutants, the utricular otolith was not affected in rolling stones mutants either. These similarities between the two mutants were surprising, considering that *α-tectorin* mRNA expression was not affected in *dak*^{to273b} mutants.

The saccular otoliths of the *dak*^{to273b} mutant ear grew at a slower rate compared to the wild-types, while their shape was also slightly altered. Consistent with these observations, *otolith matrix protein* and *starmaker* genes, whose expression have been reported to control otolithic size and shape respectively, were found reduced in the mutants (Söllner, 2003; Murayama et al., 2005).

Mice lacking the sulphatase enzymes required for HS modification (*Sulf1* and *Sulf2*) showed an abnormal increase in the number of hair cells of the cochlea, suggesting that HS sulphation plays a role in the development of mechanosensory hair cells. In the *dak*^{to273b} mutant ear, hair cells of the maculae differentiated normally, as shown by *myo7aa* expression, but the macula did appear disorganised and misshapen. Although hair cells in the *dak*^{to273b} mutant ear were not counted, this shape defect of the macula could be due to hair cells being supernumerary, but this hypothesis requires further investigation.

Finally, I demonstrate that, in *dak*^{to273b} mutants, *adgrg6* was up-regulated in the lateral line and showed ectopic expression in a region presumed to be the cerebral vein. The up-regulation of *adgrg6* in the lateral line could be due to the previously reported imbalance between FGF and Wnt/β-catenin signalling in this region (Venero Galanternik et al., 2015). As the Wnt/β-catenin pathway was found to be ectopically activated in the lateral line of *dak*^{to273b} mutants (VeneroGalanternik et al., 2015), the ectopic *adgrg6* expression observed in the cerebral vein could be the result of the angiogenic properties of Wnt/β-catenin

signalling activation in this tissue (Daneman et al., 2009).This hypothesis could be tested by analysing the mRNA expression of Wnt target genes, such as *wnt10a, axin2*, and *fgf10*.

4.4 CONCLUSIONS

- HS contribute to the elongation of the epithelial projections into the otic vesicle from around 48 hpf, possibly by propulsing the epithelial tissue towards the inside of the lumen.
- HS contribute to otolithic growth and maintenance of otolithic adhesion to the posterior macula, by controlling *otogelin, otolith matrix protein* and *starmaker* expression.

CHAPTER 5.

In vivo drug screening using the *adgrg6* zebrafish mutant

5.1 INTRODUCTION

Adgrg6 (formerly Gpr126) is an adhesion G-protein coupled receptor (aGPCR) with important roles in neural, cardiac and ear development (reviewed in Patra et al., 2014). Although the majority of adhesion GPCRs are orphan receptors, Adgrg6 is activated via a tethered-peptide-agonist mechanism, which can be triggered by interaction of the extracellular domain with endogenous ECM ligands (Liebscher et al., 2014; Stoveken et al., 2015; Monk et al., 2015; for more details on Adgrg6, see section 1.3.5).

In *adgrg6* zebrafish and mouse mutants, peripheral myelination is severely impaired; Schwann cells (SCs) associate with axons but do not spiral their membrane to generate a myelin sheath, resulting in reduced or absent *myelin basic protein* (*mbp*) gene expression on the lateral line (Glenn et al., 2013). Mouse knockouts in particular, show additional abnormal phenotypes, such as limb deformities, axon degeneration and embryonic lethality, due to cardiovascular failure (Waller-Evans et al., 2010; Monk et al., 2011).

Apart from abnormalities in the lateral line, *adgrg6* zebrafish mutants have been reported to exhibit a severe morphological inner ear phenotype (Geng et al., 2013); the epithelial projections that form the semicircular canal ducts fail to adhere and fuse as per normal. Instead, they grow past one another without fusing, resulting in no pillar formation (Geng et al., 2013). Analysis of the gene expression pattern in the *adgrg6* mutant ear showed a dramatic alteration in the expression of ECM genes, with the *versican* genes displaying abnormally high levels of expression (Geng et al., 2013).

There are several *adgrg6* alleles that have been identified in zebrafish, for example *tb233c* (Whitfield et al., 1996; Geng et al., 2013), *fr24* (Geng et al., 2013), *st49* and *st63* (Monk et al., 2009) (Figure 5.1). Treatment with cAMP agonists, such as forskolin and IBMX, was shown to ameliorate the myelination defects present in *adgrg6*^{st49} mutants (Monk et al.,

2009) and ameliorate the ear defects present in *adgrg6 tb233c* and *fr24* mutants (Geng et al., 2013). The molecular mechanism of Adgrg6 action in Schwann cells was later described; unmasking of the *Stachel* agonistic peptide leads to cAMP elevation via $G\alpha_s$-protein activation. This triggers a signalling cascade involving activation of PKA, the cAMP-response element binding protein (CREB) pathway and, ultimately, expression of transcription factors that induce the expression of myelination genes (Liebscher et al., 2014; Monk et al., 2015). However, the underlying mechanism of Adgrg6 signalling in the inner ear is yet largely uncharacterised.

In this chapter, I used otic *versican b* overexpression in the zebrafish *adgrg6*^{tb233c} mutant larvae as the basis for an *in vivo* drug screening assay to identify compounds that can suppress *versican b* mRNA levels back to wild-type levels. In parallel, *mbp* expression in the lateral line of these mutants was used as the basis for a counter-screen assay with a dual role; First, it enabled the elimination of compounds that down-regulate both *vcanb* and *mbp* expression, and secondly it allowed for the identification of compounds that rescue the expression of both genes. In conclusion, the ultimate aims of this section were:

(1) the identification of chemical compounds able to down-regulate *versican* expression in *adgrg6*^{tb233c} mutants.
(2) the identification of compounds capable of rescuing the defective expression of *vcanb* and *mbp* genes in *adgrg6*^{tb233c} mutants, thus representing potential modulators of the Adgrg6 signalling pathway.
(3) to investigate whether any of the successful hit compounds can potentially interact with Adgrg6 receptor directly, using the nonsense allele *fr24*, which, unlike *tb233c,* is an early truncation predicting a protein lacking the CTF altogether.

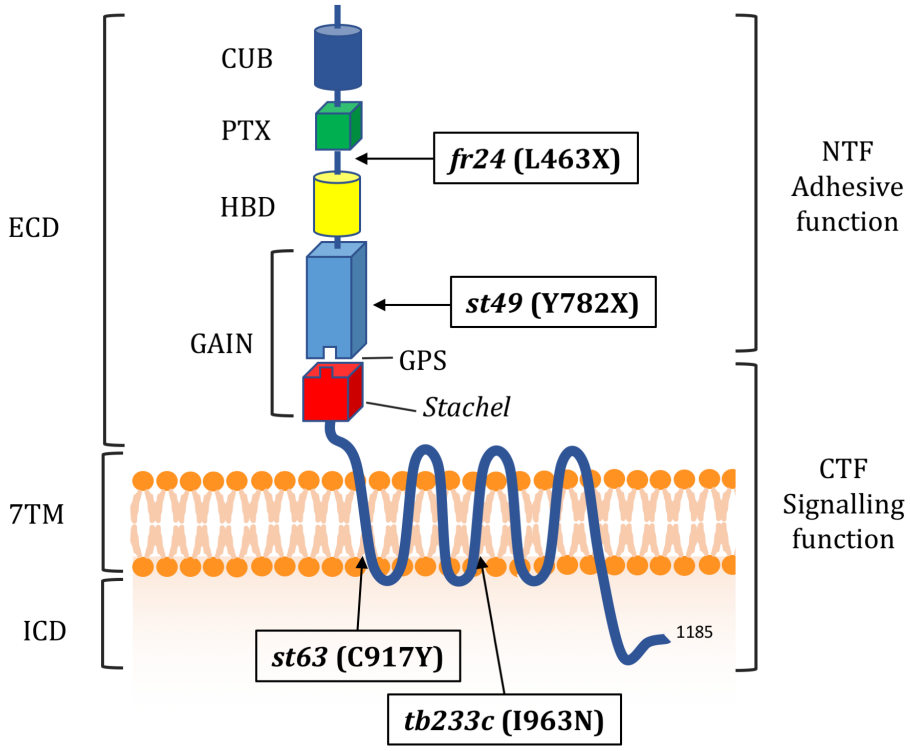

Figure 5.1 Schematic showing the positions of the most studied *adgrg6* mutant alleles. *tb233c* (Whitfield et al., 1996) is a missense point mutation allele that introduces an amino acid substitution in the fourth 7TM region (Geng et al., 2013); *st63* (Monk et al., 2009) is a point mutation that substitutes a conserved amino acid (cysteine) located in the first loop of the 7TM domain; *st49* (Monk et al., 2009) is a point mutation that introduces a premature stop codon in the GAIN domain; *fr24* (Geng et al., 2013) is a nonsense mutation predicting a truncated protein with intact CUB and PTX domains, but with no GPS and 7TM domains. Abbreviations: CTF, carboxy-terminal fragment; CUB, Complement C1r/C1s, Uegf, BMP1 domain; ECD, extracellular domain; GAIN, GPCR auto-proteolysis domain; GPS, GPCR proteolytic site; HBD, hormone binding domain; ICD, intracellular domain; NTF, amino-terminal fragment; PTX, Pentraxin domain; 7TM, 7-transmembrane domain.

5.2 RESULTS

5.2.1 Small molecules that rescue *versican* mRNA expression in *adgrg6* mutants

In order to identify compounds that suppress *versican* expression in the *adgrg6* mutant ear, I took advantage of the viability of the *adgrg6*^{tb233c} homozygous zebrafish mutants and generated batches of 100% homozygous mutant embryos. Using these, 3120 compounds from Tocriscreen Total (Tocris) and Spectrum Collection (Microsource Discovery Systems) libraries were screened, covering a wide spectrum of molecular space (Table 5.1). Although screening of the Tocris library was a product of my personal work, the screening of the Spectrum library had started prior to my arrival in the Whitfield lab, by C.J. Holdsworth and Dr. S. Baxendale. Building upon their work, I completed the screening of the Spectrum library compounds and developed the scoring system that is used throughout this study.

Table 5.1 Brief description of the two compound libraries used for the versican screening assay.

Library	Tocris Total	Spectrum Collection
Number of compounds	1120	2000
Description	Small, biologically active compounds targeting GPCRs, kinases, ion channels, nuclear receptors, transporters.	Bioactive compounds and natural products with a wide range of activities and structures: 60% FDA-approved drugs, 25% natural products, 15% other (enzyme inhibitors, receptor blockers, membrane active compounds, toxins).

All assay plates included IBMX (100 μM) as a positive control (Geng et al., 2013), 1% DMSO as a negative control, as well as untreated *nacre/mitfa-/-* mutants, which were used as a phenotypically wild-type control, and *adgrg6*^{tb233c} homozygous mutants. Three embryos were placed in each well of a 96-well plate and treated with drugs at 25 μM in E3 medium, from 60 to 90 hpf (Geng et al., 2013). At 90 hpf, embryos were fixed and analysed for mRNA expression of *versican b* (*vcanb)* by semi-automated whole-mount *in situ* hybridisation (see section 2.1.4). My findings confirmed that, at 90 hpf, there is very strong *vcanb* expression in the *adgrg6*^{tb233c} homozygous mutant inner ear and that 1% DMSO does not affect the levels of expression (Figure 5.2Ai; Geng et al., 2013).

To score the efficacy of the drugs in down-regulating *vcanb* mRNA levels, a scoring system from 0 to 3 was used, with 0 being the score for a very efficient drug (hit) that can suppress *vcanb* expression back to almost wild-type levels and 3 the score for a drug that did not have any effect on *vcanb* mRNA levels expressed in the mutant ear. Scores 1 and 2 were given to drugs that showed an ability to down- regulate *vcanb* expression to some extent, with 1 given for a stronger down- regulation than 2 (Figure 5.2A). Drugs were then classified into categories A-E, according to the average score from the three embryos that were treated with each drug (Figure 5.2B). Drugs categorised A, B or C were considered successful, and were cherry-picked into new drug assay plates for further testing. Drugs D and E were considered to show incomplete or no inhibition of *vcanb* expression, respectively, and therefore were not followed further. Drugs from category F caused severe developmental abnormalities/heart edema/brain edema or death at the end of the treatment and therefore were characterised as toxic. Category G represented drugs that were possibly corrosive, as no fish were found in these wells at the end of the treatment. Drugs that fell under categories F and G were eliminated from the assay and were not followed further.

After the completion of the screens for all 3120 compounds, 92 (8%) compounds from the Tocris Total library and 205 (10%) from Spectrum Collection that scored A-C were identified (Figure 5.2B,C,E). 5% of the drugs from each library were found to be toxic or corrosive, while 99 (9%) drugs from Tocris and 269 (13%) from Spectrum were found to cause incomplete/partial inhibition of *vcanb* expression (category D).

I identified 130 compounds that were common between the Tocris and Spectrum libraries, 60% of which (78/130) had exactly the same *vcanb* score average following the two individual screens. 33 out of the 130 (25.3%) compounds yielded a *vcanb* score average that only slightly differed by 0.33-0.67 units; 14 (10.7%) of the compounds yielded a *vcanb* score average that differed by 1-2 units, while only 4 (3%) compounds had a score average that differed by 2.33-3 units. In summary, 85.3% (111/130) of the compounds common to both libraries showed similar efficacy in down-regulating *vcanb* in parallel testing, while 13.8% (18/130) of the compounds induced different levels of down-regulation. This variability could be either due to differences in the compound purity or length of storage between the two providers affecting the efficacy or due to experimental error (e.g. in the concentration used, or during the ISH protocol).

Analysis of the hit compounds with respect to their chemical structure was conducted by Dr Antonio de la Vega de Leon (Information school, University of Sheffield). Drugs were

ordered into a dendrogram based on similarities of their chemical scaffold and this information was presented as individual dots on a polar scatterplot (Figure 5.2D,F); dots that are closer to each other are likely to be structurally similar. Due to the wide diversity of scaffolds found in the Tocris library, less clustering of hit compounds (A-C) can be observed compared to the molecules of the Spectrum library, where less scaffold diversity was found. In the Tocris scatterplot, the most prominent cluster was observed between positions 300 and 400, where 19 hit compounds from categories A-C were clustered closely. In the Spectrum library, several clusters were identified; the first comprised 22 compounds (A-C) around position 200, the second comprised 19 compounds categorised A-C around position 1400, and the third comprised 16 compounds (A-C) at position 1700. Many smaller clusters were observed, such as the group between positions 600 and 700, where 13 compounds from categories A-C were clustered closely.

In order to compare the results from the two libraries, the drugs were displayed in one combined scatterplot (Figure 5.3B). Although the drugs were widespread on the scatterplot, two regions were identified to have the most dense populations, with 36 and 39 drugs displayed in the dashed rectangular boxes in Figure 5.3B. Interestingly, one of these areas included IBMX, which has been previously reported to rescue *vcanb* expression in *tb233c* mutants and which was used as a positive control in the screen, and colforsin in the other. Colforsin is a derivative of forskolin, which has been reported to rescue *vcanb* expression in *tb233c* mutants and *mbp* expression in *st49* mutants (Monk et al., 2009; Geng et al., 2013). Forskolin itself was also included in the Spectrum library and was identified as toxic in the screen presented herein. This is easily explained by the fact that the duration of the treatment in this screen was significantly longer (30 hours) compared to the one used in Monk et al. (2009; 7 hours).

At this stage, the compounds from groups A-C did not show a strong clustering in the combined polar scatterplot, but this was expected for two reasons: (1) the compounds were only tested once and (2) *versican* down-regulation could be achieved in more than one ways, as the different compounds could have different targets, thus affecting different regulatory pathways.

A

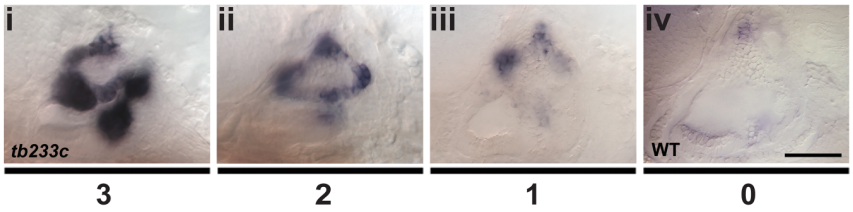

B

Category	*vcanb* score average (n=3)	No. of drugs in Tocris	No. of drugs in Spectrum
A	0-0.33	25	68
B	0.66-1.33	52	56
C	1.66-2	15	81
D	2.33	99	269
E	2.66-3	869	1413
F	Toxic	37	68
G	No fish	23	45

C

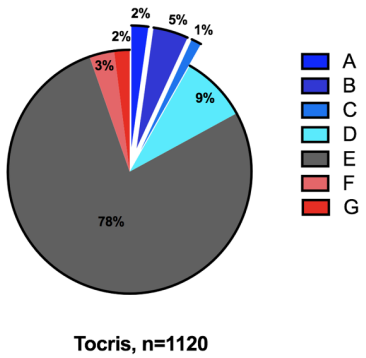

Tocris, n=1120

D

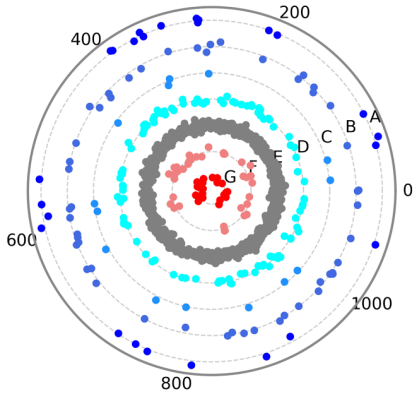

E

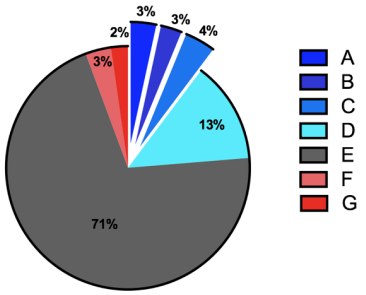

Spectrum, n=2000

F

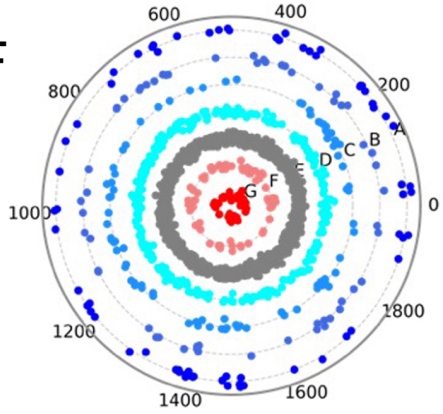

Figure 5.2 A Primary drug screen identified 92 (Tocris) and 205 (Spectrum) putative hit compounds able to down-regulate *versican* mRNA expression in *adgrg6*^{tb233c} mutants. Three *adgrg6*^{tb233c} homozygous embryos were exposed to each compound of the Tocris and Spectrum libraries at a final concentration of 25 µM. IBMX (100 µM) was used as a positive control, while DMSO (1%) was used as a negative control. Embryos were treated between 60-90 hpf prior to fixation and analysis for *vcanb* expression by whole-mount *in situ* hydridisation. **(A)** Scoring system used to assess *vcanb* mRNA expression levels in the inner ear of *adgd6*^{tb233c} embryos after treatment. **(Ai)** *vcanb* mRNA expression in the untreated/DMSO-treated *adgd6*^{tb233c} mutant ear (score 3). Scores 2 **(Aii)** and 1 **(Aiii)** were given embryos that showed reduced *vcanb* mRNA expression to some extent, with 1 given for a stronger down-regulation than 2. **(Aiv)** Score 0 was given to embryos where *vcanb* mRNA levels were equivalent to wild-type levels. **(B)** Compounds were categorised A-G according to the average *vcanb* score from the three embryos treated. **(C,E)** Pie charts showing the distribution of compounds from Tocris **(C)** and Spectrum **(E)** libraries in categories A-G. **(D,F)** Compounds from Tocris and Spectrum libraries were ordered according to similarities in their chemical scaffold and presented as individual dots in polar scatterplots in D and F, respectively. Scale bar: 50 µM, for Ai-iv.

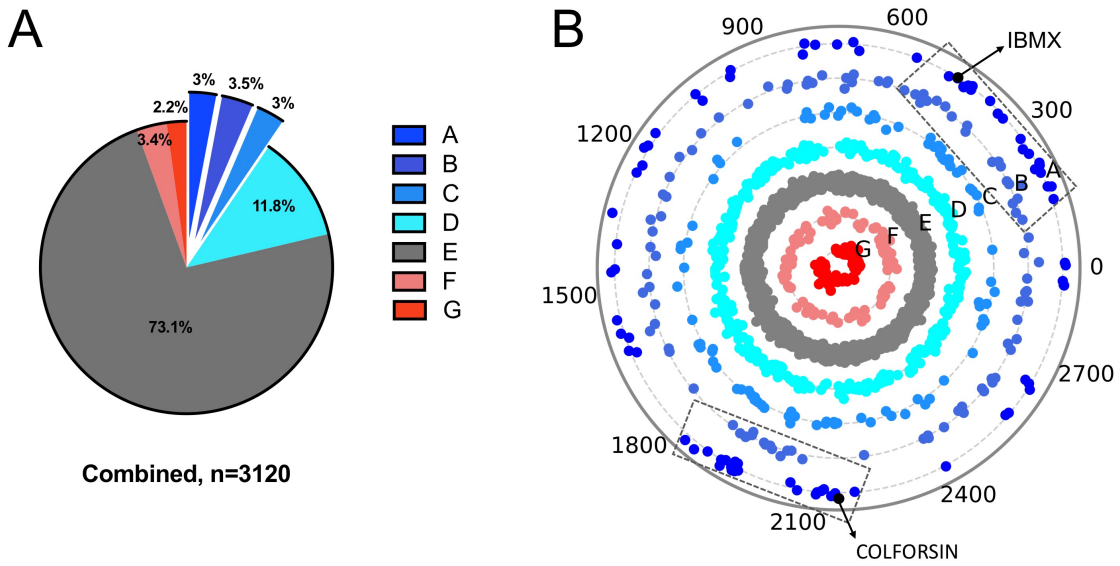

Figure 5.3 Combined data from the Tocris and Spectrum libraries revealed widespread chemical clustering. (A) Pie chart showing the distribution of compounds from both Tocris and Spectrum libraries in categories A-G. **(B)** Compounds from both libraries were ordered according to similarities in their chemical scaffold and presented as individual dots in the same polar scatterplot. Dashed rectangular boxes mark the two most densely populated areas.

In order to eliminate false-positive results and increase the number of embryos treated per drug, a large subset of the possible hit compounds categorised A-C was selected for retesting, using the same assay format. Specifically, 83 out of the 92 possible hit compounds from the Tocris library and 145 of the 205 possible hits from the Spectrum library, were retested. The selection of compounds was blind and dependent on stock availability. It is worth mentioning, that the 18 compounds that were common to the two libraries and initially showed a different degree of *vcanb* down-regulation in the two independent assays, configured a similar average *vcanb* score after the retest (for more details, see Appendix).

Out of the 83 possible hits identified from the first screen of the Tocris library, 28 compounds (34%) were classified as categories A-C following retesting. 12 and 37 compounds classed in groups D and E, respectively. Groups F and G each contained 3 compounds (Figure 5.4A). Compounds classified as D-G were eliminated from subsequent assays, whereas the 28 compounds that were confirmed from the first retest were selected for a second round of retesting, using the same assay format. Following the second retest, 24 of the 28 hit compounds (85.7%) were confirmed to be A-C, 3 (10.7%) and 1 (3.6%)

were classified in D and E, respectively, while there were no toxic (F) or corrosive (G) compounds found (Figure 5.4A').

Out of the 145 possible hits from the Spectrum library, 62 compounds (43%) were classified again as A-C, following the first round of retesting. 15 and 61 compounds were classed in categories D and E, respectively, while groups F and G had 5 and 2 compounds, respectively (Figure 5.4B). The 62 compounds that were confirmed from the first retest were selected for a second round of retesting, using the same assay format. Compounds classified as D-G were eliminated from subsequent assays. Similarly to the results obtained from the second retest in the Tocris library, 85.5% (53) of the hit compounds were confirmed to be A-C, 9.7% (6) and 4.8% (3) were grouped in D and E, respectively and there were no compounds classified F or G (Figure 5.4B'). In this instance, the compounds classified as D or E in the second retest assay were not eliminated from the assays that followed, as they all had scored A-C in both previous assays.

The top 77 *versican* hit compounds from both libraries (24 from Tocris, 53 from Spectrum) that scored A-C in the initial screen and both retests, covered a wide spectrum of naturally derived and synthetic molecules, with known and unknown functions (listed in table 5.3). The hit compounds included one compound (Gedunin) that was identified as a hit separately, in both libraries. The hit compounds with known functions included calcium channel blockers, antifungal, anti-inflammatory, antihyperlipidemic, antibacterial and anthelmintic agents, as well as compounds with known antineoplastic and vasodilatory properties.

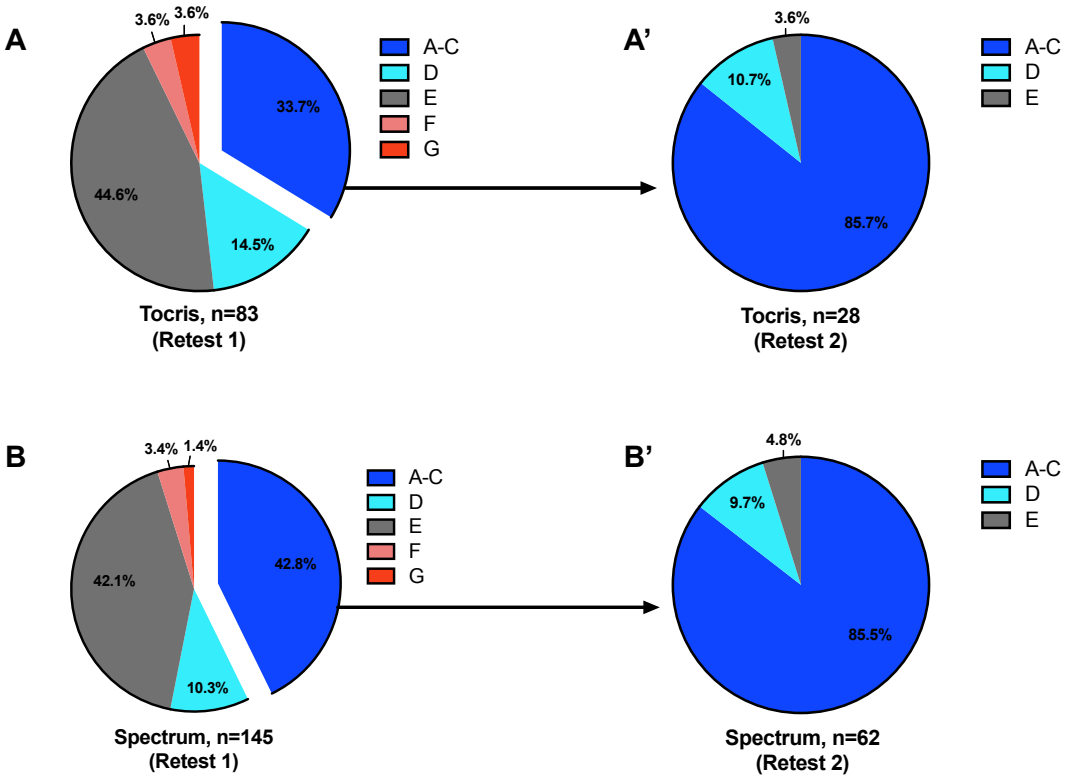

Figure 5.4 85% of the hit compounds that passed the first retest scored A-C in the second retest. (A,B) Pie charts showing the distribution of the compounds from Tocris **(A)** and Spectrum **(B)** libraries into categories A-G, following the first hit retest. **(A',B')** The compounds that scored A-C in the first retest (dark blue, exploded part of the pie chart) were chosen for a second round of retesting, after which, approximately 85% of the compounds of each library were confirmed to be A-C.

Table 5.2 Overview of the hit compounds (A-C) identified in *versican* screens.

Library	No of compounds	No of hits after the 1st screen	No of hits after two rounds of retesting
Tocris	1120	92 (8.2%)	24 (2.1%)
Spectrum	2000	205 (10.25%)	53 (2.65%)
Total	**3120**	**297 (9.5%)**	**77 (2.5%)**

Table 5.3 Hit compounds best able to down-regulate *versican* mRNA expression in the ear of *adgrg6*^{tb233c} mutants. The compounds listed were classed as A-C in both rounds of retesting.

#	Compounds best able to down-regulate *versican* expression	*vcanb* score mean ±SD (n=9)	Source library
1	COLFORSIN	0.00 ±0.00	Spectrum
2	CARAPIN-8(9)-ENE	0.00 ±0.00	Spectrum
3	3-DEOXO-3BETA-ACETOXYDEOXYDIHYDROGEDUNIN	0.00 ±0.00	Spectrum
4	DEMETHYLNOBILETIN	0.00 ±0.00	Spectrum
5	ROSUVASTATIN CALCIUM	0.00 ±0.00	Spectrum
6	HEXAMETHYLQUERCETAGETIN	0.00 ±0.00	Spectrum
7	NOBILETIN	0.00 ±0.00	Spectrum
8	LOVASTATIN	0.00 ±0.00	Spectrum
9	CLOTRIMAZOLE	0.00 ±0.00	Spectrum
10	BAICALEIN	0.00 ±0.00	Spectrum
11	CYPROHEPTADINE HYDROCHLORIDE	0.00 ±0.00	Spectrum
12	DEOXYSAPPANONE B 7,3'-DIMETHYL ETHER ACETATE	0.00 ±0.00	Spectrum
13	DEOXYSAPPANONE B 7,4'-DIMETHYL ETHER	0.00 ±0.00	Spectrum
14	5-FLUOROINDOLE-2-CARBOXYLIC ACID	0.00 ±0.00	Spectrum
15	ALBENDAZOLE	0.00 ±0.00	Spectrum
16	FENBENDAZOLE	0.00 ±0.00	Spectrum
17	GEDUNIN	0.00 ±0.00	Spectrum
18	GEDUNIN	0.00 ±0.00	Tocris
19	CHAULMOOGRIC ACID	0.00 ±0.00	Spectrum
20	PODOFILOX	0.00 ±0.00	Spectrum
21	LONIDAMINE	0.00 ±0.00	Tocris
22	ARTENIMOL	0.00 ±0.00	Spectrum
23	3ALPHA-ACETOXYDIHYDRODEOXYGEDUNIN	0.11 ±0.33	Spectrum
24	NIMODIPINE	0.11 ±0.33	Spectrum
25	CMPD-1, 2'-FLUORO-N-(4-HYDROXYPHENYL)-[1,1'-BIPHENYL]-4-BUTANAMIDE	0.11 ±0.33	Tocris
26	GTP 14564	0.22 ±0.44	Tocris
27	DANAZOL	0.33 ±0.71	Spectrum
28	XANTHYLETIN	0.33 ±0.50	Spectrum
29	2,3-DIHYDROXY-4-METHOXY-4'-ETHOXYBENZOPHENONE	0.33 ±0.50	Spectrum
30	MEPIROXOL	0.33 ±0.71	Spectrum
31	DISULFIRAM	0.33 ±0.50	Spectrum
32	METHIOTHEPIN MALEATE	0.33 ±0.50	Tocris
33	IMILOXAN HYDROCHLORIDE	0.33 ±0.52	Tocris
34	TANGERITIN	0.44 ±0.73	Spectrum
35	GITOXIN	0.44 ±0.53	Spectrum
36	DIGITOXIN	0.44 ±0.73	Spectrum
37	SULCONAZOLE NITRATE	0.44 ±0.73	Spectrum
38	BHQ (1,4-DIHYDROXY-2,5-DI-TERT-BUTYLBENZENE)	0.44 ±0.53	Tocris
39	FPL 64176	0.44 ±0.53	Tocris
40	DIHYDROGEDUNIN	0.56 ±0.88	Spectrum
41	3-ISOBUTYL-1-METHYLXANTHINE (IBMX)	0.67 ±0.50	Spectrum
42	DEOXYGEDUNIN	0.67 ±0.87	Spectrum
43	EZETIMIBE	0.67 ±1.00	Spectrum
44	3BETA-ACETOXYDEOXODIHYDROGEDUNIN	0.67 ±1.00	Spectrum

45	3-DEOXO-3BETA-HYDROXYMEXICANOLIDE 16-ENOL ETHER	0.67 ±1.00	Spectrum
46	MEBENDAZOLE	0.67 ±0.50	Spectrum
47	ECONAZOLE NITRATE	0.67 ±1.00	Spectrum
48	CILNIDIPINE	0.67 ±0.50	Tocris
49	TMS, (E)-2,3',4,5'-TETRAMETHOXYSTILBENE	0.67 ±1.00	Tocris
50	IVERMECTIN	0.78 ±0.97	Spectrum
51	ALPHA-DIHYDROGEDUNOL	0.78 ±0.67	Spectrum
52	7-DESHYDROXYPYROGALLIN-4-CARBOXYLIC ACID	0.78 ±0.67	Spectrum
53	TRACAZOLATE HYDROCHLORIDE	0.78 ±0.44	Tocris
54	DIHYDROFISSINOLIDE	0.89 ±0.78	Spectrum
55	11ALPHA-HYDROXYPROGESTERONE HEMISUCCINATE	0.89 ±0.78	Spectrum
56	DECOQUINATE	1.00 ±0.87	Spectrum
57	(RS)-(TETRAZOL-5-YL)GLYCINE	1.00 ±0.87	Tocris
58	SKF 91488 DIHYDROCHLORIDE	1.00 ±0.87	Tocris
59	1,3-DIPROPYL-8-PHENYLXANTHINE	1.11 ±0.93	Tocris
60	SD 208	1.11 ±0.33	Tocris
61	NITRENDIPINE	1.17 ±1.33	Spectrum
62	DICLOFENAC SODIUM	1.22 ±1.09	Spectrum
63	CGP 37157	1.22 ±0.67	Tocris
64	(S)-(+)-NIGULDIPINE HYDROCHLORIDE	1.22 ±0.83	Tocris
65	PP1 (1-(1,1-DIMETHYLETHYL)-1-(4-METHYLPHENYL)-1H-PYRAZOLO[3,4-D]PYRIMIDIN-4-AMINE)	1.33 ±0.87	Tocris
66	2-METHOXYESTRADIOL, (17B)-2-METHOXYESTRA-1,3,5(10)-TRIENE-3,17-DIOL	1.33 ±0.50	Tocris
67	SINENSETIN	1.44 ±0.53	Spectrum
68	HARMINE	1.44 ±0.53	Spectrum
69	NIFEDIPINE	1.44 ±0.53	Tocris
70	ETHAMIVAN	1.56 ±0.53	Spectrum
71	PREGNENOLONE SUCCINATE	1.56 ±0.53	Spectrum
72	CPT 11, IRINOTECAN, CAMPTOTHECIN 11	1.56 ±0.53	Tocris
73	AMIODARONE HYDROCHLORIDE	1.67 ±0.50	Spectrum
74	MANNITOL	1.67 ±0.50	Spectrum
75	CGS 15943	1.78 ±0.44	Tocris
76	SC-10	1.89 ±0.33	Tocris
77	DL-TBOA(DL-THREO-B-BENZYLOXYASPARTIC ACID)	2.00 ±0.00	Tocris

Although the two retests significantly reduced the possibility of false-positive results due to experimental error (e.g. failure of the ISH protocol) or due to the qualitative nature of the assay, this list could still contain compounds that may generally inhibit transcription or cause developmental arrest of the embryo. In order to eliminate such compounds, I exploited the expression of another gene that is affected in *adgrg6* mutants, *myelin basic protein* (*mbp)*. A detailed description and analysis of the hit compounds that specifically down-regulated *versican* and not *mbp* expression, can be found in the next section (5.2.3).

5.2.3 Secondary assay based on *myelin basic protein* (*mbp*) expression

As mentioned earlier, although *mbp* expression is not affected in the Central Nervous System (CNS) of *adgrg6* mutants, it is reduced in the Schwann cells of the lateral line nerves and ganglia to a degree that is dependent on the severity of the allele (Monk et al., 2009; Geng et al., 2013). In *adgrg6*^{st49} homozygous mutants for example, *mbp* expression is missing from the lateral line altogether (Monk et al., 2009). In *adgrg6*^{tb233c} homozygous mutants, *mbp* expression is reduced in the anterior lateral line nerves and completely missing from the posterior lateral line ganglion (PLLg) (Figure 5.5Aiii). The expression is also reduced from three small regions near the cristae of the inner ear, presumed to be expression in Schwann cells myelinating afferent neurons that transmit signals from the ear to the hindbrain (asterisks in Figure 5.5i,iii). However, the *mbp* expression in the posterior lateral line nerves is not significantly affected by the mutation (Figure 5.5Aiii).

In this assay, I used the absence of *mbp* expression in the PLLg of *adgrg6*^{tb233c} mutants as the basis for a scoring system to investigate which of the hit compounds found in the *versican* screens can rescue the myelination phenotype, thus representing putative Adgrg6 pathway modulators (Figure 5.5A; scores 2 or 3). At the same time, the presence of *mbp* expression in the posterior lateral line nerves of *tb233c* mutants, provided an excellent opportunity to identify compounds that exacerbate the phenotype, and thus may be general transcription blockers (Figure 5.5A; score 0). To this end, the compounds that passed the first retest for *versican* (90 compounds in total; 28 from Tocris and 62 from Spectrum) were subjected to a secondary assay, detecting *mbp* mRNA. The assay format was identical to the one followed for *versican* and the treatment timeframe was the same.

Following two experimental repeats (n=6 fish tested per drug), drugs were categorised in groups H, I and J according to their average *mbp* score, as shown in Figure 5.5B. I identified 42 compounds (12 from Tocris, 30 from Spectrum) that rescued *mbp* expression and thus represent possible modulators of the Adgrg6 pathway (Group H), 26 compounds (14 from Tocris, 12 from Spectrum) that did not affect *mbp* mRNA expression (Group I) and 22 compounds (2 from Tocris, 20 from Spectrum) that reduced the expression of *mbp* and therefore assumed to be general inhibitors of transcription or development, and thus likely to have been false positives in the *vcanb* assay (Group J; Figure 5.5C). The compounds classified in groups H, I and J are listed and analysed with respect to their chemical class and known functions in the three subsections that follow.

A

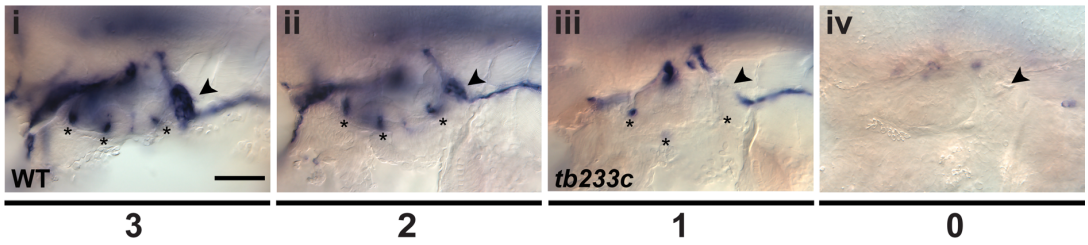

B

Category	*mbp* score average (n=6)	No. of drugs in Tocris	No. of drugs in Spectrum	Total no. of drugs
H	1.17-3	12	30	42
I	0.6-1.17	14	12	26
J	0-0.5	2	20	22

C

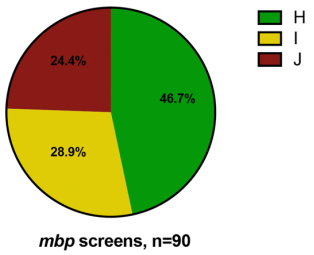

Figure 5.5 *mbp* scoring system and classification of the compounds. Six *adgrg6*^{tb233c} homozygous embryos were exposed to the 90 compounds identified as hits for *vcanb* at a final concentration of 25 µM. IBMX (100 µM) was used as a positive control, while DMSO (1%) was used as a negative control. Embryos were treated between 60-90 hpf prior to fixation and analysis for *mbp* expression by whole-mount *in situ* hydridisation **(A)** Scoring system used to assess *mbp* mRNA expression levels in the PLLg (arrowhead) of *adgd6*^{tb233c} embryos after treatment. **(Ai)** Score 3 was given to embryos were *mbp* mRNA expression was similar to the wild-type levels. **(Aii)** Score 2 was given to embryos that showed *mbp* expression in the PLLg (arrowhead), but this was weaker than 3. **(Aiii)** Score 1 was given to embryos that showed no *mbp* expression on the PLLg (arrowhead), ie. the *mbp* expression was identical to the one seen in untreated *adgd6*^{tb233c} mutants. Note the reduced expression in the Schwann cells myelinating afferent neurons (asterisks)**. (Aiv)** Score 0 was used to indicate embryos where *mbp* mRNA expression was not only absent from the PLLg, but also reduced from the Schwann cells of both the posterior and anterior lateral line. **(B)** Compounds were categorised H-J according to the average *mbp* score from the six embryos treated. **(C)** A pie chart showing the distribution of the compounds tested for *mbp* in categories H-J. Scale bar: 50 µM for Aii-iv.

5.2.3i *Versican* hit compounds that also rescued *myelin basic protein* (*mbp*) expression are putative modulators of the Adgrg6 pathway (Group H)

I identified 42 compounds that down-regulate *vcanb* expression and upregulate *mbp* expression to wild-type levels. In order to compare their combined activities, I calculated the mean score for *vcanb* and *mbp* in each assay and subtracted the *vcanb* mean from the mean *mbp* score. Higher values of this parameter represent compounds with better potency in rescuing the expression of both genes. Positive values indicate compounds where *mbp* score was higher than *vcanb*, while negative values indicate compounds where *vcanb* score was higher than *mbp* (Table 5.4). The individual mean scores were colour-coded to aid visualisation of the data, with darker green colour representing higher potency in restoring gene expression to wild-type levels.

Analysis of the hit compounds that rescued the expression of both genes showed that most of the compounds were aromatic, containing one or more π-conjugated cyclic ring structures. The chemical classes that contained five or more compounds were the pyridines, the tetranotriterpenoids (gedunin derivatives) and the *O*-methylated flavonoids (Figure 5.6A). The pyridines identified included one pyrazolopyridine and six dihydropyridines, a class of Ca^{2+}-channel blockers with vasodilatory properties. It is worth mentioning, that six was the total number of dihydropyridines tested for *mbp* expression, and they were all clustered in this group. The gedunins are a family of naturally occuring compounds, previously attributed with antineoplastic and neuroprotective effects (Jang et al., 2010; Subramani et al., 2017). In addition, some gedunin derivatives have been recently reported to act as partial agonists for the GPCRs Adgrg1 and Adgrg5 (Stoveken et al., 2018). Six gedunin derivatives were identified as hits in this screen, with deoxygedunin being one of the top ten most potent drugs (Table 5.4, compound #8). Five *O*-methylated flavonoids were identified, with various known functions, some of them undetermined. Similarly to dihydropyridines, there were no *O*-methylated flavonoids classified in other groups, but H.

Eight calcium channel blockers were identified, which were type L-, N-, T-, or a combination of each. Six of the calcium channel blockers were dihydropyridines and also known to act as α- or β-adrenoceptor antagonists. These molecules could act on Adgrg6 pathway in two ways; first, adrenoceptors are coupled with $G\alpha_s$-proteins that can stimulate the formation of cAMP (Waller et al., 2010; chapter 5) and secondly, dihydropyridines have been previously reported to inhibit cAMP degradation by phosphodiesterases (Sakamoto et al., 1978), and so may act in a similar way to the

positive control compound IBMX, a phosphodiesterase inhibitor. In both cases, this group of compounds is presumed to act downstream of the Adgrg6 receptor, by raising cAMP levels. Seven other hit compounds are known to act by elevating cAMP levels; three of these were adenosine receptor antagonists, two were NMDA receptor agonists and one was an adenylate cyclase activator. The compounds identified also included three glucocorticoids, two compounds with antineoplastic and two with antihyperlipidemic activities.

Table 5.4 List of the 42 hit compounds that were able to rescue the expression of *vcanb* and *mbp* in *adgrg6*^{tb233c} mutants, thus representing putative Adgrg6 pathway modulators (group H).

#	Compounds able to restore *vcanb* and *mbp* expression in *tb233c* mutants (group H)	*vcanb* score mean ±SD (n=9)	*mbp* score mean ±SD (n=6)	Combined potency (*mbp* mean-*vcanb* mean)
1	COLFORSIN	0.00 ±0.00	3.00 ±0.00	**3.00**
2	CARAPIN-8(9)-ENE	0.00 ±0.00	2.83 ±0.41	**2.83**
3	3ALPHA-ACETOXYDIHYDRODEOXYGEDUNIN	0.11 ±0.33	2.83 ±0.41	**2.72**
4	IMILOXAN HYDROCHLORIDE	0.33 ±0.52	3.00 ±0.00	**2.67**
5	NIMODIPINE	0.11 ±0.33	2.33 ±0.82	**2.22**
6	3-ISOBUTYL-1-METHYLXANTHINE (IBMX)	0.67 ±0.50	2.83 ±0.41	**2.17**
7	3-DEOXO-3BETA-ACETOXYDEOXYDIHYDROGEDUNIN	0.00 ±0.00	2.17 ±0.75	**2.17**
8	DEOXYGEDUNIN	0.67 ±0.87	2.67 ±0.82	**2.00**
9	DEMETHYLNOBILETIN	0.00 ±0.00	2.00 ±0.00	**2.00**
10	ROSUVASTATIN CALCIUM	0.00 ±0.00	2.00 ±0.89	**2.00**
11	EZETIMIBE	0.67 ±1.00	2.50 ±0.55	**1.83**
12	HEXAMETHYLQUERCETAGETIN	0.00 ±0.00	1.83 ±0.41	**1.83**
13	NOBILETIN	0.00 ±0.00	1.67 ±0.52	**1.67**
14	DIHYDROFISSINOLIDE	0.89 ±0.78	2.50±0.84	**1.61**
15	IVERMECTIN	0.78 ±0.97	2.33 ±0.82	**1.56**
16	CILNIDIPINE	0.67 ±0.50	2.17 ±0.41	**1.50**
17	TANGERITIN	0.44 ±0.73	1.83 ±0.41	**1.39**
18	DANAZOL	0.33 ±0.71	1.67 ±0.52	**1.33**
19	NITRENDIPINE	1.17 ±1.33	2.33 ±0.58	**1.17**
20	XANTHYLETIN	0.33 ±0.50	1.50 ±0.55	**1.17**
21	DIHYDROGEDUNIN	0.56 ±0.88	1.67 ±0.82	**1.11**
22	1,3-DIPROPYL-8-PHENYLXANTHINE	1.11 ±0.93	2.17 ±0.75	**1.06**
23	CGP 37157	1.22 ±0.67	2.17 ±0.98	**0.94**
24	NIFEDIPINE	1.44 ±0.53	2.33 ±0.82	**0.89**
25	3BETA-ACETOXYDEOXODIHYDROGEDUNIN	0.67 ±1.00	1.50 ±0.55	**0.83**
26	HYDROCORTISONE HEMISUCCINATE	1.22 ±0.97	2.00 ±1.10	**0.78**
27	TRACAZOLATE HYDROCHLORIDE	0.78 ±0.44	1.50 ±0.55	**0.72**
28	(RS)-(TETRAZOL-5-YL) GLYCINE	1.00 ±0.87	1.67 ±0.52	**0.67**
29	(S)-(+)-NIGULDIPINE HYDROCHLORIDE	1.22 ±0.83	1.83 ±0.41	**0.61**
30	ALPHA-DIHYDROGEDUNOL	0.78 ±0.67	1.33 ±0.52	**0.56**
31	AMIODARONE HYDROCHLORIDE	1.67 ±0.50	2.17 ±1.17	**0.50**
32	11ALPHA-HYDROXYPROGESTERONE HEMISUCCINATE	0.89 ±0.78	1.33 ±0.52	**0.44**
33	SKF 91488 DIHYDROCHLORIDE	1.00 ±0.87	1.33 ±0.52	**0.33**
34	SC-10	1.89 ±0.33	2.17 ±0.98	**0.28**
35	ETHAMIVAN	1.56 ±0.53	1.67 ±0.52	**0.11**
36	EFONIDIPINE HYDROCHLORIDE MONOETHANOLATE	1.22 ±0.97	1.33 ±0.52	**0.11**
37	FERULIC ACID	1.22 ±1.20	1.33 ±0.52	**0.11**
38	ASTEMIZOLE	1.56 ±0.73	1.50 ±0.55	**-0.06**
39	LOMEFLOXACIN HYDROCHLORIDE	1.78 ±0.83	1.67 ±0.82	**-0.11**
40	PREGNENOLONE SUCCINATE	1.56 ±0.53	1.33 ±0.82	**-0.22**
41	CGS 15943	1.78 ±0.44	1.50 ±0.55	**-0.28**
42	SINENSETIN	1.44 ±0.53	1.17±0.75	**-0.28**

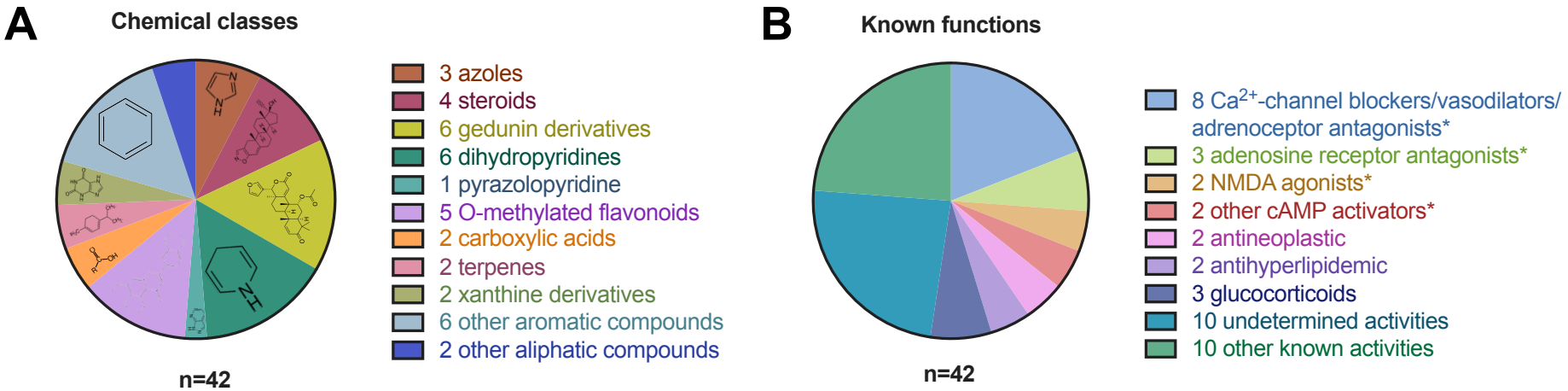

Figure 5.6 Classification of putative Adgrg6 modulators (group H). The 42 hit compounds that have been described as putative Adgrg6 modulators have been categorised according to their chemical classes **(A)** and known functions **(B)**, with the relative proportions of each group indicated in the corresponding pie chart. An asterisk indicates groups with functions known to raise cAMP levels.

In order to identify which of the compounds listed in Table 5.4 are likely to interact with the Adgrg6 receptor directly, the same *vcanb* assay was repeated with 37 of these 42 compounds using three *fr24* embryos, which, unlike *tb233c*, are predicted to be null mutants (see Figure 3.1). The idea was that compounds that rescued *vcanb* and *mbp* expression in *tb233c* mutants, but did not rescue *vcanb* expression in *fr24* mutants, are likely to interact with the Adgdg6 receptor directly. The 26 compounds that were classified in this group (group Hi) are listed in Table 5.5. This list includes 12 compounds (coloured in dark green) that did not cause any down-regulation in any of the *fr24* mutants tested, and 14 compounds (lighter green shades) that caused a slight down-regulation in one of the fish tested (Table 5.5). 11 of the compounds listed in Table 5.4 induced a strong down-regulation of *vcanb* expression in *fr24* mutants (*fr24* average *vcanb* score<2.63; list shown in Appendix) and are thus presumed to act downstream of the Adgrg6 receptor. Five of the compounds listed in Table 5.4 (nitrendipine, nifedipine, imiloxan hydrochloride, pregnenolone succinate and 3alpha-acetodihydrodeoxygedunin) were not tested on *fr24* mutants and thus, I have not been able to draw conclusions for these particular molecules.

Although these are useful preliminary data, a dose-response assay is needed to confirm that these compounds do not rescue *vcanb* expression in *fr24* mutants at concentrations higher than 25 μM. For example, IBMX only slightly rescued *vcanb* expression in *fr24* mutants at 25 μM (average *vcanb* score 2.83), but it did cause a stronger down-regulation at 100 μM (average *vcanb* score 2), which was added as a control for this assay. This might suggest that compounds with an average *vcanb* score of 2.83 or 2.67 are likely to rescue *fr24 vcanb* expression at higher concentrations, but this needs further investigation.

The top 12 compounds that did not cause any *vcanb* down-regulation (*vcanb* mean score 3) were coloured in black on the combined polar scatterplot of Figure 5.3 (Figure 5.7). Interestingly, 5 out of the 12 compounds clustered very tightly in the area around 1900. This suggests that these 5 molecules share structural similarities that may be important characteristics of agonistic ligands that can interact with the Adgrg6 receptor.

Table 5.5 List of the hit compounds that were unable to rescue the expression of *vcanb* in *adgrg6*^{fr24} mutants, thus representing putative Adgrg6 receptor modulators (group Hi).

#	Compounds unable to rescue *vcanb expression* in *fr24* mutants, thus likely to interact with Adgrg6 receptor (group Hi)	*vcanb* score mean ±SD	Number of embryos tested (n)
1	SC-10/ 5-CHLORO-N-HEPTYLNAPHTHALENE-1-SULFONAMIDE **	3.00±0.00	6
2	CILNIDIPINE**	3.00±0.00	3
3	SKF 91488 DIHYDROCHLORIDE	3.00±0.00	6
4	CGS 15943**	3.00±0.00	6
5	DEOXYGEDUNIN	3.00±0.00	6
6	ALPHA-DIHYDROGEDUNOL	3.00±0.00	6
7	DIHYDROFISSINOLIDE	3.00±0.00	6
8	AMIODARONE HYDROCHLORIDE**	3.00±0.00	3
9	DANAZOL	3.00±0.00	6
10	ETHAMIVAN	3.00±0.00	6
11	FERULIC ACID	3.00±0.00	3
12	CARAPIN-8(9)-ENE	3.00±0.00	6
13	3-ISOBUTYL-1-METHYLXANTHINE (IBMX)*, **	2.83±0.41	6
14	1,3-DIPROPYL-8-PHENYLXANTHINE **	2.83±0.41	6
15	(RS)-(TETRAZOL-5-YL) GLYCINE**	2.83±0.41	6
16	EFONIDIPINE HYDROCHLORIDE MONOETHANOLATE**	2.83±0.41	6
17	3-DEOXO-3BETA-ACETOXYDEOXYDIHYDROGEDUNIN	2.83±0.41	6
18	HYDROCORTISONE HEMISUCCINATE	2.83±0.41	6
19	LOMEFLOXACIN HYDROCHLORIDE	2.83±0.41	6
20	ASTEMIZOLE	2.83±0.41	6
21	11ALPHA-HYDROXYPROGESTERONE HEMISUCCINATE	2.83±0.41	6
22	CGP 37157	2.67±0.58	3
23	(S)-(+)-NIGULDIPINE HYDROCHLORIDE**	2.67±0.58	3
24	TRACAZOLATE HYDROCHLORIDE	2.67±0.58	3
25	IVERMECTIN	2.67±0.52	3
26	XANTHYLETIN	2.67±0.58	3

***** IBMX did not rescue *vcanb* mRNA expression in *fr24* mutants at 25 μM, but it did induce partial down-regulation (score 2) at the concentration of 100 μM, which was used as a control for this assay.

** Compounds presumed to act by raising cAMP levels.

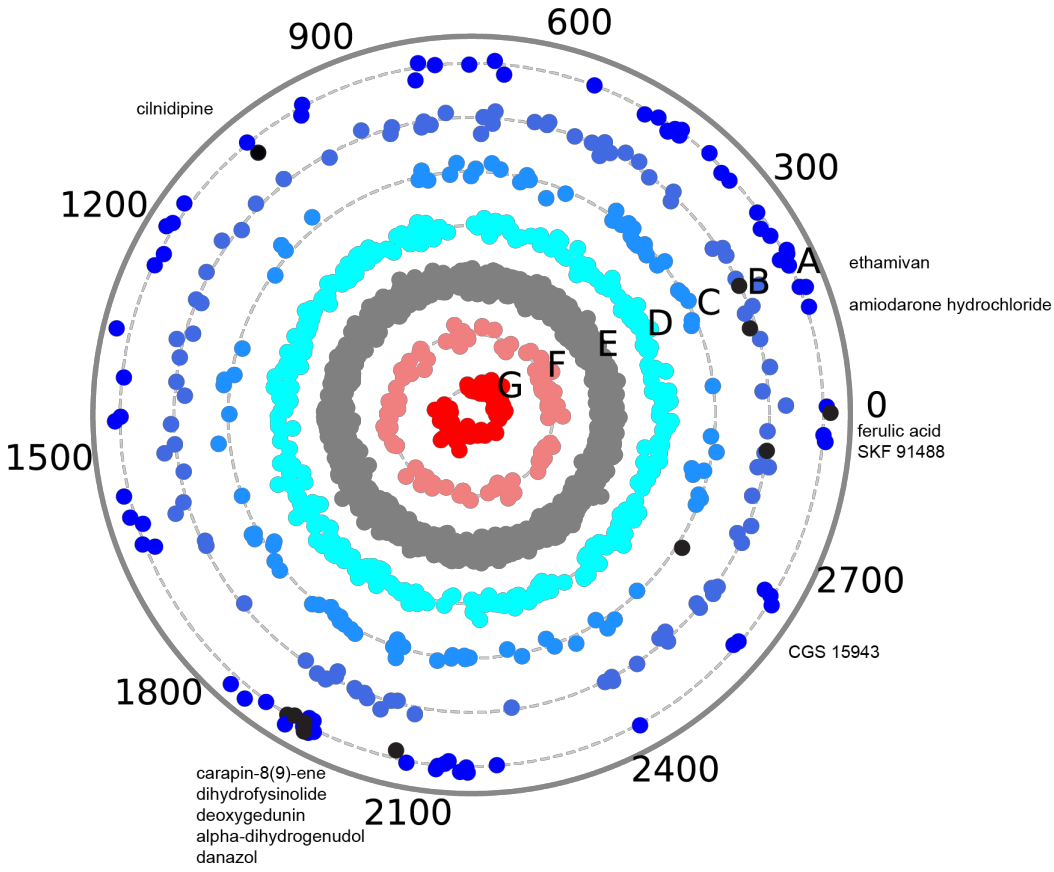

Figure 5.7 Visualisation of the compounds presumed to interact with the Adgrg6 receptor directly. Compounds that rescued the expression of *vcanb* and *mbp* in *adgrg6*^{tb233c} mutants, but did not induce any down-regulation of *vcanb* in *adgrg6*^{fr24} mutants (average *vcanb* score of 3) are shown in black.

5.2.3ii *Versican* hit compounds that did not affect *myelin basic protein* expression (Group I)

I found 26 hit compounds that strongly down-regulated *vcanb* expression and did not affect *mbp* expression in *adgrg6*^{tb233c} mutants (Table 5.6). However, as all my assays have been carried out at a single concentration (25 µM), it is possible that some or all of these compounds may rescue *mbp* expression at a higher concentration. The members of group I consist of a wide range of structures with numerous functions (Figure 5.8), which was expected, as the down-regulation of *versican* may arise from targeting different components from different pathways that regulate *versican* expression in the zebrafish ear.

Table 5.6 List of the 26 *versican* hit compounds that did not affect *mbp* expression in *adgrg6*^{tb233c} mutants (group I).

#	Compounds able to rescue *vcanb expression,* without affecting *mbp* expression (group I)	*vcanb* score mean ±SD (n=9)	*mbp* score mean ±SD (n=6)
1	CMPD-1 /2'-FLUORO-N-(4-HYDROXYPHENYL)-[1,1'-BIPHENYL]-4-BUTANAMIDE	0.11 ±0.33	0.83 ±0.41
2	GTP 14564/ 3-PHENYL-1H-BENZOFURO[3,2-C] PYRAZOLE	0.22 ±0.44	1.00 ±0.63
3	2,3-DIHYDROXY-4-METHOXY-4'-ETHOXYBENZOPHENONE	0.33 ±0.50	1.17 ±0.41
4	MEPIROXOL/ 3-PYRIDINEMETHANOL N-OXIDE	0.33 ±0.71	1.17 ±0.41
5	METHIOTHEPIN MALEATE	0.33 ±0.50	1.00 ±0.00
6	BHQ/ 1,4-DIHYDROXY-2,5-DI-TERT-BUTYLBENZENE	0.44 ±0.53	1.17 ±0.41
7	FPL 64176	0.44 ±0.53	1.00 ±0.00
8	3-DEOXO-3BETA-HYDROXYMEXICANOLIDE 16-ENOL ETHER	0.67 ±1.00	1.00 ±0.00
9	TMS/ (E)-2,3',4,5'-TETRAMETHOXYSTILBENE	0.67 ±1.00	0.83 ±0.41
10	7-DESHYDROXYPYROGALLIN-4-CARBOXYLIC ACID	0.78 ±0.67	1.00 ±0.00
11	ANGOLENSIN (R)	0.78 ±1.20	0.67 ±0.52
12	DECOQUINATE	1.00 ±0.87	1.00 ±0.00
13	CHOLIC ACID	1.11 ±1.05	1.17 ±0.41
14	SD 208/ 2-(5-CHLORO-2-FLUOROPHENYL)-4-[(4-PYRIDYL)AMINO]PTERIDINE	1.11 ±0.33	1.00 ±0.00
15	DICLOFENAC SODIUM	1.22 ±1.09	1.00 ±0.00
16	D-64131/ (5-METHOXY-1H-INDOL-2-YL) PHENYLMETHANONE	1.22 ±0.97	0.83 ±0.41
17	GBR 12935 DIHYDROCHLORIDE	1.33 ±1.22	1.17 ±0.41
18	PP1 /1-(1,1-DIMETHYLETHYL)-1-(4-METHYLPHENYL)-1H-PYRAZOLO[3,4-D]PYRIMIDIN-4-AMINE)	1.33 ±0.87	1.00 ±0.00
19	2-METHOXYESTRADIOL/ (17B)-2-METHOXYESTRA-1,3,5(10)-TRIENE-3,17-DIOL	1.33 ±0.50	0.83 ±0.41
20	HARMINE	1.44 ±0.53	1.00 ±0.00
21	IOPANOIC ACID	1.44 ±1.13	0.83 ±0.41
22	CPT 11/ IRINOTECAN/ CAMPTOTHECIN 11	1.56 ±0.53	1.00 ±0.00
23	MANNITOL	1.67 ±0.50	1.17 ±0.41
24	CGP 7930	1.67 ±0.87	1.00 ±0.00
25	CARBIMAZOLE	1.78 ±0.83	1.00 ±0.00
26	DL-TBOA/ DL-THREO-B-BENZYLOXYASPARTIC ACID	2.00 ±0.00	1.17 ±0.41

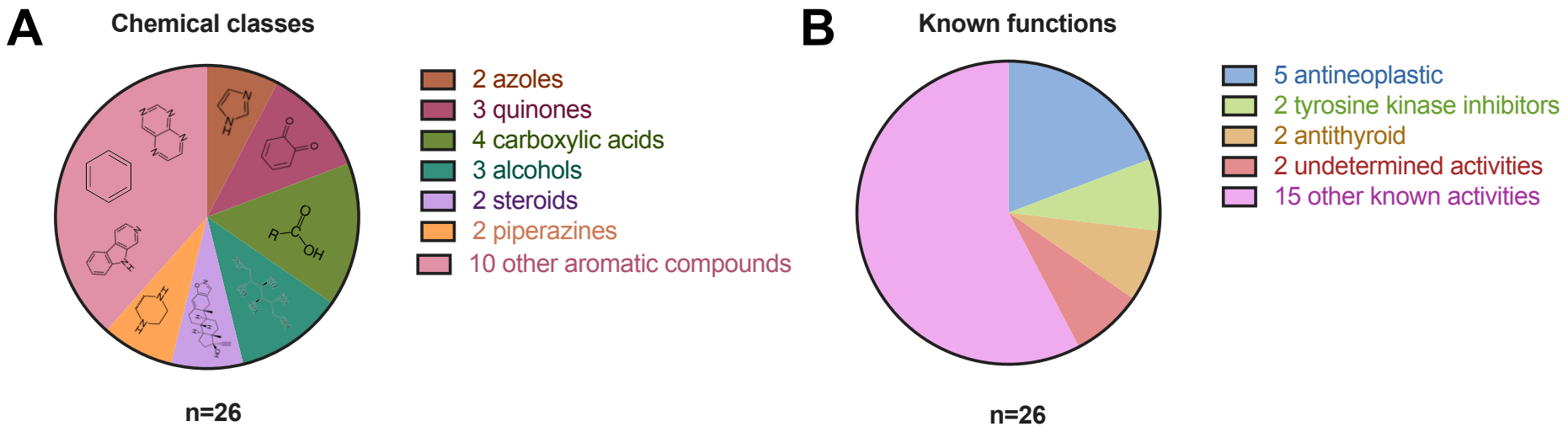

Figure 5.8 Classification of the *versican* hit compounds that did not affect *mbp* expression (group I). The 26 *versican* hit compounds have been categorised according to their broad chemical classes **(A)** and known functions **(B)**, with the relative proportions of each group indicated in the corresponding pie chart.

5.2.3iii *Versican* hit compounds that also down-regulated *myelin basic protein* mRNA expression (General transcription inhibition) (Group J)

I found 22 hit compounds that down-regulated the expression of both *vcanb* and *mbp,* and thus, were presumed to inhibit transcription or cause developmental arrest of the embryo (Table 5.7). Gedunin was a member of both libraries and was tested for *mbp* in duplicate, giving the same score (0), so, the number of unique compounds of group J is actually 21. This group included various natural toxins, as well as synthetic antifungal, anthelmintic, antiviral and antineoplastic compounds that impede proliferation (Figure 5.9). It is worth mentioning, that six out of the six azoles with antifungal or anthelmintic properties tested for *mbp*, were clustered in this group.

Table 5.7 List of the 21 *versican* hit compounds that also down-regulated *mbp* expression in *adgrg6*^{tb233c} mutants, which may represent general transcription inhibitors (group J).

#	Compounds that down-regulated the expression of both *vcanb* and *mbp* expression (group J)	*vcanb* score mean ±SD (n=9)	*mbp* score mean ±SD (n=6)
1	LOVASTATIN	0.00 ±0.00	0.50 ±0.55
2	BAICALEIN	0.00 ±0.00	0.50 ±0.55
3	CLOTRIMAZOLE	0.00 ±0.00	0.50 ±0.55
4	GITOXIN	0.44 ±0.53	0.33 ±0.52
5	CYPROHEPTADINE HYDROCHLORIDE	0.00 ±0.00	0.33 ±0.52
6	DEOXYSAPPANONE B 7,3'-DIMETHYL ETHER ACETATE	0.00 ±0.00	0.33 ±0.52
7	DEOXYSAPPANONE B 7,4'-DIMETHYL ETHER	0.00 ±0.00	0.17 ±0.41
8	5-FLUOROINDOLE-2-CARBOXYLIC ACID	0.00 ±0.00	0.17 ±0.41
9	LARIXOL ACETATE	1.44 ±1.33	0.17 ±0.41
10	MEBENDAZOLE	0.67 ±0.50	0.17 ±0.41
11	ALBENDAZOLE	0.00 ±0.00	0.17 ±0.41
12	LONIDAMINE	0.00 ±0.00	0.00 ±0.00
13	GEDUNIN	0.00 ±0.00	0.00 ±0.00
14	PODOFILOX	0.00 ±0.00	0.00 ±0.00
15	DIGITOXIN	0.44 ±0.73	0.00 ±0.00
16	ARTENIMOL	0.00 ±0.00	0.00 ±0.00
17	DISULFIRAM	0.33 ±0.50	0.00 ±0.00
18	CHAULMOOGRIC ACID	0.00 ±0.00	0.00 ±0.00
19	SULCONAZOLE NITRATE	0.44 ±0.73	0.00 ±0.00
20	ECONAZOLE NITRATE	0.67 ±1.00	0.00 ±0.00
21	FENBENDAZOLE	0.00 ±0.00	0.00 ±0.00

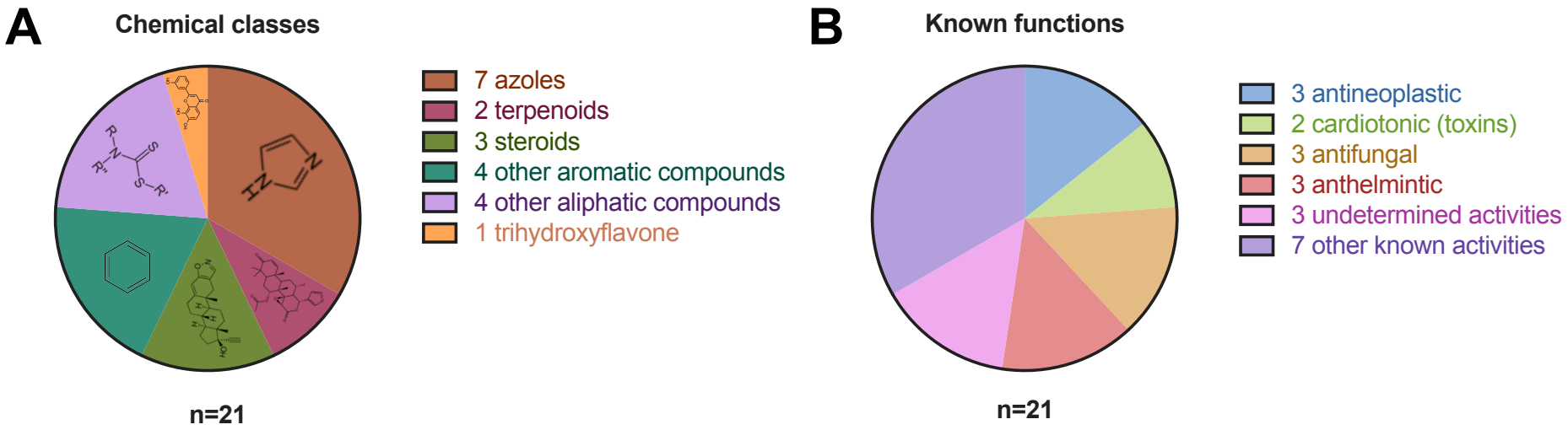

Figure 5.9 Classification of the *versican* hit compounds that also down-regulated *mbp* expression, which may represent general transcription inhibitors (group J). The 21 compounds in group J have been categorised according to their chemical classes **(A)** and known functions **(B)**, with the relative proportions of each group indicated in the corresponding pie chart.

5.2.4 Tracazolate hydrochloride, FPL 64176, nifedipine and cilnidipine down-regulate *versican* mRNA expression in a dose-dependent manner.

In order to further analyse the activity of some hit compounds further and determine if their action is dose-dependent, four hit compounds (three from group H and one from group I) were selected for dose-response assessment. As many of the compounds classified as putative Adgrg6 pathway modulators were dihydropyridines, I chose two compounds from this class (cilnidipine and nifedipine). The third compound that was chosen from group H was tracazolate hydrochloride, a nonbenzodiazepine, γ-aminobutyric acid A ($GABA_A$) modulator. Based on its potent efficacy in down-regulating versican and the fact that it was the only calcium channel blocker that was not classified in group H, FPL 64176 was the compound chosen from group I.

The four compounds selected for dose-response assessment were initially tested in a three-fold dilution series, by exposing three *adgrg6*^{tb233c} embryos to concentrations ranging from 0.3 μM to 222.2 μM, between 60-90 hpf. *In situ* hybridisation analysis of the 90 hpf larvae revealed a dose-dependent down-regulation of *vcanb* mRNA expression in response to treatment with all four drugs, with concentration efficacy windows that differ for each drug (Figure 5.10A-D). To determine the concentration at which the drugs can affect the health of the embryo, three LWT wild-type embryos were exposed to the same concentrations of compounds as mentioned above. At the end of the treatment (90 hpf), the number of heartbeats per minute was monitored for one embryo per concentration (Figure 5.10E-H). I found that 1% DMSO slightly reduced heartbeats from 150 (untreated) to 130 per minute, in all four embryos checked (Figure 5.10E-H). Among the four drugs, FPL 64176 affected heartbeats the most, as even at low concentrations (e.g. 2.7 μM) heartbeats were significantly reduced compared to the DMSO-treated embryos. This reduction in heartbeats induced by FPL 64176 was accompanied by a slight edema, which developed to moderate in higher concentrations (data not shown). Tracazolate, nifedipine and cilnidipine did not result in heart oedema, but all four drugs resulted in complete arrest of the heart beat at the highest concentrations tested (Figure 5.10).

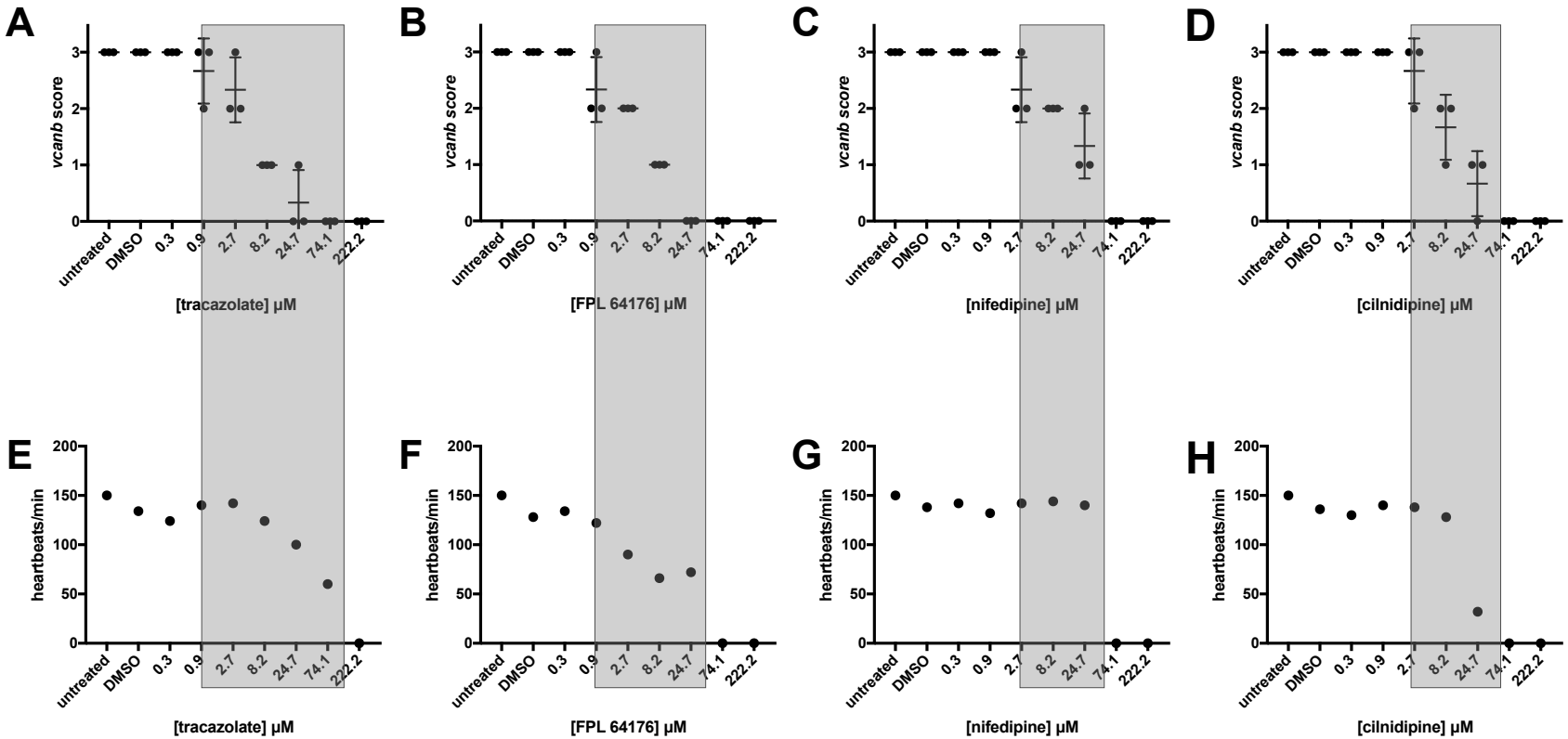

Figure 5.10 Tracazolate hydrochloride, FPL 64176, nifedipine and cilnidipine down-regulate *versican* mRNA expression in the *adgrg6*^{tb233c} mutant ear in a dose-dependent manner. Three *adgrg6*^{tb233c} homozygous embryos (A-D) and three LWT wild-type embryos (E-H) were exposed to each one of a three-fold dilution series of concentrations, ranging from 0.3 µM to 222.2 µM, between 60-90 hpf. DMSO (1%) was used as a negative control. **(A-D)** *In situ* hybridisation analysis of the *adgrg6*^{tb233c} larvae revealed a dose-dependent down-regulation of *vcanb* mRNA expression in response to treatment with all four drugs. **(E-F)** At the end of the treatment (90 hpf), the number of heartbeats per minute was measured from one LWT wild-type embryo per concentration.

Based on the information about the efficacy and toxicity of each drug, I designed an optimised assay, by increasing the number of *adgrg6*^{tb233c} embryos treated per concentration to nine, adjusting the exposure time to 50 hours (60-110 hpf, instead of 60-90 hpf) and testing a 1.5-fold dilution series of concentrations, tailored to the known toxicity of each drug. *In situ* hybridisation analysis of the 110-hpf larvae revealed a robust, dose-dependent down-regulation of *vcanb* mRNA expression in response to treatment with all four drugs. *versican* (*vcanb*) mRNA expression was assessed by annotating each embryo with two scores, one representing the intensity of the stain (0-3; Figure 5.11A) and the other representing the number of projections stained (0p-3; Figure 5.11B). I found that all four drugs were able to reduce both the intensity of the mRNA staining and the number of projections stained, in a dose-dependent manner. For each of the four drugs, the intensity of the *vcanb* staining was found decreased after treatment with low doses, while a relatively higher dosage was needed to decrease the number of the projections stained.

An LD_{50} was plotted for the adjusted exposure time (60-110 hpf), using 16 LWT wild-type embryos per concentration. Each LWT embryo was kept in a separate 96-well-plate well and at the end of each treatment, the number of dead larvae was counted (Figure 5.12). The assessment of the embryos as alive or dead was based on microscopic observation of the heart for 10 seconds; dead embryos were considered the ones where no heartbeat was recorded in this timeframe. The lowest LD_{50}among the four drugs was the one calculated for cilnidipine (19.2 μM). The LD_{50} concentrations for nifedipine, FPL 64176 and tracazolate were calculated 40 μM, 47.3 μM and 51.7 μM, respectively. In terms of mortality rate, nifedipine and cilnidipine behaved in a similar way, as it can be deduced from the two respective steep curves (Figure 5.12 C,D). Tracazolate and FPL 64176 curves followed a different pattern, with a more gradual sigmoid curvature (Figure 5.12 A,B).

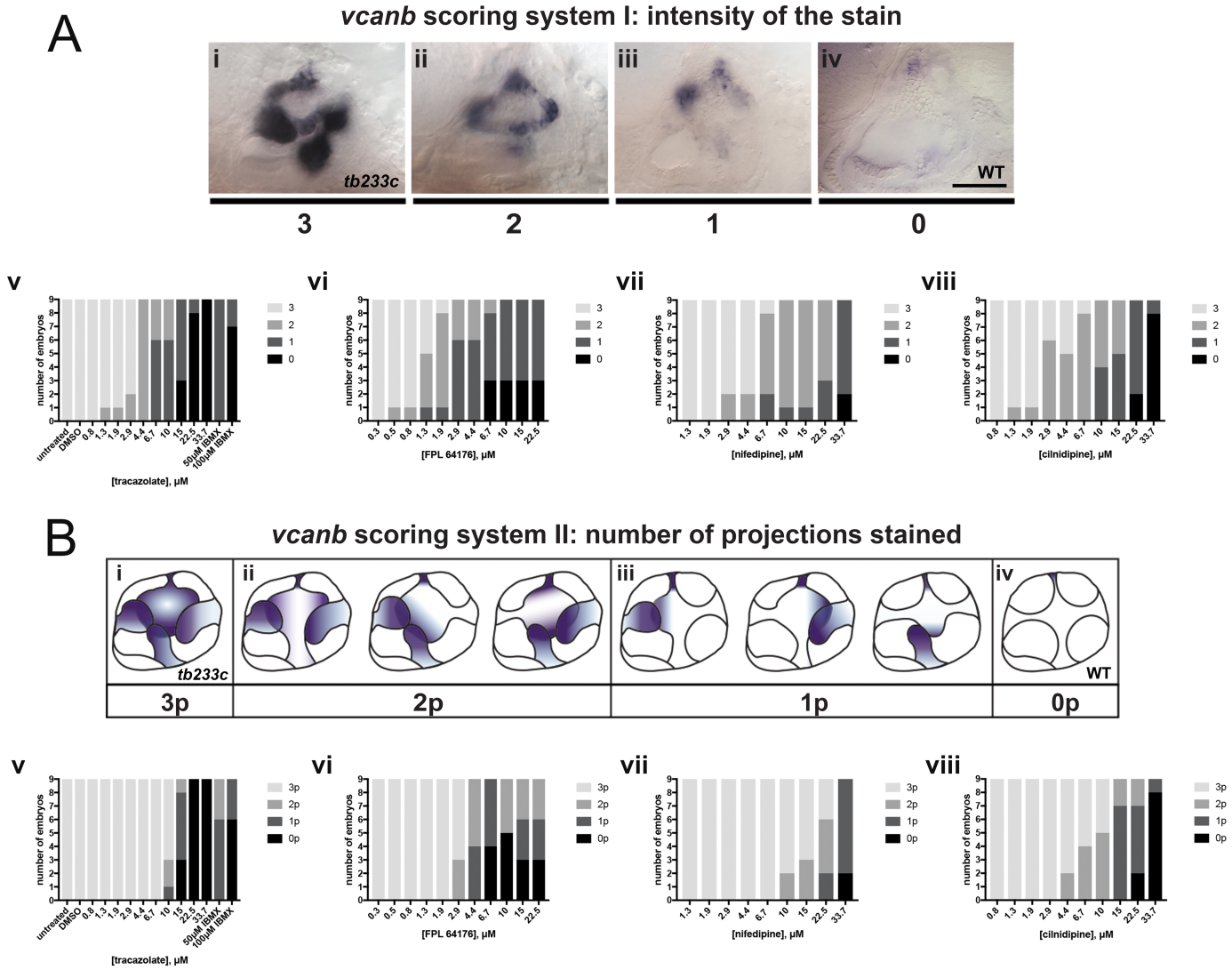

Figure 5.11 Tracazolate hydrochloride, FPL 64176, nifedipine and cilnidipine down-regulate *versican* levels of expression and reduce the number of projections that express *versican* in the *adgrg6*^{tb233c} mutant ear, in a dose-dependent manner. Nine *adgrg6*^{tb233c} homozygous embryos were exposed to a 1.5-fold dilution series of concentrations (ranging from 0.3 µM to 33.7 µM), that was tailored to the following drugs: tracazolate hydrochloride, FPL 64176, nifedipine and cilnidipine. IBMX (50 µM and 100 µM) was used as a positive control, while DMSO (1%) was used as a negative control. Embryos were treated between 60-110 hpf prior to fixation and analysis for *vcanb* expression by whole-mount *in situ* hydridisation. **(Ai-iv)** Scoring system used to assess the intensity of *vcanb* staining, i.e. the mRNA expression levels. **(Av-viii)** Chart bars showing the number of embryos that scored 0, 1, 2, or 3. **(Bi-iv)** Scoring system used to assess the number of projections that express *vcanb*. **(Bv-viii)** Chart bars showing the number of embryos that scored 0p, 1p, 2p, or 3p.

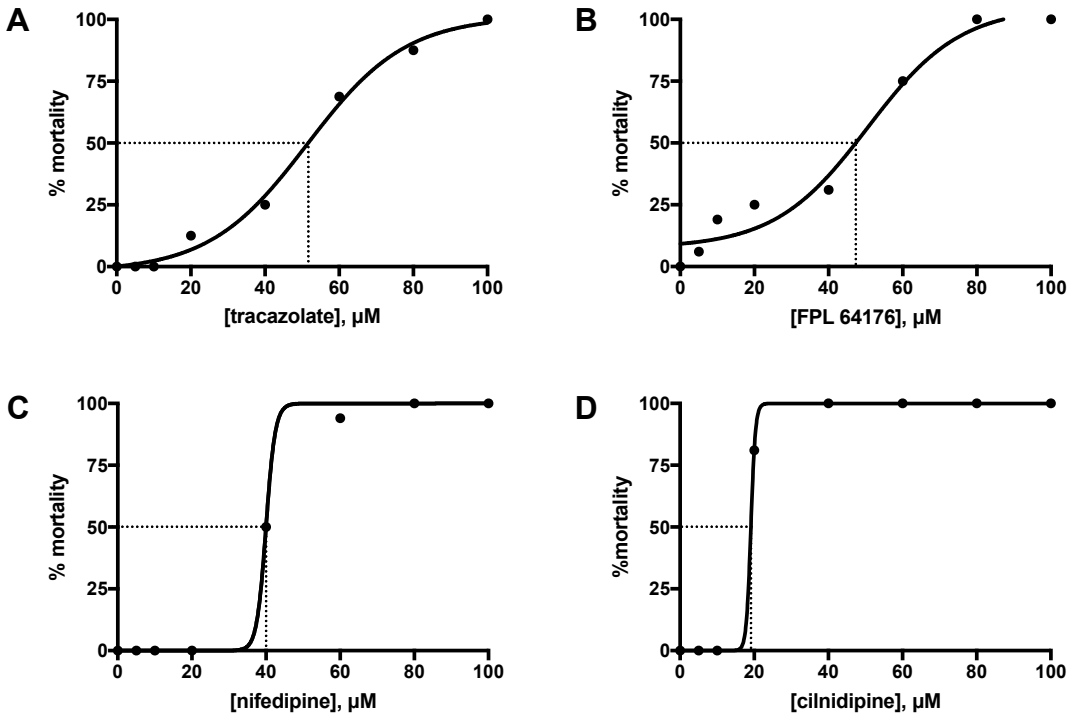

Figure 5.12 LD_{50} curves from the treatment of wild-type embryos for the adjusted exposure time (60-110 hpf). 16 LWT wild-type embryos, each kept in a separate 96-well-plate well, were treated with each one of the following concentrations: 5, 10,20,40, 60, 80 and 100 µM from 60 to 110 hpf. At the end of the treatment, the number of alive versus dead embryos was counted and the mortality percentage was plotted against concentration. PRISM LD_{50}, nonlinear fit algorithm was used to draw the curves for tracazolate hydrochloride **(A)**, FPL 64176 **(B)**, nifedipine **(C)** and cilnidipine **(D)**. LD_{50} was calculated as the concentration at which 50% of the embryos were dead.

5.2.5 Tracazolate hydrochloride, FPL 64176, nifedipine and cilnidipine restore pillar formation in the *adgrg6* mutant ear in a dose-dependent manner.

In order to investigate whether reduction of the number of projections expressing *vcanb* correlated with an increase in the number of the pillars formed, the inner ears of the treated larvae were observed and photographed at 110 hpf. Consistent with the *versican* scores for the number of projections stained, live DIC images of the inner ear revealed a dose-dependent rescue of pillar formation, which was greater at higher doses (Figure 5.13A-F'). This finding demonstrates that *versican* mRNA expression is a reliable indicator of the epithelial projection fusion to form pillars taking place in the zebrafish inner ear.

As *adgrg6*^{tb233c} mutants have been reported to have a swollen ear phenotype (Geng et al., 2013), measurements of the ear-to-ear width (A) were taken from photographs of live embryos mounted dorsally. To eliminate any stage/size differences among the larvae and normalise the data, I subtracted the width of the rest of the head (B) and then divided by the width of the body (C), as defined by the points where the edge of the ear joins the rest of the body (see section 2.1.3 and Figure 2.1 for more details on the experimental approach). The results showed a dose-dependent reduction in the normalised ear width with increased concentration of the four drugs (Figure 5.13G-J).

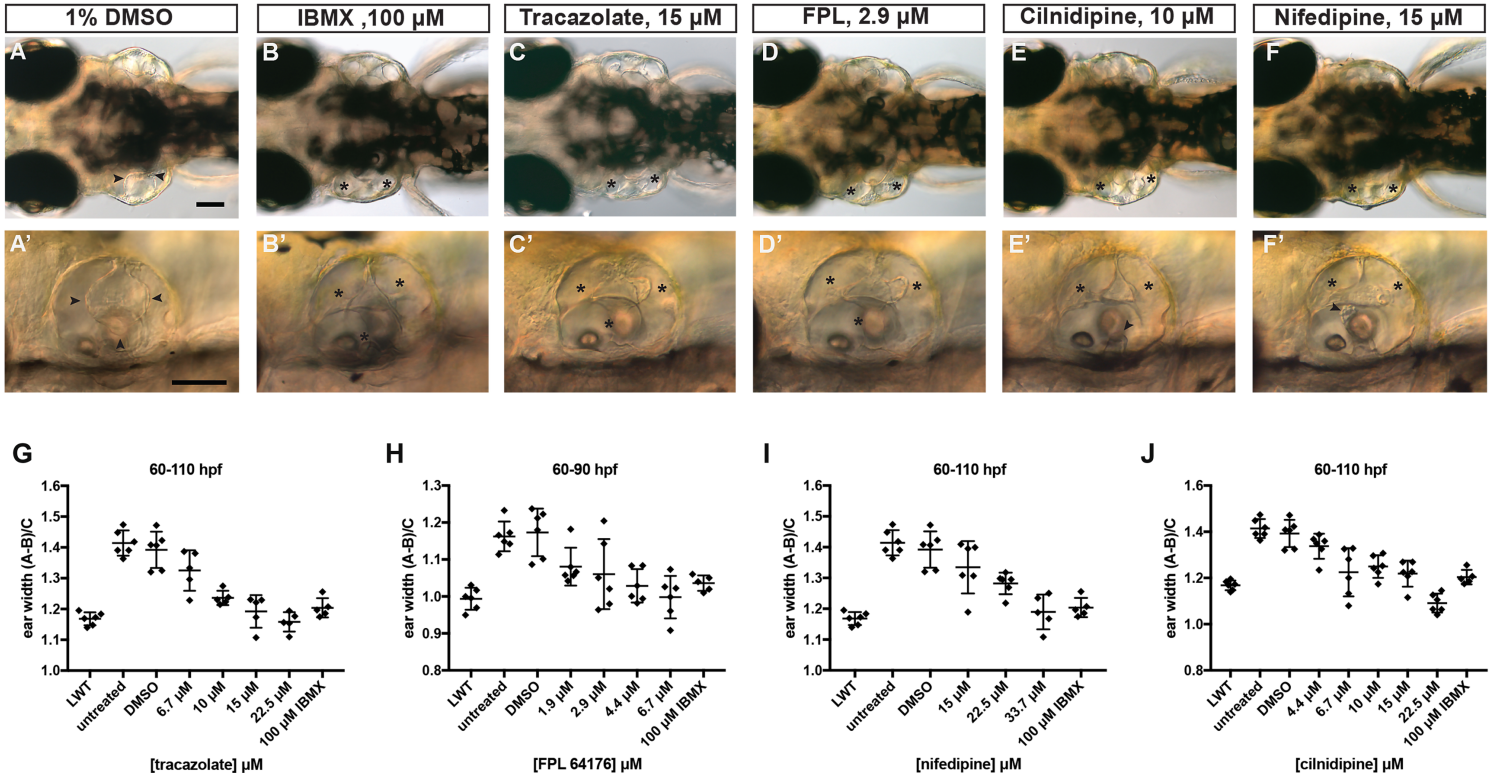

Figure 5.13 Tracazolate hydrochloride, FPL 64176, nifedipine and cilnidipine restore pillar formation and ameliorate the swelling in the *adgrg6*^{tb233c} mutant ear in a dose-dependent manner. Six *adgrg6*^{tb233c} homozygous embryos were exposed to each one of a geometric series of concentrations, that was tailored for each drug. Embryos were treated with tracazolate hydrochloride, nifedipine and cilnidipine between 60-110 hpf and with FPL 64176 between 60-90 hpf. IBMX (100 µM) was used as a positive control, while DMSO (1%) was used as a negative control. At the end of each treatment, live embryos were mounted and photographed. **(A-F)** Live dorsal DIC images of the inner ear of 110 hpf *adgrg6*^{tb233c} homozygous mutants. **(A'-F')** Side views of the same embryos depicted in A-F. **(G-J)** Measurements of the ear-to-ear width were taken from live embryos mounted dorsally and photographed at a focal plane that highlighted the largest visible dimensions. Scale bars: in A, 50 µm for B-F; in A', 50 µm for B'-F'. Asterisks mark fused pillars, while arrowheads mark unfused projections.

5.3 DISCUSSION

5.3.1 Primary *versican* screens

In this chapter, I present a high-throughput, phenotypic drug screening assay, in which I and other members of the Whitfield lab tested the efficacy of 3120 compounds from the Tocris and Spectrum libraries in down-regulating the expression of *versican* in the *adgrg6*^{tb233c} mutant ear. As all the compounds were administered at the same, arbitrary concentration (25 μM), it is not safe to deduce conclusions for the compounds that failed these assays, as their lack of efficacy could be due to this concentration being suboptimal.

After the first round of primary screens, I found that 8% and 10% of the compounds included in the Tocris library and Spectrum libraries, respectively, were identified as successful in down-regulating *versican* expression in *adgrg6*^{tb233c} homozygous mutants. When the successful compounds were retested for the first time, the hit rates from the Tocris and Spectrum libraries were 34% and 43%, respectively. The relatively low hit rates after the first re-test implies the existence of a high number of false-positive results in the primary screen, but could also be due to slight variations in the concentration at which a compound is administered between the primary library plate and the subsequent, manually cherry-picked plates. When these compounds were selected and retested for a third time, more than 85% of the compounds from both libraries retested positive. This finding suggests that two experimental repeats (i.e. data from 6 embryos) are enough to eliminate false-positive results that could arise from *in situ* hybridisation limitations, such as low penetration of the RNA probe. The fact that 85.3% of the compounds that were common between the two libraries (and therefore tested in duplicate) showed a similar efficacy in down-regulating *vcanb* expression in the two independent experiments, highlights the robustness of the assay and the consistency of the scoring process.

The fact that IBMX and colforsin were independently identified through the screen as category A hits and that many of the hit compounds were structurally similar to IBMX and colforsin, is in line with previously published data reporting that IBMX and forskolin (of which colforsin is a derivative) ameliorate the *adgrg6*^{tb233c} mutant ear phenotype by elevating cAMP levels (Monk et al., 2009; Geng et al., 2013).

In order to obtain insight into the way the hit compounds act to trigger down-regulation of *versican* expression, I exploited the absence of *mbp* expression in the PLLg of *adgrg6*^{tb233c} mutants and used it as the basis of a secondary screening assay.

5.3.2 Secondary *myelin basic protein* screens

After testing how the successful versican hit compounds affect *mbp* expression in the PNS of *adgrg6*^{tb233c} mutants, three groups of compounds were identified: The biggest group included 42 out of the 90 hit compounds (46.7%) that down-regulated *vcanb* expression; these compounds up-regulated *mbp* expression in the PLLg to some extent, presumably by targeting components of the Adgrg6 signalling pathway. The second group included 26 (28.9%, n=90) versican hit compounds which did not affect *mbp* expression, while the third group comprised of 22 (24.4%, n=90) compounds, which down-regulated *mbp* expression in the anterior and posterior lateral line nerves and ganglia. These findings suggest that there are both shared and distinct signalling mechanisms that regulate the expression of *vcanb* and *mbp* genes.

The screening assay format followed for the assessment of *mbp* expression was the same with the one used to analyse *versican* expression. As the latter had been tailored to semicircular canal formation, the treatment was applied from 60 to 90 hpf. However, this may not be the optimal time window for the development of lateral line nerves and ganglia, and therefore compounds that did not seem to affect *mbp* in this assay may be efficacious in a different experimental format.

Using the expression of *mbp*, I identified compounds that rescue the myelination defects of the PLL ganglia in *adgrg6* homozygous mutants. However, further experiments are needed to investigate whether these compounds are also capable of restoring the functionality of the nerves, or have any effects on nerve regeneration (e.g. after a nerve crush). Furthermore, a follow-up counter-screen of the hit compounds using other mutant lines characterised by myelination defects (e.g. gle1; Seytanoglu et al., 2016) would provide useful insight in relation to drug promiscuity.

5.3.3 Putative downstream effectors of the Adgrg6 pathway

5.3.3i cAMP modulators

Previous studies have managed to restore the PNS defects of *Adgrg6*-/- mouse and zebrafish mutants by elevating cAMP levels and activating protein kinase A (PKA), demonstrating that Adgrg6, via interactions with G-proteins, elevates cAMP levels in Schwann cells and controls differentiation and myelination, through CREB activation (Monk et al., 2009; Mogha et al., 2013). In apparent agreement with these findings, 15 out

of 42 compounds that rescued both *versican* and *mbp* expression in *adgrg6*^{tb233c} mutants are known to increase cAMP in different ways, suggesting that Adgrg6 may act by elevating cAMP not only in Schwann cells, but also in the zebrafish inner ear cells. Consistent with the finding of Monk et al. (2009) that forskolin rescues *mbp* expression in *st49* mutants, the forskolin derivative colforsin rescued *vcanb* and *mbp* expression in both *tb233c* and *fr24* alleles used in this assay. Although four out of the 15 compounds known to raise cAMP (cilnidipine, amiodarone hydrochloride, SC-10, CGS 15943) showed no efficacy in restoring *fr24* mutants at 25 μM, it seems unlikely that they interact directly with the receptor. However, this requires further experimentation and may be elucidated by performing dose-response assays using the *fr24* allele.

5.3.3ii Calcium-channel blockers (CCBs): dihydropyridines

Calcium channels are transmembrane, voltage-gated ion channels, whose activity can be modulated by compounds directly or indirectly, by intracellular signals from other receptors (Waller et al., 2010; chapter 1). For example, L-type calcium channels can be inactivated either by calcium-channel blockers (CCBs) or indirectly by reducing intracellular signalling from β1-adrenoceptors. When calcium channels are open, they permit the passive diffusion of cations passively into the cell, making the cytosolic electrical potential more positive and causing depolarisation of excitable tissues (Waller et al., 2010; chapter 1).

Although it is known that active Ca^{2+} transport plays an important role in the formation of the otoliths (Mugiya & Yoshida, 1995), Cruz et al. (2008) suggested additional roles in the zebrafish ear, whereby the Ca^{2+} ATPase Atp2b1a is also required for hair cell growth and semicircular canal formation. The fact that *vcanb* expression and pillar formation in *adgrg6* mutants are rescued by nifedipine and cilnidipine, two CCBs, but also by FPL 64176, which is a calcium-channel activator, further supports the importance of [Ca^{2+}] balance inside and outside the cell in semicircular canal development.

In CNS, reducing intracellular Ca^{2+} is known to be neuroprotective in rat retinal ganglion cells (Farell et al., 2014). More specifically, CCBs limit chronic secondary degeneration following neurotrauma, by preserving axonal density and reducing the number of axons with de-compacted myelin (Savigni et al., 2013). Our finding that eight out of forty-two hit compounds that rescued both *versican* and *mbp* expression in *tb233c* mutants are Ca^{2+}-channel blockers, suggests that regulation of intracellular Ca^{2+} levels may be crucial in

both the inner ear and the PNS, and that Ca^{2+} may interfere with Adgrg6 pathway, possibly by controlling calcium ATPases and/or by elevating cAMP levels.

The most smooth-muscle-selective class of CCBs are the dihydropyridines. Because of their high vascular selectivity, these drugs are primarily used to reduce systemic vascular resistance and arterial pressure, and therefore are used to treat hypertension. The finding that six (nifedipine, cilnidipine, nitrendipine, nimodipine, niguldipine, efonidipine) out of these eight CCBs are dihydropiridines is in agreement with previous studies in mammals, reporting that nimodipine triggers remyelination in a mouse model of multiple sclerosis and in rats, by ameliorating peripheral nerve crush injuries (Schampel et al., 2017; Tang et al., 2015). As dihydropiridines have been previously reported to inhibit cAMP phosphodiesterases (Sakamoto et al., 1978), protection of cAMP from degradation might be another mechanism whereby these molecules exert their ameliorating action.

5.3.3iii Flavonoids and MAPK signalling

The flavonoids are a group of molecules with well-known antioxidant and neuroprotective properties (Maurer et al., 1997; Schroeter et al., 2002). Flavonoid members have been reported to display various functions, including calcium homeostasis and modulation of various enzyme systems, affecting inflammation, cardiovascular disease and cancer (Yule et al., 1994; Schroeter et al., 2002). Although the final outcome of their bioactivity could be different among members and dependent on the metabolites each compound produces, flavonoids have been reported to exert their function through interaction with MAPK/ERK signalling pathway (Kong et al., 2000; Schroeter et al., 2002; Cheng et al., 2016). All five *O*-methylated flavonoids that rescued *vcanb* and *mbp* expression in *tb233c* mutants, seemed to also rescue *fr24* allele, suggesting that they act down-stream of the Adgrg6 receptor. Therefore, MAPK signalling and its downstream effect on CREB pathway, could be a possible mechanism of action of these five flavonoid members. This finding is consistent with human melanoma studies, where *VCAN* transcription was shown to be activated through ERK/MAPK and JNK signalling pathways acting on the AP-1 site of the *VCAN* promoter (Domenzain-Reyna et al., 2009). Taken together, these data suggest that *versican* regulatory mechanisms may be conserved from teleosts to human, and thus, insight obtained from zebrafish screening studies could be applied to regulate *versican* expression in human malignant cells. This is the subject of Chapter 6, where the efficacy of some hit compounds identified in this Chapter is interrogated in an *in vitro* human cell model.

5.3.4 Putative Adgrg6 receptor modulators

As discussed in section 5.2.3i, I found twelve hit compounds that rescued *vcanb* and *mbp* expression in *tb233c* mutants, but not in *fr24* mutants; these compounds may therefore interact directly with the Adgrg6 receptor. Five out of the twelve compounds, namely deoxygedunin, alpha-dihydrogedunol, dihydrofissinolide, carapin-8(9)-ene and danazol, share structural similarities, that may be important for binding and activation of the Adgrg6 receptor, thereby acting as receptor agonists (Figure 5.14). However, further binding and activity assays (e.g. luciferase reporter assays) are needed to confirm this interaction.

Although the mechanism of action of dihydrofissinolide, carapin-8(9)-ene and danazol is unknown, gedunin derivatives have been reported to be partial agonists for human aGPCRs ADGRG1 and ADGRG5 (Stoveken et al., 2018). Deoxygedunin in particular, has been shown to activate TrkB receptor signalling in mice, thus mediating neuroprotective and learning enhancement properties (Jang et al., 2010). With suspected roles in other signalling pathways, it would be important to characterise the specificity each of the five target molecules has for Adgrg6 in relation to Adgrg1 and Adgrg5 in parallel binding or activity assays. However, the promising results described here give an indication of the structural characteristics required for the drug molecules to mimic the activity of the endogenous Adgrg6 peptide agonists and warrants further investigation.

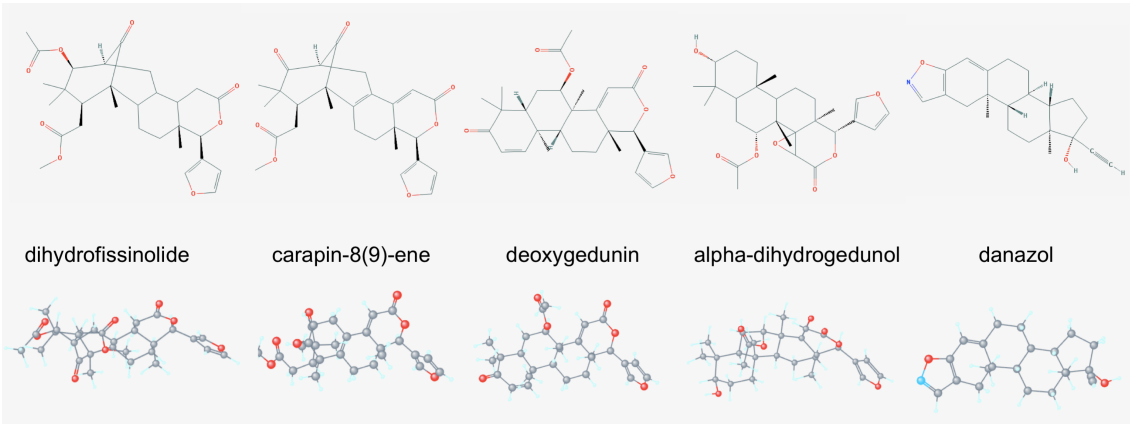

Figure 5.14 Dihydrofissinolide, carapin-8(9)-ene, deoxygedunin, alpha-dihydrogedunol and danazol share 2D (upper panels) and 3D (lower panels) structural similarities that may be important for interaction with the binding pocket of Adgrg6 receptor. The molecular structure of all five compounds is steroid-like. Dihydrofissinolide, carapi-8(9)-ene, deoxygedunin and alpha-dihydrogedunol share a limonoid skeleton, thus having a furanolactone core (Roy and Saraf, 2006; Stoveken et al., 2018).

In summary, these data show that *versican* overexpression in the *adgrg6* mutant ear provides an easily identifiable phenotype, which can be used as a robust, preliminary screening tool to seek for compounds that may target components of the Adgrg6 pathway. The availability of various *adgrg6* mutant alleles provides an excellent *in vivo* system, which can facilitate the investigation of the target molecule. The fact that some of the compounds presented in this study have been previously reported to promote myelination in mammals, highlights the value of phenotypic screens in zebrafish. It also suggests that zebrafish *adgrg6* mutants constitute a powerful model which recapitulates the PNS and ear defects present in some human hereditary peripheral myelinopathies in human, such as Charcot-Marie-Tooth syndrome, where sensorimotor deficits and deafness are attributed to mutations in *KROX 20*, myelin genes, and others (Pogoda et al., 2006).

5.4 CONCLUSIONS

- Phenotypic screening of a broad range of chemical compounds revealed a wide spectrum of compounds that can rescue *vcanb* expression in the hypomorphic allele of the *adgrg6* mutant, *tb233c*.
- Subsequent analysis of the hit compounds from the *versican* screens in a secondary screen using *mbp* expression, identified molecules that up-regulate, down-regulate or do not affect *mbp* expression in the lateral line of *adgrg6*^{tb233c} mutants.
- Molecules that were able to rescue the expression defects of both *vcanb* and *mbp* genes in *adgrg6*^{tb233c} mutants, represent putative modulators of the Adgrg6 pathway.
- Compounds presumed to act downstream of the Adgrg6 receptor included calcium channel blockers of the dihydropyridine type, *O*-methylated flavonoids and other molecules known to trigger cAMP elevation, such as NMDA receptor agonists, phosphodiesterase inhibitors and adenosine receptor antagonists.
- Compounds presumed to interact directly with Adgrg6 receptor included compounds from the gedunin family and other compounds with a similar, limonoid skeleton.
- The dose-response assays highlight that *versican* expression is a reliable indicator of epithelial projection fusion in the zebrafish inner ear that can be modulated by both calcium channel blockers and activators.

CHAPTER 6.

Regulation of Versican in Human Fibroblasts

6.1 INTRODUCTION

As discussed in section 1.4.2., Versican (VCAN) isoforms play pivotal and often contradicting roles during cancer progression. While V0, V1 and V3 isoforms have been strongly associated with increased cancer cell motility and proliferation (reviewed in Ricciardelli et al., 2009), V3 has also been reported to inhibit cancer cell growth *in vitro* and *in vivo* (Miquel-Serra et al., 2006; Fanhchaksai et al., 2016). The main source of VCAN in a malignant lesion is the tumour microenvironment, primarily cancer-associated fibroblasts (CAFs, also called myofibroblasts; see section 1.4.1). TGF-β has been shown to be the major cytokine that drives fibroblast differentiation to an activated, myofibroblastic, CAF phenotype, by up-regulating the expression of a number of genes, including α-smooth muscle actin (*α-SMA*) and *VCAN* (Gabbiani, 2003; Yeung et al., 2013). Increased secretion of VCAN activates the NFκB signalling pathway in cancer cells, which in turn up-regulates the expression of genes promoting contractility and invasion, such as *CD44* and *MMP9* (Yeung et al., 2016).

In this chapter, I have used TGF-β-induced normal and cancer-associated fibroblasts as an *in vitro* system in which to interrogate two of the compounds that down-regulated *versican* expression in zebrafish in a dose-dependent manner. The compounds tested in this system were two L-type calcium channel blockers (CCBs) of the dihydropyridipine family (Tikhonov and Zhorov, 2009), which, as shown in Chapter 5, were presumed to modulate Adgrg6 pathway by raising cAMP levels. As the human *VCAN* promoter has been reported to possess a functional CREB domain (Naso et al., 1994), I wanted to investigate whether these cAMP-raising compounds would be able to modulate *VCAN* expression in human fibroblasts. The aim of this chapter was to investigate whether the *VCAN* regulatory pathways are conserved from zebrafish to human and, by extension, whether zebrafish data could provide a basis for future translational studies on the tumour microenvironment.

6.2 RESULTS

6.2.1 TGF-β1 upregulates *VCAN* mRNA expression in oral fibroblasts to an extent that is dependent on the cell type.

In order to investigate the effect of TGF-β1 on VCAN expression, normal and cancer-associated oral fibroblasts were seeded in 6-well plates and exposed to TGF-β1 (5 ng/mL) for 48 hours, after being serum-starved for 24 hours. At the end of the treatment, fibroblasts were harvested and total cDNA was synthesised from the extracted RNA and subjected to qRT-PCR analysis. Primers specific for V0, V1 and V3 isoforms were used to evaluate VCAN mRNA expression in normal (NOF804, NOF316) and cancer-associated (CAF003) fibroblasts. C_T values for *VCAN* isoforms were normalised to the reference expression levels of β2 microglobulin (*B2M*) and plotted as the fold-change relative to the expression levels of control samples that had not been treated with TGF- β1.

The quantification of the results showed that, in all three cell types, V0 and V1 isoforms showed a greater up-regulation in response to TGF-β1 treatment, compared to V3 (Figure 6.1). The fold increase of *VCAN* expression following TGF-β1 treatment varied among different cell types, with the variation being greater between NOFs and CAFs. While NOF316 and NOF804 cells showed a 10- and 100-fold increase in V0 expression, respectively, CAFs responded to TGF-β1 treatment with a 3000-fold increase. Similarly, V1 expression in NOF316 and NOF804 cells increased by 4- and 6-fold respectively, while CAF003 saw a 10-fold increase in V1 after being treated with TGF-β1. The difference in the response of NOFs and CAFs could perhaps be due to the fact that CAFs possess a higher amount of TGF-β receptors compared to NOFs, as previously suggested (Yeung et al., 2013).

The up-regulation of V3 transcript in response to TGF-β1 was not as great as the results observed for V1 and V0; NOF804 showed a three-fold increase in V3 expression following TGF-β1 treatment, while NOF316 and CAF003 showed increases of two-fold or less (Figure 6.1C). Taken together, these data suggest that TGF-β1 up-regulates the expression of all three VCAN isoforms tested, to a degree that is dependent on the cell type.

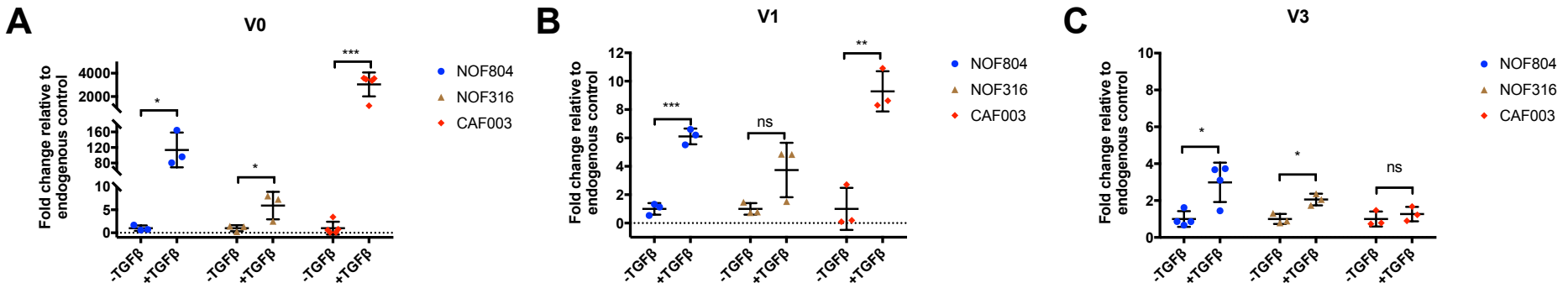

Figure 6.1 The effect of TGF-β1 on *VCAN* mRNA expression in normal and cancer-associated oral fibroblasts. Primary NOF804, NOF316 and CAF003 oral fibroblasts were seeded in 6-well plates, serum-starved and treated with 5 ng/mL TGF-β1 or serum-free media as control, for 48 hours. At the end of the treatment, fibroblasts were harvested, the RNA was isolated and total cDNA was synthesised by *in vitro* reverse transcription. Specific primers were used in qRT-PCR to amplify V0, V1, V3 and B2M cDNA fragments, with the latter being used as a reference gene. Each data point represents the relative quantification of V0 **(A)**, V1 **(B)** and V3 **(C)** transcript levels in a well, compared to the endogenous expression of *B2M*. All data points are expressed as a fold change relative to the average expression levels of untreated samples (-TGFβ). Statistical analysis was performed by two-tailed, unpaired Student's *t*-tests and asterisks are used to show statistical significance; *p<0.05, **p<0.01, ***p<0.001 or ns, not significant. Error bars represent the SD.

6.2.2 The effect of nifedipine on *VCAN* expression in TGF-β-induced oral fibroblasts

Nifedipine is an L-type calcium-channel blocker of the dihydropyridine type found to be efficacious in down-regulating *VCAN* expression in zebrafish *adgrg6* mutants in a dose-dependent manner (Chapter 5). Expression of L-type calcium channels has been shown in fibroblasts, with recent studies reporting altered expression in samples from patients with different types of cancer (Jacquemet et al., 2016; Jeng et al., 2006). Studies in nude mice have shown that calcium-channel blockers (CCBs) can inhibit cancer growth (Taylor and Simpson, 1992; Jensen and Wurster, 2001), while recent drug screening data demonstrate that L-type CCBs impede cancer cell invasion by destabilising filopodia, suggesting a previously uncharacterised role for these receptors (Jacquemet et al., 2016).

In order to investigate whether *VCAN* modulation could be one of the underlying mechanisms granting L-type CCBs antineoplastic functions, I used TGF-β-induced normal and cancer-associated oral fibroblasts, as a system to assess the effect of nifedipine on *VCAN* expression levels. Primary normal (NOF804 and NOF316) and cancer-associated (CAF003) fibroblasts were seeded in 6-well plates and exposed to TGF-β1 (5 ng/mL) for 24 hours, after being serum-starved for 24 hours. At the end of the 24-hour TGF-β1 treatment, fibroblasts were treated with a concentration series of nifedipine in DMSO, in a solution that also contained TGF-β1 at a final concentration of 5 ng/mL. After the 24-hour nifedipine treatment, fibroblasts were harvested, with the total cDNA synthesised from the extracted RNA and subjected to qRT-PCR analysis. At the same time, cells from one well per treatment group were stained with trypan blue (0.1%) and viable cells were counted using a hemocytometer. Primers specific for V0, V1 and V3 isoforms were used to evaluate *VCAN* mRNA expression, while *B2M* was used as a reference gene. C_T values for *VCAN* isoforms were normalised to the endogenous expression levels of *B2M* and plotted as fold-change relative to the expression levels of control samples that were not treated with TGF-β1. The statistical significance of the data was then evaluated with one-way ANOVA statistical tests.

6.2.2i The effect of nifedipine on *VCAN* expression in TGF-β-induced normal oral fibroblasts

Treatment of NOF804 cells (passage 6) with a 10-fold dilution series of nifedipine giving concentrations ranging from 0.05-50 ng/mL did not have an impact on the viability of cells, as shown by trypan blue assay data (data not shown). Although the average V0 expression levels of every treatment group was lower than the average V0 expression of the DMSO-treated control group, this reduction was not statistically significant (Figure 6.2A). Interestingly, treatment with TGF-β1 and DMSO (0.1%) seemed to cause an average decrease of 48% in V0 expression levels compared to samples treated with TGF-β1 alone.

Contrary to V0, V1 levels only showed a 13% average reduction after DMSO treatment compared to the untreated TGF-β1 control (Figure 6.2B). Although no significant reduction in V1 expression was observed after treatment with 0.5 or 5 ng/mL nifedipine, it was reduced by approximately 37% after treatment with 0.05 ng/mL or 50 ng/mL of nifedipine compared to the vehicle control and this reduction was statistically significant (p values 0.019 and 0.02, respectively; Figure 6.2B).

Nifedipine at 0.05 ng/mL and 50 ng/mL also reduced V3 expression by 32-34% when compared to the vehicle control, but none of the concentrations tested induced a statistically significant reduction in V3 levels of expression (Figure 6.2C). V3 expression was not affected by the DMSO treatment (average V3 expression for TGF-β1-treated group and for TGF-β1 plus DMSO group were 2.05 and 1.87, respectively).

In order to increase sample size, the experiment was repeated using NOF804 cells at a later passage (passage 11). Interestingly, C_T values obtained for V0 and V1 were too high (>38) in all samples, implying that these isoforms are not expressed or are expressed at very low levels. Values obtained for V3 were normal (<37) and were used to plot the graph shown in Figure 6.2D. The average V3 expression levels in the three nifedipine-treated groups were found to be lower than that observed in the DMSO-treated control group. However, only the 5 ng/mL concentration caused a statistically significant decrease (p value=0.021). The V3 expression data obtained from the two independent experiments described above were combined in Figure 6.2E. It was observed that the reduction induced by the 5 ng/mL nifedipine treatment was of a stronger statistical significance (p value=0.026), while the reduction induced by 50 ng/mL nifedipine was not statistically significant.

Immunoblot analysis showed VCAN protein as a single band of 65 kDa, the intensity of which was reduced in the 5 ng/mL nifedipine-treated group (Figure 6.2F). The observed molecular weight (MW) of the VCAN band was lower than the predicted MW (73 kDa) for V3 protein, which could be either due to post-transcriptional cleavage of V3 isoform by matrix metalloproteases (MMPs) or differences in glycosylation. In the immunoblotting procedure, α-SMA protein expression was used to confirm the myofibroblastic phenotype following induction with TGF-β1 and GAPDH was used as a loading control. In line with previously reported data, α-SMA protein levels were found significantly increased following TGF-β1 treatment (Hinz et al., 2001). As well as the reduction in VCAN protein abundance, treatment with 5 ng/mL nifedipine, also induced a reduction in α-SMA protein levels, but the mechanistic basis for this requires further investigation.

In summary, my results show that V0 expression in NOF804 cells was not significantly affected by nifedipine treatments, however this experiment was limited by sensitivity to DMSO. Although there was a reduction trend in V1 and V3 expression after treatment with nifedipine, this effect was variable and not dose-dependent.

In order to investigate whether different types of normal fibroblasts would behave in the same way as NOF804, NOF316 fibroblasts (passage 7) were treated with 5 ng/mL nifedipine in DMSO, while ethanol was also tested as an alternative option of solvent in future assays (water was eliminated as an option, as nifedipine is not water-soluble). qRT-PCR results showed no reduction in V1 or V0 levels of expression with respect to the DMSO control group (Figure 6.3A,B). Ethanol induced a higher reduction in V0 and V1 expression levels compared to DMSO and therefore was not considered a suitable solvent choice for future experiments.

Immunoblotting confirmed that VCAN expression levels are similar amongst all treatment groups, although α-SMA protein expression is clearly upregulated following TGF-β1 treatment (Figure 6.3C). However, the appearance of VCAN immunoblot signal was different in this case; multiple bands of sizes 73-370 kDa were detected, suggesting the existence of various, cleaved or non-cleaved isoforms, with chondroitin sulphate chains of differing lengths. This laddering appearance of VCAN signal from total protein lysates makes any changes in versican protein levels difficult to distinguish in immunoblots.

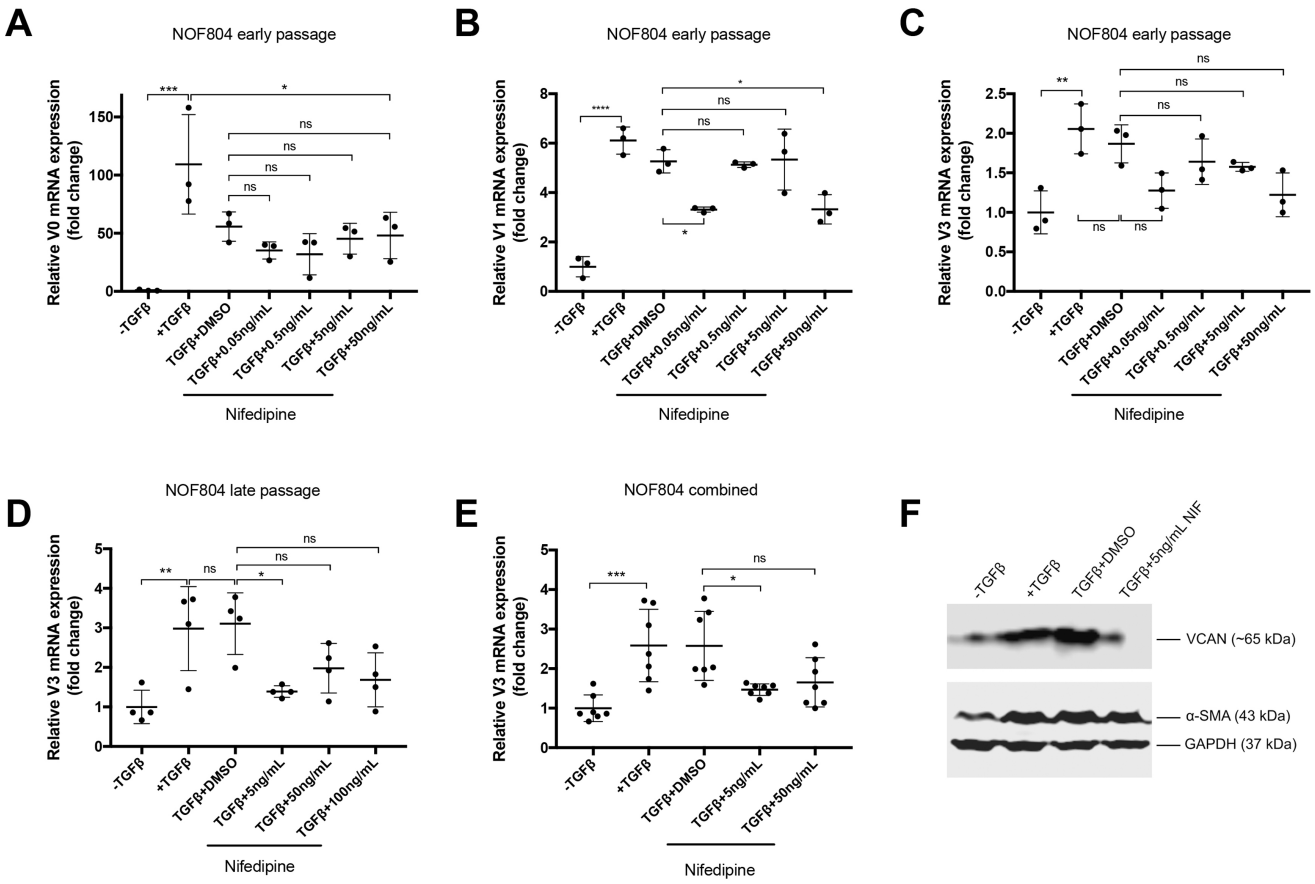

Figure 6.2 Nifedipine induced a variable decrease in *VCAN* expression in TGF-β1-induced NOF804 oral fibroblasts, which was not dose-dependent. Primary NOF804 normal oral fibroblasts of passage 6 (A-C) or passage 11 (D,F) were treated with 5 ng/mL TGF-β1 (or serum-free media as control), for 24 hours, before being treated with a concentration series of nifedipine in DMSO (0.1%), in a solution that also contained TGF-β1 (5 ng/mL). 24 hours later, RNA and protein were extracted and analysed by qRT-PCR (A-E) and immunoblot (F), respectively. **(A-E)** Specific primers were used in qRT-PCR to amplify V0, V1, V3 and B2M cDNA fragments, with the latter being used as a reference gene. Each data point represents the relative quantification of V0 **(A)**, V1 **(B)** and V3 **(C-E)** transcript levels in a well, compared to the endogenous expression of B2M. All data points are expressed as a fold change relative to the average expression levels of untreated samples (-TGFβ). **(E)** Combined results from graphs C and D. Statistical analysis was performed by one-way ANOVA tests and asterisks are used to show statistical significance; *p<0.05, **p<0.01, ***p<0.001, ****p<0.0001 or ns, not significant. Error bars represent the SD. **(F)** Total protein lysates (15 μg) from NOF804 cells (passage 11) were resolved in Tris-acetate gel and transferred to a nitrocellulose membrane, which was immunoblotted with α-SMA, VCAN and GAPDH antibodies, with the latter being used as a loading control.

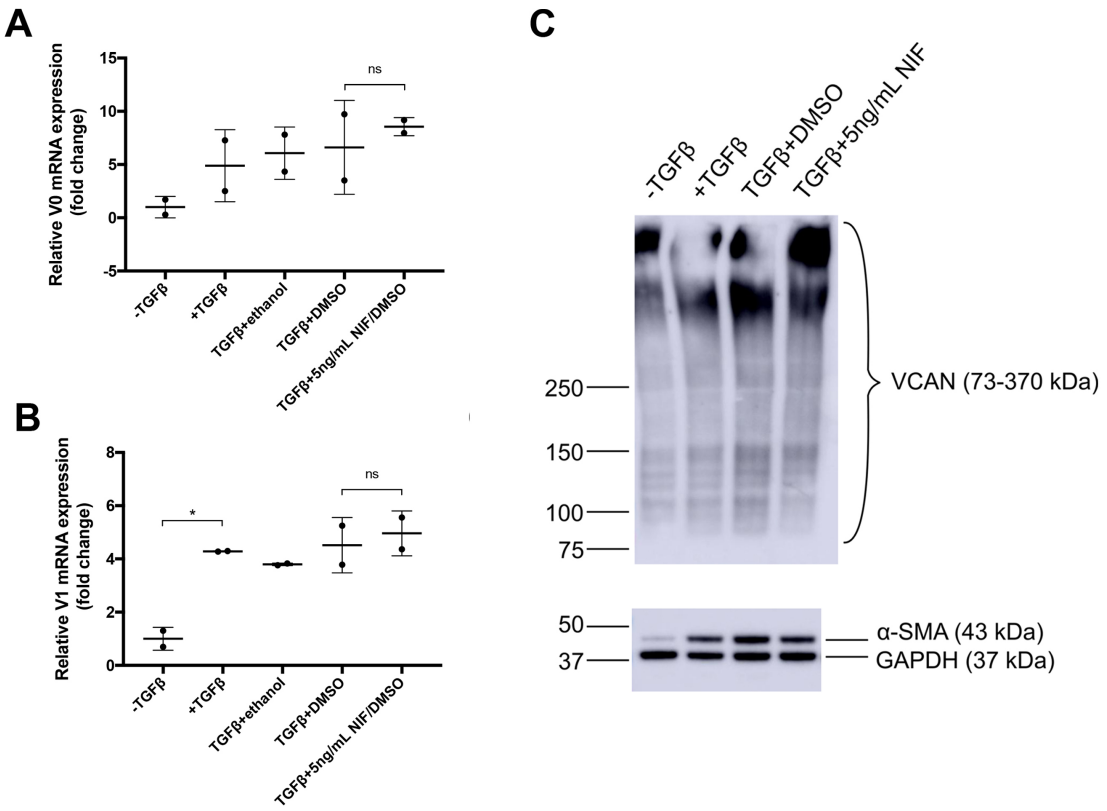

Figure 6.1 Treatment of TGF-β1 induced NOF316 fibroblasts with nifedipine did not affect V0 or V1 expression levels. TGF-β1-induced primary NOF316 fibroblasts were treated with 5 ng/mL nifedipine in DMSO (0.1%) for 24 hours, before being analysed by qRT-PCR and immunoblot. **(A,B)** Graphs showing the relative V0 **(A)** and V1 **(B)** mRNA expression in NOF316 cells. Each data point represents the relative quantification of V0 and V1 transcript levels in a well, compared to the endogenous expression of B2M. All data points are expressed as a fold change relative to the average expression levels of untreated samples (-TGFβ). Statistical analysis was performed by one-way ANOVA tests and asterisks are used to show statistical significance; *p<0.05. Error bars represent the SD. **(C)** Total protein lysates (15 µg) were resolved in an 8% (w/v) Tris-acetate gel and transferred to a nitrocellulose membrane, which was immunoblotted with α-SMA, VCAN and GAPDH antibodies, with the latter being used as a loading control. Abbreviations: NIF, nifedipine; ns, not significant.

6.2.2ii The effect of nifedipine on *VCAN* expression in TGF-β-induced cancer-associated oral fibroblasts

Treatment of cancer-associated fibroblasts (CAF003, passage 5) with a 10-fold concentration series of nifedipine ranging from 0.05-50 ng/mL, resulted in dose-dependent reduction in V0 levels of expression with increasing nifedipine concentrations (Figure6.4A). However, only treatment with 50 ng/mL nifedipine induced a statistically significant, 2-fold decrease in V0 expression compared to the vehicle. Similarly to the data obtained from NOF804 cells, treatment with 0.1% DMSO resulted in an approximately 2-fold (60%) average reduction in V0 levels, compared to the control (+TGFβ) group.

DMSO had less impact on V1 expression levels of CAF003 cells compared to V0, with a 37% average reduction in V1 compared to the control (+TGFβ) group (Figure 6.4B). V1 expression levels were further reduced by 57% and 7% after treatment with 0.5 and 5 ng/mL nifedipine, respectively, compared to the vehicle control. However, these results were not statistically significant (Figure 6.4B).

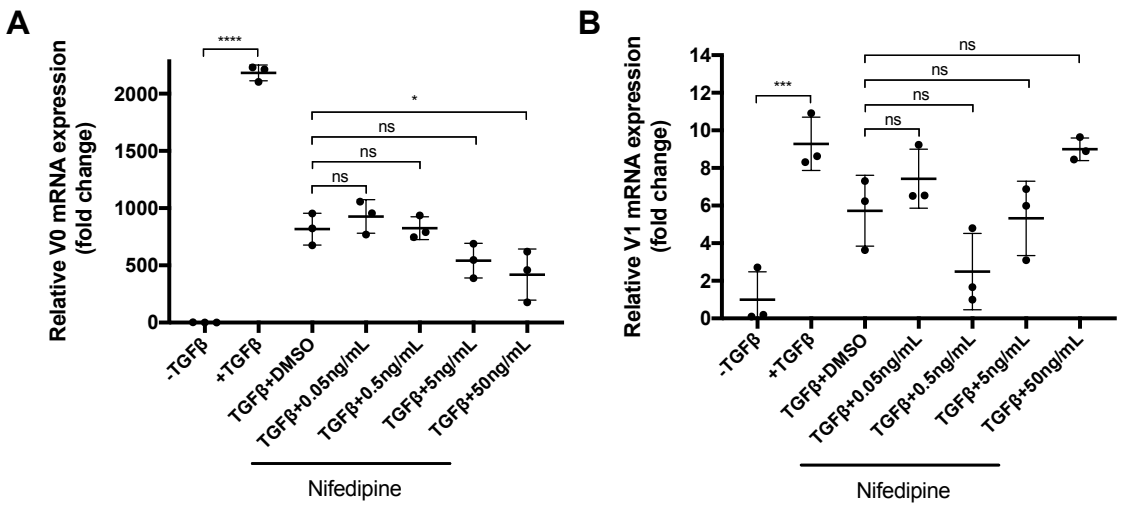

Figure 6.4 Treatment of cancer-associated fibroblasts with nifedipine induced a dose-dependent down-regulation of V0, but not V1 expression. TGF-β1-induced primary CAF003 fibroblasts were treated with a 10-fold concentration series of nifedipine in DMSO (0.1%) for 24 hours, before being analysed by qRT-PCR. Each data point represents the relative quantification of V0 **(A)** and V1 **(B)** transcript levels in a single well, compared to the endogenous expression of B2M. All data points are expressed as a fold change relative to the average expression levels of untreated samples (-TGFβ). Statistical analysis was performed by one-way ANOVA tests and asterisks are used to show statistical significance; *p<0.05, **p<0.01, ***p<0.001, ****p<0.0001 or ns, not significant. Error bars represent the SD.

In summary, these data show that V0 in CAF003 cells decreased in a dose-dependent manner with increasing nifedipine concentrations, with the highest average reduction

(49%) following treatment with 50 ng/mL. However, not all concentrations tested induced a statistically significant reduction and thus more experimental repeats are needed. In contrast, low doses of nifedipine (0.5 ng/mL) were more efficacious in decreasing V1 expression levels in CAF003 cells compared to higher doses.

6.2.3 The effect of cilnidipine on *VCAN* expression in TGF-β-induced oral fibroblasts

Cilnidipine is an antihypertensive drug, which inhibits L- and N-type calcium channels with higher potency compared to other dihydropyridines (Chandra and Ramesh, 2013). As nifedipine did show some efficacy in down-regulating *VCAN* levels, but the inhibition was not consistent between samples, I wanted to test a dihydropyridine of higher specificity and potency, using the same system of TGF-β1-induced oral fibroblasts.

To this end, NOF316 fibroblasts (passage 9) were treated with 5 or 20 ng/mL of cilnidipine in DMSO in an identical assay format to that used for nifedipine treatments. The results showed that V0 expression levels of the samples belonging to the same treatment group varied considerably. This observation in combination with the small sample size (n=2), obscured the deduction of conclusions from the experiment. However, it was seen that treatment with 5 and 20 ng/mL cilnidipine reduced the average V0 expression in NOF316 cells by 76% and 42% respectively, compared to the vehicle control. Contrary to V0, V1 expression levels between the samples of the same treatment group showed less variability. However, none of the two cilnidipine dosages tested affected the expression levels of V1 transcript in NOF316 cells (Figure 6.5B).

Immunoblot analysis confirmed that α-SMA was activated following TGF-β1 treatment, but VCAN protein levels were difficult to assess due to the dense laddering of the protein bands (Figure 6.5C). Interestingly, the reduction in V0 mRNA expression levels after treatment with 20 ng/mL cilnidipine was accompanied by a reduction in α-SMA protein levels (Figure 6.5C).

In summary, these data show that there is no strong association between cilnidipine or nifedipine treatments and reduced *VCAN* levels, with the response highly dependent on the cell type. Of the fibroblasts tested in this study, NOF804 cells were the most responsive to nifedipine, as all three isoforms showed reduced expression following treatment. In order to investigate why these cells were more responsive to dihydropyridipine

treatment, in the next sub-section, I compare the levels of *ADGRG6* gene expression among the cell types that were treated in this section.

.

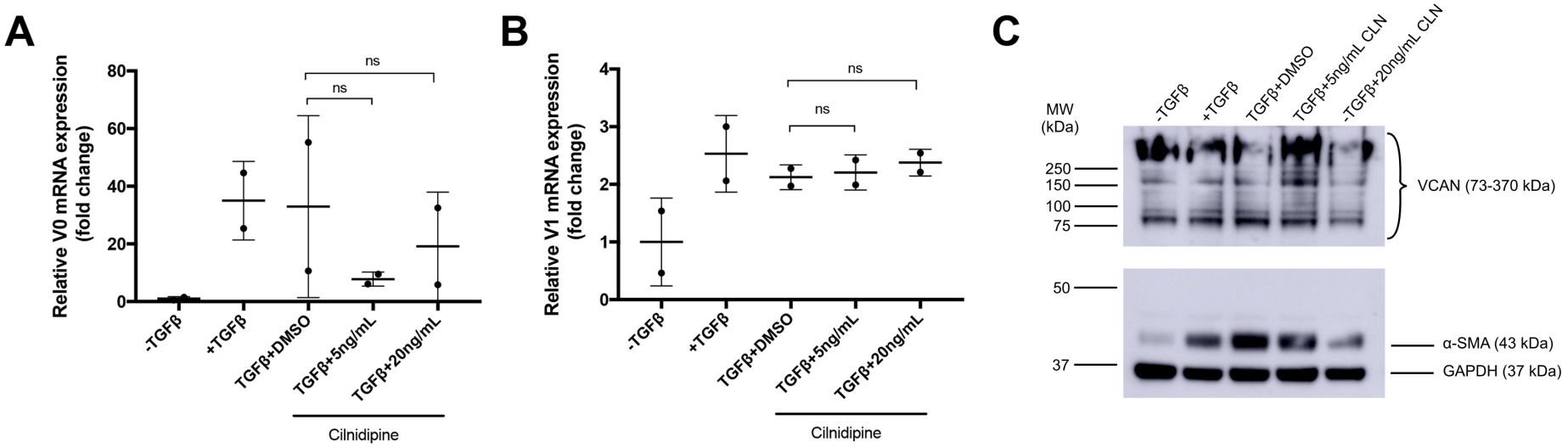

Figure 6.5 Treatment of TGF-β1-induced normal fibroblasts with cilnidipine induced a down-regulation of V0, but not V1 expression. TGF-β1-induced primary NOF316 fibroblasts were treated with 5 or 20 ng/mL cilnidipine in DMSO (0.1%) for 24 hours, before being analysed by qRT-PCR and immunoblot. **(A,B)** Graphs showing the relative V0 **(A)** and V1 **(B)** mRNA expression in NOF316 cells. Each data point represents the relative quantification of V0 and V1 transcript levels in a well, compared to the endogenous expression of B2M. All data points are expressed as a fold change relative to the average expression levels of untreated samples (-TGFβ). Statistical analysis was performed by one-way ANOVA tests and error bars represent the SD. **(C)** Total protein lysates (15 µg) were resolved in an 8% (w/v) Tris-acetate gel and transferred to a nitrocellulose membrane, which was immunoblotted with α-SMA, VCAN and GAPDH antibodies, with the latter being used as a loading control. Abbreviations: CLN, cilnidipine; ns, not significant.

6.2.4 *ADGRG6* is expressed in oral fibroblasts

As dihydropyridines were presumed to act downstream of the Adgrg6 pathway in zebrafish to down-regulate *VCAN* (Chapter 5), in this section, I wanted to investigate whether *ADGRG6* is expressed in oral fibroblasts, as there is no relevant literature available on this to date. In addition, I wanted to elucidate whether different levels of *ADGRG6* expression could account for the different responsiveness observed among fibroblasts of different type in terms of *VCAN* down-regulation.

To this end, cDNA from untreated NOF804, NOF316 and CAF003 cells grown in serum-free medium that was used as a negative control in nifedipine and cilnidipine treatments, was subjected to qRT-PCR in order to analyse *ADGRG6* expression. The results were quantified with respect to *B2M* expression and normalised against the sample with the lowest expression levels, in order to facilitate direct comparison among the three different cell groups tested (Figure 6.6). The two samples with the lowest *ADGRG6* expression levels were obtained from the NOF316 cells used in the nifedipine treatment (in Figure 6.3). Compared to those samples, CAF003 cells were found to express twice the amount of *ADGRG6* transcripts, while the two NOF316 cell samples used in the cilnidipine treatment (Figure 6.5) showed six-fold higher *ADGRG6* expression levels. The inconsistency between the two sets of NOF316 samples could be attributable either to the varying passage or to differences in the health condition of the individuals. NOF804 cells showed by far the highest levels of *ADGRG6* expression, which were on average 200-fold higher compared to the expression of the NOF316 control, and 100-fold higher compared to the average expression of CAF003 cells.

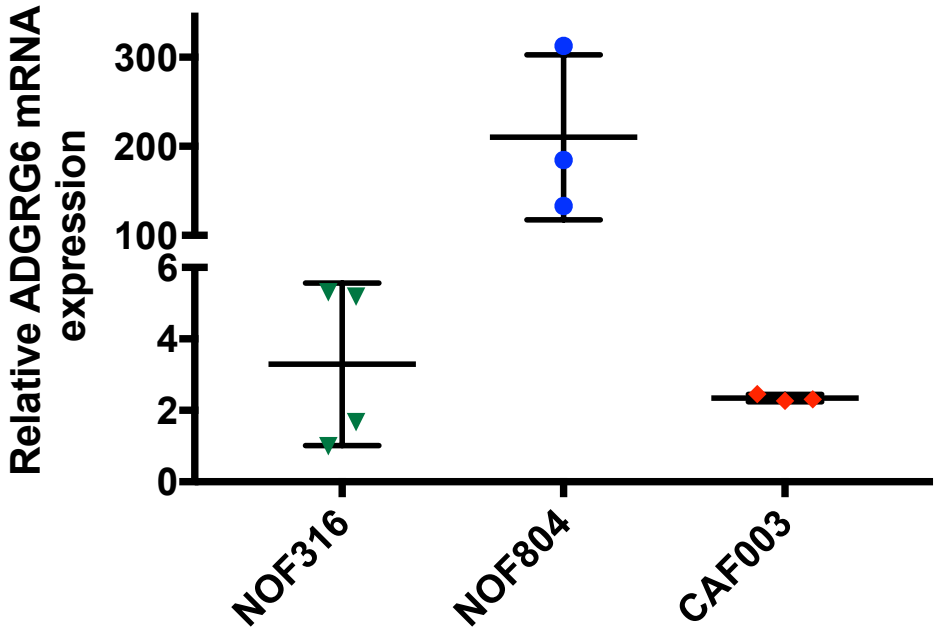

Figure 6.6 *ADGRG6* is expressed in low levels in NOF316 and CAF003 cells, but is found expressed at high levels in NOF804 cells. The cDNA from untreated NOF804, NOF316 and CAF003 cells grown in serum-free medium that was used as a negative control in nifedipine and cilnidipine treatments, was subjected to qRT-PCR, in order to analyse *ADGRG6* expression. The results were quantified with respect to *B2M* endogenous expression and shown as fold change relative to the minimum expression levels detected (the first sample from the left-hand side). Error bars represent the SD.

These preliminary findings on *ADGRG6* expression seem to correlate well with the response of each cell type to the dihydropyridine treatments in terms of *VCAN* expression. However, further experimentation is needed to assess whether *ADGRG6* expression is involved in the regulation of *VCAN* expression in human fibroblasts.

6.3 DISCUSSION

6.3.1 The effect of TGF-β1 on *VCAN* expression in oral fibroblasts

In agreement with previously reported data, the data presented herein showed that TGF-β1 treatment induced an increase in the expression of *VCAN* isoforms V0, V1 and V3, to an extent that was dependent on the cell type (Yeung et al., 2013). This finding demonstrates that treatment with TGF-β1 offers the advantage of up-regulating all three isoforms, unlike TGF-β2 and TGF-β3, which have been shown to preferentially increase only the expression of the V0 and V1 isoforms (Berdiaki et al., 2008).

CAFs showed greater up-regulation of the V0 and V1 transcripts in response to TGF-β1 treatment compared to NOFs, which could be attributable to the amount of TGF-β1 receptors each cell type possesses and is in line with previously reported data demonstrating that CAFs have got a higher number of TGF-β receptors than NOFs (Yeung et al., 2013). In all three cell types tested, V0 was the most greatly up-regulated isoform, while V3 displayed the least up-regulation following TGF-β1 treatment.

6.3.2 The use of DMSO as a solvent for drug treatments on oral fibroblasts

As the drugs used in this study were not water-soluble, 0.1% (v/v) DMSO was used as a solvent throughout. DMSO at 0.1% was found to reduce the expression levels of the V1 and V0 isoforms, with the magnitude of this effect higher for V0, but varying among different cell types and different samples from the same cell batch. Although there is no literature to support the apparent DMSO-mediated effect on *VCAN* expression, it has been reported that DMSO at 2% (v/v) can inhibit gene expression in mice fibroblast cultures, while at concentrations as low as 0.05% (v/v) can affect the oncogenic potential of myeloma cells (Srinivas et al., 1991; Wen et al., 2015). Ethanol was investigated as an alternative solvent, but was found to induce a reduction in V0 and V1 levels to a degree similar to that caused by DMSO. This variable, DMSO-mediated reduction in *VCAN* expression limited the reproducibility of the data presented in this study and may have also compromised the validity of the results, as the combined effects of evaluated drugs and DMSO may not be additive.

6.3.3 CCBs as a tool to down-regulate *VCAN* in fibroblasts

The importance of calcium in proliferating cells and its mitogenic effect to stimulate growth is well-established. However, the response of cancer cells to extracellular calcium is highly dependent on the cancer type (Taylor and Simpson, 1992). L-type calcium channels are expressed in fibroblasts and cancer cells and their expression is altered in patients suffering from different types of cancer (Jacquemet et al., 2016; Jeng et al., 2006). Although concerns that CCBs may promote cancer in the elderly have been raised (Mason, 1996), there is also data showing that CCBs can inhibit cancer growth in nude mice (Taylor and Simpson, 1992; Jensen and Wurster, 2001). Additional drug screening data suggests that L-type CCBs in particular act downstream of integrins to potently inhibit the formation of filopodia, thus impeding cancer cell invasion (Jacquemet et al., 2016).

In this chapter, I studied the effect of the CCBs nifedipine and cilnidipine on *VCAN* expression in normal and cancer-associated fibroblasts of the oral cavity. I found no strong association between cilnidipine or nifedipine treatments and reduced *VCAN* levels, while I observed that the cell response is variable and highly dependent on the cell type. Of the fibroblasts tested in this study, NOF804 cells were the most responsive to nifedipine treatment, as all three *VCAN* isoforms showed reduced expression following treatment. V0 transcript levels were also reduced in nifedipine-treated CAFs and cilnidipine-treated NOF316 cells, but this reduction was not accompanied by a down-regulation in V1 expression.

Apart from CCBs, flavonoids, another group of putative Adgrg6 down-stream effectors identified in zebrafish, represent good candidates that may down-regulate *VCAN* expression in human fibroblast or cancer cell lines. This is because flavonoids act by interacting with the MAPK/ERK signalling pathway, which is already known to activate the human *VCAN* promoter in melanoma cells (Schroeter et al., 2002; Domenzain-Reyna et al., 2009).

NOF804 cells were shown to express significantly higher levels of *ADGRG6* compared to the other two cell types used in this study. This finding may account for the fact that the same cells responded to nifedipine treatments with a more robust down-regulation of *VCAN* expression compared to other cells, but this hypothesis warrants further investigation.

6.4 CONCLUSIONS

- TGF-β1 up-regulates the expression of *VCAN* V0, V1 and V3 isoforms in normal and cancer-associated oral fibroblasts.
- No strong association was observed between cilnidipine or nifedipine treatments and reduced *VCAN* levels in normal and cancer-associated oral fibroblasts. The cell response to the treatment was variable and highly dependent on the cell type.
- The normal and cancer-associated fibroblasts tested in this study expressed *ADGRG6* at different levels.

CHAPTER 7.

Synopsis

7.1 OVERVIEW OF THE RESULTS

This thesis presents data on the role of chondroitin and heparan sulphate proteoglycans of the ECM in the development of the inner ear (Chapters 3 and 4) and provides insight on the regulation of versican expression in zebrafish and human (Chapters 5 and 6).

The study of *vcana* and *vcanb* single and double zebrafish mutants in Chapter 3, showed that *versican* genes individually exert a dispensable role in the projection elongation and fusion processes that lead to semicircular canal formation. Although incompletely penetrant, single *vcana* and *vcanb* mutations caused a delay in the elongation and fusion of the projections, which was amended before 5 dpf. Between the two genes, *vcana* seems to be more important for the above processes than *vcanb*, as the corresponding *vcana* mutation showed a higher degree of penetration in the ear. Double *vcana*;*vcanb* mutants displayed the same otic phenotype observed in single mutants, but the ear abnormalities in some homozygous mutants persisted until 5 dpf. The incomplete penetrance of the *versican* mutant phenotype may be due to a compensatory network of other proteoglycans of the ECM that are activated when *versican* genes are mutated.

The investigation of *ext2* zebrafish mutants (Chapter 4), where heparan sulphate biosynthesis is severely impaired (*dak*^{to273b}), showed that heparan sulphates exert an indispensable role in the elongation of the projections that is required for semicircular canal formation in the inner ear. Apart from their role in semicircular canal formation, heparan sulphates were shown to be important for otolith adhesion to the macula, as well as for the control of otolith shape and size, through regulation of *otogelin*, *starmaker and otolith matrix protein* expression, respectively. In addition, *adgrg6* expression in the inner ear and the lateral line of *dak*^{to273b} mutants was found to be up-regulated, while ectopic *adgrg6* expression was detected in a region presumed to be the cerebral vein.

In Chapter 5, the *adgrg6*^{tb233c} mutant ear was used as a screening platform which allowed the identification of several chemical compounds able to down-regulate the abnormally

high expression levels of *versican*. Subsequent counter-screens of the hit compounds using *mbp* expression, identified molecules that up-regulate, down-regulate or do not affect *mbp* expression in the lateral line of *adgrg6*^{tb233c} mutants. Consequently, compounds were categorised as putative Adgrg6 pathway modulators, general transcription blockers or compounds that only down-regulate *versican* expression. Almost half of the *versican* hit compounds were found to also rescue *mbp* expression, suggesting that Adgrg6 signalling is one of the main pathways that regulate *versican* expression in the zebrafish inner ear. Calcium channel blockers of the dihydropyridine chemical class were one of the groups of molecules identified to restore the expression of both genes, most likely by acting downstream of the Adgrg6 receptor and raising cAMP levels. The screening results implicated additional pathways that may be involved in the regulation of *versican* expression in zebrafish, such as ERK/MAPK and JNK signalling pathways (section 5.3.3iii). Using the nonsense *adgrg6*^{fr24} allele in a counter-screen, I was able to identify 25 compounds that rescued both alleles to a variable extent and 12 compounds that only rescued *tb233c* mutants, presumably by interacting directly with the Adgrg6 receptor. Five out of the 12 hit compounds share profound structural similarities that may be important for the interaction with the Adgrg6 receptor.

The efficacy of two hit compounds from the dihydropyridine class, in down-regulating human *VCAN* expression in TGF-β1-activated normal and cancer-associated fibroblasts was evaluated in Chapter 6. Contrary to zebrafish-derived data, the effect of dihydropyridine treatment on *VCAN* expression was variable and inconsistent among different fibroblasts. However, it was shown that NOF804 fibroblasts, which expressed higher *ADGRG6* levels compared to the other cells tested, showed a decreased expression of *VCAN* isoforms V0, V1 and V3 after nifedipine treatment, but this reduction was neither statistically significant nor dose-dependent.

7.2 THE ROLE OF CHONDROITIN AND HEPARAN SULPHATES IN THE DEVELOPMENT OF THE INNER EAR

Versican is the only chondroitin sulphate proteoglycan yet known to be expressed in the zebrafish inner ear. However, based on the findings of this study, *versican* genes seem to exert a dispensable role in the projection elongation and fusion processes that lead to semicircular canal formation. Li et al. (2010) observed a more severe otic phenotype after antisense-morpholino knockdown of *chsy1* in zebrafish. Morphants were characterised by abnormally sized epithelial projections that were either too small or too large and failed to fuse properly, while injection of synthetic *chsy1* mRNA in wild-type ears resulted in very similar phenotypes (Li et al., 2010). Consistent to this, in cases such as *adgrg6* and *ext2* mutants, where *versican* genes remain up-regulated, otic projections are either too swollen or too small and fail to fuse. Taken together, these data indicate that either loss or gain of function of CSPGs results in malformed epithelial projections and interferes with the fusion process that leads to semicircular canal development. The fact that *chsy1* morphants displayed a more severe phenotype than double *vcana;vcanb* mutants suggests a central role for CS chains and implies that there may be additional CSPGs expressed in the zebrafish inner ear, whose CS chains compensate for the loss of versican.

I found that heparan sulphates play an indispensable role in the elongation of the epithelial projections, as *dak*^{to273b} homozygous mutants were characterised by small projections that never elongate sufficiently to form the semicircular canal ducts. In combination with the apparent *versican* up-regulation in the unfused projections of the *dak*^{to273b} ear, these data suggest that HSPGs and versican exert similar roles in the zebrafish inner ear and that *versican* expression may be part of the compensatory network that is activated in the *ext2* mutant ear. *adgrg6*, whose expression has been shown to be required for projection fusion (Geng et al., 2013), was also up-regulated in the unfused projections of the *dak*^{to273b} mutant ear. Taken together, these findings suggest that CSPGs, HSPGs and Adgrg6 are all members of a network that intercommunicates to facilitate projection elongation and fusion.

Ugdh activity is required for the biosynthesis of hyaluronic acid, heparan sulphate and chondroitin sulphate glycosaminoglycans. Live images of 72 hpf *ugdh* homozygous mutant embryos display a very similar ear phenotype to the one observed in *versican* mutants, where projections fail to reach one another and fuse to form pillars, but is not as severe as that displayed by *dak*^{to273b} mutants (Walsh and Stainier, 2001). Although both *ugdh* and

ext2 RNAs are maternally provided in zebrafish embryos, the early (36 hpf) down-regulation of HS may perhaps account for the stronger otic phenotype of *dak*^{to273b} mutants (Clément et al., 2008).

The otic *dak*^{to273b} phenotype is very similar to those observed after hyaluronidase injections in the epithelial projections of wild-type zebrafish embryos, where the injected projections collapsed and were not able to elongate (Geng et al., 2013). These data combined suggest that hyaluronan, CSPGs and HSPGs act in a similar, most likely cooperative way, to aid the elongation of the epithelial projections into the otic vesicle, possibly by propulsing the epithelial tissue towards the inside of the lumen, as previously proposed for *Xenopus* (Haddon and Lewis, 1991). One possible mechanism underlying this cell propulsion is the HS of the cell surface using components of the adjacent ECM, such as hyaluronan or CS, as anchoring points.

In conclusion, the data presented above, in conjunction with the results of previously reported literature, highlight the importance of ECM in cell movement that takes place during the morphogenetic processes that give rise to the complex structure of the semicircular canals in zebrafish.

7.3 DRUG SCREENING APPROACH: THE TRANSLATION FROM *IN VIVO* TO *IN VITRO* SYSTEMS

The finding that some of the hit compounds identified through the zebrafish screen presented here have been previously reported to promote myelination in mammals, suggests that zebrafish *adgrg6* mutants constitute a promising, phenotypic *in vivo* drug screening platform. Target-based drug screening has been the most popular approach to therapeutics for the last 30 years, but its yield of new marketed drugs has not been outstanding. While target-based strategies can only be applied to disease models where one single target is affected, phenotypic screens provide the advantage of assessing multifactorial pathological conditions, such as hereditary neuropathies and cancer (Baxendale et al., 2017). In cases like this, *in vivo* phenotypic drug screening allows for the metabolism of the administered compounds into metabolites that may act synergistically by targeting different components to produce a desirable response.

In this study, data from *in vivo* zebrafish screens were applied to an *in vitro* human cell culture system. One limitation in such a translative approach is that some of the available targets and metabolites that are present *in vivo* might be absent from *in vitro* cell culture systems. Apart from genetic differences in the versican promoter between zebrafish and human, the lack of important targets or metabolites might also account for the apparent decreased potency of the CCBs nifedipine and cilnidipine to induce a significant reduction in *VCAN* expression in human fibroblasts. Therefore, future evaluation of these and other hit compounds identified by this screen in mice models would be an attractive *in vivo* direction for the continuation of this work.

7.4 RELEVANCE OF MY STUDY TO OTHER FIELDS OF RESEARCH AND THERAPEUTICS

It is clear that versican functions in a variety of organisms, tissues and circumstances, with a complexity that is poorly understood. The elucidation of its role in the development of the semicircular canals in zebrafish will not only advance the understanding of inner ear development in the host organism, but also provide information that may be related to other organisms, due to the high conservation of the *versican* gene among vertebrates. In addition, the role of versican in the morphogenesis of the inner ear could provide useful information relevant to other developmental processes in which versican participates, such as the development of the heart valves. The identification of compounds able to modulate *versican* expression could provide a useful tool to manipulate canal formation *in vivo* in other mutant lines where versican is overexpressed, such as *ext2* mutants, allowing the delineation of compounds that work in the context of a specific mutation.

As versican is overexpressed in a number of human pathologies, including neoplasia, lung disorders and inflammation, the ability to chemically modulate *versican* expression could provide a valuable tool with promising wide therapeutic benefits, which are summarised below:

- The development of therapeutic methods to suppress *versican* expression, reduce its catabolism to more active fragments or inhibit its function in the tumour microenvironment, may prevent tumour invasion in many cancer types. In addition, better understanding of the mechanisms involved in its regulation and activity will assist the development of specific inhibitors of versican-mediated metastasis.
- Chemical suppression of *versican* expression might also have applications to the treatment of pathological conditions such as COPD and asthma, where fibroblasts from distal airways overexpress versican. Similarly, chemical down-regulation of versican alone or along with other GAGs in pulmonary fibrosis may have a positive impact on the patient outcome.
- Since versican can bind to a wide variety of receptors and other inflammatory components to regulate their availability and activity, manipulation of versican expression might also have applications to the control of inflammation, thus alleviating the symptoms of some inflammatory diseases. For example, targeting the versican-enriched cable-like structures that have been found in lesions of

atherosclerosis and inflammatory bowel disease (IBD) (de la Motte et al., 2003) may provide a successful therapeutic approach to these conditions.

The identification of compounds able to rescue *mbp* expression in *adgrg6* mutants could have applications in hereditary peripheral myelinopathies in human, such as Charcot-Marie-Tooth syndrome, where sensorimotor deficits and deafness are attributed to mutations in *KROX 20* and myelin genes, including *MBP* (Pogoda et al., 2006). The same data might also have applications to the treatment of human diseases where *ADGRG6* is mutated, such as congenital contracture syndrome 9, where peripheral nerves from affected individuals also show significantly reduced expression of *MBP* (Ravenscroft et al., 2015). Some of the putative Adgrg6 agonists presented in this study (such as the gedunin derivatives) have been previously reported to activate other GPCR members. Future specificity assays would be valuable for the identification of the range of GPCR receptors targeted by each hit compound, thus expanding the possible therapeutic applications of these data into other GPCR-associated pathological conditions.

7.5 CONCLUDING REMARKS

Zebrafish provide an animal model that affords numerous advantages ideal for the requirements of the research undertaken in this thesis. The transparency of the zebrafish embryo was a fascinating opportunity to microscopically observe the formation of the semicircular canal system in real time. The rapid development of its embryo, as well as the large amount of offspring allowed for the performance of experiments with big sample size in a short time frame. The location of the lateral line, ideally placed on the surface of the body, facilitated the accessibility and visualisation of this organ. Maternally-provided RNA offered the chance to study surviving *ext2* homozygous zebrafish larvae during the first five days of development, when gene-knockout mice experiments have been hindered by the lethality of null embryos (Lin et al., 2000). In addition, the small size of the zebrafish embryo in combination with the permeability of its body to small chemical compounds allowed for high-throughput drug screening, where three embryos could fit in just one well of a 96-well-plate. Zebrafish embryos offer the advantages of both phenotypic and whole-organism drug screening, allowing for early insight into toxicity and metabolism of the tested compounds, due to the existence of fully integrated and functioning organs such as liver, kidney and blood-brain barriers in the larvae.

This thesis highlights the importance of the ECM in the development and morphogenesis of the inner ear in zebrafish. At the same time, it describes how phenotypic drug screening based on *versican* expression is an easily assessible, preliminary platform for the identification of compounds that interact with various components of the Adgrg6 signalling pathway. In combination with the numerous mutation alleles available for *adgrg6* in zebrafish, this *in vivo* platform provides an excellent opportunity to determine the potential target of the hit compounds in counter-screens. The chemical analysis and structural comparison of the compounds shown to be putative Adgrg6 receptor agonists will contribute to the elucidation of the physical properties responsible for this interaction and by extension, will provide further insight on the underlying mechanism of Adgrg6 signalling.

BIBLIOGRAPHY

Abbas, L. and Whitfield, T.T. (2010). The zebrafish inner ear. In *Fish Physiology: Zebrafish*, A.P. Farrell and C.J. Brauner, ed. (London, UK: Elsevier Inc.), pp. 123-171.

Adany, R., Heimer, R., Caterson, B., Sorrell, J.M., and Iozzo, R.V. (1990). Altered expression of chondroitin sulfate proteoglycan in the stroma of human colon carcinoma. Hypomethylation of PG-40 gene correlates with increased PG-40 content and mRNA levels. The Journal of Biological Chemistry *265*(19), 11389–11396.

Ahuja, S., Dogra, D., Stainier, D.Y.R., and Reischauer, S. (2016). Id4 functions downstream of Bmp signaling to restrict TCF function in endocardial cells during atrioventricular valve development. Developmental Biology *412*, 71–82.

Andersson-Sjöland, A., Hallgren, O., Rolandsson, S., Weitoft, M., Tykesson, E., Larsson-Callerfelt, A.-K., Rydell-Törmänen, K., Bjermer, L., Malmström, A., Karlsson, J.C. and Westergren-Thorsson, G. (2014). Versican in inflammation and tissue remodeling: The impact on lung disorders. Glycobiology *25*(3), 243–251.

Armulik, A., Genové, G., and Betsholtz, C. (2011). Pericytes: Developmental, Physiological, and Pathological Perspectives, Problems, and Promises. Developmental Cell *21*(2):193-215.

Arslan, F., Bosserhoff, A.K., Nickl-Jockschat, T., Doerfelt, A., Bogdahn, U. and Hau, P. (2007). The role of versican isoforms V0/V1 in glioma migration mediated by transforming growth factor-beta 2. British Journal of Cancer *96*, 1560-1568.

Ashikari-Hada, S., Habuchi, H., Kariya, Y., Itoh, N., Reddi, A.H. and. Kimata K. (2004). Characterization of growth factor-binding structures in heparin/heparan sulfate using an octasaccharide library. The Journal of Biological Chemistry *279*, 12346–12354.

Aspberg, A., Binkert, C. and Ruoslahtit, E. (1995). The versican C-type lectin domain recognizes the adhesion protein tenascin-R. Proceedings of the National Academy of Sciences *92*, 10590–10594.

Attieh, Y., and Vignjevic, D.M. (2016). The hallmarks of CAFs in cancer invasion. European Journal of Cell Biology *95*, 493–502.

Baker, J.R., Roden, L., Stoolmiller, A.C. (1972). Biosynthesis of Chondroitin Sulphate Proteoglycans. The Journal of Biological Chemistry *247*, 3838–3847.

Balkwill, F.R. and Hagemann, T. (2012). The tumor microenvironment at a glance. Journal of Cell Science *125*, 5591–5596.

Baraban, S.C., Dinday, M.T., and Hortopan, G.A. (2013). Drug screening in Scn1a zebrafish mutant identifies clemizole as a potential Dravet syndrome treatment. Nature Communications *4*, 1–10.

Barry, S., Chelala, C., Lines, K., Sunamura, M., Wang, A., Marelli-Berg, F.M., and Crnogorac-Jurcevic, T. (2013). S100P is a metastasis-associated gene that facilitates transendothelial migration of pancreatic cancer cells. Clinical and Experimental Metastasis *30*(3), 251–264.

Baxendale, S. and Whitfield, T.T. (2014). Zebrafish Inner Ear Development and Function. In Development of Auditory and Vestibular Systems, R. Romand and I. Varela-Nieto, eds. (Cambridge, USA: Academic Press), pp. 63–106.

Baxendale, S., Eeden, F. Van, and Wilkinson, R. (2017). The Power of Zebrafish in Personalised Medicine. Advances in Experimental Medicine and Biology *1007*, 179–197.

Baxendale, S., Holdsworth, C.J., Santoscoy, P.L.M., Harrison, M.R.M., Fox, J., Parkin, C.A., Ingham, P.W., and Cunliffe, V.T. (2012). Identification of compounds with anti-convulsant properties in a zebrafish model of epileptic seizures. Disease models and mechanisms *5*, 773–784.

Becker, C.G. and Becker, T. (2002). Repellent Guidance of Regenerating Optic Axons by Chondroitin Sulfate Glycosaminoglycans in Zebrafish. The Journal of Neuroscience *22*, 842–853.

Berdiaki, A., Zafiropoulos, A., Fthenou, E., Katonis, P., Tsatsakis, A., Karamanos, N.K. and Tzanakakis, G.N. (2008). Regulation of hyaluronan and versican deposition by growth factors in fibrosarcoma cell lines. Biochimica et Biophysica Acta *1780*, 194–202.

Bjarnadóttir, T.K., Gloriam, D.E., Hellstrand, S.H., Kristiansson, H., Fredriksson, R., and Schiöth, H.B. (2006). Comprehensive repertoire and phylogenetic analysis of the G protein-coupled receptors in human and mouse. Genomics *88*, 263–273.

Bockaert, J., Pin, J.P. (1999). Molecular tinkering of G protein-coupled receptors: an evolutionary success. The EMBO Journal *18*, 1723–1729.

Bok, J., Chang, W., and Wu, D.K. (2007). Patterning and morphogenesis of the vertebrate inner ear. International Journal of Developmental Biology *51*(6–7), 521–533.

Bossé, G.D., and Peterson, R.T. (2017). Development of an opioid self-administration assay to study drug seeking in zebrafish. Behavioural Brain Research *335*, 158–166.

Bremer, J., Skinner, J., and Granato, M. (2017). A small molecule screen identifies *in vivo* modulators of peripheral nerve regeneration in zebrafish. PLoS ONE *12*, 1–17.

Brösamle, C., and Halpern, M.E. (2002). Characterization of myelination in the developing zebrafish. Glia *39*, 47–57.

Bruni, G., Rennekamp, A.J., Velenich, A., Mccarroll, M., Lorello, P.J., Huang, X., Kolczewski, S., Carey, G., and Caldarone, B.J. (2016). Zebrafish behavioral profiling identifies multitarget antipsychotic-like compounds. Nature Chemical Biology *12*, 559–566.

Burighel, P., Caicci, F., and Manni, L. (2011). Hair cells in non-vertebrate models: Lower chordates and molluscs. Hearing Research *273*, 14–24.

Busch-Nentwich, E., Söllner, C., Roehl, H., and Nicolson, T. (2004). The deafness gene dfna5 is crucial for ugdh expression and HA production in the developing ear in zebrafish. Development *131*, 943–951.

Carney, T.J., Feitosa, N.M., Sonntag, C., Slanchev, K., Kluger, J., Kiyozumi, D., Gebauer, J.M., Talbot, J.C., Kimmel, C.B., Sekiguchi, K., et al. (2010). Genetic analysis of fin development in zebrafish identifies furin and Hemicentin1 as potential novel fraser syndrome disease genes. PLoS Genetics *6*.

Chandra, K.S., and Ramesh, G. (2013). The fourth-generation Calcium channel blocker: Cilnidipine. Indian Heart Journal *65*, 691–695.

Chen, X., and Song, E. (2018). Turning foes to friends: targeting cancer-associated

fibroblasts. Nature Reviews Drug Discovery, *1.*

Cheng, H.-L., Hsieh, M.-J., Yang, J.-S., Lin, C.-W., Lue, K.-H., Lu, K.-H., and Yang, S.-F. (2016). Nobiletin inhibits human osteosarcoma cells metastasis by blocking ERK and JNK-mediated MMPs expression. Oncotarget *7*.

Choudhry, P., and Trede, N.S. (2013). DiGeorge Syndrome Gene tbx1 Functions through wnt11r to Regulate Heart Looping and Differentiation. PLoS ONE *8*.

Christensen, C.B., Lauridsen, H., Christensen-Dalsgaard, J., Pedersen, M., and Madsen, P.T. (2015). Better than fish on land? Hearing across metamorphosis in salamanders. Proceedings of the Royal Society B: Biological Sciences *282*, 1802.

Clark, A.G., and Vignjevic, D.M. (2015). Modes of cancer cell invasion and the role of the microenvironment. Current Opinion in Cell Biology *36*, 13–22.

Clément, A., Wiweger, M., Von Der Hardt, S., Rusch, M.A., Selleck, S.B., Chien, C. Bin, and Roehl, H.H. (2008). Regulation of zebrafish skeletogenesis by *ext2/dackel* and *papst1/pinscher*. PLoS Genetics *4*.

Colotta, F., Allavena, P., Sica, A., Garlanda, C. and Mantovani, A. (2009) Cancer-related inflammation, the seventh hallmark of cancer: links to genetic instability. Carcinogenesis *30*, 1073–1081.

Coster, L., Carlstedt, I. and Malmstrom, A. (1979). Isolation of 35S- and 3H-labelled proteoglycans from cultures of human embryonic skin fibroblasts. Biochemical Journal *183*, 669–681.

Cruz, S., Shiao, J., Liao, B., Huang, C., and Hwang, P. (2009). Plasma membrane calcium ATPase required for semicircular canal formation and otolith growth in the zebrafish inner ear. The Journal of Experimental Biology *212*, 639–647.

Cummings, R.D. and McEver, R.P. (2017). C-Type Lectins. In *Essentials of Glycobiology,* A. Varki, R.D. Cummings, J.D. Esko, et al., eds. (New York: Cold Spring Harbor Laboratory Press).

Cusick, M.F., Libbey, J.E., Trede, N.S., Eckels, D.D., and Fujinami, R.S. (2012). Human T cell expansion and experimental autoimmune encephalomyelitis inhibited by

Lenaldekar, a small molecule discovered in a zebrafish screen. Journal of Neuroimmunology *244*, 35–44.

Daneman, R., Agalliu, D., Zhou, L., Kuhnert, F., Kuo, C.J., and Barres, B.A. (2009). Wnt/ -catenin signaling is required for CNS, but not non-CNS, angiogenesis. Proceedings of the National Academy of Sciences *106*, 641–646.

de la Motte, C.A., Hascall, V.C., Drazba, J., Bandyopadhyay, S.K. and Strong, S.A. (2003). Mononuclear leukocytes bind to specific hyaluronan structures on colon mucosal smooth muscle cells treated with polyinosinic acid: polycytidylic acid: inter-alpha-trypsin inhibitor is crucial to structure and function. The American Journal of Pathology *163*, 121-133.

de Wit, M., Belt, E.J.T., Delis-van Diemen, P.M., Carvalho, B., Coupé, V.M.H., Stockmann, H.B., and Meijer, G.A. (2013). Lumican and Versican Are Associated with Good Outcome in Stage II and III Colon Cancer. Annals of Surgical Oncology *20*, 348–359.

Detrich, H.W., Westerfield, M. and Zon L.I. (2010). The Zebrafish: Cellular and Developmental Biology (Cambridge, USA: Academic Press).

Diakos, C.I., Charles, K.A., Mcmillan, D.C., and Clarke, S.J. (2014). Cancer-related inflammation and treatment effectiveness. The Lancet Oncology *15*, 493–503.

Ding, L., Bailey, M.H., Porta-Pardo, E., and Wheeler, D.A. (2018). Perspective on Oncogenic Processes at the End of the Beginning of Cancer Genomics Article Perspective on Oncogenic Processes at the End of the Beginning of Cancer Genomics. Cell *173*, 305–320.

Domenzain-Reyna, C., Hernández, D. and Miquel-Serra, L. (2009). Structure and Regulation of the Versican Promoter: The versican promoter is regulated by AP-1 and TCF transcription factors in invasive Human Melanoma cells. The Journal of Biological Chemistry *284*(18), 12306-12317.

Drews, J. (2000). Drug discovery: A historical perspective. Science *287*, 1960–1964.

Du, W.W., Fang, L., Yang, W., Sheng, W., Zhang, Y., Seth, A., and Yee, A. (2012). The role of versican G3 domain in regulating breast cancer cell motility including effects on

osteoblast cell growth and differentiation *in vitro*-evaluation towards understanding breast cancer cell bone metastasis. BMC Cancer *12*(1), 341.

Du, W.W., Fang, L., Yang, X., Sheng, W., Yang, B.L., Seth, A., and Yee, A.J. (2013). The role of versican in modulating breast cancer cell self-renewal. Molecular Cancer Research *11*(5), 443–55.

Dunkelberger, D.G., Dean, J.M., and Watabe, N. (1980). The ultrastructure of the otolithic membrane and otolith in the juvenile mummichog, Fundulus heteroclitus. Journal of Morphology *163*, 367–377.

Dutt, S., Kle, M., Matasci, M., Sommer, L., and Zimmermann, D.R. (2006). Versican V0 and V1 Guide Migratory Neural Crest Cells. The Journal of Biological Chemistry *281*(17), 12123–12131.

Eames, B.F., Singer, A., Smith, G.A., Wood, Z.A., Yan, Y.-L., He, X., and Postlethwait, J.H. (2010). UDP xylose synthase 1 is required for morphogenesis and histogenesis of the craniofacial skeleton. Developmental Biology *341*(2), 400–415.

El-haibi, C.P., Bell, G.W., Zhang, J., Collmann, A.Y., Wood, D., and Scherber, C.M. (2012). Critical role for lysyl oxidase in mesenchymal stem cell-driven breast cancer malignancy. PNAS *109*, 17460–17465.

Ernest, S., Rauch, G.J., Haffter, P., Geisler, R., Petit, C., and Nicolson, T. (2000) Mariner is defective in myosin VIIA: a zebrafish model for human hereditary deafness. Human Molecular Genetics *9*, 2189-2196.

Esko, J.D., and Zhang, L. (1996). Influence of core protein sequence on glycosaminoglycan assembly. Current Opinion in Structural Biology *6,* 663–670.

Evanko, S.P., Angello, J.C. and Wight, T.N. (1999). Formation of hyaluronan- and versican-rich pericellular matrix is required for proliferation and migration of vascular smooth muscle cells. Arteriosclerosis, Thrombosis, and Vascular Biology *19*, 1004–1013.

Evanko, S.P., Potter-Perigo, S., Bollyky, P.L., Nepom, G.T., Wight, T.N. (2012). Hyaluronan and versican in the control of human T-lymphocyte adhesion and migration. Matrix Biology *31*, 90–100.

Fang, L., Du, W.W., Yang, X., Chen, K., Ghanekar, A., Levy, G., and Yang, B.B. (2013). Versican 3′-untranslated region (3′-UTR) functions as a ceRNA in inducing the development of hepatocellular carcinoma by regulating miRNA activity. The Federation of American Societies for Experimental Biology Journal *27*(3), 907–919.

Fanhchaksai, K., Okada, F., Nagai, N., Pothacharoen, P., Kongtawelert, P., Hatano, S., and Watanabe, H. (2016). Host stromal versican is essential for cancer-associated fibroblast function to inhibit cancer growth. International Journal of Cancer *138*(3), 630–641.

Farrell, S.R., Rankin, D.R., Brecha, N.C., and Barnes, S. (2014). Somatostatin receptor subtype 4 modulates L-type calcium channels via Gβγ and PKC signaling in rat retinal ganglion cells. Channels *8*, 519–527.

Fredriksson, R., Gloriam, D.E.I., Hoglund, P.J., Lagerstrom, M.C. and Schiöth, H.B. (2003). There exist at least 30 human G-protein-coupled receptors with long Ser/Thr-rich N-termini. Biochemical and Biophysical Research Communications *301*, 725–734.

Freeman, S.D., Keino-Masu, K., Masu, M., and Ladher, R.K. (2015). Expression of the heparan sulfate 6-O-endosulfatases, Sulf1 and Sulf2, in the avian and mammalian inner ear suggests a role for sulfation during inner ear development. Developmental Dynamics *244*, 168–180.

Fritzsch, B., and Elliott, K.L. (2017). Evolution and Development of the Inner Ear Efferent System: Transforming a Motor Neuron Population to Connect to the Most Unusual Motor Protein via Ancient Nicotinic Receptors. Frontiers in Cellular Neuroscience *11*, 1–9.

Fritzsch, B., Barald, K.F. and Lomax, M.I. (1998). Early Embryology of the Vertebrate Ear. In *Development of the Auditory System*, E. W. Rubel, A. N. Popper and R. R. Fay, eds. (New York: SpringerVerlag), pp. 80-145.

Gabbiani, G. (2003). The myofibroblast in wound healing and fibrocontractive diseases. Journal of Pathology *200*, 500–503.

Gao, D., Joshi, N., Choi, H., Ryu, S., Hahn, M., Catena, R., and Stiles, B. (2012). Myeloid Progenitor Cells in the Premetastatic Lung Promote Metastases by Inducing Mesenchymal to Epithelial Transition. Cancer Research *72*(6), 1384–1395.

Garrity, D.M., Childs, S., and Fishman, M.C. (2002). The heartstrings mutation in zebrafish causes heart/fin Tbx5 deficiency syndrome. Development (Cambridge, England) *129*, 4635–4645.

Gay, L.J., and Felding-habermann, B. (2011). Contribution of platelets to tumour metastasis Laurie. Nature reviews *11*, 123–134.

Geng, F.-S.F.-S., Abbas, L., Baxendale, S., Holdsworth, C.J., Swanson, G., Slanchev, K., Hammerschmidt, M., Topczewski, J., and Whitfield, T.T. (2013). Semicircular canal morphogenesis in the zebrafish inner ear requires the function of *gpr126* (*lauscher*), an adhesion class G protein-coupled receptor gene. Development (Cambridge, England) *140*, 4362–4374.

Gerchman, E., Hilfer, S.R., and Brown, J.W. (1995). Involvement of Extracellular Matrix in the Formation of the Inner Ear. Developmental Dynamics *202,* 421–432.

Ghysen, A., and Dambly-Chaudie, C. (2004). Development of the zebrafish lateral line. Current Opinion in Neurobiology *14*, 67–73.

Gilkes, D.M., Chaturvedi, P., Bajpai, S., Wong, C.C., Wei, H., Pitcairn, S., and Semenza, G.L. (2013). Collagen Prolyl Hydroxylases Are Essential for Breast Cancer Metastasis. Cancer Research *73*(11), 3285–3297.

Glenn, T.D., and Talbot, W.S. (2013). Analysis of Gpr126 function defines distinct mechanisms controlling the initiation and maturation of myelin. Development *140*(15), 3167–75.

Griffin, A., Hamling, K.R., Knupp, K., Hong, S., Lee, L.P., and Baraban, S.C. (2017). Clemizole and modulators of serotonin signalling suppress seizures in Dravet syndrome. Brain 140, 669–683.

Haddon, C.M., and Lewis, J.H. (1991). Hyaluronan as a propellant for epithelial movement: the development of semicircular canals in the inner ear of *Xenopus*. Development *550*, 541–550.

Haddon, C.M., and Lewis, J.H. (1991). Hyaluronan as a propellant for epithelial movement: the development of semicircular canals in the inner ear of *Xenopus*. Development *550*, 541–550.

Hallgren, O., Nihlberg, K., Dahlbäck, M., Bjermer, L., Eriksson, L.T., Erjefält, J.S., Löfdahl, C.G. and Westergren-Thorsson, G. (2010). Altered fibroblast proteoglycan production in COPD. Respiratory Research *11*, 55.

Han, W., Chen, S., Yuan, W., Fan, Q., Tian, J., Wang, X., and Chen, L. (2016). Oriented collagen fibers direct tumor cell intravasation. PNAS *113*, 11208–11213.

Hanahan, D., and Weinberg, R.A. (2011). Review Hallmarks of Cancer : The Next Generation. Cell *144*, 646–674.

Hanahan, D., Weinberg, R.A. (2000). The Hallmarks of Cancer. Cell *100*, 57-70.

Hascall, V. and Esko, J.D. (2017). Hyaluronan. In *Essentials of Glycobiology,* A. Varki, R.D. Cummings, J.D. Esko, et al., eds. (New York: Cold Spring Harbor Laboratory Press).

Hearnden, V., Lomas, H., MacNeil, S., Thornhill, M., Murdoch, C., Lewis, A., Madsen, J., Blanazs, A., Armes, S., and Battaglia, G. (2009). Diffusion studies of nanometer polymersomes across tissue engineered human oral mucosa. Pharmaceutical Research *26*, 1718–1728.

Henderson, D.J., and Copp, A.J. (1998). Versican expression is associated with chamber specification, septation, and valvulogenesis in the developing mouse heart. Circulation Research *83*, 523-532.

Henikoff, S., and Henikoff, J.G. (1992). Amino acid substitution matrices from protein blocks. PNAS *89*, 10915–10919.

Hester, E. (2005). The evolution of the auditory system: A tutorial. Contemporary Issues in Communication Science and Disorders, *32*, 5-10.

Hetherington, T.E. (1987). Timing of development of the middle ear of Anura (Amphibia). Zoomorphology *106*, 289–300.

Hinek, A., Mecham, R.P., Keeley, F., and Rabinovitch, M. (1991). Impaired elastin fiber assembly related to reduced 67-kD elastin-binding protein in fetal lamb ductus arteriosus and in cultured aortic smoothmuscle cells treated with chondroitin sulfate. Journal of Clinical Investigation *88*, 2083–2094.

Hinz, B., Celetta, G., Tomasek, J.J., Gabbiani, G. and Chaponnier, C. (2001). Alpha-Smooth Muscle Actin Expression Upregulates Fibroblast Contractile Activity. Molecular Biology of the Cell *12*, 2730–2741.

Hinz, B., Celetta, G., Tomasek, J.J., Gabbiani, G., and Chaponnier, C. (2001). Alpha-Smooth Muscle Actin Expression Upregulates Fibroblast Contractile Activity. Molecular Biology of the Cell *12*, 2730–2741.

Hitchcock, A.M., Costello, C.E. and Zaia J. (2006). Glycoform quantification of chondroitin/dermatan sulfate using a liquid chromatography-tandem mass spectrometry platform. Biochemistry *45*, 2350–2361.

Holmborn, K., Habicher, J., Kasza, Z., Eriksson, A.S., Filipek-Gorniok, B., Gopal, S., and Ledin, J. (2012). On the roles and regulation of chondroitin sulfate and heparan sulfate in zebrafish pharyngeal cartilage morphogenesis. Journal of Biological Chemistry *287*(40), 33905–33916.

Howe, K., Clark, M.D., Torroja, C.F., Torrance, J., Berthelot, C., Muffato, M., and Stemple, D.L. (2013). The zebrafish reference genome sequence and its relationship to the human genome. Nature *496*, 498-503.

Iozzo, R.V., Naso, M.F., Cannizzaro, L.A., Wasmuth, J.J. and McPherson, J.D. (1992). Mapping of the versican proteoglycan gene (CSPG2) to the long arm of human chromosome 5 (5q12-5q14). Genomics *14*, 845-851.

Jacquemet, G., Baghirov, H., Georgiadou, M., Sihto, H., Peuhu, E., Cettour-janet, P., Kronqvist, P., Joensuu, H., Ivaska, J., He, T., et al. (2016). L-type calcium channels regulate filopodia stability and cancer cell invasion downstream of integrin signalling. Nature communications *7.*

Jang, S., Liu, X., Chan, C.B., France, S.A., Sayeed, I., Tang, W., Lin, X., Andero, R., Chang, Q., Ressler, K.J., et al. (2010). Deoxygedunin , a Natural Product with Potent Neurotrophic Activity in Mice. PLoS ONE *5*.

Jeng, J.H., Lan, W.H., Wang, J.S., Chan, C.P., Ho, Y.S., Lee, P.H., Wang, Y.J., Wang, T.M., Chen, Y.J., and Chang, M.C. (2006). Signaling mechanism of thrombin-induced gingival fibroblast-populated collagen gel contraction. British Journal of Pharmacology *147*, 188–198.

Jensen, R.L., and Wurster, R.D. (2001). Calcium channel antagonists inhibit growth of subcutaneous xenograft meningiomas in nude mice. Surgical Neurology *55*, 275–283.

Jochmann, K., Bachvarova, V., and Vortkamp, A. (2014). Reprint of: Heparan sulfate as a regulator of endochondral ossification and osteochondroma development. Matrix Biology *35*, 239–247.

Jones, P.A., and Baylin, S.B. (2002). The fundamental role of epigenetic events in cancer. Nature Reviews Genetics *3*, 415–428.

Joyce, J.A., and Pollard, J.W. (2009). Microenvironmental regulation of metastasis. Nature Reviews Cancer *9*(4), 239–252.

Kang, I., Barth, J.L., Sproul, E.P., Yoon, D.W., Workman, G.A., Braun, K.R., Argraves, W.S., and Wight, T.N. (2015). Expression of V3 Versican by Rat Arterial Smooth Muscle Cells Promotes Differentiated and Anti-inflammatory. The Journal of Biological Chemistry *290*(35), 21629–21641.

Kang, I., Yoon, D.W., Braun, K.R., and Wight, T.N. (2014). Expression of Versican V3 by Arterial Smooth Muscle Cells Alters Tumor Growth Factor β (TGF-β)-, Epidermal Growth Factor (EGF)-, and Nuclear Factor κB (NFκB)-dependent signaling Pathways, Creating a Microenvironment That Resists Monocyte Adhesion. The Journal of Biological Chemistry *289*(22), 15393–15404.

Kang, J.S., Oohashi, T., Kawakami, Y., Bekku, Y., Izpisúa Belmonte, J.C., and Ninomiya, Y. (2004). Characterization of *dermacan*, a novel zebrafish lectican gene, expressed in dermal bones. Mechanisms of Development *121*, 301–312.

Kaslin, J., and Gibert, Y. (2017). Using Zebrafish to Study Human Genetic Disease. In: eLS. John Wiley & Sons, Ltd: Chichester.

Keire, P.A., Bressler, S.L., Lemire, J.M., Edris, B., Rubin, B.P., Rahmani, M., and Wight, T.N. (2014). A Role for Versican in the Development of Leiomyosarcoma. Journal of Biological Chemistry *289*(49), 34089–34103.

Kessenbrock, K., Plaks, V., and Werb, Z. (2010). Matrix Metalloproteinases : Regulators of the Tumor Microenvironment. Cell *141*, 52–67.

Kim, J., Kim, H., Koun, S., Ham, H., and Kim, M. (2014). Zebrafish Crip2 plays a critical role in atrioventricular valve development by downregulating the expression of ECM genes in the endocardial cushion. Molecules and Cells *37*(5), 406–411.

Kimmel, C.B., Ballard, W.W., Kimmel, S.R., Ullmann, B., and Schilling, T.F. (1995). Stages of embryonic development of the zebrafish. Developmental Dynamics *203*, 253–310.

Kokenyesi, R., and Bernfields, M. (1994). Core Protein Structure and Sequence Determine the Site and Presence of Heparan Sulfate and Chondroitin Sulfate on Syndecan-l. The Journal of Biological Chemistry *269*(16), 12304–12309.

Kong, A.N.T., Yu, R., Chen, C., Mandlekar, S., and Primiano, T. (2000). Signal Transduction Events Elicited by Natural Products: Role of MAPK and Caspase Pathways in Homeostatic Response and Induction of Apoptosis. Archives of Pharmacal Research *23*, 1–16.

Koyama, H., Hibi, T., Isogai, Z., Yoneda, M., Fujimori, M., Amano, J., Kawakubo, M., Kannagi, R., Kimata, K., Taniguchi, S., et al. (2007). Hyperproduction of Hyaluronan in Neu-Induced Mammary Tumor Accelerates Angiogenesis through Stromal Cell Recruitment. The American Journal of Pathology *170*, 1086–1099.

Kreuger, J., Spillmann, D., Li, J., and Lindahl, U. (2006). Interactions between heparan sulfate and proteins: the concept of specificity. The Journal of Cell Biology *174*(3), 323–327.

Kung, H., Hoyert, D.L., Xu, J. and Murphy S.L. (2008). Deaths: final data for 2005. National Vital Statistics System *56*, 1-120.

Lambert, A.W., Pattabiraman, D.R., and Weinberg, R.A. (2016). Review Emerging Biological Principles of Metastasis. Cell *168*, 670–691.

Langenhan, T., Aust, G., and Hamann, J. (2013). Sticky Signaling - Adhesion Class G Protein-Coupled Receptors Take the Stage. Cell Biology *6*(276), 1–22.

Lee, H., Lo, H., Lo, D., Su, M., and Hu, J. (2015). Amiodarone Induces Overexpression of Similar to Versican b to Repress the EGFR / Gsk3b / Snail Signaling Axis during Cardiac Valve Formation of Zebrafish Embryos. PLoS ONE *10*, 1–14.

Lee, J.S., Von Der Hardt, S., Rusch, M. a., Stringer, S.E., Stickney, H.L., Talbot, W.S., Geisler, R., Nüsslein-Volhard, C., Selleck, S.B., Chien, C. Bin, et al. (2004). Axon sorting in the optic tract requires HSPG synthesis by *ext2* (*dackel*) and *extl3* (*boxer*). Neuron *44*, 947–960.

Levental, K.R., Yu, H., Kass, L., Lakins, J.N., Egeblad, M., Erler, J.T., Fong, S.F.T., Csiszar, K., Giaccia, A., Weninger, W., *et al.* (2009). Matrix Crosslinking Forces Tumor Progression by Enhancing Integrin Signaling. Cell *139*, 891–906.

Li, B. and Wang, J.H. (2011). Fibroblasts and myofibroblasts in wound healing: Force generation and measurement. Journal of Tissue Viability *20*, 108–120.

Li, D., Wang, X., Wu, J.L., Quan, W.Q., Ma, L., Yang, F., and Wan, H.Y. (2013). Tumor-Produced Versican V1 Enhances hCAP18/LL-37 Expression in Macrophages through Activation of TLR2 and Vitamin D3 Signaling to Promote Ovarian Cancer Progression *In Vitro*. PLoS ONE *8*(2).

Li, Y., Laue, K., Temtamy, S., Aglan, M., Kotan, L.D., Yigit, G., Canan, H., Pawlik, B., Nürnberg, G., Wakeling, E.L., et al. (2010). Temtamy preaxial brachydactyly syndrome is caused by loss-of-function mutations in chondroitin synthase 1, a potential target of BMP signaling. American Journal of Human Genetics *87*, 757–767.

Liebscher, I., Schön, J., Petersen, S.C., Fischer, L., Auerbach, N., Demberg, L.M., and Schöneberg, T. (2014). A Tethered Agonist within the Ectodomain Activates the Adhesion G Protein-Coupled Receptors GPR126 and GPR133. Cell Reports *9*(6), 2018–2026.

Lin, X., Wei, G., Shi, Z., Dryer, L., Esko, J.D., Wells, D.E., and Matzuk, M.M. (2000). Disruption of gastrulation and heparan sulfate biosynthesis in EXT1-deficient mice. Developmental Biology *224*, 299–311.

Lindahl, U., Couchman, J., Kimata, K., et al. (2017) Proteoglycans and Sulfated Glycosaminoglycans. In *Essentials of Glycobiology,* A. Varki, R.D. Cummings, J.D. Esko, et al., eds. (New York: Cold Spring Harbor Laboratory Press).

Lister, J.A., Robertson, C.P., Lepage, T., Johnson, S.L., and Raible, D.W. (1999). Nacre Encodes a Zebrafish Microphthalmia-Related Protein That Regulates Neural-Crest-Derived Pigment Cell Fate. Development (Cambridge, England) *126*, 3757–3767.

Livak, K.J., and Schmittgen, T.D. (2001). Analysis of Relative Gene Expression Data Using Real-Time Quantitative PCR and the 2−ΔΔCT Method. Methods *25*, 402–408.

Lu, Z., DeSmidt, A.A. (2013). Early Development of Hearing in Zebrafish. Journal of the Association for Research in Otolaryngology 521, 509–521.

Macrae, C.A., and Peterson, R.T. (2015). Zebrafish as tools for drug discovery. Nature Reviews drug discovery *14*, 721–731.

Mamuya, F.A., and Duncan, M.K. (2012). αV integrins and TGF-β-induced EMT: a circle of regulation. Journal Of Cellular And Molecular Medicine *16*(3), 445–455.

Masuda, A., Yasuoka, H., Satoh, T., Okazaki, Y., Yamaguchi, Y., and Kuwana, M. (2013). Versican is upregulated in circulating monocytes in patients with systemic sclerosis and amplifies a CCL2-mediated pathogenic loop. Arthritis Research and Therapy *15*(4), 1–15.

Maurer, K., Ihl, R., Dierks, T., and Frolich, L. (1997). Clinical efficacy of Gingko biloba special extract EGb 761 in dementia of the Alzheimer type. Journal of Psychiatric Research *31*, 645–655.

Mauri, P., Scarpa, A., Nascimbeni, A.C., Benazzi, L., Parmagnani, E., Mafficini, A., Della Peruta, M., Bassi, C., Miyazaki, K. and Sorio, C. (2005). Identification of proteins released by pancreatic cancer cells by multidimensional protein identification technology: a strategy for identification of novel cancer markers. Federation of American Societies for Experimental Biology Journal *19*(9), 1125–1127.

McBride, W.H., and Bard, J.B.L. (1979). Hyaluronidase-sensitive halos around adherent cells. Their role in blocking lymphocyte-mediated cytolysis. Journal of Experimental Medicine *149*, 507–515.

Mcculloch, D.R., Nelson, C.M., Dixon, L.J., Silver, D.L., Wylie, J.D., Lindner, V., and Apte, S.S. (2009). ADAMTS Metalloproteases Generate Active Versican Fragments that Regulate Interdigital Web Regression. Developmental Cell *17*(5), 687–698.

Meeker, N.D., Hutchinson, S.A., Ho, L., and Trede, N.S. (2007). Method for isolation of PCR-ready genomic DNA from zebrafish tissues. BioTechniques *43*, 610–614.

Mehta, P., and Piao, X. (2017). Adhesion G-Protein Coupled Receptors and Extracellular Matrix Proteins: Roles in Myelination and Glial Cell Development. Developmental Dynamics *246*, 275–284.

Miquel-Serra, L., Serra, M., Hernández, D., Domenzain, C., Docampo, M.J., Rabanal, R.M., de Torres, I., Wight, T.N., Fabra, A. and Bassols, A. (2006). V3 versican isoform expression has a dual role in human melanoma tumor growth and metastasis. Laboratory Investigation *86*(9), 889–901.

Mizumoto, S., Mikami, T., Yasunaga, D., Kobayashi, N., Yamauchi, H., Miyake, A., Itoh, N., Kitagawa, H., and Sugahara, K. (2009). Chondroitin 4-O-sulfotransferase-1 is required for somitic muscle development and motor axon guidance in zebrafish. The Biochemical Journal *419*, 387–399.

Mjaatvedt, C.H., Yamamura, H., Capehart, A.A., Turner, D., and Markwald, R.R. (1998). The Cspg2 Gene , Disrupted in the hdf Mutant , Is Required for Right Cardiac Chamber and Endocardial Cushion Formation. Developmental Biology *66*, 56–66.

Mogha, A., Benesh, A.E., Patra, C., Engel, F.B., Schoneberg, T., Liebscher, I., and Monk, K.R. (2013). Gpr126 Functions in Schwann Cells to Control Differentiation and Myelination via G-Protein Activation. Journal of Neuroscience *33*(46), 17976–17985.

Mogha, X.A., Harty, X.B.L., Carlin, D., Joseph, J., Sanchez, N.E., Suter, U., Piao, X., Cavalli, V., and Monk, K.R. (2016). Gpr126 / Adgrg6 Has Schwann Cell Autonomous and Nonautonomous Functions in Peripheral Nerve Injury and Repair. The Journal of Neuroscience *36*(49), 12351–12367.

Monk, K.R., Feltri, M.L., and Taveggia, C. (2015). New Insights on Schwann Cell Development. Glia *63*, 1376–1393.

Monk, K.R., Naylor, S.G., Glenn, T.D., Mercurio, S., Perlin, J.R., Dominguez, C., Moens, C.B., and Talbot, W.S. (2009). A G protein-coupled receptor is essential for Schwann cells to initiate myelination. Science *325*, 1402–1405.

Monk, K.R., Oshima, K., Jörs, S., Heller, S., and Talbot, W.S. (2011). Gpr126 is essential for peripheral nerve development and myelination in mammals. Development *138*(13), 2673–80.

Montague, T.G., Cruz, J.M., Gagnon, J.A., Church, G.M., and Valen, E. (2014). CHOPCHOP: A CRISPR/Cas9 and TALEN web tool for genome editing. Nucleic Acids Research *42*, 401–407.

Moro-Balbás, J.A., Gato, A., Alonso, M.I., Martín, P., and De la Mano, A. (2000). Basal lamina heparan sulphate proteoglycan is involved in otic placode invagination in chick embryos. Anatomy and Embryology *202*, 333–343.

Mugiya, Y., and Yoshida, M. (1995). Effects of Calcium Antagonists and Other Metabolic Modulators on *in Vitro* Calcium Deposition on Otoliths in the Rainbow Trout Oncorhynchus mykiss. Fisheries Science *61*, 1026–1030.

Müller-Deile, J., Gellrich, F., Schenk, H., Schroder, P., Nyström, J., Lorenzen, J., Haller, H., and Schiffer, M. (2016). Overexpression of TGF-β Inducible microRNA-143 in Zebrafish Leads to Impairment of the Glomerular Filtration Barrier by Targeting Proteoglycans. Cellular Physiology and Biochemistry *40*, 819–830.

Murayama, E., Herbomel, P., Kawakami, A., Takeda, H., and Nagasawa, H. (2005). Otolith matrix proteins OMP-1 and Otolin-1 are necessary for normal otolith growth and their correct anchoring onto the sensory maculae. Mechanisms of Development *122*, 791–803.

Nandadasa, S., Foulcer, S., and Apte, S.S. (2014). The multiple, complex roles of versican and its proteolytic turnover by ADAMTS proteases during embryogenesis. Matrix Biology *35*, 34–41.

Naso, M.F., Morgan, J.L., Buchberg, M., Siracusa, L.D., and Iozzo, R.V. (1995). Expression pattern and mapping of the murine versican gene (Cspg2) to chromosome 13. Genomics *29*, 297–300.

Naso, M.F., Zimmermanng, D.R., and Iozzo, R.V. (1994). Characterization of the Complete Genomic Structure of the Human Versican Gene and Functional Analysis of Its Promoter. The Journal of Biological Chemistry *269*(52), 32999–33008.

Nawaz, M., Shah, N., Zanetti, B.R., Maugeri, M., Silvestre, R.N., Fatima, F., Neder, L., and Valadi, H. (2018). Extracellular Vesicles and Matrix Remodeling Enzymes: The Emerging Roles in Extracellular Matrix Remodeling, Progression of Diseases and Tissue Repair. Cells *7*, 1–26.

Nelson, C.M., and Bissell, M.J. (2006). Of Extracellular Matrix, Scaffolds, and Signaling: Tissue Architecture Regulates Development, Homeostasis, and Cancer. Annual Review of Cell and Developmental Biology *22*, 287–309.

Neuhauss, S.C., Solnica-Krezel, L., Schier, A.F., Zwartkruis, F., Stemple, D.L., Malicki, J., Abdelilah, S., Stainier, D.Y., Driever, W. (1996). Mutations affecting craniofacial development in zebrafish. Development *123*, 357–367.

Ng, M.R., and Brugge, J.S. (2009). A stiff blow from the stroma: collagen crosslinking drives tumor progression. Cancer Cell *16*, 455–457.

Nieman, K.M., Kenny, H.A., Penicka, C.V., Ladanyi, A., Buell-, R., Zillhardt, M.R., Romero, I.L., Carey, M.S., Mills, G.B., and Gökhan, S. (2011). Adipocytes promote ovarian cancer metastasis and provide energy for rapid tumor growth. Nature Medicine *17*(11), 1498–1503.

O'Hayre, M., Vázquez-Prado, J., Kufareva, I., Stawiski, E.W., Handel, T.M., Seshagiri, S., and Gutkind, J.S. (2013). The emerging mutational landscape of G proteins and G-protein-coupled receptors in cancer. Nature Reviews Cancer *13*(6), 412–424.

Onken, J., Moeckel, S., Leukel, P., Leidgens, V., Baumann, F., Bogdahn, U., Vollmann-Zwerenz, A., and Hau, P. (2014). Versican isoform V1 regulates proliferation and migration in high-grade gliomas. Journal of Neuro-Oncology *120*, 73–83.

Owens, K.N., Santos, F., Roberts, B., Linbo, T., Coffin, A.B., Knisely, A.J., Simon, J.A., Rubel, E.W., and Raible, D.W. (2008). Identification of Genetic and Chemical Modulators of Zebrafish Mechanosensory Hair Cell Death. PLoS Genetics *4,* e1000020.

Parrie, L.E., Renfrew, E.M., Wal, A. Vander, Mueller, R.L., and Garrity, D.M. (2013). Zebrafish tbx5 paralogs demonstrate independent essential requirements in cardiac and pectoral fin development. Developmental Dynamics *242*, 485–402.

Patra, C., Diehl, F., Ferrazzi, F., van Amerongen, M.J., Novoyatleva, T., Schaefer, L., Muhlfeld, C., Jungblut, B., and Engel, F.B. (2011). Nephronectin regulates atrioventricular canal differentiation via Bmp4-Has2 signaling in zebrafish. Development *138*, 4499–4509.

Patra, C., Monk, K.R. and Engel, F.B. (2014). The multiple signaling modalities of adhesion G protein-coupled receptor GPR126 in development. Receptors of Clinical Investigation *1*(3), 1–14.

Petersen, S.C., Luo, R., Liebscher, I., Giera, S., Jeong, S.J., Mogha, A., Ghidinelli, M., Feltri, M.L., Schöneberg, T., Piao, X., et al. (2015). The Adhesion GPCR GPR126 Has Distinct, Domain-Dependent Functions in Schwann Cell Development Mediated by Interaction with Laminin-211. Neuron *85*, 755–769.

Pietras, K., and Östman, A. (2010). Hallmarks of cancer: Interactions with the tumor stroma. Experimental Cell Research *316*(8), 1324–1331.

Pogoda, H., Sternheim, N., Lyons, D.A., Diamond, B., Hawkins, T.A., Woods, I.G., Bhatt, D.H., Franzini-armstrong, C., Dominguez, C., Arana, N., et al. (2006). A genetic screen identifies genes essential for development of myelinated axons in zebrafish. Developmental Biology *298*, 118–131.

Popper, A.N. and Fay, R.R. (1973). Sound detection and processing by teleost fishes: a critical review. The Journal of the Acoustical Society of America *53*(6), 1515–29.

Potter-Perigo, S., Johnson, P.Y., Evanko, S.P., Chan, C.K., Braun, K.R., Wilkinson, T.S., Altman, C., and Wight, T.N. (2010). Polyinosine-Polycytidylic Acid Stimulates Versican Accumulation in the Extracellular Matrix Promoting Monocyte Adhesion. American Journal of Respiratory Cell and Molecular Biology *17*, 109–120.

Prajapati, P., and Lambert, D.W. (2016). Cancer-associated fibroblasts – Not-so-innocent bystanders in metastasis to bone? Journal of Bone Oncology *5*(3), 128–131.

Preston Mason, R. (1996). Calcium channel blockers and cancer: A biological link remains elusive. American Journal of Hypertension *9*, 1047–1049.

Pukkila, M., Kosunen, A., Ropponen, K., Virtaniemi, J., Kellokoski, J., Kumpulainen, E., and Kosma, V.-M. (2007). High stromal versican expression predicts unfavourable outcome in oral squamous cell carcinoma. Journal of Clinical Pathology *60*(3), 267–272.

Rahmani, M., Read, J.T., Carthy, J.M., McDonald, P.C., Wong, B.W., Esfandiarei, M., Si, X., Luo, Z., Luo, H., Rennie, P.S., et al. (2005). Regulation of the versican promoter by the β-

catenin-T-cell factor complex in vascular smooth muscle cells. The Journal of Biological Chemistry *280*, 13019–13028.

Ravenscroft, G., Nolent, F., Rajagopalan, S., Meireles, A.M., Paavola, K.J., Gaillard, D., and Laing, N.G. (2015). Mutations of GPR126 Are Responsible for Severe Arthrogryposis Multiplex Congenita. American Journal of Human Genetics *96*(6), 955–961.

Ricciardelli, C., Sakko, A.J., Ween, M.P., Russell, D.L., and Horsfall, D.J. (2009). The biological role and regulation of versican levels in cancer. Cancer and Metastasis Reviews *28*, 233–245.

Ridges, S., Heaton, W.L., Joshi, D., Choi, H., Eiring, A., Batchelor, L., Choudhry, P., Manos, E.J., Sofla, H., Sanati, A., et al. (2018). Zebrafish screen identifies novel compound with selective toxicity against leukemia. Blood *119*, 5621–5632.

Riley, B.B. and Moorman, S.J. (2000). Development of utricular otoliths, but not saccular otoliths, is necessary for vestibular function and survival in zebrafish. Journal of Neurobiology *43*, 329–337.

Riley, B.B., Zhu, C., Janetopoulos, C., and Aufderheide, K.J. (1997). A critical period of ear development controlled by distinct populations of ciliated cells in the zebrafish. Developmental Biology *191*, 191–201.

Ronan, S.M., Tran-Viet, K.N., Burner, E.L., Metlapally, R., Toth, C., and Young, T.L. (2009). Mutational hot spot potential of a novel base pair mutation of the CSPG2 gene in a family with Wagner syndrome. Archives of Ophthalmology *127*(11), 1511–1519.

Rossi, A., Kontarakis, Z., Gerri, C., Nolte, H., Hölper, S., Krüger, M., and Stainier, D.Y.R.R. (2015). Genetic compensation induced by deleterious mutations but not gene knockdowns. Nature *524*, 230–233.

Roy, A., and Saraf, S. (2006). Limonoids: Overview of Significant Bioactive Triterpenes Distributed in Plants Kingdom. Biological & Pharmaceutical Bulletin *29*, 191–201.

Rozario, T. and Desimone, D.W. (2010). The Extracellular Matrix In Development and Morphogenesis: A Dynamic View. Developmental Biology *341*, 126–140.

Said, N., Sanchez-Carbayo, M., Smith, S.C., and Theodorescu, D. (2012). RhoGDI2 suppresses lung metastasis in mice by reducing tumor versican expression and macrophage infiltration. Journal of Clinical Investigation *122*(4), 1503–1518.

Sakamoto, N., Terai, M., Takenaka, T., and Maeno, H. (1978). Inhibition of cyclic amp phosphodiesterase by 2,6-dimethyl-4-(3-nitrophenyl)-1,4-dihydropyridine-3,5-dicarboxylic acid 3-[2-(N-benzyl-N-methylamino)] ethyl ester 5-methyl ester hydrochloride (YC-93), a potent vasodilator. Biochemical Pharmacology *27*, 1269–1274.

Savigni, D.L., O'Hare Doig, R.L., Szymanski, C.R., Bartlett, C.A., Lozić, I., Smith, N.M., and Fitzgerald, M. (2013). Three Ca^{2+} channel inhibitors in combination limit chronic secondary degeneration following neurotrauma. Neuropharmacology *75*, 380–390.

Schaff, M., Receveur, N., Bourdon, C., Wurtz, V., Denis, V., Orend, G., Gachet, C., and Mangin, P.H. (2011). Novel Function of Tenascin-C , a Matrix Protein Relevant to Atherosclerosis , in Platelet Recruitment and Activation Under Flow. Arteriosclerosis, Thrombosis, and Vascular Biology *31*, 117–124.

Schampel, A., Volovitch, O., Koeniger, T., Scholz, C.-J., Jörg, S., Linker, R.A., Wischmeyer, E., Wunsch, M., Hell, J.W., Ergün, S., et al. (2017). Nimodipine fosters remyelination in a mouse model of multiple sclerosis and induces microglia-specific apoptosis. Proceedings of the National Academy of Sciences *114*, 3295–3304.

Schmale, G.A., Conrad, E.U., and Raskind W.H. (1994). The natural history of hereditary multiple exostoses. The Journal of Bone and Joint Surgery-American Volume *76* (7), 986–992.

Schmalfeldt, M., Dours-Zimmermann, M.T., Winterhalter, K.H. and Zimmermann, D.R. (1998). Versican V2 is a major extracellular matrix component of the mature bovine brain. The Journal of Biological Chemistry *273*(25), 15758–15764.

Schroeder, J.A., Jackson, L.F., Lee, D.C., and Camenisch, T.D. (2003). Form and function of developing heart valves: coordination by extracellular matrix and growth factor signalling. Journal of Molecular Medicine *81*, 392-403.

Schroeter, H., Boyd, C., Spencer, J.P.E., Williams, R.J., Cadenas, E., and Rice-Evans, C. (2002). MAPK signaling in neurodegeneration: Influences of flavonoids and of nitric oxide. Neurobiology of Aging *23*, 861–880.

Schwander, M., Kachar, B. and Müller, U. (2010). The cell biology of hearing. The Journal of Cell Biology *190*, 9–20.

Serra, M., Miquel, L., Domenzain, C., Fabra, A., and Wight, T.N. (2005). V3 versican isoform expression alters the phenotype of melanoma cells and their tumorigenic potential. International Journal of Cancer *886*, 879–886.

Seytanoglu, A., Alsomali, N.I., Valori, C.F., McGown, A., Kim, H.R., Ning, K., Ramesh, T., Sharrack, B., Wood, J.D., and Azzouz, M. (2016). Deficiency in the mRNA export mediator Gle1 impairs Schwann cell development in the zebrafish embryo. Neuroscience *322*, 287–297.

Sharma, D., Brummel-ziedins, K.E., Bouchard, B.A., and Holmes, C.E. (2014). Platelets in Tumor Progression : A Host Factor That Offers Multiple Potential Targets in the Treatment of Cancer. Journal of Cellular Physiology *229*, 1005–1015.

Sheng, W., Wang, G., Pierre, D.P. La, Wen, J., Deng, Z., Wong, C.A., and Yang, B.B. (2006). Versican Mediates Mesenchymal – Epithelial Transition. Molecular Biology of the Cell *17*, 2009–2020.

Sheng, W., Wang, G., Wang, Y., Liang, J., Wen, J., Zheng, P.S., and Yang, B.B. (2005). The roles of Versican V1 and V2 isoforms in cell proliferation and apoptosis. Molecular Biology of the Cell *16*(3), 1330-1340.

Shinomura, T., Nishida, Y., Ito, K., and Kimatas, K. (1993). cDNA Cloning of PG-M, a Large Chondroitin Sulfate Proteoglycan Expressed during Chondrogenesis in Chick Limb Buds. The Journal of Biological Chemistry *268*, 14461–14469.

Shintani, Y., Hollingsworth, M.A., Johnson, K.R. and Wheelock, M.J. (2006). Collagen I Promotes Metastasis in Pancreatic Cancer by Activating c-Jun NH 2 -Terminal Kinase 1 and Up-regulating N-Cadherin Expression. Cancer Research *66*, 11745–11754.

Shoulders, M.D., and Raines R.T. (2009). Collagen structure and stability. Annual Review of Biochemistry *78*, 929–958.

Silbert, J.E., and DeLuca, S. (1969) Biosynthesis of chondroitin sulfate: III. Formation of sulfated glycosaminoglycan with a microsomal preparation from chick cartilage. The Journal of Biological Chemistry *244*, 876–881.

Silbert, J.E., and Sugumaran, G. (2002). Biosynthesis of Chondroitin / Dermatan Sulfate. IUBMB Life *54*, 177–186.

Singh, M., Yelle, N., Venugopal, C., and Singh, S.K. (2018). EMT : Mechanisms and therapeutic implications. Pharmacology and Therapeutics *182*, 80–94.

Singha, N.C., Nekoroski, T., Zhao, C., Symons, R., Jiang, P., Gregory, I., Huang, Z., and Shepard, H.M. (2015). Tumor-Associated Hyaluronan Limits Efficacy of Monoclonal Antibody Therapy. Molecular Cancer Therapeutics *20*, 523–533.

Singleton, P.A. (2014). Hyaluronan regulation of endothelial barrier function in cancer. Advances in Cancer Research *123*, 191–209.

Sisson, B.E., Dale, R.M., Mui, S.R., Topczewska, J.M., and Topczewski, J. (2015). A role of glypican4 and wnt5b in chondrocyte stacking underlying craniofacial cartilage morphogenesis. Mechanisms of Development *138*, 279–290.

Smyth, M.J., Ngiow, S.F., Ribas, A., and Teng, M.W.L. (2016). Combination cancer immunotherapies tailored to the tumour microenvironment. Nature reviews *13*, 143–158.

Snyder, J.M., Washington, I.M., Birkland, T., Chang, M.Y., and Frevert, C.W. (2015). Correlation of Versican Expression, Accumulation, and Degradation during Embryonic Development by Quantitative Immunohistochemistry. Journal of Histochemistry and Cytochemistry *63*(12), 952–967.

Söllner, C. (2003). Control of Crystal Size and Lattice Formation by Starmaker in Otolith Biomineralization. Science *302*, 282–286.

Sotoodehnejadnematalahi, F., Staples, K.J., Chrysanthou, E. and Pearson, H. (2015). Mechanisms of Hypoxic Up-Regulation of Versican Gene Expression in Macrophages. PLoS One *10*(6), e0125799.

Srinivas, S., Sironmani, T.A., and Shanmugam, G. (1991). Dimethyl sulfoxide inhibits the expression of early growth-response genes and arrests fibroblasts at quiescence. Experimental Cell Research *196*, 279–286.

Stankunas, K., Hang, C.T., Tsun, Z.Y., Chen, H., Lee, N. V., Wu, J. I., Shang, C., Bayle, J. H., Shou, W., Iruela-Arispe, M.L., et al. (2008). Endocardial Brg1 represses ADAMTS1 to maintain the microenvironment for myocardial morphogenesis. Developmental Cell *14,* 298-311.

Stehlik, C., Kroismayr, R., Dorfleutner, A., Binder, B.R., and Lipp, J. (2004). VIGR – a novel inducible adhesion family G-protein coupled receptor in endothelial cells. Federation of European Biochemical Societies Letters *569*, 149–155.

Stooke-Vaughan, G.A., Obholzer, N.D., Baxendale, S., Megason, S.G., and Whitfield, T.T. (2015). Otolith tethering in the zebrafish otic vesicle requires Otogelin and Alpha - Tectorin. Development (Cambridge, England) *142*, 1137–1145.

Stoveken, H.M., Larsen, S.D., Smrcka, A. V, and Tall, G.G. (2018). Gedunin- and Khivorin-Derivatives Are Small-Molecule Partial Agonists for Adhesion G Protein-Coupled Receptors. Molecular Pharmacology *93*, 477–488.

Subramani, R., Gonzalez, E., and Nandy, S.B. (2017). Gedunin inhibits pancreatic cancer by altering sonic hedgehog signaling pathway. Oncotarget *8*, 10891–10904.

Syrokou, A., Tzanakakis, G.N., Hjerpe, A., Karamanos, N.K. (1999). Proteoglycans in human malignant mesothelioma. Stimulation of their synthesis induced by epidermal, insulin and platelet-derived growth factors involves receptors with tyrosine kinase activity. Biochimie *81*, 733-744.

Tamkun, J.W., Desimone, D.W., Fonda, D., Patel, R.S., Buck, C., Horwitz, A.F., and Hynes, R. (1986). Structure of Integrin, a Glycoprotein Involved in the Transmembrane Linkage between Fibronectin and Actin. Cell *46*, 271–282.

Tang, Y., Zheng, X., Ying, T., Yuan, Y., and Li, S. (2015). Nimodipine-mediated re-myelination after facial nerve crush injury in rats. Journal of Clinical Neuroscience *22*, 1661–1668.

Taylor, J.M., and Simpson2, R.U. (1992). Inhibition of Cancer Cell Growth by Calcium Channel Antagonists in the Athymic Mouse. Cancer Research *52*, 2413–2418.

The UniProt Consortium; UniProt: the universal protein knowledgebase, Nucleic Acids Research, Volume *45*, Issue D1, 4 January 2017, Pages D158–D169.

Theocharis, A.D., Skandalis, S.S., Gialeli, C., and Karamanos, N.K. (2016). Extracellular matrix structure. Advanced Drug Delivery Reviews *97*, 4–27.

Thisse, B., and Thisse, C. (2004). Fast release clones: a high throughput expression analysis. ZFIN Direct Data Submission (http://zfin.org).

Thisse, B., Pflumio, S., Fürthauer, M., Loppin, B., Heyer, V., Degrave, A., Woehl, R., Lux, A., Steffan, T., Charbonnier, X.Q., and Thisse, C. (2001). Expression of the zebrafish genome during embryogenesis (NIH R01 RR15402). ZFIN Direct Data Submission (http://zfin.org).

Thisse, C., and Thisse, B. (2008). High-resolution *in situ* hybridization to whole-mount zebrafish embryos. Nature Protocols *3*, 59–69.

Tian, J., Ling, L., Shboul, M., Lee, H., O'Connor, B., Merriman, B., Nelson, S.F., Cool, S., Ababneh, O.H., Al-Hadidy, A., et al. (2010). Loss of CHSY1, a secreted FRINGE enzyme, causes syndromic brachydactyly in humans via increased NOTCH signaling. American Journal of Human Genetics *87*(6), 768–778.

Tikhonov, D.B., and Zhorov, B.S. (2009). Structural model for dihydropyridine binding to L-type calcium channels. The Journal of Biological Chemistry *284*, 19006–19017.

Van Eeden, F.J.M., Granato, M., Schach, U., Brand, M., Furutani-Seiki, M., Haffter, P., Hammerschmidt, M., Heisenberg, C.P., Jiang, Y.J., Kane, D.A., et al. (1996). Genetic analysis of fin formation in the zebrafish, Danio rerio. Development *123*, 255–262.

Venero-Galanternik, M., Kramer, K.L., and Piotrowski, T. (2015). Heparan Sulfate Proteoglycans Regulate Fgf Signaling and Cell Polarity during Collective Cell Migration. Cell Reports *10*, 414–428.

Venning, F.A., Wullkopf, L., and Erler, J.T. (2015). Targeting ECM Disrupts Cancer Progression. Frontiers in Oncology *5*, 1–15.

Walker, C., Mojares, E., and del Rio Hernandez, A. (2018). Role of Extracellular Matrix in Development and Cancer Progression. International Journal of Molecular Sciences *19*, 3028.

Waller-Evans, H., Promel, S., Langenhan, T., Dixon, J., Zahn, D., Colledge, W.H., Doran, J., Carlton, M.B.L., Davies, B., Aparicio, S.A.J.R., et al. (2010). The Orphan Adhesion-GPCR GPR126 Is Required for Embryonic Development in the Mouse. PLoS ONE *5*, 1–10.

Waller, D., Renwick, A.G., Hillier, K. (2010). Medical Pharmacology and Therapeutics (London, UK: Elsevier Inc.), pp.3–30.

Walsh, E.C., and Stainier, D.Y.R. (2001). UDP – Glucose Dehydrogenase Required for Cardiac Valve Formation in Zebrafish. Science *293*, 1670–1674.

Waterman, R.E., and Bell, D.H. (1984). Epithelial Fusion During Early Semicircular Canal Formation in the Embryonic Zebrafish, Brachydanio rerio. The Anatomical Record *210*, 101–114.

Ween, M.P., Hummitzsch, K., Rodgers, R.J., Oehler, M.K., and Ricciardelli, C. (2011). Versican induces a pro-metastatic ovarian cancer cell behavior which can be inhibited by small hyaluronan oligosaccharides. Clinical and Experimental Metastasis *28*, 113–125.

Wen, J., Tong, Y., Zu, Y., Saverio, S. Di, and Dwyer, D.S. (2015). Low Concentration DMSO Stimulates Cell Growth and *In vitro* Transformation of Human Multiple Myeloma Cells. British Journal of Medicine & Medical Research *5*, 65–74.

White, R.M., Cech, J., Ratanasirintrawoot, S., Lin, C.Y., Rahl, P.B., Burke, C.J., Langdon, E., Tomlinson, M.L., Mosher, J., Kaufman, C., et al. (2011). DHODH modulates transcriptional elongation in the neural crest and melanoma. Nature *471*, 518–522.

Whitfield, T.T. (2015). Development of the inner ear. Current Opinion in Genetics and Development *32*, 112–118.

Whitfield, T.T., Granato, M., van Eeden, F.J., Schach, U., Brand, M., Furutani-Seiki, M., Haffter, P., Hammerschmidt, M., Heisenberg, C.P., Jiang, Y.J., et al. (1996). Mutations

affecting development of the zebrafish inner ear and lateral line. Development (Cambridge, England) *123*, 241–254.

Whitfield, T.T., Riley, B.B., Chiang, M.-Y., and Phillips, B. (2002). Development of the zebrafish inner ear. Developmental Dynamics *223*(4), 427–458.

Wight, T.N. (2002). Versican: a versatile extracellular matrix proteoglycan in cell biology. Current Opinion in Cell Biology *14*, 617–623.

Wight, T.N., Kinsella, M.G., Evanko, S.P., Potter-Perigo, S., and Merrilees, M.J. (2014). Versican and the regulation of cell phenotype in disease. Biochimica et Biophysica Acta *1840*(8), 2441–2451.

Wu, Y.J., La Pierre, D.P., Wu, J., Yee, A.J. and Yang, B.B. (2005). The interaction of versican with its binding partners. Cell Research *15*(7), 483–494.

Xiao, Q., and Ge, G. (2012). Lysyl Oxidase , Extracellular Matrix Remodeling and Cancer Metastasis. Cancer Microenvironment *5*, 261–273.

Xu, L., Xue, T.A.O., Zhang, J., and Qu, J. (2016). Knockdown of versican V1 induces a severe inflammatory response in LPS-induced acute lung injury via the TLR2-NF-κB signaling pathway in C57BL/6J mice. Molecular Medicine Reports *13*, 5005–5012.

Yang, W., and Yee, A.J. (2013). Versican V2 isoform enhances angiogenesis by regulating endothelial cell activities and fibronectin expression. Federation of European Biochemical Societies Letters *587*(2), 185–192.

Yang, W., and Yee, A.J.M. (2014). Versican 3'-untranslated region (3'UTR) promotes dermal wound repair and fibroblast migration by regulating miRNA activity. Biochimica et Biophysica Acta *1843*, 1373-1385.

Yeung, K.T., and Yang, J. (2017). Epithelial – mesenchymal transition in tumor metastasis. Molecular oncology *11*, 28–39.

Yeung, T.L., Leung, C.S., Li, F., Wong, S.S.T., and Mok, S.C. (2016). Targeting stromal-cancer cell crosstalk networks in ovarian cancer treatment. Biomolecules *6*, 1-19.

Yeung, T.L., Leung, C.S., Wong, K.K., Samimi, G., Thompson, M.S., Liu, J., and Mok, S.C. (2013). TGF-β Modulates ovarian cancer invasion by upregulating CAF-Derived versican in the tumor microenvironment. Cancer Research *73*(16), 5016–5028.

Yeung, T.L., Leung, C.S., Wong, K.K., Samimi, G., Thompson, M.S., Liu, J., Zaid, T.M., Ghosh, S., Birrer, M.J., and Mok, S.C. (2013). TGF-β Modulates ovarian cancer invasion by upregulating CAF-Derived versican in the tumor microenvironment. Cancer Research *73*, 5016–5028.

Yilmaz, M., and Christofori, G., Lehembre, F. (2007). Distinct mechanisms of tumor invasion and metastasis. Trends in Molecular Medicine *13*(12), 535–541.

Yoon, H., Liyanarachchi, S., Wright, F.A., Davuluri, R., Lockman, J.C., de la Chapelle, A., et al. (2002). Gene expression profiling of isogenic cells with different TP53 gene dosage reveals numerous genes that are affected by TP53 dosage and identifies CSPG2 as a direct target of p53. The Proceedings of the National Academy of Science *99*(24), 15632–15637.

Yule, D., Kim, E., and A, W.J. (1994). Tyrosine kinase inhibitors attenuate "capacitative" Calcium influx in rat pancreatic acinar cells. Biochemical and Biophysical Research Communications *202*, 1697–1704.

Zhang, Z., Miao, L. and Wang, L. (2012). Inflammation Amplification by Versican: The First Mediator. International Journal of Molecular Sciences *13*, 6873–6882.

Zhang, Z., Zhang, J., Miao, L., Liu, K., Yang, S., Pan, C., and Jiao, B. (2012). Interleukin-11 promotes the progress of gastric carcinoma via abnormally expressed versican. International Journal of Biological Sciences *8*(3), 383–393.

Zheng, P., Wen, J., Ang, L.C., Sheng, W., Viloria-petit, A., Wang, Y., Wu, Y., Kerbel, R.S., Yang, B.B., and Centre, S. (2004). Versican/PG-M G3 domain promotes tumor growth and angiogenesis. Journal of The Federation of American Societies for Experimental Biology *18*(6), 754–756.

Zheng, P.S., Vais, D., Lapierre, D., Liang, Y.Y., Lee, V., Yang, B.L., and Yang, B.B. (2004). PG-M/ versican binds to P-selectin glycoprotein ligand-1 and mediates leukocyte aggregation. Journal of Cell Science *117*, 5887–5895

APPENDIX

Appendix Table 1. Nucleotide sequence of *vcana* and *vcanb* anti-sense RNA probes used for *in situ* hybridisation.

Target gene	5'-3' RNA sequence	Length and targeting mRNA position
vcana	AGAAGAAACUGUCCGGCUGGUUCGGUCUCCAGUUUUCAUAUUGCACAACUCUACCA UCUGUCCACCGGAAAUCAUUCUCAAACAUCUUAUCAUUCAGACCAAUCCACUGGUA GUCAUGGCCAAGACGGUUGAUGUAUUGCUGCUCAUCAUGGGACAGGACACUAGCAA GAUGUGCCCCCUGGAGACGACAUUCACGCUCUGCUGUGUCCCAGUUACGUCGAUGGG GAAAGUAUUUGUAGCAAUGACCCUGGAACUUAUGCCAGCCAUAGCUGCAUGUUUCAG UAUCUUGUUCACAUAGUGCUCCUGCAUAACUUGGAAGACAUAGACAGGUGAAUGAGU UUAGGCCAUCAAUGCAUGUUCCUCCAUUACGACAAGGGUUUGUGUGACAUUCAUCAAU GUCUAUUUCACAUUGUUCACCACUGUAUCCAGGUUGACAUAUGCAGAUUUGAGCACCG CCUGUUUUUAUACAUGUACCACCAUUCAAGCAAACAGCAUCAGAACAGGAGUGGACACC UUGGAA	520 bp long, spanning nt 963-1482 of the mRNA sequence (NCBI Reference Sequence: NM_001326557.1)
vcanb	ACAUCUUCUGGAAGGUGGACGGAUUCAAGCAUGUGAUUUUGGGCUUGUCCCACUGUC CGUCUUCUCUGCAUCUGAUAGUAGGGACAUGUCUCUGGAUGAAGCCUUCUUUACAGU GAUAUCGAACCAGAGAGUUGAUCUCGUAUCGCGGCUUCAUGCUGCCAUAGACUUGAG CGUCCUUUAUGAGAGGAGGCUGACCGCAGGACACUGUGCCCUUCUUACAGGUGAAGG UCAGGUGGUAGUUGCAGGGCACAUCGUUCCACUGUCCGCUCUCAUGCCAGAUCAUGA CCACACAGUCCUCACCGGUGGAGAAGAAGCUGUCCGGCUGACCAUCACGCCAGUUCUC GAAUUGCAUAGGAUGUCCAUCAGUCCAGCGGAAAUCAUUGUCAAACAUUUUAUCAUU CAGGCCGAUCCACUGAUAGUCAUGACCCAAACGAUUUACGAAGAGCUGCUCCUCGUGG GACAGGACGCUGGUCAGGUGUCCGCCCUGCAGACGACACUCUCUUUCUGCUGCCUCCCA CGUCCGCCGGUGGGUGAAGUACUUAUAGCAGUGGCUCUGAAACUUCUGCCAACCAAAGU CGCACACCUCCGUAUCUUGUUCACAGA	603 bp long, spanning nt 4041-4643 of the mRNA sequence (NCBI Reference Sequence: NM_214688.1)

Appendix Table 2. List of the compounds able to rescue *vcanb expression* in both *fr24 and tb233c* mutants, thus presumed to act downstream of the Adgrg6 receptor.

#	Compounds able to rescue *vcanb expression* in both *fr24 and tb233c* mutants, thus presumed to act downstream of the Adgrg6 receptor	*vcanb* score mean ±SD	Number of embryos tested (n)
1	NIMODIPINE	1.83± 0.41	6
2	3BETA-ACETOXYDEOXODIHYDROGEDUNIN	1.33± 0.52	6
3	SINENSETIN	0.17± 0.41	6
4	TANGERITIN	1.17± 1.33	6
5	DIHYDROGEDUNIN	0.67±1.15	3
6	COLFORSIN	0.00± 0.00	3
7	EZETIMIBE	0.00± 0.00	3
8	DEMETHYLNOBILETIN	0.00± 0.00	3
9	ROSUVASTATIN CALCIUM	0.00± 0.00	3
10	HEXAMETHYLQUERCETAGETIN	0.00± 0.00	6
11	NOBILETIN	0.00± 0.00	6

Appendix Table 3. List of compounds that were common between Tocris and Spectrum Libraries with the corresponding versican scores. Dark green colour indicates no difference between the scores obtained, light green indicates a small difference (<1) and orange indicates a difference of 1 or higher.

COMPOUND NAME	Tocris initial *vcan* score (0-3), n=3	Tocris average after retests	Spectrum initial *vcan* score(0-3), n=3	Spectrum average after retests	Initial Difference	Difference after retests
7-NITROINDAZOLE	3.00	3.00	3.00	3.00	0.00	0.00
ACARBOSE	3.00	3.00	3.00	3.00	0.00	0.00
ACYCLOVIR	3.00	3.00	3.00	3.00	0.00	0.00
ALRESTATIN	3.00	3.00	3.00	3.00	0.00	0.00
AMBROXOL HYDROCHLORIDE	3.00	3.00	3.00	3.00	0.00	0.00
AMILORIDE HYDROCHLORIDE	3.00	3.00	3.00	3.00	0.00	0.00
ANIRACETAM	3.00	3.00	3.00	3.00	0.00	0.00
ANISOMYCIN	3.00	3.00	3.00	3.00	0.00	0.00
ARTEMISININ	3.00	3.00	3.00	3.00	0.00	0.00
BENAZEPRIL HYDROCHLORIDE	3.00	3.00	3.00	3.00	0.00	0.00
BUDESONIDE	3.00	3.00	3.00	3.00	0.00	0.00
CANTHARIDIN	3.00	3.00	3.00	3.00	0.00	0.00
CARBETAPENTANE CITRATE	3.00	3.00	3.00	3.00	0.00	0.00
CARBOPLATIN	3.00	3.00	3.00	3.00	0.00	0.00
CARVEDILOL	3.00	3.00	3.00	3.00	0.00	0.00
CILOSTAZOL	3.00	3.00	3.00	3.00	0.00	0.00
CIMETIDINE	3.00	3.00	3.00	3.00	0.00	0.00
CLOFIBRIC ACID	3.00	3.00	3.00	3.00	0.00	0.00
COLCHICINE	3.00	3.00	3.00	3.00	0.00	0.00
CYCLOTHIAZIDE	3.00	3.00	3.00	3.00	0.00	0.00
DEXAMETHASONE	3.00	3.00	3.00	3.00	0.00	0.00
DIHYDROERGOTAMINE MESYLATE	3.00	3.00	3.00	3.00	0.00	0.00
DILTIAZEM HYDROCHLORIDE	3.00	3.00	3.00	3.00	0.00	0.00
DIPYRIDAMOLE	3.00	3.00	3.00	3.00	0.00	0.00
DOBUTAMINE HYDROCHLORIDE	3.00	3.00	3.00	3.00	0.00	0.00
DOXEPIN HYDROCHLORIDE	3.00	3.00	3.00	3.00	0.00	0.00
EFAROXAN HYDROCHLORIDE	3.00	3.00	3.00	3.00	0.00	0.00
ELETRIPTAN HYDROBROMIDE	3.00	3.00	3.00	3.00	0.00	0.00
ETICLOPRIDE HYDROCHLORIDE	3.00	3.00	3.00	3.00	0.00	0.00

ETOMIDATE	3.00	3.00	3.00	3.00	0.00	0.00
FEXOFENADINE HYDROCHLORIDE	3.00	3.00	3.00	3.00	0.00	0.00
GENISTEIN	3.00	3.00	3.00	3.00	0.00	0.00
GUANABENZ ACETATE	3.00	3.00	3.00	3.00	0.00	0.00
HARMANE	3.00	3.00	3.00	3.00	0.00	0.00
HISTAMINE DIHYDROCHLORIDE	3.00	3.00	3.00	3.00	0.00	0.00
IDAZOXAN HYDROCHLORIDE	3.00	3.00	3.00	3.00	0.00	0.00
ISOGUVACINE HYDROCHLORIDE	3.00	3.00	3.00	3.00	0.00	0.00
KAEMPFEROL	3.00	3.00	3.00	3.00	0.00	0.00
KAINIC ACID	3.00	3.00	3.00	3.00	0.00	0.00
KETANSERIN TARTRATE	3.00	3.00	3.00	3.00	0.00	0.00
KETOTIFEN FUMARATE	3.00	3.00	3.00	3.00	0.00	0.00
LANSOPRAZOLE	3.00	3.00	3.00	3.00	0.00	0.00
LOBELINE HYDROCHLORIDE	3.00	3.00	3.00	3.00	0.00	0.00
MAPROTILINE HYDROCHLORIDE	3.00	3.00	3.00	3.00	0.00	0.00
MEMANTINE HYDROCHLORIDE	3.00	3.00	3.00	3.00	0.00	0.00
METHYSERGIDE MALEATE	3.00	3.00	3.00	3.00	0.00	0.00
MEXILETINE HYDROCHLORIDE	3.00	3.00	3.00	3.00	0.00	0.00
MINOXIDIL	3.00	3.00	3.00	3.00	0.00	0.00
NOSCAPINE HYDROCHLORIDE	3.00	3.00	3.00	3.00	0.00	0.00
OCTOPAMINE HYDROCHLORIDE	3.00	3.00	3.00	3.00	0.00	0.00
ORLISTAT	3.00	3.00	3.00	3.00	0.00	0.00
OUABAIN	3.00	3.00	3.00	3.00	0.00	0.00
PIMOZIDE	3.00	3.00	3.00	3.00	0.00	0.00
PINDOLOL	3.00	3.00	3.00	3.00	0.00	0.00
PRAZOSIN HYDROCHLORIDE	3.00	3.00	3.00	3.00	0.00	0.00
RAUWOLSCINE HYDROCHLORIDE	3.00	3.00	3.00	3.00	0.00	0.00
REPAGLINIDE	3.00	3.00	3.00	3.00	0.00	0.00
RESERPINE	3.00	3.00	3.00	3.00	0.00	0.00
RESVERATROL	3.00	3.00	3.00	3.00	0.00	0.00
ROSMARINIC ACID	3.00	3.00	3.00	3.00	0.00	0.00
SCOPOLAMINE HYDROBROMIDE	3.00	3.00	3.00	3.00	0.00	0.00
SERTRALINE HYDROCHLORIDE	3.00	3.00	3.00	3.00	0.00	0.00
SOTALOL	3.00	3.00	3.00	3.00	0.00	0.00

HYDROCHLORIDE						
SPAGLUMIC ACID	3.00	3.00	3.00	3.00	0.00	0.00
TAMOXIFEN CITRATE	3.00	3.00	3.00	3.00	0.00	0.00
TERAZOSIN HYDROCHLORIDE	3.00	3.00	3.00	3.00	0.00	0.00
THALIDOMIDE	3.00	3.00	3.00	3.00	0.00	0.00
TOPIRAMATE	3.00	3.00	3.00	3.00	0.00	0.00
TROPICAMIDE	3.00	3.00	3.00	3.00	0.00	0.00
VINBLASTINE SULFATE	3.00	3.00	3.00	3.00	0.00	0.00
VINCRISTINE SULFATE	3.00	3.00	3.00	3.00	0.00	0.00
ZAPRINAST	3.00	3.00	3.00	3.00	0.00	0.00
PIROXICAM	TOXIC	TOXIC	TOXIC	TOXIC	0.00	0.00
FENRETINIDE	3.00	3.00	3.00	3.00	0.00	0.00
NIMODIPINE	0.00	0.00	0.00	0.11	0.00	0.11
BAICALEIN	0.00	0.17	0.00	0.00	0.00	0.17
GEDUNIN	0.00	0.00	0.00	0.00	0.00	0.00
MEVASTATIN	0.00	0.00	0.00	0.00	0.00	0.00
MIANSERIN HYDROCHLORIDE	2.00	2.34	2.33	2.33	0.33	0.00
IVERMECTIN	2.33	2.33	2.00	0.78	0.33	1.56
ROLIPRAM	2.33	2.33	3.00	3.00	0.67	0.67
1-PHENYLBIGUANIDE HYDROCHLORIDE	2.33	2.33	3.00	3.00	0.67	0.67
BROMOCRIPTINE MESYLATE	2.33	2.33	3.00	3.00	0.67	0.67
CISPLATIN	2.33	2.33	3.00	3.00	0.67	0.67
CLOMIPRAMINE HYDROCHLORIDE	2.33	2.33	3.00	3.00	0.67	0.67
CLONIDINE HYDROCHLORIDE	2.33	2.33	3.00	3.00	0.67	0.67
ETOPOSIDE	2.33	2.33	3.00	3.00	0.67	0.67
GALANTHAMINE HYDROBROMIDE	2.33	2.33	3.00	3.00	0.67	0.67
NALOXONE HYDROCHLORIDE	2.33	2.33	3.00	3.00	0.67	0.67
OXYMETAZOLINE HYDROCHLORIDE	2.33	2.33	3.00	3.00	0.67	0.67
QUINOLINIC ACID	2.33	2.33	3.00	3.00	0.67	0.67
ACETAMINOPHEN	3.00	3.00	2.33	2.33	0.67	0.67
AMLODIPINE BESYLATE	3.00	3.00	2.33	2.33	0.67	0.67
BUSPIRONE HYDROCHLORIDE	3.00	3.00	2.33	2.33	0.67	0.67
CLOZAPINE	3.00	3.00	2.33	2.33	0.67	0.67
DIAZOXIDE	3.00	3.00	2.33	2.33	0.67	0.67
IPRATROPIUM BROMIDE	3.00	3.00	2.33	2.33	0.67	0.67
LOPERAMIDE HYDROCHLORIDE	3.00	3.00	2.33	2.33	0.67	0.67

MELATONIN	3.00	3.00	2.33	2.33	0.67	0.67
METERGOLINE	3.00	3.00	2.33	2.33	0.67	0.67
MYCOPHENOLIC ACID	3.00	3.00	2.33	2.33	0.67	0.67
PARTHENOLIDE	3.00	3.00	2.33	2.33	0.67	0.67
PRIMIDONE	3.00	3.00	2.33	2.33	0.67	0.67
QUERCETIN	3.00	3.00	2.33	2.33	0.67	0.67
SULFISOXAZOLE	3.00	3.00	2.33	2.33	0.67	0.67
TACRINE HYDROCHLORIDE	3.00	3.00	2.33	2.33	0.67	0.67
TRANILAST	3.00	3.00	2.33	2.33	0.67	0.67
URAPIDIL HYDROCHLORIDE	3.00	3.00	2.33	2.33	0.67	0.67
YOHIMBINE HYDROCHLORIDE	3.00	3.00	2.33	2.33	0.67	0.67
CAMPTOTHECIN	TOXIC	TOXIC	NO FISH	NO FISH	TOXICITY	TOXICITY
NIMESULIDE	TOXIC	TOXIC	NO FISH	NO FISH	TOXICITY	TOXICITY
NICERGOLINE	2.00	2.17	3.00	3.00	1.00	0.84
NITRENDIPINE	0.00	1.17	1.00	0.50	1.00	0.67
CYPROHEPTADINE HYDROCHLORIDE	1.00	1.84	0.00	0.00	1.00	1.84
ZARDAVERINE	1.00	1.00	2.00	2.00	1.00	1.00
KETOCONAZOLE	2.33	2.33	1.00	1.84	1.33	0.50
RITANSERIN	2.33	2.33	1.00	2.00	1.33	0.33
RALOXIFENE HYDROCHLORIDE	1.00	1.00	2.33	2.33	1.33	1.33
NIFEDIPINE	1.00	1.17	2.50	2.50	1.50	1.34
OMEPRAZOLE	1.00	2.00	3.00	3.00	2.00	1.00
ASTEMIZOLE	3.00	3.00	1.00	1.55	2.00	1.45
ISOPROTERENOL HYDROCHLORIDE	2.33	2.33	0.00	1.34	2.33	1.00
LOVASTATIN	2.33	2.33	0.00	0.00	2.33	2.33
NILUTAMIDE	3.00	3.00	0.00	1.34	3.00	1.67
APIGENIN	0.00	1.50	3.00	3.00	3.00	1.50
SIMVASTATIN	3.00	3.00	TOXIC	TOXIC	TOXICITY	TOXICITY
SULINDAC	TOXIC	TOXIC	3.00	3.00	TOXICITY	TOXICITY
FLURBIPROFEN	TOXIC	TOXIC	3.00	3.00	TOXICITY	TOXICITY
INDOMETHACIN	2, TOXIC	2, TOXIC	2.33	2.33	TOXICITY	TOXICITY

Appendix Table 4. List of the chemical compounds included in the Tocris Total Library.

Product Name	Cat. No.	CAS No.	Product Name	Cat. No.	CAS No.
(-)-[3R,4S]-Chromanol 293B	1475	[163163-24-4]	(R)-3,4-DCPG	1395	
(-)-Bicuculline methobromide	0109	[73604-30-5]	(R)-AMPA	0253	[83654-13 -1]
(-)-Bicuculline methochloride	0131	[53552-05-9]	(RS)-(±)-Sulpiride	0894	[15676-16-1]
(-)-Cytisine	1390	[485-35-8]	(RS)-(Tetrazol-5-yl)glycine	0312	[138199-51-6]
(-)-MK 801 maleate	0955	[77086-19-2]	(RS)-3,4-DCPG	1394	
(-)-Quinpirole hydrochloride	1061	[85760-74-3]	(RS)-3,5-DHPG	0342	[19641-83-9]
(-)-U-50488 hydrochloride	0496	[67198-19-0]	(RS)-4-Carboxy-3-hydroxyphenylglycine	0310	[134052-66-7]
(+)-AJ 76 hydrochloride	0678	[85379-09-5]	(RS)-AMPA	0169	[74341-63-2]
(+)-Bicuculline	0130	[485-49-4]	(RS)-AMPA hydrobromide	1074	[77521-29-0]
(+)-MK 801 maleate	0924	[77086-22-7]	(RS)-Atenolol	0387	[29122-68-7]
(+)-PD 128907 hydrochloride	1243	[300576-59-4]	(S)-(-)-Carbidopa	0455	[28860-95-9]
(+)-SK&F 10047 hydrochloride	1079	[58640-82-7]	(S)-(-)-HA-966	0282	[111821-58-0]
(+)-U-50488 hydrochloride	0471	[67198-17-8]	(S)-(-)-Pindolol	1060	[26328-11-0]
(+)-UH 232 maleate	0775	[95999-12-5]	(S)-(-)-Propranolol hydrochloride	0834	[4199-10-4]
(±)-1-(1,2-Diphenylethyl)piperidine maleate	0360	[36794-52-2]	(S)-(-)-Sulpiride	0895	[23672-07-3]
(±)-Bisoprolol hemifumarate	0914	[104344-23-2]	(S)-(+)-a-Methylhistamine dihydrobromide	0572	[75614-93-6]
(±)-Palmitoylcarnitine chloride	0609	[6865-14-1]	(R)-(+)-HA-966	0281	[123931-04-4]
(±)-U-50488 hydrochloride	0495	[67198-13-4]	(R)-(+)-Propranolol hydrochloride	0835	[5051-22-9]
(±)-Vesamicol hydrochloride	0653	[22232-64-0]	(R)-3-Carboxy-4-hydroxyphenylglycine	0328	[13861-03-5]
(E)-Capsaicin	0462	[404-86-4]	(R)-(+)-8-Hydroxy-DPAT hydrobromide	1080	[80300-09-0]
(R)-(-)-a-Methylhistamine dihydrobromide	0569	[75614-87-8]	(S)-(+)-Niguldipine hydrochloride	1123	[113165-32-5]
(R)-(-)-Deprenyl hydrochloride	1095	[14611-52-0]	(S)-(+)-Rolipram	1350	[85416-73-5]
(R)-(-)-Niguldipine hydrochloride	1124	[113145-70-3]	(S)-3-Carboxy-4-hydroxyphenylglycine	0329	[55136-48-6]
(R)-(-)-Rolipram	1349	[85416-75-7]	(S)-3,4-DCPG	1302	
(S)-3,5-DHPG	0805	[162870-29-3]	2-Hydroxysaclofen	0245	[117354-64-0]
(S)-4-Carboxy-3-hydroxyphenylglycine	0320	[85148-82-9]	2-Iodomelatonin	0737	[93515-00-5]
(S)-AMPA	0254	[83643-88-3]	2-Methoxyestradiol	1807	[362-07-2]

(S)-Timolol maleate	0649	[26921-17-5]	2-Methyl-5-hydroxytryptamine hydrochloride	0558	[78263-90-8]
(S)-WAY 100135 dihydrochloride	1253	[133025-23-7]	2-Phenylmelatonin	0680	[151889-03-1]
(Z)-Capsaicin	0463	[25775-90-0]	2-Pyridylethylamine	2478	[3343-39-3]
1-Acetyl-4-methylpiperazine hydrochloride	0351	[60787-05-5]	2,3-DCPE	2137	[418788-90-6]
1-BCP	1048	[34023-62-6]	2'-MeCCPA	2281	[205171-12-6]
1-Deoxymannojirimycin hydrochloride	1259	[84444-90-6]	3-(4-Allylpiperazin-1-yl)-2-quinoxalinecarbonitrile maleate	0666	
1-Deoxynojirimycin	1258	[19130-96-2]	3-[2-[4-(2-Methoxyphenyl)piperazin-1-yl] ethyl]pyrimido[5,4-b] indole-2,4-dione	0581	
1-EBIO	1041	[10045-45-1]	3-Aminobenzamide	0788	[3544-24-9]
1-Phenylbiguanide hydrochloride	0969	[55-57-2]	3-Bromo-7-nitroindazole	0735	[74209-34-0]
1,2,3,4,5,6-Hexabromocyclohexane	2291	[1837-91-8]	2-(1-Thienyl)ethyl 3,4-dihydroxybenzylidenecyanoacetate	0645	2-(1-Thienyl)ethyl 3,4-dihydroxybenzylidenecyanoacetate
1,3-Dipropyl-8-phenylxanthine	0486	[85872-53-3]	2-[(4-Phenylpiperazin-1-yl)methyl]-2,3-dihydroimidazo[1,2-c]quinazolin-5(6H)-one	0627	2-[(4-Phenylpiperazin-1-yl)methyl]-2,3-dihydroimidazo[1,2-c]quinazolin-5(6H)-one
10-DEBC	2558	[201788-90-1]	2-[[4-(2-Methoxyphenyl)piperazin-1-yl] methyl]-6-methyl-2,3-dihydroimidazo[1,2c]quinazolin-5(6H)-one	0661	2-[[4-(2-Methoxyphenyl)piperazin-1-yl] methyl]-6-methyl-2,3-dihydroimidazo[1,2c]quinazolin-5(6H)-one
1400W dihydrochloride	1415	[180001-34-7]	2-[1-(4-Piperonyl)piperazinyl]benzothiazole	0736	2-[1-(4-Piperonyl)piperazinyl]benzothiazole
17-PA	2681	[694438-95-4]	2-Chloro-N6-cyclopentyladenosine	1705	[37739-05-2]
2-APB	1224	[524-95-8]	2-Cl-IB-MECA	1104	[163042-96-4]
2-BFI hydrochloride	0348	[89196-95-2]	7-NINA	0800	[2942-42-9]
2-Chloro-11-(4-methylpiperazino)dibenz[b,f]oxepin maleate	0782		7-Nitroindazole	0602	[2942-42-9]
3-MATIDA	2196	[518357-51-2]	8-Bromo-cAMP, sodium salt	1140	[76939-46-3]
3-Methyl-GABA (2:1 salt with naphthalene-1,5-disulfonic acid)	0386	[71424-95-8]	8-Bromo-cGMP, sodium salt	1089	[51116-01-9]
3'-Fluorobenzylspiperone maleate	0701		8-Hydroxy-DPAT hydrobromide	0529	[78950-78-4]

3a-[(4-Chlorophenyl)phenylmethoxy] tropane hydrochloride	0917		8-Hydroxy-PIPAT	0797	[159651-91-9]
3a-Bis-(4-fluorophenyl) methoxytropane hydrochloride	0918		8-M-PDOT	1035	[134865-70-6]
4-Acetyl-1,1-dimethylpiperazinium iodide	0352	[75667-84-4]	9-AC	0963	[723-62-6]
4-Aminopyridine	0940	[504-24-5]	A 205804	2524	[251992-66-2]
4-Chlorophenylguanidine hydrochloride	0442	[14279-91-5]	A 61603 hydrobromide	1052	[107756-30-9]
4-DAMP	0482	[1952-15-4]	A 77636	1701	[145307-34-2]
4-HQN	2192	[491-36-1]	A-3 hydrochloride	0366	
4-IBP	0748		A-7 hydrochloride	0378	
4-Methylhistamine	2342	[36376-47-3]	a-Methyl-5-hydroxytryptamine maleate	0557	[304-52-9]
4-P-PDOT	1034	[134865-74-0]	A23187, free acid	1234	[52665-69-7]
4-Phenyl-1,2,3,4-tetrahydroisoquinoline hydrochloride	0730	[75626-12-9]	ABT 702 2HCl	2372	[214697-26-4]
4-Phenylbutyrate, sodium	2682	[1716-12-7]	ABT 724 trihydrochloride	2214	[70006-24-5]
4-PPBP maleate	0620		AC 55649	2436	[59662-49-6]
4F 4PP oxalate	0523		AC 7954, (±)-	2484	[477313-09-0]
5-Carboxamidotryptamine maleate	0458	[74885-09-9]	Acarbose	2673	[56180-94-0]
5-Iodo-A-85380	1518	[213764-92-2]	ACDPP	2254	[37804-11-8]
5-Methylfurmethiodide	0588	[1197-60-0]	Acetaminophen	1706	[103-90-2]
5-Nonyloxytryptamine oxalate	0901	[157798-12-4]	Acifran	1762	[72420-38-3]
5,7-Dichlorokynurenic acid	0286	[131123-76-7]	Actinomycin D	1229	[50-76-0]
6-Chloromelatonin	0443	[63762-74-3]	Acyclovir	2513	[59277-89-3]
6-Hydroxydopamine	2547	[28094-15-7]	AEG 3482	2651	[63735-71-7]
6-Iodonordihydrocapsaicin	1975		AF-DX 116	1105	[102394-31-0]
7-Chlorokynurenic acid	0237	[18000-24-3]	AF-DX 384	1345	[118290-27-0]
7-Hydroxy-DPAT hydrobromide	0706	[74938-11-7]	Amthamine dihydrobromide	0668	[142437-67-0]
7-Hydroxy-PIPAT maleate	0719	[159559-71-4]	Anabasine hydrochloride	1971	[53912-89-3]

AG 18	0493	[118409-57-7]	Aniracetam	0867	[72432-10-1]
AG 213	0503	[122520-86-9]	Anisomycin	1290	[22862-76-6]
AG 490	0414	[133550-30-8]	Anpirtoline hydrochloride	0703	[98330-05-3]
AG 494	0619	[133550-35-3]	Antazoline hydrochloride	0791	[2508-72-7]
AG 555	0618	[133550-34-2]	API-2	2151	[35943-35-2]
AG 556	0616	[133550-41-1]	Apigenin	1227	[520-36-5]
AG 825	1555	[149092-50-2]	Apomorphine	2073	[314-19-2]
AG 99	0497	[122520-85-8]	Apoptosis Activator 2	2098	[79183-19-0]
AGN 192403 hydrochloride	1072	[175521-95-6]	AQ-RA 741	2292	[123548-16-3]
AH 11110 hydrochloride	0998	[179388-65-9]	ARC 239 dihydrochloride	0928	[67339-62-2]
AH 6809	0671	[33458-93-4]	Arctigenin	1777	[7770-78-7]
Alprostadil	1620	[745-65-3]	Arcyriaflavin A	2457	[118458-54-1]
Alrestatin	0485	[51411-04 -2]	Arecaidine but-2-ynyl ester tosylate	0382	[499-04-7]
Altanserin	1809	[76330-71-7]	Arecaidine propargyl ester tosylate	0383	[147202-94-6]
ALX 5407	1757		ARP 101	2622	
AM 251	1117	[183232-66-8]	Artemisinin	2668	[63968-64-9]
AM 281	1115	[202463-68-1]	ATPA	1107	[140158-50-5]
AM 404	1116	[198022-70-7]	AY 9944	1639	[366-93-8]
AM 580	0760	[102121-60-8]	AZ 10417808	2172	[331645-84-2]
AM 630	1120	[164178-33-0]	b-CCB	0405	[84454-35-3]
AM 92016 hydrochloride	0876	[178894-81-0]	b-Funaltrexamine hydrochloride	0926	[72786-10-8]
Ambenonium dichloride	0388	[52022-31-8]	B-HT 920	2759	[36085-73-1]
Ambroxol	2404	[23828-92-4]	BADGE	1326	[1675-54-3]
AMG 9810	2316	[545395-94-6]	Baicalein	1761	[491-67-8]
Amiloride hydrochloride	0890	[2016-88-8]	Bax channel blocker	2160	[335165-68-9]
Aminoguanidine hydrochloride	0787	[1937-19-5]	Bay 11-7085	1743	[196309-76-9]
Aminopurvalanol A	2072	[220792-57-4]	Bay 11-7821	1744	[19542-67-7]
Amisulpride	2132	[71675-85-9]	Bay 36-7620	2501	[232605-26-4]
Amlodipine	2571	[111470-99-6]	Bay 59-3074	2500	[406205-74-1]
AMN 082	2385	[83027-13-8]	BRL 54443	1129	

AMT hydrochloride	0871	[21463-31-0]	Bromocriptine mesylate	0427	[22260-51-1]
Bay K 8644, R (+)-	1545	[98791-67-4]	BTCP maleate	0702	[112726-66-6]
Bay K 8644, S(-)-	1546	[98625-26-4]	BTS	1870	[1576-37-0]
Bay K 8644,(±)-	1544	[71145-03-4]	BTS 54-505	2322	[84484-78-6]
BD 1008 dihydrobromide	0511	[138356-08-8]	BU 224 hydrochloride	0725	[187173-05-3]
BD 1047 dihydrobromide	0956	[138356-20-4]	BU 226 hydrochloride	1091	
BD 1063 dihydrochloride	0883	[150208-28-9]	BU 239 hydrochloride	0726	[187753-87-3]
Benazepril	2578	[86541-74-4]	Budesonide	2671	[51333-22-3]
Benzoquinonium dibromide	0424	[311-09-1]	Buspirone hydrochloride	0962	[33386-08-2]
Bestatin	1956	[58970-76-6]	Butabindide oxalate	1323	[175553-48-7]
Betaxolol hydrochloride	0906	[63659-19-8]	BVT 948	2176	[39674-97-0]
BHQ	1236	[88-58-4]	BW 373U86	1663	[155836-52-5]
BIBU 1361	2417	[793726-84-8]	BW 723C86 hydrochloride	1059	[160521-72-2]
BIBX 1382	2416	[196612-93-8]	BW-B 70C	1304	[134470-38-5]
Bicuculline methiodide, (-)-	2503	[40709-69-1]	C-1	0543	[84468-24-6]
Bifemelane	0767	[90293-01-9]	Cabergoline	2664	[81409-90-7]
BIIE 0246	1700	[246146-55-4]	Caffeic acid phenethyl ester	2743	[104594-70-9]
Blebbistatin, (±)-	1760	[674289-55-5]	Calcipotriol	2700	[112965-21-6]
BML-190	1383	[2854-32-2]	Calmidazolium chloride	2561	[57265-65-3]
BMS 182874 hydrochloride	1441	[153042-42-3]	Calpeptin	0448	[117591-20-5]
BMS 191011	2665	[202821-81-6]	Camptothecin	1100	[7689-03-4]
BMY 14802 hydrochloride	1440	[105565-55-7]	Cantharidin	1548	[56-25-7]
BMY 45778	1442	[152575-66-1]	Capsazepine	0464	[138977-28-3]
BMY 7378 dihydrochloride	1006	[21102-95-4]	Carbetapentane citrate	0454	[23142-01-0]
BNTX maleate	0899	[129468-28-6]	Carboplatin	2626	[41575-94-4]
BP 554 maleate	0556	[82900-57-0]	Carboxy-PTIO, potassium salt	0772	[148819-94-7]
Brefeldin A	1231	[20350-15-6]	Carmoxirole	2193	[98323-83-2]
BRL 15572 hydrochloride	1207	[193611-72-2]	Carvedilol	2685	[72956-09-3]
BRL 37344, sodium salt	0948	[127299-93-8]	Castanospermine	0759	[79831-76-8]
BRL 44408 maleate	1133	[118343-19-4]	CCCP	0452	[555-60-2]

BRL 50481	2237	[433695-36-4]	CI 898 trihydrochloride	2039	[82952-64-5]
BRL 52537 hydrochloride	0699	130497-33-5	CI 966	1296	[110283-66-4]
CCMQ	1238		CI 976	2227	[114289-47-3]
CCT 018159	2435	[171009-07-7]	Ciglitazone	1307	[74772-77-3]
CD 1530	2554	[107430-66-0]	Cilastatin	2709	[81129-83-1]
CD 437	1549	[125316-60-1]	Cilnidipine	2629	[132203-70-4]
Ceramide	0744	[3102-57-6]	Cilostamide	0915	[68550-75-4]
Cetirizine	2577	[83881-52-1]	Cilostazol	1692	[73963-72-1]
CFM 1571	2586	[268725-86-6]	Cimaterol	0435	[54239-37-1]
CFM-2	1082	[178616-26-7]	Cimetidine	0902	[51481-61-9]
CGH 2466	2344	[252198-68-8]	Cinalukast	2025	[128312-51-6]
CGK 733	2639	[905973-89-9]	Cinanserin hydrochloride	0460	[1166-34-3]
CGP 12177 hydrochloride	1134	[81047-99-6]	Cirazoline hydrochloride	0888	[40600-13-3]
CGP 13501	1514	[56189-68-5]	cis-ACBD	0271	[73550-55-7]
CGP 20712	1024	[105737-62-0]	cis-ACPD	0186	
CGP 37157	1114	[75450-34-9]	Cisapride	1695	[81098-60-4]
CGP 53353	2442	[145915-60-2]	Cisplatin	2251	[15663-27-1]
CGP 54626 hydrochloride	1088	[149184-21-4]	Citalopram hydrobromide	1427	[59729-33-8]
CGP 55845	1248	[149184-22-5]	CL 218872	1709	[66548-69-4]
CGP 57380	2731	[522629-08-9]	CL 82198	2632	[307002-71-7]
CGP 71683 hydrochloride	2199	[192322-50-2]	Clemastine fumarate	1453	[14976-57-9]
CGP 78608	1493	[206648-13-7]	Clobenpropit dihydrobromide	0752	[145231-45-4]
CGP 7930	1513	[57717-80-3]	Clofarabine	2600	[123318-82-1]
CGS 15943	1699	[104615-18-1]	Clofibric acid	0825	[882-09-7]
CGS 20625	2467	[111205-55-1]	Clomipramine hydrochloride	0457	[17321-77-6]
CGS 21680 hydrochloride	1063	[124182-57-6]	Clonidine hydrochloride	0690	[4205-91-8]
CGS 9343B	2255	[109826-27-9]	Clopidogrel, (+/-)-	2490	[90055-48-4]
Ch 55	2020	[110368-33-7]	Cloprostenol sodium salt	2295	[55028-72-3]
Chlorisondamine diiodide	1001	[69-27-2]	Clozapine	0444	[5786-21-0]
Chlormethiazole hydrochloride	0881	[533-45-9]	CMPD1	2186	[41179-33-3]

Chlormezanone	0456	[80-77-3]	CNQX	0190	[115066-14-3]
CHPG	1049		Daunorubicin hydrochloride	1467	[23541-50-6]
Chromanol 293B	1412	[163163-23-3]	DCA	2755	[2156-56-1]
CNQX disodium salt	1045	[115066-14-3]	DCB	1952	[6971-97-7]
Co 101244 HCl	2456	[193359-26-1]	DCEBIO	1422	[60563-36-2]
Co 102862	2642	[181144-66-1]	DCPIB	1540	[82749-70-0]
Colchicine	1364	[64-86-8]	Decitabine	2624	[2353-33-5]
Compound W	2654	[173550-33-9]	Deguelin	1770	[522-17-8]
Cordycepin	2294	[73-03-0]	Demethylasterriquinone B1	1819	[78860-34-1]
Corynanthine hydrochloride	1143	[66634-44-4]	Desmethyl-YM 298198	2447	[299901-57-8]
Costunolide	2483	[553-21-9]	Devazepide	2304	[103420-77-5]
CP 339818 hydrochloride	1399	[185855-91-8]	Dexamethasone	1126	[50-02-2]
CP 55,940	0949	[83002-04-4]	DFB	1625	[15332-10-2]
CP 93129 dihydrochloride	1032	[127792-75-0]	DH 97	1218	
CP 94253 hydrochloride	1317	[131084-35-0]	DHBP dibromide	0839	[6159-05-3]
CPCCOEt	1028	[179067-99-3]	Diazoxide	0964	[364-98-7]
CPT 11	2688	[100286-90-6]	Dibutyryl-cAMP, sodium salt	1141	[16980-89-5]
Cromakalim	1377	[94470-67-4]	Dihydrexidine hydrochloride	0884	[123039-93-0]
CV 1808	1710	[53296-10-9]	Dihydroergocristine mesylate	0474	[24730-10-7]
CY 208-243	1249	[100999-26-6]	Dihydroergotamine mesylate	0475	[6190-39-2]
Cyanopindolol hemifumarate	0993	[106469-57-2]	Dilazep dihydrochloride	0481	[35898-87-4]
Cycloheximide	0970	[66-81-9]	Diltiazem hydrochloride	0685	[33286-22-5]
Cyclopiazonic Acid	1235	[18172-33-3]	Dimaprit dihydrochloride	0506	[23256-33-9]
Cyclosporin A	1101	[59865-13-3]	Diphenyleneiodonium chloride	0504	[244-54-2]
Cyclothiazide	0713	[2259-96-3]	Dipyridamole	0691	[58-32-2]
Cyproheptadine hydrochloride	0996	[969-33-5]	DL-TBOA	1223	
Cytochalasin D	1233	[22144-77-0]	DMAB-anabaseine	2241	[32013-69-7]
D-64131	1643	[74588-78-6]	DMeOB	1953	[40252-74-2]
D609	1437	[83373-60-8]	DMNB	2088	[20357-25-9]
Daidzein	1417	[486-66-8]	DMP 543	2330	[160588-45-4]

Danazol	0687	[17230-88-5]	DNQX	0189	[2379-57-9]
Dantrolene, sodium salt	0507	[14663-23-1]	DNQX disodium salt	2312	[2379-57-9]
DAPT	2634	[208255-80-5]	FCCP	0453	[370-86-5]
DAU 5884	2096	[131780-47-7]	Felbamate	0869	[25451-15-4]
Dobutamine hydrochloride	0515	[49745-95 1]	Fenobam	2386	[57653-26-6]
Domoic acid	0269	[14277-97-5]	Fenoldopam	1659	[67227-56-9]
Domperidone	2536	[57808-66-9]	Fenretinide	1396	[65646-68-6]
Doxepin hydrochloride	0508	[1668-19-5]	Fexaramine	2563	[574013-66-4]
Doxorubicin hydrochloride	2252	[25316-40-9]	Fexofenadine HCl	2429	[153439-40-8]
DPCPX	0439	[102146-07-6]	FG 7142	0554	[78538-74-6]
DPN	1494	[1428-67-7]	FGIN-1-27	0658	[142720-24-9]
DPO-1	2533	[43077-30-1]	FGIN-1-43	0659	[145040-29-5]
DPPE fumarate	0743		FIT	1480	[85951-63-9]
DR 2313	2496	[284028-90-6]	FK 888	2400	[138449-07-7]
DTG	0841	[97-39-2]	Flecainide acetate	1470	[54143-56-5]
DuP 697	1430	[88149-94-4]	Flumazenil	1328	[78755-81-4]
DY131	2266	[95167-41-2]	Flunarizine dihydrochloride	0522	[30484-77-6]
E-4031 dihydrochloride	1808	[113559-13-0]	Fluoxetine hydrochloride	0927	[56296-78-7]
EBPC	0518	[57056-57-2]	Flurbiprofen	1769	[5104-49-4]
Efaroxan hydrochloride	0792	[89197-00-2]	Flurofamide	0478	[70788-28-2]
EIT hydrobromide	0873	[625-53-6]	Fluticasone propionate	2007	[80474-14-2]
Eliprodil	2195	[119431-25-3]	Fluvoxamine maleate	1033	[61718-82-9]
Eltoprazine	1860	[98224-03-4]	Formoterol hemifumarate	1448	[43229-80-7]
Embelin	2156	[550-24-3]	Forskolin	1099	[66575-29-9]
EMD 386088	2382	[54635-62-0]	FPL 55712	2276	[40786-08-1]
EMD 66684	1849	[187683-79-0]	FPL 64176	1403	[120934-96-5]
Eplerenone	2397	[107724-20-9]	FR 122047	1507	[130717-51-0]
ER 27319	2471	[201010-95-9]	FR 139317	1210	[142375-60-8]
Etazolate hydrochloride	0438	[51022-77-6]	Gabexate	1798	[39492-01-8]
Eticlopride	1847	[97612-24-3]	Galanthamine hydrobromide	0686	[1953-04-4]

Etomidate	1471	[33125-97-2]	Galnon	2085	[475115-35-6]
Etoposide	1226	[33419-42-0]	Ganaxolone	2531	[38398-32-2]
Exo1	1850	[461681-88-9]	Gavestinel	2348	[153436-22-7]
Fananserin	2645	[127625-29-0]	GW 0742	2229	317318-84-6
Fasudil hydrochloride	0541	[103745-39-7]	GW 1929	1664	[196808-24-9]
GBR 12783 dihydrochloride	0513	[67469-57-2]	GW 311616	1959	[198062-54-3]
GBR 12909 dihydrochloride	0421	[67469-78-7]	GW 3965	2474	[405911-09-3]
GBR 12935 dihydrochloride	0514	[76778-22-8]	GW 405833	2374	[180002-83-9]
GBR 13069 dihydrochloride	0420	[77862-93-2]	GW 4064	2473	[278779-30-9]
Genistein	1110	[446-72-0]	GW 441756	2238	[504433-23-2]
GF 109203X	0741	[133052-90-1]	GW 5074	1381	[220904-83-6]
Ginkgolide B	1657	[15291-77-7]	GW 583340 dihydrochloride	2239	[388082-81-3]
Glibenclamide	0911	[10238-21-8]	GW 6471	2271	[436159-64-7]
Glimepiride	2396	[93479-97-1]	GW 7647	1677	[265129-71-3]
GNTI dihydrochloride	1282		GW 9508	2649	[885101-89-3]
Gossypol	1964	[303-45-7]	GW 9662	1508	[22978-25-2]
GP 1a	2764		GYKI 52466 hydrochloride	1454	[102771-26-6]
GP 2a	2678	[919077-81-9]	H-7 dihydrochloride	0542	[84477-87-2]
GR 103691	1109	[162408-66-4]	H-9 dihydrochloride	0396	[84468-17-7]
GR 113808	1322	[144625-51-4]	HA 1100	2415	[105628-72-6]
GR 125487	1658	[144625-67-2]	HA14-1	1541	[65673-63-4]
GR 127935 hydrochloride	1477	[148672-13-3]	Haloperidol hydrochloride	0931	[52-86-8]
GR 135531	0896	[190277-13-5]	Harmane hydrochloride	1132	[486-84-0]
GR 144053 trihydrochloride	1263	[201304-22-5]	HEAT hydrochloride	0535	[30007-39-7]
GR 159897	1274	[158848-32-9]	HEMADO	1579	[403842-38-6]
GR 32191	1958	[85505-64-2]	HomoAMPA	1026	
GR 46611	0864	[185259-85-2]	Homoharringtonine	1416	[26833-87-4]
GR 55562 dihydrochloride	1054	[172854-55-6]	Homoquinolinic acid	0197	[490-75-5]
GR 79236	1957	[124555-18-6]	HTMT dimaleate	0646	[195867-54-0]
GR 89696	1483	[126766-32-3]	IB-MECA	1066	[152918-18-8]

GS 39783	2001	[39069-52-8]	IBC 293	2469	[306935-41-1]
GTP 14564	2086	[34823-86-4]	Ibotenic acid	0285	[2552-55-8]
Guanabenz acetate	0885	[23256-50-0]	Ibudilast	1694	[50847-11-5]
Guanfacine hydrochloride	1030	[29110-48-3]	ICI 118,551 hydrochloride	0821	[72795-19-8]
Guggulsterone	2013		Isamoltane hemifumarate	0992	[55050-95-8]
Guvacine hydrochloride	0234	[498-96-4]	Isoguvacine hydrochloride	0235	[64603-90-3]
ICI 162,846	0833	[84545-30-2]	Isoproterenol	1747	[51-30-9]
ICI 182,780	1047	[129453-61-8]	Isradipine	2004	[75695-93-1]
ICI 185,282	0836	[106393-80-0]	ITE	1803	[448906-42-1]
ICI 192,605	0837	[117621-64-4]	Ivachtin	2636	
ICI 199,441 hydrochloride	0778	[115199-84-3]	Ivermectin	1260	[70288-86-7]
ICI 204,448 hydrochloride	0822	[121264-04-8]	J 104129	2507	[244277-89-2]
ICI 215,001 hydrochloride	0929	[141269-99-0]	JLK 6	2677	[62252-26-0]
ICI 63197	1816	[27277-00-5]	JNJ 10191584	2441	[869497-75-6]
ICI 89406	0832	[53671-71-9]	JNJ 16259685	2333	[409345-29-5]
Icilin	1531	[36945-98-9]	JTC 801	2481	[244218-51-7]
Idazoxan hydrochloride	0793	[79944-56-2]	JTE 013	2392	[547756-93-4]
IDRA 21	1219	[22503-72-6]	JTE 907	2479	[282089-49-0]
IEM 1460	1636	[121034-89-7]	JWH 015	1341	[155471-08-2]
Ifenprodil	0545	[23210-56-2]	JX 401	2657	[349087-34-9]
IKK 16	2539		Kainic acid	0222	[487-79-6]
IMD 0354	2611	[978-62-1]	KB-R7943 mesylate	1244	[182004-65-5]
Imetit dihydrobromide	0729	[32385-58-3]	Kenpaullone	1398	[142273-20-9]
Imiloxan hydrochloride	0986	[81167-16-0]	Ketanserin tartrate	0908	[83846-83-7]
Immepip dihydrobromide	0932	[164391-47-3]	Ketoconazole	1103	[65277-42-1]
Immethridine	2315	[87976-03-2]	Ketotifen fumarate	0784	[34580-14-8]
Impentamine 2HBr	1858	[34973-91-6]	KF 38789	2748	[257292-29-8]
INCA-6	2162	[3519-82-2]	Ki 8751	2542	[228559-41-9]
Indatraline	1588	[86939-10-8]	KU14R	1131	[189224-48-4]
Indirubin-3-oxime	1813	[160807-49-8]	Kynurenic acid	0223	[492-27-3]

Indomethacin	1708	[53-86-1]	L-(-)-a-Methyldopa	0584	[555-30-6]
Iodophenpropit dihydrobromide	0779	[143407-29-8]	L-152,804	1382	[6508-43-6]
IPAG	0544		L-161,982	2514	[147776-06-5]
Ipratropium bromide	0692	[22254-24-6]	L-165041	1856	[79558-09-1]
Ipsapirone	1869	[95847-70-4]	L-168049	2311	[191034-25-0]
IRL 2500	1838	[169545-27-1]	Levcromakalim	1378	[94535-50-9]
Irsogladine	2504	[84504-69-8]	LFM-A13	1300	[62004-35-7]
L-368899	2641	[148927-60-0]	Linomide	1461	[84088-42-6]
L-655,708	1327	[130477-52-0]	Linopirdine	1999	[105431-72-9]
L-655240	1698	[103253-15-2]	Lobeline hydrochloride	1077	[134-63-4]
L-670596	1949	[121083-05-4]	LOE 908	2314	[149759-26-2]
L-689,560	0742	[139051-78-8]	Lofepramine	2545	[23047-25-8]
L-690,330	0681	[142523-38-4]	Lonidamine	1646	[50264-69-2]
L-692585	2261	[145455-35-2]	Loperamide hydrochloride	0840	[34552-83-5]
L-693,403 maleate	0426	[137730-52-0]	Loratidine	1944	[79794-75-5]
L-694,247	0781	[137403-12-4]	Loreclezole hydrochloride	1295	[117857-45-1]
L-701,252	0705	[151057-13-5]	Lovastatin	1530	[75330-75-5]
L-701,324	0907	[142326-59-8]	Luzindole	0877	[117946-91-5]
L-732,138	0868	[148451-96-1]	LY 2183240	2452	[874902-19-9]
L-733,060 hydrochloride	1145	[148700-85-0]	LY 225910	1018	[133040-77-4]
L-741,626	1003		LY 255283	2208	[117690-79-6]
L-741,742 hydrochloride	1004	[156337-32-5]	LY 288513	1524	[147523-65-7]
L-745,870 trihydrochloride	1002	[158985-00-3]	LY 294002 hydrochloride	1130	[154447-36-6]
L-755507	2197	[159182-43-1]	LY 303511	2418	[154447-38-8]
L-803,087	1979	[217480-26-7]	LY 320135	2387	[176977-56-3]
L-Cysteinesulfinic acid	0216	[1115-65-7]	LY 341495	1209	[201943-63-7]
L-NAME	0665	[51298-62-5]	LY 344864	2451	[186544-26-3]
L-NIL hydrochloride	1139	[150403-89-7]	LY 364947	2718	[396129-53-6]
L-Quisqualic acid	0188	[52809-07-1]	m-3M3FBS	1941	[200933-14-8]
Lamotrigine	1611	[84057-84-1]	m-Chlorophenylbiguanide hydrochloride	0440	[2113-05-5]

Lamotrigine isethionate	2289	[113170-86-8]	m-CPP hydrochloride	0875	[65369-76-8]
Lansoprazole	2582	[103577-45-3]	Malonoben	0479	[10537-47-0]
Lazabemide	2460	[103878-83-7]	Maprotiline hydrochloride	0935	[10347-81-6]
LE 135	2021	[155877-83-1]	MCI-186	0786	[89-25-8]
LE 300	1674	[274694-98-3]	McN 5652, (+/-)	2148	[96795-89-0]
Leelamine	2139	[1446-61-3]	MDL 11,939	0870	[107703-78-6]
Leflunomide	2228	[75706-12-6]	MDL 72832 hydrochloride	0412	[113777-33-6]
MDL 73005EF hydrochloride	0411	[124756-23-6]	MPMQ	2390	[338738-57-1]
Medetomidine	2023	[106807-72-1]	MR 16728 hydrochloride	0537	[147614-21-9]
Melperone hydrochloride	2495	[1622-79-3]	MRS 1220	1217	[183721-15-5]
Memantine hydrochloride	0773	[19982-08-2]	MRS 1334	1385	[192053-05-7]
Mepyramine maleate	0660	[59-33-6]	MRS 1754	2752	[264622-58-4]
Metaphit	0568	[82824-01-9]	MRS 1845	1866	[544478-19-5]
Metergoline phenylmethyl ester	0590	[17692-51-2]	MRS 3777	2403	
Methiothepin maleate	0582	[20229-30-5]	MTPG	0855	[169-209-66-9]
Methotrexate	1230	[59-05-2]	Muscimol	0289	[2763-96-4]
Methyl 2,5-dihydroxycinnamate	0577	[63177-57-1]	MY-5445	0432	[78351-75-4]
Methylergometrine maleate	0549	[113-42-8]	Mycophenolic acid	1505	[24280-93-1]
Methyllycaconitine citrate	1029	[21019-30-7]	N-[2-(Piperidinylamino)ethyl]-4-iodobenzamide	0763	
Methysergide maleate	1064	[129-49-7]	N-Acetylglycyl-D-glutamic acid	0395	[135701-69-8]
Mevastatin	1526	[73573-88-3]	N-Acetyltryptamine	0357	[1016-47-3]
Mexiletine	2596	[5370-01-4]	N-ArachidonylGABA	1814	[128201-89-8]
MG 132	1748	[133407-82-6]	N-Benzylnaltrindole hydrochloride	0754	
MG 624	1356	[77257-42-2]	N-Desmethylclozapine	1007	[6104-71-8]
Mianserin hydrochloride	0997	[21535-47-7]	N-Methyl-N-[(1S)-1-phenyl-2-(1-pyrrolidinyl)ethyl]phenylacetamidehydrochloride	0783	
Mibefradil	2198	[116644-53-2]	N-Methyllidocaine iodide	1042	[29199-61-9]
Mifepristone	1479	[84371-65-3]	N-Methylquipazine dimaleate	0566	[28614-26-8]
Milrinone	1504	[78415-72-2]	N20C hydrochloride	2213	[76991-05-4]
Minoxidil	0583	[38304-91-5]	N6-Cyclopentyladenosine	1702	[41552-82-3]

Mirtazepine	2018	[85650-52-8]	Na-Methylhistamine dihydrochloride	0573	[673-50-7]
ML 9 hydrochloride	0431	[105637-50-1]	Nafadotride	1347	[149649-22-9]
MM 77 dihydrochloride	0933	[159311-94-1]	Naftopidil hydrochloride	0597	[57149-07 2]
MMPX	0552	[78033-08-6]	Naloxone benzoylhydrazone	1419	[119630-94-3]
MNITMT	2492	[177653-76-8]	Naloxone hydrochloride	0599	[357-08-4]
Moexipril	2691	[82586-52-5]	Naltrexone hydrochloride	0677	[16676-29-2]
Monastrol	1305	254753-54-3	Naltriben mesylate	0892	[111555-58-9]
Moxonidine hydrochloride	2282	[75438-57-2]	Naltrindole hydrochloride	0740	[111469-81-9]
MPEP hydrochloride	1212	[96206-92-7]	MPMQ	2390	[338738-57-1]
NAN-190 hydrobromide	0553	[115388-32-4]	NECA	1691	[35920-39-9]
Naproxen	2655	[26159-34-2]	Necrostatin-1	2324	[4311-88-0]
NAS-181	1413	[205242-62-2]	Nefazodone hydrochloride	2777	[82752-99-6]
NBI 27914	1591	[184241-44-9]	Nemonapride	1746	[75272-39-8]
NBQX	0373	[118876-58-7]	NF 449	1391	[389142-38-5]
NBQX disodium salt	1044	[118876-58-7]	NGB 2904	2635	[189060-98-8]
NCS-382	0780	[131733-92-1]	Nicergoline	0604	[27848-84-6]
Nicorandil	2147	[65141-46-0]	O-1918	2288	[536697-79-7]
Nifedipine	1075	[21829-25-4]	O-2050	1655	
Nilutamide	1759	[63612-50-0]	o-3M3FBS	1942	[313981-55-4]
Nimesulide	2470	[51803-78-2]	OBAA	0606	
Nimodipine	0600	[66085-59-4]	Octopamine hydrochloride	2242	[770-05-8]
Nisoxetine hydrochloride	1025	[57754-86-6]	ODQ	0880	[41443-28-1]
Nitrendipine	0601	[39562-70-4]	OLDA	1641	[105955-11-1]
Nitrocaramiphen hydrochloride	0469		Oleamide	0878	[301-02-0]
NMDA	0114	[6384-92-5]	Oleylethanolamide	1484	[111-58-0]
NNC 05-2090 hydrochloride	2747	[184845-43-0]	Olomoucine	1284	[101622-51-9]
NNC 26-9100	2440	[199522-35-5]	Olvanil	0934	[58493-49-5]
NNC 55-0396	2268	[357400-13-6]	OMDM-2	1797	
NNC 63-0532	1780	[250685-44-0]	Omeprazole	2583	[73590-58-6]
NNC 711	1779	[145645-62-1]	OR-486	0483	[7659-29-2]

Nocodazole	1228	[31430-18-9]	Ouabain	1076	[630-60-4]
nor-Binaltorphimine dihydrochloride	0347	[105618-26-6]	Oxaliplatin	2623	[61825-94-3]
Norketamine	1970	[35211-10-0]	Oxotremorine M	1067	[63939-65-1]
Noscapine	1697	[912-60-7]	Oxotremorine sesquifumarate	0843	[17360-35-9]
NPC 15199	0675	[35661-60-0]	Oxymetazoline hydrochloride	1142	[2315-02-8]
NPPB	0593	[107254-86-4]	Ozagrel	1510	[74003-18-2]
NS 398	0942	[123653-11-2]	P1075	1355	[60559-98-0]
NSC 23766	2161	[733767-34-5]	PAC 1	2581	[315183-21-2]
NSC 3852	2521	[3565-26-2]	PACOCF3	1460	[141022-99-3]
NSC 625987	2152	[141992-47-4]	PALDA	2203	[136181-87-8]
NSC 632839	2647	[157654-67-6]	Palmitoylethanolamide	0879	[544-31-0]
NSC 663284	1867	[383907-43-5]	Paroxetine maleate	2141	[64006-44-6]
NSC 693868	1937	[40254-90-8]	Parthenolide	0610	[20554-84-1]
NSC 95397	1547	[93718-83-3]	Paxilline	2006	[57186-25-1]
NTNCB hydrochloride	2155	[486453-65-0]	PCA 4248	0571	[123875-01-4]
nTZDpa	2150	[118414-59-8]	PD 102807	1671	[23062-91-1]
NU 1025	1401	[90417-38-2]	PD 123319	1361	[130663-39-7]
PD 158780	2615	[171179-06-9]	PK 11195	0670	[85532-75-8]
PD 160170	2200	181468-88-2	PMPA (NAALADase inhibitor)	1380	[173039-10-6]
PD 166793	2520	[199850-67-4]	PNU 120596	2498	[501925-31-1]
PD 168077 maleate	1065		PNU 22394 hydrochloride	2201	[15923-78-1]
PD 198306	2605	[212631-61-3]	PNU 282987	2303	[123464-89-1]
PD 407824	2694	[622864-54-4]	PNU 37883 hydrochloride	2095	[57568-80-6]
PD 81723	1363	[132861-87-1]	PP 1	1397	[172889-26-8]
PD 98059	1213	[167869-21-8]	PP 2	1407	[172889-27-9]
Pentylenetetrazole	2687	[54-95-5]	PPNDS	1309	
PETCM	1758	[10129-56-3]	PPT	1426	[263717-53-9]
PG-9 maleate	0750		Practolol	0831	[6673-35-4]
PHA 665752	2693	[477575-56-7]	Pravastatin	2318	[81131-70-6]
PHCCC	1027		Prazosin hydrochloride	0623	[19237-84-4]

PHTPP	2662	[805239-56-9]	PRE-084 hydrochloride	0589	[138847-85-5]
Physostigmine hemisulfate	0622	[64-47-1]	PRIMA-1	1862	[5608-24-2]
Piceatannol	1554	[10083-24-6]	Primidone	0830	[125-33-7]
Pifithrin-a hydrobromide	1267	[63208-82-2]	Procaterol hydrochloride	1102	[62929-91-3]
Pifithrin-mu	2653	[64984-31-2]	Pronethalol hydrochloride	0829	[51-02-5]
Pilocarpine hydrochloride	0694	[54-71-7]	Propranolol hydrochloride	0624	[3506-09-0]
Pimozide	0937	[2062-78-4]	Prostaglandin E2	2296	[363-24-6]
Pinacidil	1503	[60560-33-0]	Proxyfan	2477	[177708-09-7]
Pindolol	0994	[13523-86-9]	PSB 06126	2574	
Pirfenidone	1093	[53179-13-8]	PSB 069	2573	
Piribedil hydrochloride	1031	[78213-63-5]	PSB 11	2012	[444717-56-0]
Pirlindole mesylate	0724	[60762-57-4]	PSB 1115	2009	[409344-71-4]
Piroxicam	0960	[36322-90-4]	PSB 36	2019	[524944-72-7]
PIT	1682	[56583-49-4]	Purvalanol A	1580	[212844-53-6]
Purvalanol B	1581	[212844-54-7]	Ro 20-1724	0415	[29925-17-5]
Pyrrolidinedithiocarbamate ammonium	0727	[5108-96-3]	Ro 25-6981	1594	[169274-78-6]
Quercetin	1125	[117-39-5]	Ro 26-4550	1794	[193744-04-6]
Quipazine dimaleate	0629	[5786-68-5]	Ro 31-8220	2002	[125314-64-9]
QX 222	1043	[21236-55-5]	Ro 60-0175	1854	[169675-09-6]
QX 314	1014	[21306-56-9]	Ro 90-7501	2408	[293762-45-5]
QX 314 chloride	2313	[5369-03-9]	Rolipram	0905	[61413-54-5]
R 59-022	2194	[93076-89-2]	Rosmarinic acid	0630	[20283-92-5]
R-96544	1742	[167144-79-8]	Rottlerin	1610	[82-08-6]
Raclopride	1810	[84225-95-6]	RS 100329 hydrochloride	1325	[232953-52-5]
Raloxifene hydrochloride	2280	[84449-90-1]	RS 102221 hydrochloride	1050	[185376-97-0]
Ranitidine	1967	[66357-35-5]	RS 102895	2089	[300815-41-2]
Rauwolscine hydrochloride	0891	[6211-32-1]	RS 16566 dihydrochloride	1015	[175729-69-8]
Reboxetine	1982	[71620-89-8]	RS 17053 hydrochloride	0985	[169505-93-5]
Remacemide	1622	[111686-79-4]	RS 23597-190 hydrochloride	0728	[149719-06-2]
Remoxipride hydrochloride	0916	[73220-03-8]	RS 39604 hydrochloride	0991	[167710-87-4]

Reserpine	2742	[50-55-5]	RS 45041-190 hydrochloride	0889	[170034-96-5]
Resveratrol	1418	[501-36-0]	RS 504393	2517	[300816-15-3]
Retinoic acid	0695	[302-79-4]	RS 56812 hydrochloride	0988	[143137-35-3]
RHC 80267	1842	[83654-05-1]	RS 67333 hydrochloride	0989	[168986-60-5]
Rilmenidine hemifuramate	0790	[54187-04-1]	RS 67506 hydrochloride	0990	[168986-61-6]
Riluzole hydrochloride	0768	[1744-22-5]	RS 79948 hydrochloride	0987	[158854-42-3]
Rimcazole	1497	[75859-03-9]	RU 24969 hemisuccinate	0912	[107008-28-6]
RITA	2443	[213261-59-7]	RU 28318	1672	[76676-34-1]
Ritanserin	1955	[87051-43-2]	RWJ 21757	2719	[121288-39-9]
Ro 04-5595	2005	[194089-07-1]	RX 821002 hydrochloride	1324	[102575-24-6]
Ro 08-2750	2272	[37854-59-4]	Ryuvidine	2609	[265312-55-8]
Ro 10-5824	2329	[189744-46-5]	S 14506	1771	[135721-98-1]
Ro 106-9920	1778	[62645-28-7]	S-(-)-Atenolol	0393	[93379-54-5]
Ro 15-4513	1997	[91917-65-6]	S-Isopropylisothiourea hydrobromide	0897	[57200-31-4]
Ro 19-4603	1995	[99632-94-7]	S-Sulfo-L-cysteine sodium salt	0162	[1637-71 -4]
S-Trityl-L-cysteine	2191	[2799-07-7]	SC 19220	1206	[19395-87-0]
Saclofen	0246	[125464-42-8]	SC 560	1550	[188817-13-2]
Salbutamol hemisulfate	0634	[51022-70-9]	SC-10	0430	[102649-79-6]
Salmeterol	1660	[89365-50-4]	SC-9	0433	[102649-78-5]
Salsolinol-1-carboxylic acid	0636		SCH 202676 hydrobromide	1400	[70375-43-8]
Salubrinal	2347	[405060-95-9]	SCH 23390 hydrochloride	0925	[125941-87-9]
SANT-1	1974	[304909-07-7]	SCH 28080	1690	[76081-98-6]
SB 200646 hydrochloride	1371	[143797-63-1]	SCH 39166	2299	
SB 202190	1264	[152121-30-7]	SCH 442416	2463	[316173-57-6]
SB 203186 hydrochloride	0785	[135938-17-9]	SCH 58261	2270	[160098-96-4]
SB 203580	1202	[152121-47-6]	SCH 79797	1592	[245520-69-8]
SB 203580 hydrochloride	1402	[152121-47-6]	Scopolamine hydrobromide	1414	[114-49-8]
SB 205384	1512	[160296-13-9]	Scriptaid	2421	[287383-59-9]
SB 205607 dihydrobromide	0921	[148545-09-9]	SCS	2143	[3232-36-8]
SB 206553	1661	[158942-04-2]	SDM25N hydrochloride	1410	[342884-62-2]

SB 216641 hydrochloride	1242	[170230-39-4]	SDZ 205-557	2037	[137196-67-9]
SB 216763	1616	[280744-09-4]	SDZ 21009	1516	[39731-05-0]
SB 218078	2560	[135897-06-2]	SDZ 220-040	1251	[174575-40-7]
SB 218795	1376	[174635-53-1]	SDZ 220-581	1250	[174575-17-8]
SB 221284	1379	[196965-14-7]	SDZ NKT 343	2394	[180046-99-5]
SB 222200	1393	[174635-69-9]	SDZ SER 082 fumarate	1255	[141474-54-6]
SB 225002	2725	[182498-32-4]	SDZ WAG 994	2465	[130714-47-5]
SB 228357	1375	[181629-93-6]	Sertraline	2395	[79559-97-0]
SB 239063	1962	[193551-21-2]	SEW 2871	2284	[256414-75-2]
SB 258585	1961	[209480-63-7]	SG 209	0385	[83440-03-3]
SB 269970	1612	[201038-74-6]	SIB 1757	1215	[31993-01-8]
SB 334867	1960	[249889-64-3]	SIB 1893	1214	[6266-99-5]
SB 366791	1615	[472981-92-3]	Siguazodan	1148	[115344-47-3]
SB 408124	1963	[288150-92-5]	Simvastatin	1965	[79902-63-9]
SB 415286	1617	[264218-23-7]	SKF 38393 hydrobromide	0922	[81633-77-4]
SB 431542	1614	[301836-41-9]	SKF 77434	1662	[104422-04-0]
SKF 81297	1447	[71636-61-8]	SR 57227 hydrochloride	1205	[77145-61-0]
SKF 83566	1586	[99295-33-7]	SR 59230A hydrochloride	1511	[174689-39-5]
SKF 83959	2074	[80751-85-5]	SR 95531 hydrobromide	1262	[104104-50-9]
SKF 86002	2008	[72873-74-6]	SSR 69071	2506	[344930-95-6]
SKF 89976A hydrochloride	1081	[85375-15-1]	ST 91	2638	[4749-61-5]
SKF 91488 dihydrochloride	0512	[68643-23-2]	Statil	0847	[72702-95-5]
SKF 96365 hydrochloride	1147	[130495-35-1]	STO-609	1551	[52029-86-4]
SKI II	2097	312636-16-1	Streptozocin	1621	[18883-66-4]
SL 327	1969	[305350-87-2]	SU 4312	1459	[5812-07-7]
SM-21 maleate	0751	[155058-71-2]	Sulfisoxazole	0731	[127-69-5]
SN 38	2684	[86639-52-3]	Sulindac	1707	[38194-50-2]
SN-6	2184	[415697-08-4]	SUN-B 8155	2550	[345893-91-6]
SNAP 5089	2398		Suramin hexasodium salt	1472	[129-46-4]
SNAP 5114, (S)-	1561	[157604-55-2]	SYM 2206	0961	[173952-44-8]

SNC 162	1529	[178803-51-5]	T 0156	1676	[324572-92-1]
SNC 80	0764	[156727-74-1]	T 0901317	2373	[293754-55-9]
Sotalol hydrochloride	0952	[959-24-0]	T 98475	2519	[192887-28-8]
SP 600125	1496	[129-56-6]	T0070907	2301	[313516-66-4]
Spaglumic acid	0391	[4910-46-7]	Tabimorelin	2308	[193079-69-5]
Spermidine trihydrochloride	0959	[334-50-9]	Tacrine hydrochloride	0965	[1684-40-8]
Spiperone	0995	[749-02-0]	Talniflumate	2510	[66898-62-2]
Spiroxatrine	0631	[1054-88-2]	Tamoxifen citrate	0999	[54965-24-1]
Splitomicin	1542	[5690-03-9]	Taxol	1097	[33069-62-4]
SQ 22536	1435	[17318-31-9]	TBB	2275	[17374-26-4]
SR 11302	2476	[160162-42-5]	TC 1	2669	
SR 142948	2309	[184162-64-9]	TC 2559 difumarate	2737	212332-35-9]
SR 202	2022	[76541-72-5]	TCB-2	2592	
SR 2640	1804	[105350-26-3]	TCS 359	2591	[301305-73-7]
SR 27897	2190	[136381-85-6]	Telenzepine dihydrochloride	1122	[147416-96-4]
SR 33805	1806	[121346-32-5]	Temozolomide	2706	[85622-93-1]
SR 49059	2310	[150375-75-0]	Tenidap	2580	[120210-48-2]
Terazosin hydrochloride	1506	[63074-08-8]	UB 165 fumarate	1348	[200432-86-6]
Terreic acid	1405	[121-40-4]	UBP 296	2078	
Tetrabenazine	2175	[58-46-8]	UBP 302	2079	
Tetrindole mesylate	0723	[135991-95-6]	UCL 1684	1310	[199934-16-2]
Thalidomide	0652	[50-35-1]	UCL 2077	2661	
THC, (R,R)-	1990	[138090-06-9]	UK 14,304	0425	[59803-98-4]
Thioperamide maleate	0644	[106243-16-7]	UK 14,304 tartrate	2466	[59803-99-5]
THIP hydrochloride	0807	[64603-91-4]	Urapidil	1772	[64887-14-5]
Tianeptine	1972	[30123-17-2]	Verapamil hydrochloride	0654	[152-11-4]
Tiotidine	0826	[69014-14-8]	Vinblastine sulfate	1256	[143-67-9]
TMPH hydrochloride	2438	[849461-90-1]	Vincristine sulfate	1257	[2068-78-2]
TMS	1509	[24144-92-1]	Vinpocetine	0757	[42971-09-5]
Tomoxetine hydrochloride	2011	[82248-59-7]	VUF 5681 dihydrobromide	2493	

TPCA-1	2559	[507475-17-4]	VUF 8430 dihydrobromide	2494	[98021-17-1]
Tracazolate	1558	[41094-88-6]	W-13 hydrochloride	0361	[88519-57-7]
Tranilast	1098	[53902-12-8]	W-5 hydrochloride	0368	[61714-25-8]
trans-4-Hydroxycrotonic acid	0538	[24587-49-3]	W-7 hydrochloride	0369	[61714-27-0]
trans-Triprolidine hydrochloride	0662	[6138-79-0]	W-9 hydrochloride	0370	[69762-85-2]
Trap 101	2508	[873567-76-1]	WAY 161503	1801	[75704-24-4]
Trequinsin	2337	[78416-81-6]	WAY 170523	2633	[307002-73-9]
TRIM	0919	[25371-96-4]	WAY 213613	2652	[868359-05-1]
Tropanyl-3,5-dimethylbenzoate	0641		WAY 629	2173	[57756-45-3]
Tropicamide	0909	[1508-75-4]	WB 4101 hydrochloride	0946	[613-67-2]
Tropisetron	2459	[105826-92-4]	WEB 2086	2339	[105219-56-5]
TTNPB	0761	[71441-28-6]	WIN 55,212-2 mesylate	1038	[131543-23-2]
Tyrphostin B44, (+) enantiomer	0579	[133550-37-5]	WIN 55212-3	2327	[131543-25-4]
U 18666A	1638	[3039-71-2]	WIN 64338 hydrochloride	1057	[151039-63-3]
U 99194 maleate	1357	[83598-46-3]	Wortmannin	1232	[19545-26-7]
U-54494A hydrochloride	0498	[112465-94-8]	WY 14643	1312	[50892-23-4]
U0124	1868	[108923-79-1]	Xaliproden	2491	[90494-79-4]
U0126	1144	[109511-58-2]	UB 165 fumarate	1348	[200432-86-6]
Xamoterol hemifumarate	0950	[73210-73-8]	ZD 7114 hydrochloride	0930	[129689-30-1]
XE 991	2000	[122955-42-4]	ZD 7155 hydrochloride	1211	[146709-78-6]
Y 134	2676	[849662-80-2]	ZD 7288	1000	[133059-99-1]
Y-25130 hydrochloride	0380	[123040-16-4]	Zebularine	2293	[3690-10-6]
Y-26763	2076	[127408-31-5]	Zimelidine	1767	[56775-88-3]
Y-27152	2077	[127408-30-4]	ZK 164015	2183	[177583-70-9]
Y-27632 dihydrochloride	1254	[146986-50-7]	ZK 200775	2345	[161605-73-8]
Y-29794	1634	[129184-48-1]	ZK 756326	2565	[874911-96-3]
YM 022	1408	[145084-28-2]	ZK 93423	1994	[83910-44-5]
YM 298198	2448	[748758-45-4]	ZK 93426	1996	[89592-45-0]
YM 90709	1675	[163769-88-8]	ZM 226600	0882	[147695-92-9]
YM 976	1821	[191219-80-4]	ZM 241385	1036	[139180-30-6]

Yohimbine hydrochloride	1127	[146-48-5]	ZM 306416	2499	[690206-97-4]
YS-035 hydrochloride	0416	[33978-72-2]	ZM 323881	2475	[324077-30-7]
Zacopride	1795	[90182-92-6]	ZM 336372	1321	[208260-29-1]
Zamifenacin	2579	[127308-98-9]	ZM 39923 hydrochloride	1367	[58753-54-1]
ZAPA sulfate	0180	[92138-10-8]	ZM 447439	2458	[331771-20-1]
Zaprinast	0947	[37762-06-4]	Zolantidine dimaleate	1070	[104076-38-2]
Zardaverine	1046	[101975-10-4]	Zonisamide	2625	[68291-97-4]
Zatebradine hydrochloride	2202	[91940-87-3]	Zopiclone	1094	[43200-80-2]
ZD 2079	2154	[178600-17-4]			

Appendix Table 4. List of the chemical compounds included in the Spectrum Collection Library.

Product Name	ID	CAS No.	Product Name	ID	CAS No.
1-HYDROXY-3,6,7-TRIMETHOXY-2,8-DIPRENYLXANTHONE	01505909	15404-76-9	2,3-DIMERCAPTOSUCCINIC ACID	01505007	304-55-2
1-MONOPALMITIN	00300020	542-44-9	2,3,4-TRIHYDROXY-4'-ETHOXYBENZOPHENONE	00200424	
1-PHENYLBIGUANIDE HYDROCHLORIDE	01503641	55-57-2	2,3,4'-TRIHYDROXY-4-METHOXYBENZOPHENONE	00200412	
1,3,5-TRIMETHOXYBENZENE	00231043	621-23-8	2,4-DINITROPHENOL	00330008	51-28-5
1,7-DIDEACETOXY-1,7-DIOXO-3-DEACETYLKHIVORIN	00100358		2,5-DI-t-BUTYL-4-HYDROXYANISOLE	01505039	1991-52-2
10-HYDROXYCAMPTOTHECIN	01504123	19685-09-7	2,6-DIHYDROXY-4-METHOXYTOLUENE	01600025	
11a-ACETOXYPROGESTERONE	01505121	2268-98-6	2,6-DIMETHOXYQUINONE	00200413	35069-70-6
11alpha-HYDROXYPROGESTERONE HEMISUCCINATE	01505846	41238-98-6	2'-METHOXYFORMONETIN	00201310	
1R,2S-PHENYLPROPYLAMINE	02300253	14838-15-4	2',2'-BISEPIGALLOCATECHIN DIGALLATE	00201507	
2-AMINOBENZENESULFONAMIDE	01505862		2',3-DIHYDROXY-4,4',6'-TRIMETHOXYCHALCONE	01505153	38186-71-9
2-BENZOYL-5-METHOXYBENZOQUINONE	00200690		2',4-DIHYDROXY-3,4',6'-TRIMETHOXYCHALCONE	01505140	112572-59-5
2-ETHOXYCARBONYL-2-ETHOXYOXALOYLOXYDIHYDROCHRYSIN DIMETHYL ETHER	00200141		2',4-DIHYDROXYCHALCONE	01505141	13323-66-5
2-MERCAPTOBENZOTHIAZOLE	01504225	149-30-4	2',4'-DIHYDROXY-4-METHOXYCHALCONE	01505152	81674-91-1
2-METHOXY-5 (6)EPOXY-TETRAHYDROCARYOPHYLLENE	00300111		2',4'-DIHYDROXYCHALCONE	01505132	1776-30-3
2-METHOXYRESORCINOL	00211066	29267-67-2	2',4'-DIHYDROXYCHALCONE 4'-GLUCOSIDE	00200258	
2-METHOXYXANTHONE	00240736	1214-20-6	2',5'-DIHYDROXY-4-METHOXYCHALCONE	01505142	6342-92-3
2-METHYL GRAMINE	00100599		21-ACETOXYPREGNENOLONE	01505123	566-78-9
2-METHYL-4-(PIPERIDIN-1-YLCARBOXY)-5-ISOPROPYLPHENYLTRIMETHYLAMMONIUM CHLORIDE	01505165		3-ACETAMIDOCOUMARIN	01505863	
2-METHYL-5,7,8-TRIMETHOXYISOFLAVONE	00200215		3-ACETYLCOUMARIN	01505864	
2-METHYLENE-5-(2,5-DIOXOTETRAHYDROFURAN-3-YL)-6-OXO--10,10-DIMETHYLBICYCLO[7: 2: 0]UNDECANE	00300104		3-AMINO-1,2,4-TRIAZOLE	01505154	61-82-5
2-THIOURACIL	01503973	141-90-2	3-AMINO-beta-PINENE	00300106	
2,2'-AZO-bis-2-AMINOPROPANE	01505157	2997-92-4	3-AMINOPROPANESULPHONIC ACID	01501125	3687-18-1
2,3-DICHLORO-5,8-DIHYDROXYNAPTHOQUINONE	01505158	14918-65-5	3-HYDROXY-3',4'-DIMETHOXYFLAVONE	01505278	6889-80-1
2,3-DIHYDROXY-4-METHOXY-4'-ETHOXYBENZOPHENONE	00200425		3-HYDROXY-4-(SUCCIN-2-YL)-CARYOLANE delta-LACTONE	00307033	

2,3-DIHYDROXY-6,7-DICHLOROQUINOXALINE	01504232		3-HYDROXYFLAVONE	01501012	577-85-5
3-HYDROXYTYRAMINE	01505155	62-31-7	4-HYDROXYANTIPYRINE	01505870	1672-63-5
3-ISOBUTYL-1-METHYLXANTHINE (IBMX)	01505298	28822-58-4	4-METHOXYDALBERGIONE	00201092	4646-86-0
3-METHOXYCATECHOL	01600919	934-00-9	4-METHYLDAPHNETIN	01500730	
3-METHYLORSELLINIC ACID	00200640	4707-46-4	4-METHYLESCULETIN	01500729	
3-METHYLXANTHINE	01504182	1076-22-8	4-NAPHTHALIMIDOBUTYRIC ACID	01502074	
3-NOR-3-OXOPANASINSAN-6-OL	00300110		4-O-METHYLPHLORACETOPHENONE	01505349	7507-89-3
3-OXOURSAN (28-13)OLIDE	00307047		4,4'-DIISOTHIOCYANOSTILBENE-2,2'-SUFONIC ACID SODIUM SALT	01505164	67483-13-0
3-PINANONE OXIME	00300160		4,4'-DIMETHOXYDALBERGIONE	00201448	
3,16-DIDEOXYMEXICANOLIDE-3beta-DIOL	00100359		4'-DEMETHYLEPIPODOPHYLLOTOXIN	01505328	
3,3'-DIINDOLYLMETHANE	01505331	1968-05-4	4'-HYDROXYCHALCONE	00200407	2657-25-2
3,4-DIDESMETHYL-5-DESHYDROXY-3'-ETHOXYSCLEROIN	00240429		4'-METHOXYCHALCONE	00211475	22966-19-4
3,4-DIHYDROXYCARANE	01505274		4'-METHOXYFLAVONE	00240958	4143-74-2
3,4-DIMETHOXYCINNAMIC ACID	01505130	14737-89-4	5-AMINOPENTANOIC ACID HYDROCHLORIDE	01501126	
3,4-DIMETHOXYDALBERGIONE	00240828	41043-20-3	5-FLUOROINDOLE-2-CARBOXYLIC ACID	01502092	399-76-8
3,4'-DIMETHOXYFLAVONE	01500734		5-HYDROXY-2',4',7,8-TETRAMETHOXYFLAVONE	01505382	123316-61-0
3,4',5,6,7-PENTAMETHOXYFLAVONE	01505380	4472-73-5	5-METHYLFURMETHIDE	01503928	1197-60-0
3,6-DIMETHOXYFLAVONE	01500736		5,7-DIHYDROXY-4-METHYLCOUMARIN	01500728	
3,7-DIHYDROXYFLAVONE	01504130	492-00-2	5,7-DIHYDROXYISOFLAVONE	00240565	4044-00-2
3,7-DIMETHOXYFLAVONE	01500737	20950-52-1	5,7,4'-TRIMETHOXYFLAVONE	00300384	5631-70-9
3,7-EPOXYCARYOPHYLLAN-6-OL	00300118		5alpha-ANDROSTAN-3,17-DIONE	00107108	
3,7-EPOXYCARYOPHYLLAN-6-ONE	00300132		5alpha-CHOLESTAN-3beta-OL-6-ONE	00270083	
3alpha-ACETOXYDIHYDRODEOXYGEDUNIN	00100205		5alpha-CHOLESTANOL	00270078	80-97-7
3alpha-HYDROXY-3-DEOXYANGOLENSIC ACID METHYL ESTER	00100114		5beta-12-METHOXY-4,4-BISNOR-8,11,13-PODOCARPATRIEN-3-ONE	00100254	
3alpha-HYDROXY-4,4-BISNOR-8,11,13-PODOCARPATRIENE	00100618		6-AMINONICOTINAMIDE	01505315	329-89-5
3beta-ACETOXYDEOXODIHYDROGEDUNIN	00100497		6-HYDROXYANGOLENSIC ACID METHYL ESTER	00100058	
3beta-HYDROXY-23,24-BISNORCHOL-5-ENIC ACID	00270043		6-HYDROXYTROPINONE	01505865	
3beta-HYDROXYISOALLOSPIROST-9(11)-ENE	00100305		6-METHOXYHARMALAN	01506011	3589-73-9

3H-1,2-DITHIOLE-3-THIONE	01505015		6,2'-DIMETHOXYFLAVONE	01505180	
4-(3-BUTOXY-4-METHOXYBENZYL)IMIDAZOLIDIN-2-ONE	01505104	29925-17-5	6,3'-DIMETHOXYFLAVONE	01504132	79786-40-6
4-ACETOXYPHENOL	00240740	3233-32-7	ACECLIDINE	01501124	827-61-2
4-HYDROXYANTIPYRINE	01505870	1672-63-5	ACEDAPSONE	01505376	77-46-3
4-METHOXYDALBERGIONE	00201092	4646-86-0	ACEMETACIN	01500666	53164-05-9
4-HYDROXY-6-METHYLPYRAN-2-ONE	01600759	675-10-5	ACEPROMAZINE MALEATE	01505498	3598-37-6
6,4'-DIHYDROXYFLAVONE	01500717	63046-09-3	ACETAMINOPHEN	01500101	103-90-2
6,4'-DIMETHOXYFLAVONE	01500741	54401-47-7	ACETAMINOSALOL	01501170	118-57-0
6,7-DICHLORO-3-HYDROXY-2-QUINOXALINECARBOXYLIC ACID	01502070		ACETANILIDE	01501173	103-84-4
6alpha-METHYLPREDNISOLONE ACETATE	01503254		ACETARSOL	01500616	97-44-9
7-AMINOCEPHALOSPORANIC ACID	01505746	957-68-6	ACETAZOLAMIDE	01500102	59-66-5
7-DEACETOXY-7-OXOKHIVORIN	00100048	15004-51-0	ACETOHEXAMIDE	01505425	968-81-0
7-DEACETYLKHIVORIN	00100014		ACETOHYDROXAMIC ACID	01500103	546-88-3
7-DESACETOXY-6,7-DEHYDROGEDUNIN	00100146		ACETOSYRINGONE	00300610	2478-38-8
7-DESHYDROXYPYROGALLIN-4-CARBOXYLIC ACID	00201508		ACETRIAZOIC ACID	01504142	85-36-9, 129-63-5 [acetrizoate sodium]
7-HYDROXYFLAVONE	01504519	6665-86-7	ACETYL ISOGAMBOGIC ACID	00300549	
7-NITROINDAZOLE	01505342	2942-42-9	ACETYL-L-LEUCINE	01502001	99-15-0
7-OXOCHOLESTEROL	01500854	566-28-9	ACETYLCHOLINE	01500104	60-31-1, 51-84-3 [acetylcholine]
7,2'-DIHYDROXYFLAVONE	01500719	77298-66-9	ACETYLCYSTEINE	01500105	616-91-1
7,4'-DIHYDROXYFLAVONE	01500721	2196-14-7	ACETYLGLUCOSAMINE	01500715	
7,4'-DIMETHOXYISOFLAVONE	00211249		ACETYLGLUTAMIC ACID	01500703	
7,8-DIHYDROXYFLAVONE	00201315	38183-03-8	ACETYLPHENYLALANINE	01500710	
8-HYDROXYCARAPINIC ACID	00100129		ACETYLTRYPTOPHAN	01500702	1218-34-4
8beta-HYDROXYCARAPIN, 3,8-HEMIACETAL	00100105		ACETYLTRYPTOPHANAMIDE	01500699	
ABAMECTIN	01502260	65195-55-3	ACEXAMIC ACID	01503045	57-08-9
ABIETIC ACID	01502229	514-10-3	ACONITIC ACID	00310001	585-84-2
ACACETIN	00200499	480-44-4	ACONITINE	01500655	302-27-2
ACACETIN DIACETATE	00200833	5892-39-7	ACECLIDINE	01501124	827-61-2

ACADESINE	01505167	2627-69-2	ACEBUTOLOL HYDROCHLORIDE	01500665	34381-68-5, 37517-30-9
ACAMPROSATE CALCIUM	01505711	77337-73-6	ACECAINIDE HYDROCHLORIDE	02300154	34118-92-8, 32795-44-1 [acecainide]
ACARBOSE	01505172	56180-94-0	ACRIFLAVINIUM HYDROCHLORIDE	01500618	8018-07-3
ACRISORCIN	01504218	7527-91-5	ALLOPREGNANOLONE	00100303	
ACTINONIN	00210477	13434-13-4	ALLOPURINOL	01500108	315-30-0
ACYCLOVIR	01503603	59277-89-3	ALLOXAN	01500802	2244-11-3
ADENINE	01500807	73-24-5	ALOIN	01503427	5133-19-7
ADENOSINE	01500107	58-61-7	alpha-CYANO-3-HYDROXYCINNAMIC ACID	01502095	
ACTINONIN	00210477	13434-13-4	alpha-CYANO-4-HYDROXYCINNAMIC ACID	01502096	
ACYCLOVIR	01503603	59277-89-3	alpha-DIHYDROGEDUNOL	00100375	
ADENOSINE PHOSPHATE	01500667	61-19-8	alpha-ERGOCRYPTINE	01505883	511-09-1
ADIPHENINE HYDROCHLORIDE	01503073	50-42-0, 64-95-9	alpha-HYDROXYDEOXYCHOLIC ACID	00270049	83-49-8
ADONITOL	00310002	488-81-3	alpha-MANGOSTIN	01504015	6147-11-1
ADRENALINE BITARTRATE	01500274	51-42-3	alpha-TOCHOPHEROL	00310039	59-02-9
AESCULIN	01500901	531-75-9	alpha-TOCHOPHERYL ACETATE	00310040	58-95-7
AGARIC ACID	01505775	666-99-9	alpha-TOXICAROL	00211224	82-09-7
AGELASINE	00300010		ALPINETIN METHYL ETHER	01500733	36052-66-1
AGMATINE SULFATE	01503982	2482-00-0	ALPRENOLOL	02300166	13655-52-2, 13707-88-5
AJMALINE	01500656	4360-17-7	ALRESTATIN	01502053	51411-04-2, 51876-97-2
AKLOMIDE	01503014	3011-89-0	ALTHIAZIDE	01500804	5588-16-9
ALANYL-dl-LEUCINE	01500716		ALTRENOGEST	01505703	850-52-2
ALAPROCLATE	01504136	60719-82-6	ALTRETAMINE	01503065	645-05-6
ALBENDAZOLE	01503903	54965-21-8	ALVERINE CITRATE	01500109	5560-59-8, 150-59-4 [alverine]
ALBUTEROL (+/-)	01500677	18559-94-9	AMANTADINE HYDROCHLORIDE	01500110	665-66-7, 768-94-5 [amantadine]
ALCLOMETAZONE DIPROPIONATE	01505125	66734-13-2	AMBROXOL HYDROCHLORIDE	01503080	23828-92-4, 18683-91-5
ALENDRONATE SODIUM	01505166	121268-17-5	AMCINONIDE	01503816	51022-69-6
ALEURETIC ACID	01505743	533-87-9	AMIFOSTINE	01503081	20537-88-6
ALEXIDINE HYDROCHLORIDE	01503074	22573-93-9, 22782-69-0 [alexidine]	AMIKACIN SULFATE	01500111	39831-55-5, 37517-28-5 [amikacin]

ALFAXALONE	01503424	23930-19-0	ALLOPREGNANOLONE	00100303	
ALFLUZOSIN	01505263	81403-80-7	ALLOPURINOL	01500108	315-30-0
ALISKIREN HEMIFUMARATE	01505710	173334-57-1	ALLOXAN	01500802	2244-11-3
ALLANTOIN	01500801	97-59-6	ALOIN	01503427	5133-19-7
AMILORIDE HYDROCHLORIDE	01500112	17440-83-4, 2016-88-8, 2609-46-3	ANAGRELIDE HYDROCHLORIDE	01505590	58579-51-4
AMINACRINE	01500810	90-45-9, 134-50-9	ANCITABINE HYDROCHLORIDE	01504137	10212-25-6
AMINOCAPROIC ACID	01500114	60-32-2	ANDROGRAPHOLIDE	00300532	5508-58-7
AMINOCYCLOPROPANECARBOXYLIC ACID	01502130	68781-13-5	ANDROSTA-1,4-DIEN-3,17-DIONE	01701001	897-06-3
AMINOGLUTETHIMIDE	01500115	125-84-8	ANDROSTERONE	01505745	53-41-8
AMINOHIPPURIC ACID	01503069	61-78-9, 94-16-6	ANDROSTERONE ACETATE	00107113	1164-95-0
AMINOLEVULINIC ACID HYDROCHLORIDE	01504184	5451-09-2	ANETHOLE	01503705	4180-23-8
AMINOPENTAMIDE	01505650	119793-66-7	ANGOLENSIN (R)	00100616	4842-48-2
AMINOPTERIN	01500679	54-62-6, 58602-66-7	ANHYDROBRAZILIC ACID	00200457	
AMINOSALICYLATE SODIUM	01500116	6018-19-5	ANIRACETAM	01503078	72432-10-1
AMINOTHIAZOLE	01503017	96-50-4	ANISINDIONE	01502198	117-37-3
AMIODARONE HYDROCHLORIDE	02300165	1951-25-3	ANISODAMINE HYDROBROMIDE	00300047	17659-49-3
AMIPRILOSE	01503083	56824-20-5, 60414-06-4	ANISOMYCIN	01503906	22862-76-6
AMITRAZ	01505299	33089-61-1	ANTAZOLINE PHOSPHATE	01500126	154-68-7, 91-75-8 [antazoline]
AMITRIPTYLINE HYDROCHLORIDE	01500117	549-18-8	ANTHOTHECOL	00100005	10410-83-0
AMLODIPINE BESYLATE	01505202	111470-99-6	ANTHRALIN	01500127	480-22-8, 1143-38-0
AMODIAQUINE DIHYDROCHLORIDE	01500119	6398-98-7, 69-44-3, 86-42-0	ANTHRAQUINONE	01502103	84-65-1
AMOXAPINE	02300161	14028-44-5	ANTIAROL	00200110	642-71-7
AMOXICILLIN	01500120	61336-70-7, 26787-78-0	ANTIMYCIN A (A1 shown)	01502108	1397-94-0
AMPHOTERICIN B	01500122	1397-89-3	ANTIPYRINE	01500128	60-80-0
AMPICILLIN SODIUM	01500123	69-52-3, 69-53-4	APHYLLIC ACID	01504155	642-67-1
AMPROLIUM	01500124	121-25-5	APIGENIN	00200846	520-36-5
AMPYRONE	01505869	83-07-8	APIGENIN DIMETHYL ETHER	01505490	5728-44-9
AMRINONE	01503084	60719-84-8	APIIN	00350025	26544-34-3

AMSACRINE	01503256	51264-14-3	APIOLE	00390001	523-80-8
AMYGDALIN	01502244	29883-15-6	APOMORPHINE HYDROCHLORIDE	01500129	41372-20-7, 314-19-2, 58-00-4
ANABASAMINE HYDROCHLORIDE	01504156	20410-87-1(base)	APOTOXICAROL	00211949	
ANABASINE HYDROCHLORIDE	00310004	13078-04-1 (anabasine)	APRAMYCIN	01505249	37321-09-8
ARBUTIN	00300539	497-76-7	ATROPINE SULFATE	01500131	51-55-8, 5908-99-6, 55-48-1
ARCAINE SULFATE	01500706	36587-93-6	AURAPTENE	01505176	495-02-3
ARECOLINE HYDROBROMIDE	01500680	300-08-3, 63-75-2 [arecoline]	AURIN TRICARBOXYLIC ACID	01505163	4431-00-9
ARGININE HYDROCHLORIDE	01300010	1119-34-2	AUROTHIOGLUCOSE	01500132	12192-57-3
ARIPIPRAZOLE	01505851	129722-12-9	AVOBENZONE	01504190	70356-09-1
ARMODAFINIL	01504283	112111-43-0	AVOCADENOFURAN	01505807	25346-24-1
ARSANILIC ACID	01505652	98-50-0	AVOCADYNE	01505234	34524-38-4
ARSENIC TRIOXIDE	01505957	1327-53-3	AVOCADYNE ACETATE	00240929	24607-06-5
ARTEMISIN	01500659	481-05-0	AZACITIDINE	01502111	320-67-2
ARTEMISININ	01503042	63968-64-9	AZADIRACHTIN	01503802	11141-17-6
ARTENIMOL	01504143	81496-81-3	AZAPERONE	01505332	1649-18-9
ARTHONIOIC ACID	00240942	25556-24-5	AZASERINE	01502113	115-02-6
ASARININ (-)	01504180	13079-95-3	AZATHIOPRINE	01500133	446-86-6
ASARYLALDEHYDE	00200208	4460-86-0	AZELAIC ACID	01500648	123-99-9
ASCORBIC ACID	01502230	50-81-7	AZELASTINE HYDROCHLORIDE	01505340	58581-89-8
ASCORBYL PALMITATE	01505742	137-66-6	AZITHROMYCIN	01503679	83905-01-5, 117772-70-0
ASIATIC ACID	01505175	464-92-6	AZLOCILLIN SODIUM	01503101	37091-66-0
ASPARTAME	01505306	22839-47-0	AZOBENZENE	01501172	103-33-3
ASPIRIN	01500130	50-78-2	AZTREONAM	01505996	78110-38-0
ASTAXANTHIN	01502235	71772-51-5	AZTREONAM	01505122	78110-38-0
ASTEMIZOLE	02300094	68844-77-9	BACAMPICILLIN HYDROCHLORIDE	01503102	37661-08-8, 50972-17-3 [bacampicillin]
ASTRAGALOSIDE IV	01505018	84687-43-4	BACCATIN III	01505034	27548-93-2
ATENOLOL	01501127	29122-68-7	BACITRACIN	01500134	1405-87-4
ATOMOXETINE HYDROCHLORIDE	01505385	82248-59-7	BACLOFEN	01500135	1134-47-0

ATORVASTATIN CALCIUM	01503722	134523-03-8, 134523-00-5	BAICALEIN	01504002	491-67-8
ATOVAQUONE	01504210	95233-18-4	BAMBUTEROL HYDROCHLORIDE	01505173	81732-46-9
ATRANORIN	00200034	479-20-9	BARBITAL	01900040	57-44-3
ATROPINE OXIDE	01505407	4438-22-6	BATYL ALCOHOL	01503983	544-62-7
BECLAMIDE	01505827	501-68-8	beta-ESCIN	01504030	6805-41-0
BECLOMETHASONE DIPROPIONATE	01500136	5534-09-8, 4419-39-0	beta-NAPHTHOL	01504501	135-19-3
BEKANAMYCIN SULFATE	01500812	4696-76-8 (base)	BETA-PROPIOLACTONE	01503234	57-57-8
BENAZEPRIL HYDROCHLORIDE	01505200	86541-74-4	beta-SITOSTEROL	00107022	83-46-5
BENDROFLUMETHIAZIDE	01503104	73-48-3	beta-TOXICAROL	00203010	82-11-1
BENFLUOREX HYDROCHLORIDE	01500669	23602-78-0	BETAHISTINE HYDROCHLORIDE	01500670	5579-84-0, 5638-76-6
BENFOTIAMINE	01503105	22457-89-2	BETAINE HYDROCHLORIDE	01503007	590-46-5, 141-58-2, 107-43-7
BENSERAZIDE HYDROCHLORIDE	01500137	322-35-0	BETAMETHASONE	01500144	378-44-9
BENURESTAT	01505410	38274-54-3	BETAMETHASONE 17,21-DIPROPIONATE	01503210	5593-20-4
BENZALKONIUM CHLORIDE	01503610	8001-54-5	BETAMETHASONE ACETATE	01505723	987-24-6
BENZBROMARONE	01505971	117976-90-6	BETAMETHASONE VALERATE	01500145	2152-44-5
BENZETHONIUM CHLORIDE	01500138	121-54-0	BETAMETHAZONE SODIUM PHOSPHATE	01505725	151-73-5
BENZOCAINE	01500139	94-09-7	BETAMIPRON	01504244	3440-28-6
BENZOIC ACID	01503001	65-85-0	BETHANECHOL CHLORIDE	01500146	590-63-6, 674-38-4 [bethanechol]
BENZOXIQUINE	01505411	86-75-9	BETULIN	01500815	473-98-3
BENZOYL PEROXIDE	01503004	94-36-0	BETULINIC ACID	01504081	472-15-1
BENZOYLPAS	01505413	13898-58-3	BEZAFIBRATE	01502046	41859-67-0
BENZTHIAZIDE	01500141	91-33-8	BICUCULLINE (+)	01500821	485-49-4
BENZYDAMINE HYDROCHLORIDE	01505975	132-69-4	BICUCULLINE(-) METHIODIDE	01505395	55950-07-7
BENZYL BENZOATE	01503002	120-51-4	BIFONAZOLE	01505309	60628-96-8
BENZYL ISOTHIOCYANATE	01503006	622-78-6	BILIRUBIN	01500857	635-65-4
BEPHENIUM HYDROXYNAPTHOATE	01505778	3818-50-6	BIOCHANIN A	10100003	491-80-5
BEPRIDIL HYDROCHLORIDE	01503106	74764-40-2	BIOTIN	01503009	58-85-5
BERBAMINE HYDROCHLORIDE	01501019	478-61-5 (berbamine)	BIPERIDEN	01505514	514-65-8
BERBERINE CHLORIDE	01500811	633-65-8, 2086-83-1	BISACODYL	01500147	603-50-9
BERGENIN	01500819	477-90-7	BISANHYDRORUTILANTINONE	00201605	749-18-8

beta-AMYRIN	00100360	559-70-6	BISMUTH SUBSALICYLATE	01505412	14882-18-9
beta-AMYRIN ACETATE	00100552	1616-93-9	BISOPROLOL FUMARATE	01505704	104344-23-2
beta-CAROTENE	01500143	7235-40-7	BISPHENOL A	01505041	80-05-7
beta-CARYOPHYLLENE ALCOHOL	00300105		BISSALICYL FUMARATE	01505324	
BITHIONATE SODIUM	01500148	97-18-7	BITOSCANATE	01504502	4044-65-9
BIXIN	10101011	39937-23-0	CACODYLIC ACID	01503947	75-60-5
BOLDINE	01500862	476-70-0	CADAVERINE TARTRATE	01502227	462-94-2(base)
BOVINOCIDIN (3-nitropropionic acid)	01504206	504-88-1	CADIN-4-EN-10-OL	00300055	
BRAZILEIN	00200463	600-76-0	CAFESTOL	01504001	469-83-0
BRAZILIN	00200012	474-07-7	CAFESTOL ACETATE	01503986	81760-48-7
BRETYLIUM TOSYLATE	01502018	61-75-6, 59-41-6	CAFFEIC ACID	01503987	331-39-5
BROMHEXINE HYDROCHLORIDE	01503107	611-75-6, 3572-43-8	CAFFEINE	01500155	58-08-2, 5743-12-4
BROMINDIONE	01505414	1146-98-1	CAMPHOR (1R)	01500156	464-49-3; 76-22-2
BROMO-3-HYDROXY-4-(SUCCIN-2-YL)-CARYOLANE gamma-LACTONE	00300053		CAMPTOTHECIN	01502232	7689-03-4
BROMOCRIPTINE MESYLATE	01500151	22260-51-1, 25614-03-3	CAMYLOFINE DIHYDROCHLORIDE	01505785	54-30-8
BROMOPRIDE	01503108	4093-35-0	CANAVANINE	01500833	543-38-4
BROMPERIDOL	01505972	10457-90-6	CANDESARTAN CILEXTIL	01504261	139481-59-7
BROMPHENIRAMINE MALEATE	01503985	980-71-2, 86-22-6	CANRENOIC ACID, POTASSIUM SALT	01500828	2181-04-6, 4138-96-9
BROXYQUINOLINE	01500623	521-74-4	CANRENONE	01505248	976-71-6
BRUCINE	01500822	4845-99-2, 357-57-3	CANTHARIDIN	01500814	56-25-7
BUCETIN	01505772	1083-57-4	CANTHAXANTHIN (euglenanone)	01504204	514-78-3
BUCLADESINE	01503043	362-74-3	CAPERATIC ACID	00240927	29227-64-3
BUDESONIDE	01500813	51333-22-3, 51372-29-3, 51372-28-2	CAPOBENIC ACID	01505417	21434-91-3
BUFEXAMAC	01502003	2438-72-4	CAPREOMYCIN SULFATE	01500157	1405-37-4, 11003-38-6
BUFLOMEDIL HYDROCHLORIDE	01505992	35543-24-9, 55837-25-7(base)	CAPSAICIN	01501128	404-86-4
BUMETANIDE	01502004	28395-03-1	CARBACHOL	01500158	51-83-2
BUPIVACAINE HYDROCHLORIDE	01503818	14252-80-3, 2180-92-9, 18010-40-7	CARBADOX	01505294	6804-07-5

BUPROPION	01504174	31677-93-7, 34911-55-2	CARBAMAZEPINE	01500159	298-46-4
BUSSEIN	00100006	41060-14-4	CARBENICILLIN DISODIUM	01500160	4800-94-6, 4697-36-3
BUSULFAN	01500152	55-98-1	CARBENOXOLONE SODIUM	01502005	7421-40-1, 5697-56-3
BUTACAINE	01503914	149-15-5, 149-16-6	CARBETAPENTANE CITRATE	01501129	23142-01-0, 77-23-6
BUTAMBEN	01500767	94-25-7	CARBIDOPA	01502150	38821-49-7, 28860-95-9
BUTYL PARABEN	01505995	94-26-8	CARBIMAZOLE	01505323	22232-54-8
CARBINOXAMINE MALEATE	01500161	3505-38-2, 486-16-8	CEFOPERAZONE SODIUM	01502042	62893-20-3, 62893-19-0
CARBOPLATIN	01502106	41575-94-4	CEFOTAXIME SODIUM	01500165	64485-93-4, 63527-52-6
CARISOPRODOL	01500162	78-44-4	CEFOXITIN SODIUM	01502031	66309-69-1, 61622-34-2
CARMINIC ACID	01500817	1260-17-9	CEFPODOXIME PROXETIL	01505637	87239-81-4
CARMOFUR	01505317	61422-45-5	CEFPROZIL	01505364	121123-17-9
CARMUSTINE	01503110	154-93-8	CEFSULODIN SODIUM	01502029	52152-93-9, 62587-73-9
CARNITINE (dl) HYDROCHLORIDE	01500624	461-06-3	CEFTAZIDIME	01505782	72558-82-8
CARNOSIC ACID	01504120	3650-09-7	CEFTIBUTEN	01505207	97519-39-6
CARNOSINE	01500944	305-84-0	CEFTRIAXONE SODIUM TRIHYDRATE	01503111	104376-79-6, 73384-59-5
CARPROFEN	01502006	53716-49-7	CEFUROXIME AXETIL	01504175	64544-07-6, 55268-75-2
CARSALAM	01504504	2037-95-8	CEFUROXIME SODIUM	01502033	56238-63-2
CARVEDILOL	01504257	72956-09-3	CELASTROL	00201664	34157-83-0
CARYLOPHYLLENE OXIDE	01500832	1139-30-6	CELECOXIB	01503678	169590-42-5
CARYOPHYLLENE [t(-)]	01500842	87-44-5	CELLOBIOSE (D[+])	01502231	528-50-7
CARZENIDE	01504505	138-41-0	CEPHALEXIN	01502028	23325-78-2, 15686-71-2
CATECHIN PENTAACETATE	01600537		CEPHALOSPORIN C SODIUM	01500836	61-24-5
CATECHIN TETRAMETHYLETHER	00210220		CEPHALOTHIN SODIUM	01500166	58-71-9, 153-61-7
CEDRELONE	00100009	1254-85-9	CEPHAPIRIN SODIUM	01500167	24356-60-3, 21593-23-7
CEDROL	00307059	77-53-2	CEPHRADINE	01500168	38821-53-3 [anhydrous], 58456-86-3, 31828-50-9
CEDRYL ACETATE	00310015	77-54-3	CETIRIZINE HYDROCHLORIDE	01505371	83881-52-1
CEFACLOR	01500771	70356-03-5, 53994-73-3	CETRIMONIUM BROMIDE	01503200	57-09-0, 6899-10-1
CEFADROXIL	01500163	66592-87-8, 50370-12-2 [anhydrous], 119922-89-9	CETYLPYRIDINIUM CHLORIDE	01500169	6004-24-6, 123-03-5

CEFAMANDOLE NAFATE	01502041	42540-40-9, 34444-01-4	CEVADINE	01503815	62-59-9
CEFAMANDOLE SODIUM	01502038	34444-01-4	CHAULMOOGRIC ACID	00310016	502-30-7
CEFAZOLIN SODIUM	01500164	27164-46-1, 25953-19-9	CHAULMOSULFONE	01600654	473-32-5
CEFDINIR	01505208	91832-40-5	CHENODIOL	01500837	474-25-9
CEFDITORIN PIVOXIL	01505360	117467-28-4	CHICAGO SKY BLUE	01505876	2610-05-1
CEFMETAZOLE SODIUM	01502040	56796-39-5	CHINIOFON	01504510	8002-90-2
CEFONICID SODIUM	01505474	71420-79-6	CHLORALOSE	01504511	158-79-93-3
CHLORAMPHENICOL	01500174	56-75-7	CHOLESTANE	00300015	481-21-0
CHLORAMPHENICOL HEMISUCCINATE	01500173	982-57-0, 56-75-7	CHOLESTEROL	01500847	57-88-5
CHLORAMPHENICOL PALMITATE	01500172	530-43-8	CHOLIC ACID	01500840	81-25-4
CHLORCYCLIZINE HYDROCHLORIDE	01500175	1620-21-9, 82-93-9 [base]	CHOLIC ACID, METHYL ESTER	01500904	1448-36-8
CHLORDIAZEPOXIDE	01900004	438-41-5, 58-25-3	CHOLINE CHLORIDE	01503428	67-48-1, 62-49-7 [choline]
CHLORHEXIDINE	01500177	3697-42-5, 55-56-1	CHROMOCARB	01503044	4940-39-0
CHLORINDIONE	01504507	1146-99-2	CHRYSANTHEMIC ACID	01504800	10453-89-1
CHLORMADINONE ACETATE	01505327	302-22-7	CHRYSANTHEMIC ACID, ETHYL ESTER	00310019	
CHLOROCRESOL	01500178	59-50-7	CHRYSANTHEMYL ALCOHOL	00300566	5617-92-5
CHLOROGUANIDE HYDROCHLORIDE	01504211	637-32-1	CHRYSAROBIN	00300556	491-58-7
CHLOROPHYLLIDE Cu COMPLEX Na SALT	01505308	15611-43-5	CHRYSIN	01500709	480-40-0
CHLOROPYRAMINE HYDROCHLORIDE	01506064	6170-42-9, 59-32-5 (base)	CHRYSIN DIMETHYL ETHER	01500739	21392-57-4
CHLOROQUINE DIPHOSPHATE	01500179	54-05-7	CHRYSOPHANOL	00300545	481-74-3
CHLOROTHIAZIDE	01500180	58-94-6	CHUKRASIN METHYL ETHER	00100615	
CHLOROTRIANISENE	01500181	569-57-3	CICLOPIROX OLAMINE	01500189	41621-49-2
CHLOROXINE	01503202	773-76-2	CILOSTAZOL	01505230	73963-72-1
CHLOROXYLENOL	01500182	88-04-0	CIMETIDINE	01500684	51481-61-9
CHLORPHENIRAMINE (S) MALEATE	01500183	113-92-8, 132-22-9	CINCHONIDINE	01500839	485-71-2
CHLORPROMAZINE	01500184	50-53-3	CINCHONINE	01500841	118-10-5
CHLORPROPAMIDE	01500185	94-20-2	CINCHOPHEN	01504508	132-60-5
CHLORPROTHIXENE HYDROCHLORIDE	01503203	113-59-7	CINEOLE	01500294	470-82-6
CHLORPYRIFOS	00330058	2921-88-2	CINNARAZINE	01503204	298-57-7
CHLORQUINALDOL	00212151	72-80-0	CINOXACIN	01500190	28657-80-9

CHLORTETRACYCLINE HYDROCHLORIDE	01500186	64-72-2	CIPROFLOXACIN	01503614	85721-33-1
CHLORTHALIDONE	01500187	77-36-1	CISPLATIN	01502107	15663-27-1
CHLORZOXAZONE	01500188	95-25-0	CITALOPRAM	01504172	59729-33-8
CHOL-11-ENIC ACID	01500856		CITICOLINE	01505244	987-78-0
CHOLECALCIFEROL	01500838	67-97-0	CITIOLONE	01503205	1195-16-0
CHOLEST-4,6-DIEN-3-ONE	01500851	566-93-8	CITRININ	00210186	518-75-2
CHOLEST-5-EN-3-ONE	01500849	601-54-7	CITROPTEN	01500707	487-06-9
CHOLESTAN-3-ONE	00270088	566-88-1	CITRULLINE	01500855	627-77-0
CLARITHROMYCIN	01504231	81103-11-9	CLOZAPINE	01500685	5786-21-0
CLAVULANATE LITHIUM	01505124	58001-44-8(acid)	COENZYME B12	01500844	13870-90-1
CLEMASTINE	01500191	15686-51-8	COLCHICINE	01500205	64-86-8
CLEMIZOLE HYDROCHLORIDE	01505990	1163-36-6, 442-52-4(base)	COLFORSIN	01503804	66575-29-9
CLENBUTEROL HYDROCHLORIDE	01503917	37148-27-9	COLISTIMETHATE SODIUM	01500206	8068-28-8, 21362-08-3
CLIDINIUM BROMIDE	01500192	3485-62-9	COLISTIN SULFATE	01505955	1264-72-8
CLINDAMYCIN HYDROCHLORIDE	01500193	21462-39-5, 58207-19-5 [monohydrate], 18323-44-9 [clindamycin]	CONESSINE	01503990	5913-82-6, 546-06-5
CLINDAMYCIN PALMITATE HYDROCHLORIDE	01505470	25507--04-4	CONVALLATOXIN	01503994	508-75-8
CLIOQUINOL	01505114	130-26-7	CORALYNE CHLORIDE	01500861	38989-38-7
CLOBETASOL PROPIONATE	01503918	25122-46-7, 25122-41-2 [clobetasol]	CORTISONE ACETATE	01500207	50-04-4, 53-06-5 [cortisone]
CLOFAZIMINE	01505974	2030-63-9	CORYNANTHINE	01500876	123333-62-0
CLOFIBRATE	01503429	637-07-0	COTARNINE CHLORIDE	00100595	10018-19-6, 82-54-2
CLOFIBRIC ACID	01500195	882-09-7	COTININE	01500208	486-56-6, 5695-98-7[fumarate]
CLOFOCTOL	01503206	37693-01-9	COUMARIN	01400208	91-64-5
CLOMIPHENE CITRATE	01500196	50-41-9, 911-45-5 [clomiphene]	CREATININE	01600300	60-27-5
CLOMIPRAMINE HYDROCHLORIDE	02300061	17321-77-6, 303-49-1	CRESOL	01500209	1319-77-3
CLONAZEPAM	01505958	1622-61-3	CRESOPIRINE	01401414	4386-39-4
CLONIDINE HYDROCHLORIDE	01500198	4205-91-8, 4205-90-7	CROMOLYN SODIUM	01500210	15826-37-6, 16110-51-3

CLOPERASTINE HYDROCHLORIDE	01503920	3703-76-2	CROTAMITON	01505271	483-63-6
CLOPIDOGREL SULFATE	01503710	113665-84-2	CRUSTECDYSONE	01504228	5289-74-7
CLOPIDOL	01505319	2971-90-6	CRYPTOTANSHINONE	01505812	35825-57-1
CLORGILINE HYDROCHLORIDE	01506065	17780-72-2 (base)	CURCUMIN	01505345	458-37-7
CLORSULON	01505115	60200-06-8	CYCLANDELATE	01505082	456-59-7
CLOTRIMAZOLE	01500200	23593-75-1	CYCLIZINE	01500211	82-92-8
CLOVANEDIOL DIACETATE	00300133		CYCLOBENZAPRINE HYDROCHLORIDE	01503207	6202-23-9, 303-53-7
CLOXACILLIN SODIUM	01500201	7081-44-9, 642-78-4	CYCLOCREATINE	01502085	35404-50-3
CLOXYQUIN	01500202	130-16-5	CYCLOHEXIMIDE	01502112	66-81-9
CYCLOPHOSPHAMIDE HYDRATE	01500213	6055-19-2, 50-18-0	DECAHYDROGAMBOGIC ACID	00201538	
CYCLOSERINE	01500215	68-41-7	DECAMETHONIUM BROMIDE	01505991	541-22-0
CYCLOSPORINE	01502202	59865-13-3	DECOQUINATE	01505356	18507-89-6
CYCLOTHIAZIDE	01503263	2259-96-3	DEFERIPRONE	01504512	30652-11-0
CYCLOVERATRYLENE	00500123		DEFEROXAMINE MESYLATE	01500224	138-14-7, 70-51-9
CYPERMETHRIN	01503606	52315-07-8	DEGUELIN(-)	00201138	522-17-8
CYPROHEPTADINE HYDROCHLORIDE	01505973	41354-29-4	DEHYDROABIETAMIDE	00307050	
CYPROTERONE ACETATE	01500216	427-51-0	DEHYDROCHOLIC ACID	01500907	81-23-2
CYSTEAMINE HYDROCHLORIDE	01504226	60-23-1	DEHYDROROTENONE	00201154	30990-44-4
CYSTINE	01300099	56-89-3	DEHYDROVARIABILIN	00210658	
CYTARABINE	01500217	147-94-4	DEMECLOCYCLINE HYDROCHLORIDE	01500226	127-33-3
CYTIDINE	01503431	65-46-3	DEMETHYLNOBILETIN	01505030	2174-59-6
CYTISINE	01504027	485-35-8	DENATONIUM BENZOATE	01505987	3734-33-6
D-LACTITOL MONOHYDRATE	01505436	81025-04-9, 585-86-4	DEOXYADENOSINE	01502238	16373-93-6
D-PHENYLALANINE	01503391	673-06-3	DEOXYCHOLIC ACID	00100566	88-44-3
d,l-threo-3-HYDROXYASPARTIC ACID	00501000		DEOXYGEDUNIN	00100432	
DACARBAZINE	01500218	4342-03-4	DEOXYKHIVORIN	00100139	
DACTINOMYCIN	00330001	50-76-0	DEOXYSAPPANONE B 7,3'-DIMETHYL ETHER	00200848	
DALBERGIONE	00201281		DEOXYSAPPANONE B 7,3'-DIMETHYL ETHER ACETATE	00201342	
DALBERGIONE, 4-METHOXY-4'-HYDROXY-	00200798		DEOXYSAPPANONE B 7,4'-DIMETHYL ETHER	00200484	

DANAZOL	01500220	17230-88-5	DEOXYSAPPANONE B TRIMETHYL ETHER	00201331	
DANTHRON	00211468	117-10-2	DEQUALINIUM CHLORIDE	01503127	522-51-0, 6707-58-0
DANTROLENE SODIUM	01503209	24868-20-0, 14663-23-1, 7261-97-4	DERACOXIB	01505222	169590-41-4
DAPSONE	01500222	80-08-0	DERRUSNIN	01401406	14736-62-0
DARIFENACIN HYDROBROMIDE	01505714	133099-07-7	DERRUSTONE	01401419	2204-59-3
DAUNORUBICIN	01500223	20830-81-3	DESACETYL (7)KHIVORINIC ACID, METHYL ESTER	00100650	
DEACETOXY-7-OXOGEDUNIN	00100047		DESACETYLCOLFORSIN	01503805	64657-20-1
DEACETOXY(7)-7-OXOKHIVORINIC ACID	00100447		DESIPRAMINE HYDROCHLORIDE	01500227	58-28-6, 50-47-5
DEACETYLGEDUNIN	00100012		DESONIDE	01505726	638-94-8
DEBRISOQUIN SULFATE	01506066	581-88-4	DESOXYCORTICOSTERONE ACETATE	00300029	56-47-3
DESOXYPEGANINE HYDROCHLORIDE	01505169	61939-05-7	DIFLORASONE DIACETATE	01505880	33564-31-7
DEXAMETHASONE	01500230	50-02-2	DIFLUNISAL	01500245	22494-42-4
DEXAMETHASONE ACETATE	01500231	55812-90-3, 1177-87-3	DIFUCOL HEXAMETHYL ETHER	00300423	14262-07-8
DEXAMETHASONE SODIUM PHOSPHATE	01500232	2392-39-4, 312-93-6	DIGITONIN	00100325	11024-24-1
DEXCHLORPHENIRAMINE MALEATE	01505530	2438-32-6	DIGITOXIN	01500246	71-63-6
DEXPANTHENOL	01505420	81-13-0	DIGOXIGENIN	00100688	1672-46-4
DEXPROPRANOLOL HYDROCHLORIDE	01500514	13071-11-9	DIGOXIN	01500247	20830-75-5
DEXTROMETHORPHAN HYDROBROMIDE	01500233	6700-34-1, 125-69-9	DIHYDROCELASTROL	01504082	
DIACERIN	01502010	13739-02-1	DIHYDROCELASTRYL DIACETATE	00380004	
DIACETAMATE	01504515	2623-33-8	DIHYDRODEOXYGEDUNIN	00100434	
DIALLYL SULFIDE	01505293	592-88-1	DIHYDROERGOTAMINE MESYLATE	01500248	6190-39-2
DIATRIZOIC ACID	01505777	117-96-4	DIHYDROFISSINOLIDE	00100465	
DIAZOXIDE	02300206	364-98-7	DIHYDROFOLIC ACID	01500671	4033-27-6
DIBEKACIN	01503114	34493-98-6	DIHYDROGEDUNIC ACID, METHYL ESTER	00100655	
DIBENZOTHIOPHENE	01500235	132-65-0	DIHYDROGEDUNIN	00100024	
DIBUCAINE HYDROCHLORIDE	01500236	61-12-1, 85-79-0	DIHYDROJASMONIC ACID	01504104	98674-52-3
DIBUTYL PHTHALATE	00330086	84-74-2	DIHYDROMYRISTICIN	01505006	607-91-0
DICHLORISONE ACETATE	01505779	79-61-8	DIHYDROSTREPTOMYCIN SULFATE	01500249	5490-27-7, 128-46-1
DICHLOROPHENE	01500626	97-23-4	DIHYDROTANSHINONE I	01505825	

DICHLORVOS	00330018	62-73-7	DIHYDROXY (3alpha,12alpha)PREGNAN-20-ONE	00100652	
DICLOFENAC SODIUM	01500237	15307-79-6	DILOXANIDE FUROATE	01505532	3736-81-0
DICLOXACILLIN SODIUM	01500238	13412-64-1, 343-55-5	DILTIAZEM HYDROCHLORIDE	02300214	33286-22-5, 42399-41-7
DICTAMNINE	00100541	484-29-7	DIMENHYDRINATE	01500251	523-87-5
DICUMAROL	01500239	66-76-2	DIMERCAPROL	01500252	59-52-9
DICYCLOMINE HYDROCHLORIDE	01500240	67-92-5, 77-19-0	DIMETHADIONE	01500253	695-53-4
DIENESTROL	01500241	84-17-3, 13029-44-2	DIMETHYL 4,4-o-PHENYLENE-BIS (3-THIOPHANATE)	01503974	
DIETHYLCARBAMAZINE CITRATE	01500242	1642-54-2, 90-89-1	DIMETHYLCAFFEIC ACID	00210567	14737-89-4
DIETHYLSTILBESTROL	01500244	56-53-1	DINITOLMIDE	01503036	148-01-6
DIETHYLTOLUAMIDE	01601020	134-62-3	DIOSGENIN	00100318	512-04-9
DIOSMETIN	01504068	520-34-3	DUARTIN, DIMETHYL ETHER	00201364	
DIOSMIN	01503219	520-27-4	DULOXETINE HYDROCHLORIDE	01505387	136434-34-9
DIOXYBENZONE	01500255	131-53-3	DYCLONINE HYDROCHLORIDE	01500268	536-43-6, 586-60-7
DIPERODON HYDROCHLORIDE	01505780	537-12-2	DYPHYLLINE	01500269	479-18-5
DIPHENHYDRAMINE HYDROCHLORIDE	01500256	147-24-0	EBSELEN	01501188	60940-34-3
DIPHENYLPYRALINE HYDROCHLORIDE	01500258	132-18-3 147-20-6	ECONAZOLE NITRATE	01501185	68797-31-9, 27220-47-9
DIPLOSALSALATE	01504209	530-75-6	EDOXUDINE	01503214	15176-29-1
DIPTERYXIN	01505959	53948-01-9	EDROPHONIUM CHLORIDE	02300219	116-38-1, 312-48-1
DIPYRIDAMOLE	01500259	58-32-2	EFAROXAN HYDROCHLORIDE	02300218	89197-32-0
DIPYROCETYL	01503032	486-79-3	EFLOXATE	01504518	119-41-5
DIPYRONE	01503298	5907-38-0, 68-89-3 [anhydrous]	ELAIDYLPHOSPHOCHOLINE	01505337	
DIRITHROMYCIN	01504144	62013-04-1	ELETRIPTAN HYDROBROMIDE	01505819	177834-92-3, 143322-58-1(base)
DISOPYRAMIDE PHOSPHATE	01500261	3737-09-5	ELLAGIC ACID	01502245	476-66-4
DISULFIRAM	01500262	97-77-8	EMETINE	01500272	316-42-7, 483-18-1
DJENKOLIC ACID	00310008	498-59-9	EMODIN	01500898	518-82-1
DOBUTAMINE HYDROCHLORIDE	01503212	49745-95-1, 34368-04-2	ENALAPRIL MALEATE	01501214	76095-16-4, 75847-73-3
DOCOSANOL	01505729	661-19-8	ENILCONAZOLE	01506067	35554-44-0
DONEPEZIL HYDROCHLORIDE	01504403	142057-77-0	ENOXACIN	01503215	74011-58-8

DOPAMINE HYDROCHLORIDE	01500263	62-31-7, 51-61-6	ENOXOLONE	01500990	471-53-4
DOXAZOSIN MESYLATE	01505976	77883-43-3	ENROFLOXACIN	01503721	93106-60-6
DOXEPIN HYDROCHLORIDE	01500264	1229-29-4, 1668-19-5, 4698-39-9, 25127-31-5	ENTANDROPHRAGMIN	00100517	11013-05-1
DOXIFLURIDINE	01504517	3094-09-5	EPI(13)TORULOSOL	00300058	3650-30-4
DOXORUBICIN	01505483	23214-92-8	EPIAFZELECHIN (2R,3R)(-)	00202178	24808-04-6
DOXYCYCLINE HYDROCHLORIDE	01500266	17086-28-1, 564-25-0	EPIAFZELECHIN TRIMETHYL ETHER	00210211	
DOXYLAMINE SUCCINATE	01500267	562-10-7, 469-21-6	EPIANDROSTERONE	00310009	
DROFENINE HYDROCHLORIDE	01500999	1679-76-1	EPICATECHIN	00210206	490-46-0
DROPERIDOL	01501002	548-73-2	EPICATECHIN MONOGALLATE	00210238	1257-08-5
DROPROPIZINE	01501004	17692-31-8	EPICATECHIN PENTAACETATE	01504256	
DUARTIN (-)	00201177	52305-04-1	EPIESTRIOL	01504520	547-81-9
EPIGALLOCATECHIN 3,5-DIGALLATE	00201513		ESTRONE BENZOATE	00307123	
EPIGALLOCATECHIN-3-MONOGALLATE	00210239	989-51-5	ESTROPIPATE	01505116	7280-37-7
EPIRUBICIN HYDROCHLORIDE	01505708	56390-09-1	ETANIDAZOLE	01503412	22668-01-5
EPITESTOSTERONE	01505195	481-30-1	ETHACRIDINE LACTATE	01505168	1837-57-6; 6402-23-9
EPOXYGEDUNIN	00100173		ETHACRYNIC ACID	01500287	58-54-8
EQUILIN	01500275	474-86-2	ETHAMBUTOL HYDROCHLORIDE	01500288	1070-11-7, 74-55-5
ERGOCALCIFEROL	01500276	50-14-6	ETHAMIVAN	01505994	304-84-7
ERGONOVINE MALEATE	01500277	129-51-1, 60-79-7	ETHAVERINE HYDROCHLORIDE	01501000	985-13-7, 486-47-5
ERGOSTEROL	00200743	57-87-4	ETHINYL ESTRADIOL	01500291	57-63-6
ERGOSTEROL ACETATE	00200744	2418-45-3	ETHIONAMIDE	01500292	536-33-4
ERGOTAMINE TARTRATE	01505584	379-79-3	ETHIONINE	01505849	67-21-0
ERYTHROMYCIN	01500280	114-07-8	ETHISTERONE	01503221	434-03-7
ERYTHROMYCIN ESTOLATE	01501176	134-36-1, 114-07-8	ETHOPROPAZINE HYDROCHLORIDE	01500293	1094-08-2, 522-00-9
ERYTHROMYCIN ETHYLSUCCINATE	01500279	1264-62-6, 114-07-8	ETHOSUXIMIDE	01502196	77-67-8
ERYTHROMYCIN STEARATE	01500281	643-22-1; 114-07-8(base)	ETHOXYQUIN	01500998	
ERYTHROSINE SODIUM	01505751	16423-68-0	ETHOXZOLAMIDE	01505426	452-35-7
ESCITALOPRAM OXALATE	01505216	219861-08-2	ETHYL PARABEN	01400151	120-47-8
ESCULETIN	01500899	305-01-1	ETHYLNOREPINEPHRINE HYDROCHLORIDE	01504088	3198-07-0, 536-24-3

ESEROLINE FUMARATE	01505884	469-22-7	ETHYNODIOL DIACETATE	01505979	297-76-7
ESTRADIOL	01500282	50-28-2	ETICLOPRIDE HYDROCHLORIDE	01506039	97612-24-3, 84226-12-0
ESTRADIOL ACETATE	01501184	4245-41-4	ETIDRONATE DISODIUM	01505537	7414-83-7
ESTRADIOL BENZOATE	01501182	50-50-0	ETODOLAC	01501005	41340-25-4
ESTRADIOL CYPIONATE	01500283	313-06-4	ETOMIDATE	01505599	33125-97-2
ESTRADIOL METHYL ETHER	01501183	1035-77-4	ETOPOSIDE	01500903	33419-42-0
ESTRADIOL PROPIONATE	01501179	113-38-2	EUCATROPINE HYDROCHLORIDE	01500295	536-93-6, 100-91-4
ESTRADIOL VALERATE	01500284	979-32-8	EUGENOL	01500296	97-53-0
ESTRADIOL-3-SULFATE, SODIUM SALT	01501192		EUPARIN	00300007	532-48-9
ESTRAGOLE	01505117	140-67-0	EUPHOL	00201697	514-47-6
ESTRIOL	01500285	50-27-1, 514-68-1 [as, succinate]	EUPHOL ACETATE	00100583	
ESTRONE	01500286	53-16-7	EUPHORBIASTEROID	01505010	28649-59-4
EVOXINE	01504020	522-11-2	FLUCYTOSINE	01505429	2022-85-7
EXALAMIDE	01503403	53370-90-4	FLUDARABINE PHOSPHATE	01505705	75607-67-9
EXEMESTANE	01505012	107868-30-4	FLUDROCORTISONE ACETATE	01500299	514-36-3, 127-31-1
EZETIMIBE	01505203	163222-33-1	FLUFENAMIC ACID	01501015	530-78-9
FAMCICLOVIR	01505201	104227-87-4	FLUMEQUINE	01500992	42835-25-6
FAMOTIDINE	01501003	76824-35-6	FLUMETHASONE	01501196	2135-17-3
FAMPRIDINE	01501130	504-24-5	FLUMETHAZONE PIVALATE	01500300	2002-29-1, 2135-17-3
FAMPROFAZONE	01505773	22881-35-2	FLUNARIZINE HYDROCHLORIDE	01500993	30484-77-6, 52468-60-7
FARNESOL	01501022	4602-84-0	FLUNISOLIDE	01501187	77326-96-6, 3385-03-3
FENBENDAZOLE	01501016	43210-67-9	FLUNIXIN MEGLUMINE	01505113	42461-84-7
FENBUFEN	01501008	36330-85-5	FLUOCINOLONE ACETONIDE	01500302	67-73-2
FENBUTYRAMIDE	01504223	90-26-6	FLUOCINONIDE	01500303	356-12-7
FENDILINE HYDROCHLORIDE	01501026	113042-18-7	FLUORESCEIN	01505396	2321-07-5
FENOFIBRATE	01501010	49562-28-9	FLUOROMETHOLONE	01500304	426-13-1
FENOPROFEN	01501011	31879-05-7	FLUOROURACIL	01500305	51-21-8
FENOTEROL HYDROBROMIDE	01501007	13392-18-2	FLUOXETINE	01504173	54910-89-3
FENRETINIDE	01505602	65646-68-6	FLUPHENAZINE HYDROCHLORIDE	01500994	146-56-5

FENSPIRIDE HYDROCHLORIDE	01501021	5053-08-7, 5053-06-5 [fenspiride]	FLURANDRENOLIDE	01501175	1524-88-5
FERULIC ACID	01501017	1135-24-6	FLURBIPROFEN	01500308	5104-49-4
FEXOFENADINE HYDROCHLORIDE	01504179	138452-21-8	FLUROTHYL	01505430	333-36-8
FINASTERIDE	01506069	98319-26-7	FLUTAMIDE	01500995	13311-84-7
FIPEXIDE HYDROCHLORIDE	01503222	34161-24-5	FLUVASTATIN	01504911	93957-54-1
FIPRONIL	01505354	120068-37-3	FOLIC ACID	01502020	59-30-3
FIROCOXIB	01504526	189954-96-9	FOMEPIZOLE HYDROCHLORIDE	01505432	56010-888
FISETIN	01502247	528-48-3	FORMESTANE	01504116	566-48-3
FISSINOLIDE	00100031	1915-69-1	FORMONONETIN	00102007	485-72-3
FLOPROPIONE	01500629	2295-58-1	FOSCARNET SODIUM	01502019	63585-09-1
FLORFENICOL	01505978	76639-94-6	FOSFOMYCIN CALCIUM	01502039	26472-47-9, 23112-90-5(acid)
FLOXURIDINE	01503059	50-91-9	FOSFOSAL	01502012	6064-83-1
FLUCONAZOLE	01503975	86386-73-4	FRAXIDIN METHYL ETHER	00100572	
FRIEDELIN	00100551	559-74-0	GIBBERELLIC ACID	00300021	77-06-5
FTAXILIDE	01504523	19368-18-4	GINKGOLIDE A	01500984	15291-75-5
FUCOSTANOL	01504053	83-45-4	GITOXIGENIN DIACETATE	00100584	5996-03-2
FUMARPROTOCETRARIC ACID	00200054	489-50-9	GITOXIN	01500986	4562-36-1
FUMAZENIL	01505701	78755-81-4	GLAFENINE	01500996	3820-67-5
FURALTADONE	01505770	139-91-3	GLICLAZIDE	01504145	21187-98-4
FURAZOLIDONE	01500309	67-45-8	GLIPIZIDE	01505433	29094-61-9
FUROSEMIDE	01500310	54-31-9	GLUCITOL-4-GUCOPYANOSIDE	01503989	
FUSARIC ACID	01505892	536-69-6	GLUCONOLACTONE	01503092	90-80-2
FUSIDIC ACID	01500311	6990-06-3	GLUCOSAMINE HYDROCHLORIDE	01500316	3416-24-8
GABAPENTIN	01505805	60142-96-3	GLUCOSAMINIC ACID	00310298	
GABOXADOL HYDROCHLORIDE	01503648	64603-91-4	GLUTAMINE (D)	01500987	6899-04-3
GALANTHAMINE HYDROBROMIDE	01501202	357-70-0, 1953-04-4	GLUTAMINE (L)	01300018	56-85-9
GALLAMINE TRIETHIODIDE	01500312	65-29-2, 153-76-4	GLUTATHIONE	01502248	70-18-8
GALLIC ACID	00210369	149-91-7	GLYBURIDE	02300229	10238-21-8
GAMBOGIC ACID	00200007	2752-65-0	GLYCOCHOLIC ACID	01505895	475-31-0

gamma-AMINOBUTYRIC ACID	01500678	56-12-2	GLYCOPYRROLATE	01505753	596-51-0
GANGALEOIDIN	00200035	55365-63-4	GOSSYPETIN	01505143	489-35-0
GARCINOLIC ACID	00201539		GOSSYPIN	01505127	652-78-8
GARDENIN B	01505031	2798-20-1	GOSSYPOL	01504019	303-45-7
GARLICIN	01505174	2179-57-9	GRAMICIDIN	01500319	1405-97-6
GATIFLOXACIN	01504272	160738-57-8	GRAMINE	01505896	87-52-5
GEDUNIN	00100032	2753-30-2	GRISEOFULVIC ACID	00200243	469-54-5
GEDUNOL	00300558		GRISEOFULVIN	00200046	126-07-8
GEMFIBROZIL	01500313	25812-30-0	GUAIFENESIN	01500321	93-14-1
GEMIFLOXACIN MESYLATE	01505802	204519-65-3	GUAIOL(-)	01800009	489-86-1
GENETICIN	01505302	108321-42-2, 49863-47-0(base)	GUANABENZ ACETATE	01500322	23256-50-0
GENISTEIN	00210296	446-72-0	GUANETHIDINE SULFATE	01500323	60-02-6, 55-65-2
GENTAMICIN SULFATE	01500314	1405-41-0, 1403-66-3	GUANFACINE	01505435	29110-47-2
GENTIAN VIOLET	01500315	548-62-9	GYROMITRIN	01504614	16568-02-8
HAEMATOMMIC ACID, ETHYL ESTER	00205071	39503-14-5	HEXETIDINE	01500633	141-94-6
HAEMATOPORPHYRIN	00700024	14459-29-1	HEXYLRESORCINOL	01500330	136-77-6
HAEMATOXYLIN	00200010	517-28-2	HIERACIN	01504115	1621-84-7
HAEMATOXYLIN PENTAACETATE	00240944		HISTAMINE DIHYDROCHLORIDE	01500331	51-45-6 [histamine]
HALAZONE	01500324	80-13-7	HOMATROPINE BROMIDE	01500332	51-56-9, 87-00-3
HALCINONIDE	01503237	3093-35-4	HOMATROPINE METHYLBROMIDE	01500333	80-49-9, 87-00-3
HALOPERIDOL	01500325	52-86-8	HOMIDIUM BROMIDE	01503806	1239-45-8
HALOTHANE	01505434	151-67-7	HOMOPTEROCARPIN	00100743	606-91-7
HARMALINE	01500864	304-21-2	HOMOSALATE	01505020	118-56-9
HARMALOL HYDROCHLORIDE	01500865	6028-07-5	HUMULENE (alpha)	01501210	6753-98-6
HARMANE	01500866	486-84-0	HUPERZINE A	01505255	102518-79-6
HARMINE	01500867	442-51-3	HYCANTHONE	01503239	3105-97-3
HARMOL HYDROCHLORIDE	01502237	40580-83-4	HYDRALAZINE HYDROCHLORIDE	01500334	304-20-1, 86-54-4
HARPAGOSIDE	01505151	19210-12-9	HYDRASTINE (1R, 9S)	01500687	118-08-1
HECOGENIN	01500760	467-55-0	HYDRASTININE HYDROCHLORIDE	00310006	4884-68-8, 6592-85-4

HECOGENIN ACETATE	00100310	915-35-5	HYDROCHLOROTHIAZIDE	01500335	58-93-5
HEDERACOSIDE C	01504018		HYDROCORTISONE	00300024	50-23-7
HEDERAGENIN	01504016	465-99-6	HYDROCORTISONE ACETATE	01500338	50-03-3
HELENINE	00310010	546-43-0	HYDROCORTISONE BUTYRATE	01503273	13609-67-1
HELICIN	01505476	618-65-5	HYDROCORTISONE HEMISUCCINATE	01500339	83784-20-7, 2203-97-6
HEMATEIN	01502253	475-25-2	HYDROCORTISONE PHOSPHATE TRIETHYLAMINE	01500340	3863-59-0
HEMICHOLINIUM BROMIDE	01505898	312-45-8	HYDROCORTISONE VALERATE	01505438	57524-89-7
HEPTAMINOL HYDROCHLORIDE	01503218	543-15-7, 372-66-7	HYDROFLUMETHIAZIDE	01500341	135-09-1
HESPERETIN	00310012	520-33-2	HYDROLYSIS PRODUCT OF BUSSEIN	00100117	
HESPERIDIN	00310011	520-26-3	HYDROQUINIDINE	01500657	1435-55-8
HETACILLIN POTASSIUM	01500327	5321-32-4, 3511-16-8	HYDROQUININE HYDROBROMIDE HYDRATE	01505899	207386-86-5
HETEROPEUCENIN, METHYL ETHER	00100529	26213-95-6	HYDROQUINONE	01504237	123-31-9
HEXACHLOROPHENE	01500328	70-30-4	HYDROXYCHLOROQUINE SULFATE	01503978	747-36-4, 118-42-3
HEXAMETHONIUM BROMIDE	01503297	55-97-0, 60-26-4	HYDROXYPROGESTERONE	01701060	3168-01-2
HEXAMETHYLQUERCETAGETIN	01505383	1251-84-9	HYDROXYPROGESTERONE CAPROATE	01500343	630-56-8, 68-96-2
HEXESTROL	01500632	5635-50-7	HYDROXYTOLUIC ACID	00212064	83-40-9
HYDROXYUREA	01500344	127-07-1	IRIGINOL HEXAACEATATE	00211012	
HYDROXYZINE PAMOATE	01500345	10246-75-0, 68-88-2	ISAXONINE	01504617	4214-72-6
HYMECROMONE METHYL ETHER	00300540	2555-28-4	ISOBERGAPTENE	00300032	482-48-4
HYOSCYAMINE	01500346	101-31-5	ISOETHARINE MESYLATE	01505977	7279-75-6
HYPOXANTHINE	00310023	68-94-0	ISOFLUPREDNONE ACETATE	01505724	338-98-7
IBUPROFEN	01500347	15687-27-1, 58560-75-1	ISOGUVACINE HYDROCHLORIDE	01502129	64603-90-3
ICARIIN	01505257	489-32-7	ISOKOBUSONE	00300117	24173-72-6
IDAZOXAN HYDROCHLORIDE	01506073	79944-58-4	ISOLIQUIRITIGENIN	01504200	961-29-5
IDEBENONE	01505755	58186-27-9	ISONIAZID	01500355	54-85-3
IFOSFAMIDE	01505480	3778-73-2	ISOOSAJIN	01504166	5745-54-0
IMIDAZOL-4-YLACETIC ACID SODIUM SALT	01502073	56368-58-2	ISOPEONOL	01400156	493-33-4
IMIPRAMINE HYDROCHLORIDE	01500348	113-52-0, 50-49-7	ISOPIMPINELLIN	00300012	482-27-9
INDAPAMIDE	01500349	26807-65-8	ISOPROPAMIDE IODIDE	01500356	71-81-8, 7492-32-2
INDOLE-3-CARBINOL	01505320	700-06-1	ISOPROTERENOL HYDROCHLORIDE	01500357	51-30-9, 7683-59-2

INDOMETHACIN	01500350	53-86-1	ISOROTENONE	00200015	
INDOPROFEN	01500351	31842-01-0	ISOSAFROLE	00300533	120-58-1
INOSITOL	01500352	87-89-8	ISOSORBIDE DINITRATE	01500358	87-33-2
IODIPAMIDE	01500772	606-17-7, 2618-26-0	ISOSORBIDE MONONITRATE	01503807	16051-77-7
IODOQUINOL	01500353	83-73-8	ISOTECTORIGENIN, 7-METHYL ETHER	00200139	
IOPANIC ACID	01503923	96-83-3	ISOTRETINON	01502013	4759-48-2
IPRATROPIUM BROMIDE	01500354	66985-17-9, 22254-24-6	ISOXICAM	01503242	34552-84-6
IPRIFLAVONE	01400010	35212-22-7	ISOXSUPRINE HYDROCHLORIDE	01500359	579-56-6, 395-28-8
IPRONIAZID SULFATE	01500634	54-92-2, 305-33-9	ITRACONAZOLE	01505756	84625-61-6
IRBESARTAN	01504259	138402-11-6	IVERMECTIN	01300027	70288-86-7
IRETOL	00200759		JUAREZIC ACID	00203008	1552-94-9
IRIDIN	00200793	491-74-7	JUGLONE	00300038	481-39-0
IRIGENIN	00200774	548-76-5	KAEMPFEROL	01506003	520-18-3
IRIGENIN TRIMETHYL ETHER	00200873		KAINIC ACID	02300228	487-79-6
IRIGENIN, 7-BENZYL ETHER	00200763		KANAMYCIN A SULFATE	01500360	25389-94-0, 133-92-6, 59-01-8
IRIGENIN, DIBENZYL ETHER	00201181		KARANJIN	01501208	521-88-0
IRIGENOL	00201182	4935-93-7	IRIGINOL HEXAACEATATE	00211012	
KASUGAMYCIN HYDROCHLORIDE	01505038	19408-46-9, 6980-18-3	LAPPACONITINE	01505002	32854-75-4
KAWAIN	01506075	3155-48-4	LARIXINIC ACID	00310025	118-71-8
KETANSERIN TARTRATE	01505346	83846-83-7, 74050-98-9(base)	LARIXOL	00300056	
KETOCONAZOLE	01500362	65277-42-1	LARIXOL ACETATE	00300057	
KETOPROFEN	01501215	22071-15-4	LATHOSTEROL	01500843	
KETOROLAC TROMETHAMINE	01503925	74103-07-4, 74103-06-3	LECANORIC ACID	00200070	480-56-8
KETOTIFEN FUMARATE	01500668	34580-14-8, 34580-13-7	LEOIDIN	00200033	105350-54-7
KHAYANTHONE	00100049	25279-68-9	LEUCODIN	01504149	17946-87-1
KHIVORIN	00100162	2524-38-1	LEUCOVORIN CALCIUM	01500364	1492-18-8
KINETIN	01500764	525-79-1	LEVALBUTEROL HYDROCHLORIDE	01505811	50293-90-8
KINETIN RIBOSIDE	01501207		LEVAMISOLE HYDROCHLORIDE	01503245	16595-80-5, 14769-73-4
KOBUSONE	00300048	24173-71-5	LEVOCARNITINE	01505437	541-15-1

KOPARIN	00200422	65048-75-1	LEVODOPA	02300205	59-92-7
KUHLMANNIN	00240862		LEVOFLOXACIN	01504260	138199-71-0
KYNURAMINE	01500877		LEVONORDEFRIN	01500365	829-74-3, 18829-78-2
KYNURENINE	01500879		LEVULINIC ACID, 3-BENZYLIDENYL-	01504009	
L-BUTHIONINE SULFOXIMINE	01505108	83730-53-4	LIDOCAINE HYDROCHLORIDE	01500689	6108-05-0, 73-78-9, 137-58-6
L-DEOXYALLIIN	01505005	21593-77-1	LIGUSTILIDE	01504029	4431-01-0
L-LEUCYL-L-ALANINE	01502207	7298-84-2	LIMONIN	01800018	1180-71-8
L-PHENYLALANINOL	01505339	3182-95-4	LINALOOL (+)	01501212	
L(+/-)-ALLIIN	01505190	556-27-4(-)	LINAMARIN	01504124	554-35-8
LABETALOL HYDROCHLORIDE	01503243	32780-64-6, 36894-69-6	LINCOMYCIN HYDROCHLORIDE	01500368	7179-49-9, 859-18-7, 154-21-2
LACCAIC ACID A	01505847	15979-35-8	LINDANE	00330071	58-89-9
LACTOBIONIC ACID	01506004	96-82-2	LIOTHYRONINE	01500778	6893-02-3
LACTULOSE	01500363	4618-18-2	LIOTHYRONINE (L- isomer) SODIUM	01502047	55-06-1, 6893-02-3
LAGOCHILIN	01504024	23554-81-6	LIPOAMIDE	01505740	3206-73-3
LAMOTRIGINE	01505610	84057-84-1	LISINOPRIL	01501217	83915-83-7, 76547-98-3
LANOSTEROL ACETATE	00201696		LITHIUM CITRATE	01504269	6080-58-6, 919-16-4
LANSOPRAZOLE	01503926	103577-45-3	LITHOCHOL-11-ENIC ACID	01500848	
LAPACHOL	01501204	84-79-7	LAPPACONITINE	01505002	32854-75-4
LITHOCHOLIC ACID	01500906	434-13-9	MECLIZINE HYDROCHLORIDE	01500376	31884-77-2, 1104-22-9, 569-65-3
LOBARIC ACID	00300018		MECLOCYCLINE SULFOSALICYLATE	01501118	73816-42-9, 2013-58-3
LOBELINE HYDROCHLORIDE	01500758	90-69-7	MECLOFENAMATE SODIUM	01500377	6385-02-0
LOBENDAZOLE	01505440	6306-71-4	MECYSTEINE HYDROCHLORIDE	01500636	2485-62-3, 18598-63-5
LOMEFLOXACIN HYDROCHLORIDE	01502037	98079-52-8, 98079-51-7	MEDROXYPROGESTERONE ACETATE	01500379	71-58-9, 520-85-4
LOPERAMIDE HYDROCHLORIDE	02300241	34552-83-5, 53179-11-6	MEDRYSONE	01500380	2668-66-8
LORATADINE	01503712	79794-75-5	MEFENAMIC ACID	01501103	61-68-7
LOSARTAN	01504268	124750-99-8, 114798-26-4	MEFEXAMIDE	01501108	1227-61-8
LOVASTATIN	01503977	75330-75-5	MEFLOQUINE	01503070	53230-10-7
LOXAPINE SUCCINATE	02300242	27833-64-3, 1977-10-2	MEGESTROL ACETATE	01500381	595-33-5, 3562-63-8
LUFENURON	01505355	103055-07-8	MEGLUMINE	01300029	6284-40-8
LUNARINE	00100520	24185-51-1	MELATONIN	01500690	73-31-4

LUPANINE PERCHLORATE	01505242	550-90-3 (base)	MELENGESTROL ACETATE	01505727	2919-66-6
LUPANYL ACID HYDROCHLORIDE	01505240		MELEZITOSE	00300531	
LUPEOL	01505484	545-47-1	MELIBIOSE	01505757	585-99-9
LUPININE	01504021	486-70-4	MELOXICAM SODIUM	01504150	71125-38-7
MADECASSIC ACID	01505250	18449-41-7	MELPHALAN	01500382	148-82-3
MAFENIDE HYDROCHLORIDE	01500372	138-39-6	MEMANTINE HYDROCHLORIDE	01501121	19982-08-2
MANDELIC ACID, METHYL ESTER	00201466		MENADIONE	01502254	58-27-5
MANGANESE TETRAKIS(4-CARBOXYPHENYL)PORPHYRIN CHLORDE	01505109		MENAQUINONE-4	01506091	
MANGIFERIN	01505134	4773-96-0	MENTHOL(-)	01503134	1490-04-6
MANGOSTIN TRIMETHYL ETHER	01505908		MENTHONE	00300564	14073-97-3
MANNITOL	01300028	69-65-8	MENTHYL BENZOATE	01800005	
MAPROTILINE HYDROCHLORIDE	01500373	10347-81-6, 10262-69-8	MEPENZOLATE BROMIDE	01500383	76-90-4, 25990-43-6
MEBENDAZOLE	01501110	31431-39-7	MEPHENESIN	01501140	59-47-2
MEBEVERINE HYDROCHLORIDE	01501117	2753-45-9, 3625-06-7	MEPHENTERMINE SULFATE	01503250	1212-72-2, 6190-60-9, 100-92-5
MEBHYDROLIN NAPHTHALENESULFONATE	01501116	524-81-2	MEPIROXOL	01504616	6968-72-5
MECAMYLAMINE HYDROCHLORIDE	01500374	826-39-1, 60-40-2	MEPIVACAINE HYDROCHLORIDE	01504148	1722-62-9, 96-88-8
MECHLORETHAMINE	01500375	55-86-7, 51-75-2	MERBROMIN	01500637	129-16-8
			MECLIZINE HYDROCHLORIDE	01500376	31884-77-2, 1104-22-9, 569-65-3
MERCAPTOPURINE	01500387	6112-76-1, 50-44-2	METHOXYVONE	01400666	
MEROGEDUNIN	00100455		METHSCOPOLAMINE BROMIDE	01500401	155-41-9
MESALAMINE	01505993	89-57-6	METHYL 7-DESHYDROXYPYROGALLIN-4-CARBOXYLATE	00201505	77-41-8
MESNA	01502014	19767-45-4, 3375-50-6	METHYL DEOXYCHOLATE	00270051	3245-38-3
MESTRANOL	01500388	72-33-3	METHYL ORSELLINATE	00210925	3187-58-4
meta-CRESYL ACETATE	01506049	122-46-3	METHYL ROBUSTONE	01401401	
METACETAMOL	00211175	621-42-1	METHYLATROPINE NITRATE	01505445	52-88-0
METAMECONINE	00300062		METHYLBENZETHONIUM CHLORIDE	01503253	1320-44-1, 25155-18-4
METAMPICILLIN SODIUM	01502034	6489-97-0	METHYLDOPA	01500403	41372-08-1, 555-30-6
METAPROTERENOL	01500390	586-06-1, 5874-97-5	METHYLDOPATE HYDROCHLORIDE	01505384	2508-79-4

METARAMINOL BITARTRATE	01503251	33402-03-8	METHYLENE BLUE	01505444	7220-79-3
METAXALONE	01504229	1665-48-1	METHYLERGONOVINE MALEATE	01500404	57432-61-8, 7054-07-1 [replaced], 113-42-8
METERGOLINE	00300565	17692-51-2	METHYLPHENIDATE HYDROCHLORIDE	01505907	298-59-9, 113-45-1(base)
METFORMIN HYDROCHLORIDE	01505814	1115-70-4, 657-24-9	METHYLPREDNISOLONE	01500406	83-43-2
METHACHOLINE CHLORIDE	01500391	62-51-1, 55-92-5	METHYLPREDNISOLONE SODIUM SUCCINATE	01503255	2375-03-3
METHACYCLINE HYDROCHLORIDE	01501104	3963-95-9, 914-00-1	METHYLTHIOURACIL	01500408	56-04-2
METHAPYRILENE HYDROCHLORIDE	01503229	135-23-9, 91-80-5	METHYLXANTHOXYLIN	00200446	23121-32-6
METHAZOLAMIDE	01503252	554-57-4	METHYSERGIDE MALEATE	01505492	129-49-7
METHENAMINE	01500394	100-97-0	METICRANE	01506077	1084-65-7
METHICILLIN SODIUM	01500395	7246-14-2, 132-92-3, 61-32-5	METITEPINE MALEATE	01503637	20229-30-5
METHIMAZOLE	01500396	60-56-0	METOCLOPRAMIDE HYDROCHLORIDE	01500410	54143-57-6, 7232-21-5, 364-62-5
METHIMAZOLE	01506009	60-56-0	METOLAZONE	02300325	17560-51-9
METHIONINE SULFOXIMINE (L)	01506010	15985-39-4	METOPROLOL TARTRATE	01500411	56392-17-7, 37350-58-6
METHOCARBAMOL	01500397	532-03-6	METRONIDAZOLE	01500412	443-48-1, 69198-10-3
METHOPRENE (S)	01504100	40596-69-8	MEVALONIC ACID LACTONE	01506015	503-48-0
METHOTREXATE(+/-)	01500398	60388-53-6	MEVASTATIN	01601000	73573-88-3
METHOXAMINE HYDROCHLORIDE	01500399	61-16-5, 390-28-3	MEXICANOLIDE	00100060	1915-67-9
METHOXSALEN	01500400	298-81-7	MEXILETINE HYDROCHLORIDE	01503929	5370-01-4, 31828-71-4
METHOXYAMINE HYDROCHLORIDE	01503970	593-56-6	MYRICETIN	01504065	529-44-2
MIANSERIN HYDROCHLORIDE	02300292	21535-47-7, 24219-97-4	N- (9-FLUORENYLMETHOXYCARBONYL)-L-LEUCINE	01502083	35661-60-0
MICONAZOLE NITRATE	01500413	22832-87-7, 22916-47-8	N-ACETYLMURAMIC ACID	01506020	10597-89-4
MIDODRINE HYDROCHLORIDE	01503257	3092-17-9, 42794-76-3	N-ACETYLPROLINE	01500704	
MIGLITOL	01504273	72432-03-2	N-METHYL-D-ASPARTIC ACID (NMDA)	01503636	6384-92-5
MIMOSINE	01500869		N-METHYLANTHRANILIC ACID	01600964	119-68-6
MINAPRINE HYDROCHLORIDE	01501120	25953-17-7, 25905-77-5	N-METHYLBENZYLAMINE HYDROCHLORIDE	01400242	13426-94-3, 103-67-3(base)
MINOCYCLINE HYDROCHLORIDE	01500414	13614-98-7, 10118-90-8	N-METHYLISOLEUCINE	01400136	5125-98-8
MINOXIDIL	01500415	38304-91-5	N-PHENYLANTHRANILIC ACID	01505156	91-40-7
MITOMYCIN C	00330002	50-07-7	N,N-HEXAMETHYLENEAMILORIDE	01504215	

MITOTANE	00330082	53-19-0	NADIDE	01500419	53-84-9
MITOXANTHRONE HYDROCHLORIDE	01503278	70476-82-3, 65271-80-9	NADOLOL	01503260	42200-33-9
MIZORIBINE	01503416	50924-49-7	NAFCILLIN SODIUM	01500420	7177-50-6, 985-16-0, 147-52-4
MODAFINIL	01505361	68693-11-8	NAFRONYL OXALATE	01503419	3200-06-4, 31329-57-4
MOLSIDOMINE	01500673	25717-80-0	NAFTOPIDIL DIHYDROCHLORIDE	01506024	57149-07-2
MONENSIN SODIUM	01502258	22373-78-0, 17090-79-8	NALBUPHINE HYDROCHLORIDE	01501115	23277-43-2, 20594-83-6
MONOCROTALINE	01502252	315-22-0	NALOXONE HYDROCHLORIDE	01500422	357-08-4, 51481-60-8 , 465-65-6
MONTELUKAST SODIUM	01505391	151767-02-1	NALTREXONE HYDROCHLORIDE	01503262	16676-29-2, 16590-41-3
MORANTEL CITRATE	01503931	26155-31-7, 20574-50-9	NAPHAZOLINE HYDROCHLORIDE	01500424	550-99-2, 835-31-4
MORIN	01502259	480-16-0	NAPROXEN(+)	01500425	22204-53-1
MOROXYDINE HYDROCHLORIDE	01506078	3731-59-7	NAPROXOL	01503801	26159-36-4
MOXALACTAM DISODIUM	01500418	8031-09-2	NARINGENIN	01500746	480-41-1
MOXIFLOXACIN HYDROCHLORIDE	01504303	186826-86-8	NARINGIN	01500765	10236-47-2
MOXISYLYTE HYDROCHORIDE	01506079	54-32-0	NATAMYCIN	01505560	7681-93-8
MUNDOSERONE	00201477	3564-85-0	NATEGLINIDE	01504258	105816-04-4
MUNDULONE	00200011	481-94-7	NEFOPAM	01501137	23327-57-3, 13669-70-0
MUNDULONE ACETATE	01700330		NEOMYCIN SULFATE	01500427	1405-10-3, 1404-04-2
MUPIROCIN	01505706	12650-69-0	NEOSTIGMINE BROMIDE	01500428	114-80-7, 59-99-4
MUUROLLADIE-3-ONE	00307056		NEROL	01501132	106-25-2
MYCOPHENOLIC ACID	01500674	24280-93-1	MYRICETIN	01504065	529-44-2
MYOSMINE	01500870	532-12-7	N- (9-FLUORENYLMETHOXYCARBONYL)-L-LEUCINE	01502083	35661-60-0
NETILMICIN SULFATE	01505482	56391-56-1	NOREPINEPHRINE	01500436	69815-49-2, 51-40-1, 51-41-2
NIACIN	01500430	59-67-6	NORETHINDRONE	01500437	68-22-4
NIACINAMIDE	01505397	98-92-0	NORETHINDRONE ACETATE	01500438	51-98-9
NIALAMIDE	01505986	51-12-7	NORETHYNODREL	01500439	68-23-5
NICARDIPINE HYDROCHLORIDE	01501135	54527-84-3, 55985-32-5	NORFLOXACIN	01500440	70458-96-7
NICERGOLINE	01501133	27848-84-6	NORGESTIMATE	01505562	35189-28-7
NICLOSAMIDE	01503265	50-65-7	NORGESTREL	01500441	6533-00-2
NICOTINE DITARTRATE	02300259	65-31-6	NORHARMAN	01500871	244-63-3
NICOTINYL ALCOHOL TARTRATE	01503038	100-55-0	NORSTICTIC ACID	00201716	571-67-5

NIFEDIPINE	01500431	21829-25-4	NORSTICTIC ACID PENTAACETATE	00200488	
NIFENAZONE	01503230	2139-47-1	NORTRIPTYLINE	01500442	894-71-3, 72-69-5
NIFLUMIC ACID	01502015	4394-00-7	NOSCAPINE HYDROCHLORIDE	01500443	912-60-7, 128-62-1
NIFUROXAZIDE	01505788	965-52-6	NOVOBIOCIN SODIUM	01500444	1476-53-5, 303-81-1
NILUTAMIDE	01504152	63612-50-0	NYLIDRIN HYDROCHLORIDE	01500445	849-55-8
NIMESULIDE	01503231	51803-78-2	NYSTATIN	01500446	114-90-9
NIMODIPINE	01503600	66085-59-4	O-BENZYL-l-SERINE	01500705	
NIMUSTINE	01504151	42471-28-3	OBLIQUIN	00100540	
NIPECOTIC ACID	02300345	498-95-3	OBTUSAQUINONE	00200090	21105-15-7
NISOLDIPINE	01505390	63675-72-9	OCTISALATE	01505760	118-60-5
NITHIAMIDE	01505448	140-40-9	OCTODRINE	01505447	543-82-8
NITRENDIPINE	01503609	84845-75-0	OCTOPAMINE HYDROCHLORIDE	01500639	104-14-3
NITROFURANTOIN	01500433	67-20-9, 54-87-5, 17140-81-7	OFLOXACIN	01502044	82419-36-1
NITROFURAZONE	01500434	59-87-0	OLEANDOMYCIN PHOSPHATE	01500675	3922-90-5 (base)
NITROMIDE	01500435	121-81-3	OLEANOIC ACID	00100550	508-02-1
NIZATIDINE	01505985	76963-41-2	OLEANOLIC ACID ACETATE	00102058	4339-72-4
NOBILETIN	01505268	478-01-3	OLMESARTAN MEDOXOMIL	01505205	144689-63-4
NOMIFENSINE MALEATE	01503267	32795-47-4, 24526-64-5	OLSELTAMIVIR PHOSPHATE	01504912	196618-13-0
NONIC ACID	00201227		OMEGA-3-ACID ESTERS (EPA shown)	01300030	86227-47-6
NONOXYNOL-9	01505292	26027-38-3	OMEPRAZOLE	01505693	73590-58-6
NORCANTHARIDIN	01504153		ONONETIN	00212097	487-49-0
ORBIFLOXACIN	01503711	113617-63-3	OXYPHENCYCLIMINE HYDROCHLORIDE	01503932	125-52-0, 125-53-1
ORLISTAT	01504300	96829-58-2	OXYPHENONIUM BROMIDE	01505783	50-10-2
ORNIDAZOLE	01505981	16773-42-5	OXYQUINOLINE HEMISULFATE	01500456	148-24-3
ORNITHINE	01504524	70-26-8	OXYTETRACYCLINE	01500457	6153-64-6, 79-57-2
OROTIC ACID	01504525	65-86-1	OXYTHIAMINE CHLORIDE HYDROCHLORIDE	01505761	614-05-1
ORPHENADRINE CITRATE	01500447	4682-36-4, 83-98-7	p-CHLOROPHENYLALANINE	01502162	7424-00-2(dl); 14173-39-8(l)
ORSELLINIC ACID	00300001	480-64-8	p-FLUOROPHENYLALANINE	01502114	51-65-0
ORSELLINIC ACID, ETHYL ESTER	00200002	2524-37-0	PACHYRRHIZIN	00201602	10091-01-7

OSAJIN	00201595	482-53-1	PACLITAXEL	01503908	33069-62-4
OUABAIN	01500676	11018-89-6, 630-60-4	PAEONOL	01601021	552-41-0
OXACILLIN SODIUM	01500448	7240-38-2, 1173-88-2, 66-79-5	PALMATINE	01505252	3486-67-7
OXALAMINE CITRATE	01506027	959-14-8 (base)	PALMATINE CHLORIDE	01500872	10605-02-4
OXANTEL PAMOATE	01505982	68813-55-8	PANCURONIUM BROMIDE	01505692	15500-66-0
OXAPROZIN	01505267	21256-18-8	PANGAMIC ACID SODIUM	01505921	20858-86-0
OXCARBAZEPINE	01504243	28721-07-5	PANTETHINE	01505920	16816-67-4
OXEDRINE	01506085	94-07-5	PANTHENOL	01505656	16485-10-2
OXELAIDIN CITRATE	01505774	52432-72-1, 468-61-1	PANTOPRAZOLE	01505818	102625-70-7
OXETHAZAINE	01503279	126-27-2	PANTOTHENIC ACID(d) Na salt	01505715	63409-48-3
OXFENDAZOLE	01505296	53716-50-0	PAPAVERINE HYDROCHLORIDE	01500459	61-25-6, 58-74-2
OXIBENDAZOLE	01503373	20559-55-1	PARACHLOROPHENOL	01500460	106-48-9
OXICONAZOLE NITRATE	01505330	64211-46-7	PARAMETHADIONE	01505456	115-67-3
OXIDOPAMINE HYDROCHLORIDE	01500450	1199-18-4	PARAROSANILINE PAMOATE	01503223	7232-51-1, 569-61-9
OXIGLUTATIONE DISODIUM SALT	01300019	103239-24-3; 27025-41-8(acid)	PARGYLINE HYDROCHLORIDE	01500462	306-07-0, 555-57-7
OXOLINIC ACID	01502030	14698-29-4	PAROMOMYCIN SULFATE	01503228	1263-89-4, 7542-37-2, 59-04-1
OXONITINE	00100563		PAROXETINE HYDROCHLORIDE	01504085	61869-08-7
OXYBENZONE	01500451	131-57-7	PARTHENOLIDE	01503640	20554-84-1
OXYBUTYNIN CHLORIDE	01505399	1508-65-2	PASINIAZID	01503381	2066-89-9
OXYMETAZOLINE HYDROCHLORIDE	01500453	2315-02-8, 1491-59-4	PATULIN	01503904	149-29-1
OXYPHENBUTAZONE	01500455	7081-38-1, 129-20-4	PECTOLINARIN	00200115	28978-02-1
PEFLOXACINE MESYLATE	01505305	149676-40-4	PHENINDIONE	01500477	83-12-5
PELLETIERINE HYDROCHLORIDE	00300553		PHENIRAMINE MALEATE	01500478	132-20-7, 86-21-5
PEMPIDINE TARTRATE	01503383	79-55-0	PHENOLPHTHALEIN	01500480	77-09-8
PENFLURIDOL	01505691	26864-56-2	PHENOTHRIN	01504098	26002-80-2
PENICILLAMINE	01500464	52-67-5	PHENOXYBENZAMINE HYDROCHLORIDE	02300176	63-92-3, 59-96-1
PENICILLIN G POTASSIUM	01500465	69-57-8, 61-33-6	PHENTERMINE	01505660	122-09-8
PENICILLIN V POTASSIUM	01500467	132-98-9, 87-08-1	PHENTOLAMINE HYDROCHLORIDE	01500691	73-05-2, 50-60-2

PENTAMIDINE ISETHIONATE	01500641	100-33-4	PHENYL AMINOSALICYLATE	00305025	133-11-9
PENTETIC ACID	01506082	67-43-6	PHENYLBUTAZONE	01500482	50-33-9
PENTOXIFYLLINE	01503611	6493-05-6	PHENYLBUTYRATE SODIUM	01504221	90-27-7
PENTYLENETETRAZOL	02300347	54-95-5	PHENYLEPHRINE HYDROCHLORIDE	01500483	61-76-7, 59-42-7
PEONIFLORIN	01505810	23180-57-6	PHENYLETHYL ALCOHOL	01505398	60-12-8
PERGOLIDE MESYLATE	01503269	66104-23-2, 66104-22-1	PHENYLMERCURIC ACETATE	01500644	62-38-4
PERHEXILINE MALEATE	01503227	6724-53-4, 6621-47-2	PHENYLPROPANOLAMINE HYDROCHLORIDE	01500484	154-41-6
PERICIAZINE	01503936	2622-26-6	PHENYTOIN SODIUM	01500485	630-93-3, 57-41-0
PERILLIC ACID (-)	01502101	7694-45-3	PHLORACETOPHENONE	00300604	480-66-0
PERILLYL ALCOHOL	01505297	536-59-4, 18457-55-1	PHLORETIN	00300554	60-82-2
PERINDOPRIL ERBUMINE	01505212	107133-36-8; 82834-16-0	PHLORIDZIN	00300547	60-81-1
PERPHENAZINE	01503934	58-39-9	PHTHALYLSULFACETAMIDE	01505728	131-69-1
PERSEITOL	00202130	527-06-0	PHTHALYLSULFATHIAZOLE	01502021	85-73-4
PERSEITOL HEPTAACETATE	00240437	19147-10-5	PHYSCION	01504070	521-61-9
PERUVOSIDE	01501113	1182-67-2	PHYSOSTIGMINE SALICYLATE	01500486	57-64-7, 57-47-6
PEUCENIN	00100528	578-72-3	PHYTOL	00310021	
PHENACEMIDE	01500472	63-98-9	PHYTONADIONE	01505485	84-80-0
PHENACETIN	01500642	62-44-2	PICROPODOPHYLLIN	01504410	477-47-4
PHENACYLAMINE HYDROCHLORIDE	00501332	5468-37-1, 613-89-8(base)	PICROTIN	00100346	21416-53-5
PHENAZOPYRIDINE HYDROCHLORIDE	01500473	136-40-3, 94-78-0	PICROTOXININ	01501107	17617-45-7
PHENELZINE SULFATE	01500476	156-51-4, 51-71-8	PILOCARPINE NITRATE	01500487	148-72-1, 92-13-7
PHENETHICILLIN POTASSIUM	01500643	132-93-4, 147-55-7	PIMETHIXENE MALEATE	01501114	314-03-4
PHENETHYL CAFFEATE (CAPE)	01502209	104594-70-9	PIMOZIDE	01501134	2062-78-4
PHENFORMIN HYDROCHLORIDE	01505983	834-28-6	PIMPINELLIN	00300013	131-12-4
PINACIDIL	02300270	85371-64-8, 60560-33-0	PRALIDOXIME CHLORIDE	01505449	51-15-0
PINDOLOL	01500488	13523-86-9	PRAMOXINE HYDROCHLORIDE	01501139	637-58-1, 140-65-8
PIOGLITAZONE HYDROCHLORIDE	01504401	111025-46-8 (pioglitazone)	PRASTERONE	01505083	53-43-0
PIPAMPERONE	01505690	1893-33-0	PRASTERONE ACETATE	00270029	53-43-0 (praesterone)
PIPEMIDIC ACID	01502024	51940-44-4	PRAVASTATIN SODIUM	01505803	81131-70-6
PIPENZOLATE BROMIDE	01503053	125-51-9, 13473-38-6	PRAZIQUANTEL	01500494	55268-74-1

PIPERACILLIN SODIUM	01500489	59703-84-3, 66258-76-2, 61477-96-1	PRAZOSIN HYDROCHLORIDE	01500495	19237-84-4, 19216-56-9
PIPERAZINE	01500490	110-85-0, 144-29-6, 41372-10-5	PREDNISOLONE	01500496	50-24-8 , 52438-85-4
PIPERIC ACID	01505842	5285-18-7	PREDNISOLONE ACETATE	01500497	52-21-1
PIPERIDOLATE HYDROCHLORIDE	01502197	129-77-1, 82-98-4	PREDNISOLONE HEMISUCCINATE	01505450	2920-86-7
PIPERINE	01500873	94-62-2	PREDNISOLONE SODIUM PHOSPHATE	01505712	125-02-0
PIPERONYLIC ACID	00500580	94-53-1	PREDNISONE	01500499	53-03-2
PIPLARTINE	01505135	20069-09-4	PREGABALIN	01505816	148553-50-8
PIPOBROMAN	01503393	54-91-1	PREGNENOLONE	01500645	145-13-1, 4598-67-8
PIRACETAM	01502195	7491-74-9	PREGNENOLONE SUCCINATE	01505713	4598-67-8
PIRENPERONE	01504188	75444-65-4	PRENYLETIN	00100101	15870-91-4
PIRENZEPINE HYDROCHLORIDE	01501138	29868-97-1, 28797-61-7	PRIDINOL METHANESULFONATE	01503077	511-45-5
PIRIBEDIL HYDROCHLORIDE	01506031	3605-01-4	PRILOCAINE HYDROCHLORIDE	01503270	1786-81-8, 721-50-6
PIROMIDIC ACID	01502045	19562-30-2	PRIMAQUINE DIPHOSPHATE	01500500	63-45-6, 90-34-6
PIROXICAM	01500491	36322-90-4	PRIMIDONE	01500501	125-33-7
PISCIDIC ACID	00200427	35388-57-9	PRIMULETIN	01501197	491-78-1
PIZOTYLINE MALATE	01505003	5189-11-7	PRISTIMERIN	01504181	1258-84-0
PLUMBAGIN	01505129	481-42-5	PROADIFEN HYDROCHLORIDE	01502084	78997-40-7
PODOFILOX	02300332	518-28-5	PROBENECID	01500502	57-66-9
PODOPHYLLIN ACETATE	01504412	1180-34-3	PROBUCOL	01501109	23288-49-5
PODOTOTARIN	00100286		PROCAINAMIDE HYDROCHLORIDE	01500503	614-39-1, 51-06-9
POLYMYXIN B SULFATE	01500492	1405-20-5, 1404-26-8	PROCAINE HYDROCHLORIDE	01500504	51-05-8, 59-46-1 [procaine]
POMIFERIN	00201580	572-03-2	PROCHLORPERAZINE EDISYLATE	01500505	1257-78-9, 84-02-6, 58-38-8
POTASSIUM p-AMINOBENZOATE	01500113	150-13-0 (acid)	PROCYCLIDINE HYDROCHLORIDE	01500507	1508-76-5, 77-37-2
PROMAZINE HYDROCHLORIDE	01500509	53-60-1, 58-40-2	PYRITINOL	01505762	1098-97-1
PROMETHAZINE HYDROCHLORIDE	01500510	58-33-3, 60-87-7	PYROCATECHUIC ACID	00212061	303-38-8
PRONETALOL HYDROCHLORIDE	01503628	54-80-8	PYROGALLIN	00210515	
PROPAFENONE HYDROCHLORIDE	01503935	34183-22-7, 54063-53-5	PYRROMYCIN	00201604	668-17-7
PROPANTHELINE BROMIDE	01500511	50-34-0, 298-50-0	PYRVINIUM PAMOATE	01500521	3546-41-6

PROPARACAINE HYDROCHLORIDE	01505688	575-06-98	QUASSIN	00310028	76-78-8
PROPOFOL	01505022	2078-54-8	QUEBRACHITOL	01502261	642-38-6
PROPRANOLOL HYDROCHLORIDE (+/-)	01505270	318-98-9, 525-66-6	QUERCETIN	01500672	117-39-5
PROPYLTHIOURACIL	01500515	51-52-5	QUERCETIN PENTAMETHYL ETHER	01600075	
PROSCILLARIDIN	01506084	466-06-8	QUERCITRIN	01500752	522-12-3
PROTIONAMIDE	01505316	14222-60-7	QUETIAPINE	01505187	111974-69-7
PROTOPORPHYRIN IX	01501111	553-12-8	QUINACRINE HYDROCHLORIDE	01500522	6151-30-0, 69-05-6, 83-89-6
PROTOVERATRINE A	01500909	143-57-7	QUINAPRIL HYDROCHLORIDE	01503076	82586-55-8, 85441-61-8
PROTOVERATRINE B	01500938	124-97-0	QUINIC ACID	00310018	77-95-2
PROTRYPTYLINE HYDROCHLORIDE	01505984	1225-55-4	QUINIDINE GLUCONATE	01500523	7054-25-3, 6591-63-5, 56-54-2
PROXYPHYLLINE	01505915	6003-00-9	QUININE ETHYL CARBONATE	00310050	83-75-0
PSEUDO-ANISATIN	00240914	31090-37-6	QUININE SULFATE	01500524	6119-70-6, 804-63-7, 130-95-0
PSEUDOEPHEDRINE HYDROCHLORIDE	01500516	345-78-8, 90-82-4	QUINOLINIC ACID	01502102	
PTAEROXYLIN	00100513	14729-11-4	QUIPAZINE MALEATE	01503420	5786-68-5, 4774-24-7
PUERARIN	01505001	3681-99-0	RABEPRAZOLE SODIUM	01505943	117976-90-6
PUROMYCIN HYDROCHLORIDE	01501105	58-58-2, 53-79-2	RACEPHEDRINE HYDROCHLORIDE	01500525	134-71-4, 90-81-3
PURPURIN	01505300	81-54-9	RALOXIFENE HYDROCHLORIDE	01505622	82640-04-8
PURPUROGALLIN	00210505	569-77-7	RAMIFENAZONE	01503822	3615-24-5
PYRANTEL PAMOATE	01500517	22204-24-6, 15686-83-6	RAMIPRIL	01505214	87333-19-5
PYRAZINAMIDE	01500518	98-96-4	RANITIDINE	01501151	66357-35-5
PYRIDOSTIGMINE BROMIDE	01503240	101-26-8, 155-97-5	RANOLAZINE	01505366	95635-55-5
PYRIDOXINE	01505453	65-23-6	RAUWOLSCINE HYDROCHLORIDE	01503639	6211-32-1
PYRILAMINE MALEATE	01500519	59-33-6, 91-84-9	REBAMIPIDE	01505310	90098-04-7
PYRIMETHAMINE	01500520	58-14-0	REPAGLINIDE	01506035	135062-02-1
PYRITHIONE ZINC	01500260	13463-41-7	RESERPINE	01500526	50-55-5
PYRITHYLDIONE	01503085	77-04-3	RESORCINOL	01500527	108-46-3
RESORCINOL MONOACETATE	01503500	102-29-4	ROSMARINIC ACID	01502094	537-15-5
RESVERATROL	01502223	501-36-0	ROSOLIC ACID	01500762	
RESVERATROL 4'-METHYL ETHER	01504044	33626-08-3	ROSUVASTATIN CALCIUM	01505213	287714-14-4, 147098-20-2(Ca)
RETINOL	01501203	68-26-8	ROTENONE	00200013	83-79-4

RETINYL ACETATE	01503051	127-47-9	ROXARSONE	01500530	121-19-7
RETINYL PALMITATE	01503604	79-81-2	ROXITHROMYCIN	01503276	80214-83-1
RETUSIN 7-METHYL ETHER	00240645		RUBESCENSIN A	01505177	28957-04-2
RHETSININE	01504176	526-43-2	RUTILANTINONE	00201606	21288-61-9
RHIZOCARPIC ACID	01505475	18463-11-1	RUTOSIDE (rutin)	00300607	153-18-4
RHODINYL ACETATE	00310030		S-ISOCORYDINE (+)	01500860	475-67-2
RHODOCLADONIC ACID	01505217	26984-15-6	SACCHARIN	01501171	81-07-2
RHOIFOLIN	01504075	17306-46-6	SAFROLE	01503620	94-59-7
RIBAVIRIN	01503938	36791-04-5	SALICIN	01502255	138-52-3
RIBOFLAVIN	01505347	83-88-5	SALICYL ALCOHOL	01500531	90-01-7
RIBOFLAVIN 5-PHOSPHATE SODIUM	01505763	130-40-5	SALICYLAMIDE	01500532	65-45-2
RIBOSTAMYCIN SULFATE	01503939	25546-65-0	SALICYLANILIDE	00300618	87-17-2
RIFAMPIN	01500529	13292-46-1	SALIDROSIDE	01505488	10338-51-9
RIFAXIMIN	01505321	80621-81-4	SALINOMYCIN, SODIUM	01503602	53003-10-4
RIMANTADINE HYDROCHLORIDE	01505460	1501-84-4	SALSALATE	00200331	552-94-3
RISEDRONATE SODIUM HYDRATE	01505944	115436-72-1	SALSOLIDINE	01504022	493-48-1
RITANSERIN	01503421	87051-43-2	SALSOLINE	01504025	89-31-6
RITODRINE HYDROCHLORIDE	01501149	23239-51-2, 26652-09-5	SALSOLINOL HYDROBROMIDE	01506041	38221-21-5
RIZATRIPTAN BENZOATE	01505189	144034-80-0	SALVINORIN A	01505080	83729-01-5
ROBUSTIC ACID	00240673	5307-59-5	SANGUINARINE SULFATE	00310035	5578-73-4
ROCCELLIC ACID	00200428	22139-54-4	SANTONIN	00300542	481-06-1
ROFECOXIB	01504235	162011-90-7	SAPPANONE A DIMETHYL ETHER	00201136	
ROLIPRAM	01505683	61413-54-5	SARAFLOXACIN HYDROCHLORIDE	01505314	91296-87-6
ROLITETRACYCLINE	01505684	751-97-3	SARMENTOSIDE B	00100568	
RONIDAZOLE	01501154	7681-76-7	SCOPOLAMINE HYDROBROMIDE	01500534	6533-68-2, 114-49-8, 51-34-3
ROPINIROLE	01505178	91374-21-9	SCOPOLETIN	01502242	92-61-5
ROSIGLITAZONE	01504263	122320-73-4	SECURININE	01505334	5610-40-2
SELAMECTIN	01503720	165108-07-6	SOLIDAGENONE	00300003	23534-56-7
SELEGILINE HYDROCHLORIDE	01505781	14611-52-0	SOLIFENACIN SUCCINATE	01505497	242478-37-1
SEMUSTINE	01503422	13909-09-6	SORBITOL	01300043	50-70-4

SENNOSIDE A	01504078	81-27-6	SOTALOL HYDROCHLORIDE	01506043	959-24-0
SEROTONIN HYDROCHLORIDE	01505754	50-67-9	SPAGLUMIC ACID	01503630	4910-46-7
SERTRALINE HYDROCHLORIDE	01505262	79559-97-0; 79617-96-2(base)	SPARTEINE HYDROIODIDE	01505241	
SHIKIMIC ACID	01502256	138-59-0	SPARTEINE SULFATE	00300548	6160-12-9, 299-39-8, 90-39-1
SIBUTRAMINE HYDROCHLORIDE	01505210	84485-00-7; 106650-56-0 (base); 125494-59-9	SPECTINOMYCIN HYDROCHLORIDE	01500538	22189-32-8, 21736-83-4, 1695-77-8
SILIBININ	01505256	22888-70-6	SPERMINE	01505764	71-44-3
SIMVASTATIN	01504236	79902-63-9	SPHONDIN	00300005	483-66-9
SINENSETIN	01505381	2306-27-6	SPIPERONE	01501152	749-02-0
SINOMENINE	01505253	115-53-7	SPIRAMYCIN	01503423	8025-81-8
SIROLIMUS	01504008	53123-88-9	SPIRONOLACTONE	01500539	52-01-7
SISOMICIN SULFATE	01500536	53179-09-2, 32385-11-8	SR-2640	01505930	105350-26-3
SITOSTERYL ACETATE	00107023		STICTIC ACID	00300006	549-06-4
SKATOLE	01505758	83-34-1	STIGMASTA-4,22-DIEN-3-ONE	00270067	20817-72-5
SMILAGENIN	00107013	126-18-1	STIGMASTEROL	01504051	
SMILAGENIN ACETATE	00100298		STREPTOMYCIN SULFATE	01500541	3810-74-0, 57-92-1
SODIUM DEHYDROCHOLATE	01500225	145-41-5	STREPTOZOSIN	01500543	18883-66-4
SODIUM DEOXYCHOLATE	01500902	302-95-4	STROPHANTHIDIN	00100291	66-28-4
SODIUM FLUOROACETATE	00330009	62-74-8	STROPHANTHIDINIC ACID LACTONE ACETATE	00100749	
SODIUM NITROPRUSSIDE	01300037	13755-38-9	STRYCHNINE	01500651	57-24-9
SODIUM OXYBATE	01300038	502-85-2	STRYCHNINE METHIODIDE	01505840	
SODIUM SALICYLATE	01500533	54-21-7	SUCCINYLSULFATHIAZOLE	01502025	116-43-8
SODIUM TETRADECYL SULFATE	01300042	139-88-8	SUCRALOSE	01505953	56038-13-2
SODIUM THIOGLYCOLATE	01503672	367-51-1	SULCONAZOLE NITRATE	01501148	61318-91-0, 61318-90-9
SOLANESOL	01505325	13190-97-1	SULFABENZAMIDE	01500544	127-71-9
SOLANESYL ACETATE	01505326		SULFACETAMIDE	01500545	144-80-9, 127-56-0, 6209-17-2
SOLASODINE	00100537	126-17-0	SOLIDAGENONE	00300003	23534-56-7
SULFACHLORPYRIDAZINE	01501142	80-32-0	SYRINGIC ACID	01505766	530-57-4
SULFADIAZINE	01500546	68-35-9	TACRINE HYDROCHLORIDE	02300104	1684-40-8

SULFADIMETHOXINE	01501144	122-11-2	TACROLIMUS	01503968	109581-93-3, 104987-11-3
SULFADOXINE	01506086	2447-57-6	TADALAFIL	01505639	171596-29-5
SULFAGUANIDINE	01501146	57-67-0	TAMOXIFEN CITRATE	01500557	54965-24-1, 10540-29-1
SULFAMERAZINE	01500547	127-79-7	TANGERITIN	01505269	481-53-8
SULFAMETER	01501155	651-06-9	TANNIC ACID	01504105	1401-55-4
SULFAMETHAZINE	01500548	57-68-1	TANSHINONE IIA	01505824	568-72-9
SULFAMETHIZOLE	01500549	144-82-1	TANSHINONE IIA SULFONATE SODIUM	01505036	
SULFAMETHOXAZOLE	01500550	723-46-6	TARTARIC ACID	01300044	87-69-4
SULFAMETHOXYPYRIDAZINE	01501156	80-35-3	TAURINE	01505463	107-35-7
SULFAMONOMETHOXINE	01501147	1220-83-3	TEICOPLANIN [A(2-1) shown]	01505707	61036-62-2
SULFANILAMIDE	01500646	63-74-1	TELENZEPINE HYDROCHLORIDE	01504187	80880-90-6
SULFANILATE ZINC	01503301	31884-76-1	TELITHROMYCIN	01505265	191114-48-4
SULFANITRAN	01503339	122-16-7	TEMEFOS	00330062	3383-96-8
SULFAPHENAZOLE	01501143	526-08-9	TENIPOSIDE	01504094	29767-20-2
SULFAPYRIDINE	01500551	144-83-2	TENOXICAM	01503142	59804-37-4
SULFAQUINOXALINE SODIUM	01501145	59-40-5	TERAZOSIN HYDROCHLORIDE	01505576	70024-40-7
SULFASALAZINE	01500552	599-79-1	TERBINAFINE HYDROCHLORIDE	01505392	78628-80-5, 91161-71-6(base)
SULFATHIAZOLE	01500553	72-14-0	TERBUTALINE HEMISULFATE	01500558	23031-32-5, 23031-25-6
SULFINPYRAZONE	01500554	57-96-5	TERFENADINE	01503708	50679-08-8
SULFISOXAZOLE	01500555	127-69-5	TESTOSTERONE	00307023	58-22-0
SULFISOXAZOLE ACETYL	01505461	80-74-0	TESTOSTERONE PROPIONATE	00300034	57-85-2
SULINDAC	01500556	38194-50-2	TETRACAINE HYDROCHLORIDE	01500564	136-47-0, 94-24-6
SULMAZOLE	01501159	73384-60-8	TETRACHLOROISOPHTHALONITRILE	01504101	
SULOCTIDIL	01501153	54063-56-8	TETRACYCLINE HYDROCHLORIDE	01500566	64-75-5, 60-54-8
SULPIRIDE	01501150	15676-16-1	TETRAHYDROSAPPANONE A TRIMETHYL ETHER	01600480	
SUMATRIPTAN	01505372	103628-46-2	TETRAHYDROZOLINE HYDROCHLORIDE	01500567	522-48-5, 84-22-0
SUPROFEN	01501161	40828-46-4	TETRAMIZOLE HYDROCHLORIDE	01505679	5086-74-8
SURAMIN	01502032	129-46-4, 145-63-1	TETRANDRINE	01504185	518-34-3
SUXIBUZONE	01501157	27470-51-5	SYRINGIC ACID	01505766	530-57-4
TETROQUINONE	01503330	319-89-1	TIMONACIC	01503320	444-27-9

THALIDOMIDE	01503607	50-35-1	TINIDAZOLE	01502127	19387-91-8
THEAFLAVIN	00200111	4670-05-7	TIOCONAZOLE	01505581	65899-73-2
THEAFLAVIN DIGALLATE	00201515	30462-35-2	TIOXOLONE	01503094	4991-65-5
THEAFLAVIN MONOGALLATES	00210242		TIRATRICOL	01506047	51-24-1
THEANINE	01505254	3081-61-6	TOBRAMYCIN	01500579	32986-56-4
THEOBROMINE	01500649	83-67-0	TODRALAZINE HYDROCHLORIDE	01501174	14679-73-3
THEOPHYLLINE	01500568	5967-84-0, 58-55-9	TOLAZAMIDE	01501201	1156-19-0
THERMOPSINE PERCHLORATE	01504023	486-90-8(base)	TOLAZOLINE HYDROCHLORIDE	01500580	59-97-2, 59-98-3
THIABENDAZOLE	01500570	148-79-8	TOLBUTAMIDE	01500581	64-77-7
THIAMINE	01505464	67-03-8	TOLFENAMIC ACID	01501198	13710-19-5
THIAMPHENICOL	01503136	15318-45-3	TOLMETIN SODIUM	01500582	64490-92-2, 26171-23-3
THIAMYLAL SODIUM	01900002	337-47-3, 77-27-0	TOLNAFTATE	01500583	2398-96-1
THIMEROSAL	01500572	54-64-8	TOLPERISONE HYDROCHLORIDE	01501194	70312-00-4
THIOCTIC ACID	01503941	1077-24-7	TOLTRAZURIL	01505681	69004-03-1
THIOGUANINE	01500573	154-42-7, 5580-03-0	TOMATINE	01504079	86273-92-9
THIOGUANOSINE	01506044	85-31-4	TOPIRAMATE	01505801	97240-79-4
THIOPENTAL SODIUM	01900005	71-73-8, 76-75-5	TOPOTECAN HYDROCHLORIDE	01505820	119413-54-6
THIORIDAZINE HYDROCHLORIDE	01500575	130-61-0, 50-52-2	TOREMIPHENE CITRATE	01505682	89778-27-8
THIOTEPA	01503324	52-24-4	TOSYLCHLORAMIDE SODIUM	01504506	127-65-1
THIOTHIXENE	01500576	5591-45-7, 3313-26-6	TOTAROL	00100287	511-15-9
THIRAM	01503322	137-26-8	TOTAROL ACETATE	00100267	
THONZYLAMINE HYDROCHLORIDE	01503135	63-56-9, 91-85-0	TOTAROL-19-CARBOXYLIC ACID, METHYL ESTER	00100612	
THYMOQUINONE	00310299		TRAMADOL HYDROCHLORIDE	01505389	36282-47-0
TIAPRIDE HYDROCHLORIDE	01503086	51012-32-9	TRANEXAMIC ACID	01502026	1197-18-8
TICARCILLIN DISODIUM	01505678	4697-14-7	TRANILAST	01505333	53902-12-8
TICLOPIDINE HYDROCHLORIDE	01505677	53885-35-1	TRANYLCYPROMINE SULFATE	01500584	13492-01-8, 7081-36-9, 155-09-9
TIGOGENIN	00100315	77-60-1	TRAZODONE HYDROCHLORIDE	01503121	25332-39-2, 19794-93-5
TILMICOSIN	01505112	108050-54-0	TRETINON	01502016	302-79-4
TILORONE	02300009	27591-69-1, 27591-97-5	TRIACETIN	01500585	102-76-1
TIMOLOL MALEATE	01500578	26921-17-5, 91524-16-2	TIMONACIC	01503320	444-27-9

TRIACETYLRESVERATROL	01504041	42206-94-0	TRIPROLIDINE HYDROCHLORIDE	01500598	6138-79-0, 550-70-9, 486-12-4
TRIAMCINOLONE	01500586	124-94-7	TRIPTOPHENOLIDE	01504005	74285-86-2
TRIAMCINOLONE ACETONIDE	01500587	76-25-5	TRISODIUM ETHYLENEDIAMINE TETRACETATE	01500270	150-38-9
TRIAMCINOLONE DIACETATE	01500588	67-78-7	TROLOX	01506052	53188-07-1
TRIAMTERENE	01500589	396-01-0	TROPICAMIDE	01500599	1508-75-4
TRICHLORFON	01505765	52-68-6	TROXERUTIN	01505245	7085-55-4
TRICHLORMETHIAZIDE	01500590	133-67-5	TRYPTAMINE	01503922	61-54-1
TRICHLORMETHINE	00300563	555-77-1	TRYPTOPHAN	01500600	73-22-3 ['L']
TRICLABENDAZOLE	01505786	68786-66-3	TUAMINOHEPTANE SULFATE	01500601	6411-75-2, 123-82-0
TRICLOSAN	01505465	3380-34-5	TUBOCURARINE CHLORIDE	01500602	6989-98-6, 57-94-3, 41354-45-4, 57-95-4
TRIDESACETOXYKHIVORIN	00100576		TULOBUTEROL	01503954	41570-61-0
TRIENTINE HYDROCHLORIDE	01505675	38260-01-4	TYLOSIN TARTRATE	01505312	1405-54-5, 1401-69-0(base)
TRIFLUOPERAZINE HYDROCHLORIDE	01500591	440-17-5, 117-89-5	TYLOXAPOL	01506053	25301-02-4
TRIFLUPROMAZINE HYDROCHLORIDE	01503118	1098-60-8, 146-54-3	TYROSINE	01300046	60-18-4
TRIFLURIDINE	01504183	70-00-8	TYROTHRICIN	01500603	1404-88-2
TRIGONELLINE	01500880	535-83-1	UBIDECARENEONE	01504013	303-98-0
TRIHEXYPHENIDYL HYDROCHLORIDE	01500592	52-49-3	UMBELLIFERONE	00231084	93-35-6
TRIMEBUTINE MALEATE	01505011	34140-59-5(base)	UNDECYLENIC ACID	01505468	112-38-9
TRIMEDLURE	01504135	12002-53-8	URAPIDIL HYDROCHLORIDE	01503100	34661-75-1
TRIMEPRAZINE TARTRATE	01500593	4330-99-8, 41375-66-0, 84-96-8	UREA	01500604	57-13-6
TRIMETAZIDINE DIHYDROCHLORIDE	01506088	5011-34-7	URETHANE	01503304	51-79-6
TRIMETHADIONE	01505466	127-48-0	URIDINE TRIPHOSPHATE TRISODIUM	01503346	19817-92-6
TRIMETHOBENZAMIDE HYDROCHLORIDE	01500594	554-92-7, 138-56-7	URSINOIC ACID	01504167	30265-59-9
TRIMETHOPRIM	01500595	738-70-5	URSOCHOLANIC ACID	01500835	546-18-9
TRIMETHYLCOLCHICINIC ACID	01506051	3482-37-9	URSODIOL	01500605	128-13-2
TRIMETOZINE	01504214	635-41-6	URSOLIC ACID	01800031	77-52-1
TRIMIPRAMINE MALEATE	01503117	521-78-8, 739-71-9	USNIC ACID	00300147	125-46-2
TRIOXSALEN	01500596	3902-71-4	UTILIN	00100081	31218-22-1

TRIPELENNAMINE CITRATE	01500597	6138-56-3, 91-81-6	UVAOL	01504073	545-46-0
VALACYCLOVIR HYDROCHLORIDE	01505368	124832-27-5	XANTHYLETIN	00100609	553-19-5
VALERYL SALYCILATE	01505336	64206-54-8	XYLAZINE	01501200	23076-35-9, 7361-61-7
VALINOMYCIN	01505107	2001-95-8	XYLOCARPUS A	00100424	
VALPROATE SODIUM	01500606	1069-66-5, 99-66-1	XYLOMETAZOLINE HYDROCHLORIDE	01500614	1218-35-5, 526-36-3
VALSARTAN	01505209	137862-53-4	XYLOSE	01300048	58-86-6
VANCOMYCIN HYDROCHLORIDE	01500607	1404-93-9, 1404-90-6	YOHIMBIC ACID HYDRATE	01504076	522-87-2
VARDENAFIL HYDROCHLORIDE	01505374	224789-15-5	YOHIMBINE HYDROCHLORIDE	01500663	65-19-0
VECURONIUM BROMIDE	01505709	50700-72-6	ZAPRINAST	01501199	37762-06-4
VENLAFAXINE	01504171	99300-78-4, 93413-69-5	ZARDAVERINE	01506056	101975-10-4
VERAPAMIL HYDROCHLORIDE	02300307	152-11-4, 52-53-9	ZIDOVUDINE [AZT]	01502109	30516-87-1
VESAMICOL HYDROCHLORIDE	02300309	120447-62-3	ZILEUTON	01505906	111406-87-2
VIDARABINE	01500609	24356-66-9, 5536-17-4	ZINC UNDECYLENATE	01505467	557-08-4
VIGABATRIN	01502036	60643-86-9	ZOLMITRIPTAN	01505281	139264-17-8
VINBLASTINE SULFATE	01500611	143-67-9, 865-21-4	ZOMEPIRAC SODIUM	01500615	64092-49-5, 64092-48-4, 33369-31-2
VINCAMINE	01500647	1617-90-9	ZOPICLONE	01503425	43200-80-2
VINCRISTINE SULFATE	01505672	2068-78-2	ZOXAZOLAMINE	01504216	61-80-3
XANTHONE	00200523	90-47-1			
XANTHOPTERIN	00300537	119-44-8			
XANTHOXYLIN	00200441	90-24-4			
XANTHURENIC ACID	01500754	59-00-7			